



University of Strathclyde  
Department of Pure and Applied Chemistry

**Protein Nanoparticle Conjugates for use in Bioanalytical  
Applications**

by

Jane Gallagher

A thesis presented to the Department of Pure and Applied Chemistry, University of Strathclyde, in fulfilment of the requirements for the degree of Doctor of Philosophy.

2011

This thesis is the result of the author's original research. It has been composed by the author and has not been previously submitted for examination which has led to the award of a degree. The copyright of this thesis belongs to the author under the terms of the United Kingdom Copyright Acts as qualified by University of Strathclyde Regulation 3.50. Due acknowledgement must always be made of the use of any material contained in, or derived from, this thesis.

# ACKNOWLEDGEMENTS

I would like to thank my supervisors Prof. Duncan Graham and Dr Karen Faulds for their help and guidance throughout my PhD. For their assistance and direction I would like to thank Dr Jennifer Dougan, Dr Iain Larmour, Dr Andrew Ingram and Dr Robert Stokes.

For providing hilarious banter and support throughout my time wandering the corridors of the Royal College I would like to thank Colette, Jen, Sarah, Fiona, Victoria and Derek without your friendship I would not have made it to the end.

And of course the rest of the Raminators, I will always treasure the vase stealing nights!

Perhaps the greatest thank you must go to my family, friends and Neil. You have dealt with the greatest burden of listening to my various frets throughout the years. Your support has been invaluable; I would not have been able to reach my full potential without your support.

Finally I would like to dedicate this thesis to two of the most important people in my life – my parents Rita and Pat.

Their encouragement throughout my life has been consistent and never failing. They have taught me to always believe in myself and to realise my full potential.

To Mum and Dad

# ABSTRACT

Proteins are the commanders of the cell. These structures control and form the basis for cellular activity. It is hoped through the understanding of these components and their interactions the mutations and faults that cause disease can be identified and prevented.

The aim of this research was to investigate the use of employing SERS in detection of protein interactions. It is hypothesised that this technique can be utilised in a way fluorescence spectroscopy cannot. Multiplexing provides the ability to visualise and observe proteins in the real time and the path they take through the cell. One of the most commonly used markers to examine the cellular environment is fluorescent proteins (FPs).

Fluorescent Proteins are an important biomarker and are used extensively in the field of cellular biology for a better understanding of proteins and the impact of their actions within the cell. As one of the most widely used markers in cellular biology, it was thought that SERS could be employed in this instance. Ag-FP conjugates were prepared using two different methods: electrostatic attachment; and thioctic acid capped nanoparticles. This allowed for the label-free, solution based SERS detection of FPs. The detection and optimisation of this process are described within this document, which led to a competitive LOD. Furthermore the successful detection of these proteins has opened up the possibility of multiplexing of FPs using SERS. As shown in this research, vibrational peaks individual to each protein were present, indicating that very slight structural conformation changes can be detected using SERS. To transpose this Raman based technique into the cellular environment, there first must be a route into the cell. Cellular membranes are difficult to cross - even with successful entry; the cargo may not reach its eventual target within the cell.

TAT peptide is a know cell penetrating peptide that has been shown to send 'cargo' across the cellular membrane and aid with cell localisation. The route to the conjugation of fluorescein labelled TAT was investigated. It was found thioctic acid capped nanoparticles provided a conjugation method to silver nanoparticles. When incubated with HeLa cells, subsequent SERS detection of these conjugates was

obtained. This provided the platform for the use of other proteins to be conjugated to TAT to allow for *in vivo* detection.

However the cellular environment is very different from 'bench' experiments, there are many processes occurring at any one time. To visualise these events, multiplexing must be implemented. For efficient multiplexing there has to be the development of novel dyes which will provide unique vibrational peaks that can be identified in this situation. Squaraine dyes provide a peak in a region where no other commercially available dye resonates. This type of dye has been synthesised, however solubility issues plagued the formation of a linker. SERS was obtained from this previously unpublished dye. A linker was successfully synthesised and conjugated to the A/G protein. This conjugate was used in a micro-assay from which SERS was obtained. This confirmed successful interaction between the protein and an antibody, confirming protein activity remained when conjugated to the linker and nanoparticle. This application based work was carried out to prove the benefits of these compounds in protein detection.

# ABBREVIATIONS

AcOH Acetic acid

Ag Silver

Au Gold

CDI 1,1-Carbonyldiimidazole

CPPs Cell penetrating peptide

d doublet

DCM Dichloromethane

DCC N,N'-Dicyclohexylcarbodiimide

DCU N,N'-dicyclohexylurea

DIC N,N'-Diisopropylcarbodiimide

DLS Dynamic light scattering

DIPEA Diisopropylethyl amine

DMA Dimethylaniline

DMAP Dimethylamino pyridine

DMF Dimethyl formate

DNA Deoxyribose nucleic acid

DPN Dip-pen nanolithography

DTT Dithiothreitol

E-Coli Escherichia coli

EDC 1-Ethyl-3-(3-dimethylaminopropyl) carbodiimide

ER Endoplasmic reticulum

EGFP Enhanced green fluorescent protein

FAM fluorescein

FRET Förster resonance energy transfer

FP fluorescent protein

GFP Green fluorescent protein

HeLa Cells from cell line form Henrietta Lack

HGP Human genome project

HPLC High performance liquid chromatography

HUPO Human Proteome organism

IPA Isopropyl alcohol

IR Infra-red

$\lambda$  Lambda

LOD Limit of detection

m multiplet

MALDI Matrix assisted laser desorption

MALDI-TOF Matrix assisted laser desorption – Time of flight

MAPK Mitogen Activated Protein Kinase

Max maximum

MeOH Methanol

mRNA messenger Ribose nucleic acid

MS Mass spectrometry

NHS N-hydroxysuccinimide

NMR Nuclear magnetic resonance

NP Nanoparticle

Oct-4

PDDA Poly (diallyl ammonium chloride)

PBS Phosphate buffered saline

PEG Poly(ethylene) glycol

pI isoelectric point

PTD Protein transduction domains

QD Quantum Dots

RFP Red fluorescent protein

RNA Ribonucleic acid

RRS Resonance Raman Scattering

RT Room temperature

tRNA transfer Ribose nucleic acid

s singlet

SAM self assembled monolayer

SEM Scanning electron microscopy

SERS Surface Enhanced Raman Scattering

SERRS Surface enhanced resonance Raman scattering

SPB surface plasmon band

SPOS Solid phase organic synthesis

SPR surface plasmon resonance

t triplet

TA-NPs Thiocetic acid nanoparticles

TEA Triethylamine

TEM Transmission electron microscopy

TEOF Triethyl orthoformate

TFA Trifluoroacetic acid

TLC Thin layer chromatography

TMB

TMB-SAC sulphur acetate

TMSOTf Trimethylsilyl trifluoromethanesulfonate

UV Ultraviolet

Vis visible

# CONTENTS PAGE

Acknowledgements	i
Abstract	ii-iii
Abbreviations	iv-vii
Chapter 1: Introduction	1
1.1 Introduction to proteins	2
1.1.1 Amino Acids	2
1.1.2.1 Primary Structure	3-4
1.1.2.2 Secondary structure	4-5
1.1.2.3 Tertiary structure	6
1.1.2.4 Quaternary Structure	7
1.2 Protein expression	7
1.2.1 Transcription	7-9
1.2.2 Translation	9-10
1.3 Protein functions	11-13
1.4 Protein-Protein Interactions	14
1.4.1 Study of Protein-Protein Interactions	14-15
1.4.1.1 Fluorescence Microscopy	15-16
1.4.2 Quantum Dots	17-18
1.5 Fluorescent Proteins	18-20
1.6 Nanoparticles	20-23
1.6.1 Characterisation of Nanoparticles	23
1.7 Protein and Nanoparticles	24-26
1.7.1 Protein-Nanoparticle conjugates	26-27
1.8 Raman Scattering	27-28
1.8.1 Resonance Raman	29
1.8.2 Surface Enhanced Raman Scattering	29-30
1.8.2.1 Electromagnetic Enhancement	30
1.8.2.2 Chemical Enhancement	30
1.8.2.3 Surface	31

1.8.3 Surface Enhanced Resonance Raman Scattering	31-32
1.8.3.1 Aggregation- The on/off effect	32
1.9 SERS in Bio-Nanotechnology	33
1.9.1 SERS in the detection of DNA	33-35
1.9.2 SERS in protein detection	35-37
1.9.3 Use of dyes in Raman scattering	37-40
Chapter 2: Aims	41
Chapter 3: Detection of Fluorescent Proteins via SERS	42
3.1 Introduction	42-47
3.2 Previous work	47
3.2.1 Raman of EGFP	47-48
3.2.1.1 Investigation of Raman parameters for EGFP	49-51
3.2.2 SERS of EGFP	51-52
3.2.2.1 Surface based detection of EGFP	52-55
3.3 Electrostatic methodology	55-57
3.4 Investigation of pH modification of colloid	57-68
3.5 Optimisation of SERS conditions	68-70
3.6 Limit of detection study	70-77
3.7 Alternative methods of detection	77-83
3.8 Red Fluorescent Protein	83-90
3.9 Multiplexing	91
Chapter 4: The detection of nanoparticles in cells through the use of TAT	92
4.1 Introduction	92-93
4.1.1 Cell Penetrating Peptide	93-94
4.1.2 TAT Peptide	94-95
4.2 Results and discussion	96-98
4.3 Linker synthesis	99-102
4.4 Conjugate synthesis	102-103
4.4.1 PEG <sub>41</sub> -AuNP investigations	103
4.4.1.1 Gold nanoparticles and PEG <sub>41</sub>	103-104
4.4.1.1 Silver nanoparticles and PEG <sub>41</sub>	105
4.4.2 TAT conjugation to PEG <sub>41</sub> -AuNPs	106-108

4.4.3. Characterisation of TAT-linker coupling	108-112
4.4.4 SERRS Analysis of TAT-PEG <sub>41</sub> AuNP @ 514.5 nm	113-117
4.4.5 Investigation of PEG <sub>8</sub> as a linker in TAT-NPs	117-120
4.4.6 Alternative Method of formation of TAT conjugates	120-124
4.5 Cellular Experiments	124-130
Chapter 5: Synthesis of Novel compounds	131
5.1 Introduction	131-132
5.2 Previous work	132-133
5.3 Cyanine Dyes	133-135
5.3.1 Synthesis of Cyanine dyes	135-136
5.3.1.1 Synthesis of TMB groups	136-137
5.3.1.2 Synthesis of initial dyes	137-141
5.4 Solid Phase Synthesis	142-152
5.5 Squaraine dyes-An Introduction	153-154
5.5.1 Previous Work	154
5.5.2 Synthesis of Squaraine dyes	154-155
5.5.2.1 Synthesis of half squaraine	155-157
5.5.3 Indole half squaraine synthesis	157-159
5.5.4 Solid Phase Synthesis of squaraine dyes	160-167
5.5.5 One pot synthesis of squaraine	167-168
5.6 Synthesis of linker molecules	168-169
5.6.1 Cyanine PEG <sub>3</sub> Linker Synthesis	170-178
5.6.2 Squaraine PEG <sub>3</sub> Linker Synthesis	178-183
5.7 PEG <sub>41</sub> Linker molecules	183-189
5.8 Linker Free Investigations	189
5.8.1 Linker Free Squaraine dyes	189-194
5.8.2 Linker Free Cyanine Dyes	194-200
5.9 Use of Linker one as a protein detector	200-203
5.9.2 Assay Approach	204-206
Chapter 6 Conclusions	207-210
Chapter 7: Future Work	211-213
Chapter 8: Experimental	214

8.1 General	214-215
8.2 Chemical Synthesis	216-249
8.3 Nanoparticle Synthesis	250
8.3.1 Silver citrate Nanoparticles	250
8.3.2 Gold citrate Nanoparticles	250
8.4 Conjugate Synthesis	250
8.4.1 Thioctic Acid Capped AgNPs	250
8.4.2 EGFP Conjugates	250
8.4.3 RFP Conjugates	250
8.4.4 PDDA-EGFP Conjugates	251
8.4.5 PEG41/PEG8-AuNPs Conjugates	251
8.4.6 TAT Conjugates	251
8.4.7 Gold Nanoparticle Linker protein conjugates	251
8.5 Fabrication of IgG Capture Antibody Arrays	251-252
8.6 Cellular Experimental	252-253
8.7 HPLC profile for TAT coupling	253
8.8 Klarite™ Experimental	253
8.8.1 Deposition on Klarite™	253
8.8.2 SERS analysis of Klarite™ chip and assay	253
8.9 Raman Analysis of EGFP and RFP conjugates	253
8.10 UV-Vis Spectrometry	254
8.11 pH adjustment of silver citrate colloid	254
8.12 SERS Experimental	254
8.12.1 SERS of EGFP conjugates	254
8.12.2 SERS of RFP conjugates	254-255
8.12.3 SERS of PDDA-EGFP conjugates	255
8.12.4 SERS of TAT conjugates	255
8.13 Optimisation experimental for SERS of EGFP	255
8.13.1 Acquisition Investigation	256
8.13.2 Incubation time Investigation	256
8.14 Gel Electrophoresis Experimental	256
Chapter 9: References	257-264

# CHAPTER 1: INTRODUCTION

Genomics is a branch of science dedicated to the study of the genes, with the aim to provide an insight into genetic inheritance and its impact on an organism. The research in this field led to the completion of the Human Genome Project (HGP) in 2003. This project was a 13 year endeavour, which involved over 200 laboratories that were funded by the Department of Energy (DOE) and the National Institute of Health (NIH). However, limitations of genomic research quickly became apparent.<sup>1</sup> There is over 21,000 genes within the human body. These genes can code for up to ten times the amount of proteins.<sup>2</sup> The proteome is a term created in 1994 by Marc Wilkins and the study of the proteome is called Proteomics. This was the term used to describe the complete complement of proteins expressed by a genome, cell, tissue or organism.<sup>3</sup> As such an organisation has now been created to *'...represent and promote proteomics through international co-operation and collaborations by fostering the development of new technologies, techniques and training.'* This organisation is called the Human Proteome Organisation (HUPO) and in collaboration with the HGP, aims to find the causes of diseases and track their progress, with the ultimate aim of curing and preventing diseases. Their focus is to identify and determine the location & function of the proteins that make up the cell. It is now accepted within the scientific community, that it is proteins that are the driving force of cellular processes and there is a complex relationship between the genome and eventual protein complement of an organism. Consequently the focus has shifted somewhat from genomic to proteomics for the purposes of understanding disease processes.<sup>4,5</sup>

For centuries, scientists have been fascinated with the concept of genes and genetic inheritance: from Gregor Mendel's primitive experiments with peas; to the discovery of the DNA double helix; through to the remarkable achievement of the completion of the HGP. The delicate and dynamic relationship between DNA, RNA and proteins continues to be the focus of vast scientific investigation in the quest to understand, cure and prevent diseases.

## 1.1 INTRODUCTION TO PROTEINS<sup>6,7</sup>

The term protein has its origins in the Greek Language, derived from the word Proteios, meaning “first word”. Proteins are the task masters of the cell and account for over 50% of the dry weight in the average cell. They are involved in all aspects of cellular processing, either directly or in the co-ordination of many other processes. The roles which they carry out are vast. For example proteins are involved in structural support of the cell as cellular membranes; signalling to other parts of the cell; and as enzymes that regulate metabolism by selectively accelerating chemical reactions in the cell. With such a diverse range of roles, the structure, function and reactivity of proteins are inherently linked to their chemical properties. Proteins are comprised of different layers of structural complexity, which will be explored in greater detail in the subsequent sections.

### 1.1.1 AMINO ACIDS

Proteins are constructed from a handful of building blocks, known as amino acids. Amino acids are comprised of an asymmetrical carbon attached to four functional groups: a hydrogen atom; amino group; carboxyl group; and a side chain, as shown in figure 1.1

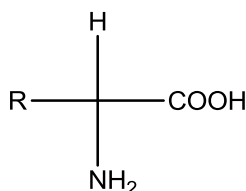


Figure 1.1: General structure of an amino acid, R group refers to the side chain.

The side chain (or residue as it is commonly referred to) determines the physical and chemical character of that specific amino acid. There are 20 essential amino acids that can be divided into two classes; hydrophobic (typically non-polar) and hydrophilic/polar. At physiological pH, the basic amino acids and acidic amino acids are dissociated and are therefore positively and negatively charged respectively.

### 1.1.2.1 PRIMARY STRUCTURE

Amino acids polymerise to form proteins and are typically made up of two or three polypeptides. The formation of a peptide bond involves a condensation reaction between the amino group of one amino acid and the carboxyl group of the other.

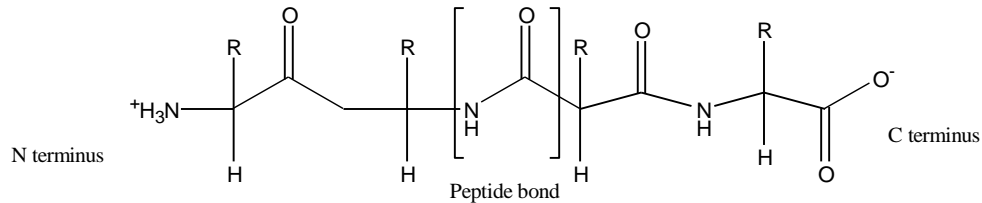


Figure 1.2: Polypeptide chain which contains a repeating peptide bond connecting the amino acids which form the protein primary structure. Every protein consists of a C terminus, free carboxylic acid at one end and an N terminus, free primary amine at the other end.

All proteins contain the basic repeating unit and polypeptide backbone, as shown in figure 1.2. The diversity present in such molecules originates from the different amino acids comprising the peptide chain. Each polypeptide varies in length and composition and it is the unique linear sequence (referred to as the primary structure) which confers the variation present in proteins.

Fredrick Sanger pioneered amino acid sequencing of proteins using enzymes that hydrolysed the polypeptide chains at specific points to produce small fragments which were then separated using chromatography.<sup>8,9</sup>

Various enzymatic proteins digested the polypeptide chain at known specific amino acids followed by separation via column chromatography, the observation of overlapping regions allowed the original primary amino acid sequence to be elucidated.

The primary structure relates to the linear amino acid sequence of the protein which is pre-determined by inherited genetic information. This genetic information is present in the nucleus of the cells, where DNA resides. The bases which comprise the DNA strand code for the eventual protein structure; this sequence of events is outlined in figure 1.3 and is known as the Central Dogma.



Figure 1.3: The process for protein synthesis.

The direct relationship between DNA and eventual protein sequence means accurate copying of information is essential. There are many different mutations that can occur in DNA sequences. If this sequence is part of a gene, the mutation can have a detrimental effect when transcription occurs. A slight change in just one of the amino acids within the sequence can have a devastating effect; this change is a consequence of a translation error. The three main mutations which occur in DNA sequences are: substitution, whereby one base is exchanged for another; insertion, in which extra bases have been added to the sequence; and finally a deletion mutation, where a section of DNA is lost or deleted. One famous example where a substitution mutation occurs is the protein Haemoglobin, which is responsible for the transportation of oxygen within the body. The mutation in the gene, where an A base is substituted with a T base causes the glutamic acid in the primary sequence to be replaced with valine. This will result in a condition called sickle cell anaemia. However the actions of proteins are not solely dictated by the primary sequence - the other tiers of protein structure have a combined affect.

#### 1.1.2.2 SECONDARY STRUCTURE

The secondary structure of a protein refers to the folding of the polypeptide chain resulting in two main types of conformation: alpha ( $\alpha$ ) helix; and beta ( $\beta$ ) sheets. Hydrogen bonding plays a crucial role in the formation of the secondary structure. The presence of oxygen, nitrogen and hydrogen allow for numerous hydrogen bonds to form at regular intervals throughout the polypeptide backbone. The  $\alpha$ -helix is a coil which is held in place through hydrogen bonding at every fourth amino acid. Whereas the  $\beta$ -sheet has two polypeptide chains that lie parallel to each other and are held together by hydrogen bonding between the chains, at various points of the backbone, as shown in figure 1.4.

The secondary structure of a protein directly influences its properties i.e. globular proteins have the tendency to form  $\alpha$ -helices with  $\beta$ -sheets separating these regions, whereas fibrous proteins tend to form predominately alpha helices without any  $\beta$ -sheet separation.

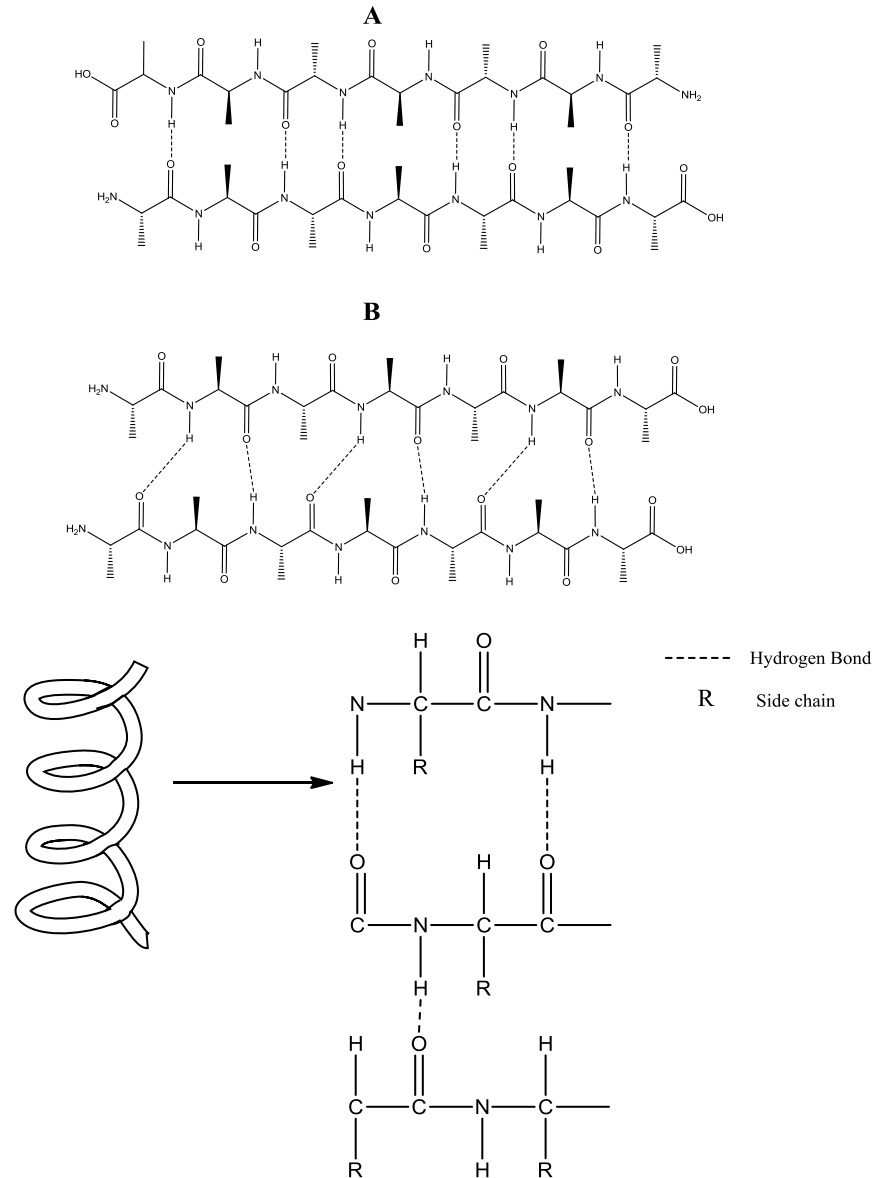


Figure 1.4: Representation of the  $\beta$ -sheet arrangement, A refers to the anti-parallel version and B to the parallel, and the  $\alpha$ -helix formed through hydrogen bonding between the amino acids in different polypeptide chains.

### 1.1.2.3 TERTIARY STRUCTURE

The third level of protein structure, describes the bonding present within the folded protein structure. There are various types of bonding that occur within the tertiary structure, however, hydrophobic interactions are the greatest contributing factor. The hydrophobic amino acids collect within the core of the protein structure to avoid the interaction with any water molecules, whilst simultaneously presenting the hydrophilic molecules toward the water. Van der Waals interactions further strengthened the hydrophobic interactions as the non-polar molecules congregate within the centre of the protein. In addition both hydrogen and ionic bonding are present which further increased the stability of the tertiary structure. As with the hydrogen bonding within the secondary structure, these interactions are individually weak but collectively they underpin the tertiary structure forming the specific shape of the protein. In addition, covalent bonding between any free cysteine amino acids can occur. The sulfhydryl groups (SH) can form disulfide bridges as the cysteine groups are brought closer together as the protein folds into its functional conformation. These various types of bonding can exist within one protein structure. This is shown in figure 1.5.

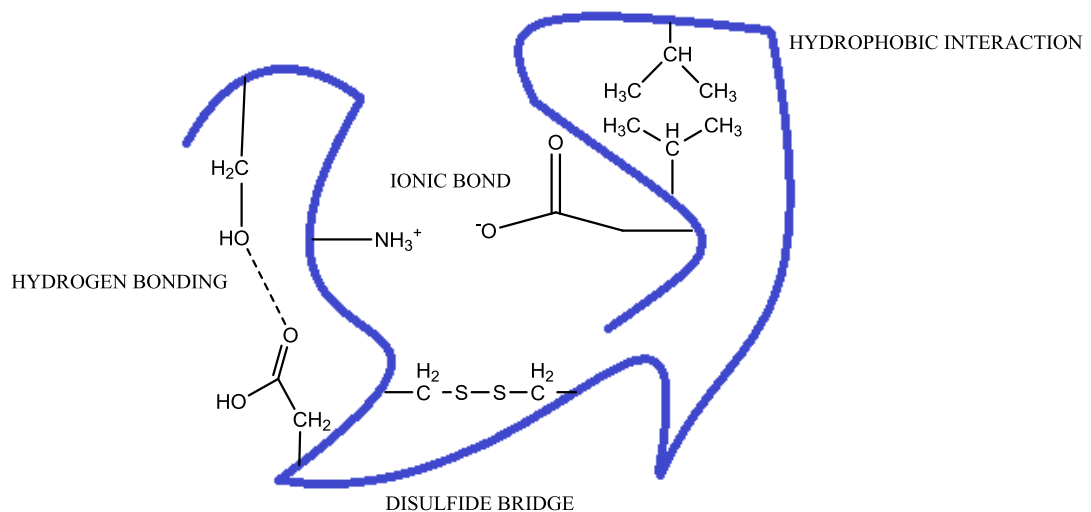


Figure 1.5: Representation of tertiary structure and the interactions between the amino acids in the polypeptide backbone which maintain the tertiary structure.

#### 1.1.2.4. QUATERNARY STRUCTURE

This fourth level of structure only exists when there are two or more polypeptide chains within the protein make-up, which then aggregate into one functional macromolecule. There are numerous examples of this type of protein including haemoglobin; this protein consists of many multi-subunit globular proteins. This larger unit is held together by a series of hydrogen bonds. However as mentioned not all proteins contain this level of structure as such their protein structure terminates at the tertiary level.

## 1.2 PROTEIN EXPRESSION

DNA and proteins are essentially both polymers made up from a combination of four nucleotides and 20 amino acids respectively. Crick proposed the Central Dogma (*figure 1.3.*) in the 1950s whereby DNA was not a functional molecule but considered as storage for genetic information. This then had to be translated into functional molecules, RNA and proteins.<sup>10, 11</sup> There are two main steps required, which are considered in detail in the subsequent sections.

### 1.2.1 TRANSCRIPTION

DNA contains an organism's full genetic information stored within chromosomes located in the nucleus of the cell. Proteins are coded by DNA; however protein synthesis takes place between the endoplasmic reticulum (ER) and Golgi apparatus, which are in the cytosol of the cell.

Ribonucleotide acid (RNA) is an intermediary molecule that transfers the data from DNA. This molecule is very similar to DNA. RNA is comprised of: a ribose sugar; a nucleobase; and a phosphate group. The main differences between DNA and RNA are that DNA contains: a deoxyribose sugar; and a thymine base. RNA replaces this base with uracil, the differences between bases is shown in figure 1.6. Finally, RNA exists as single stranded molecules compared to DNA which predominately exists as a double stranded molecule.

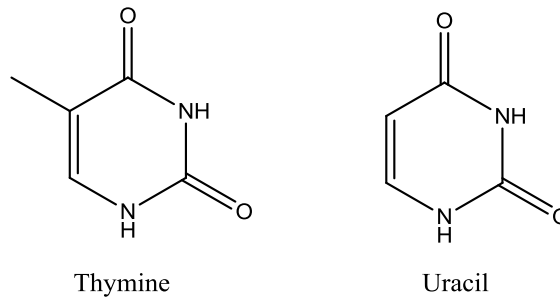


Figure 1.6: Structure of bases, thymine exists in DNA and uracil in RNA

Due to this difference, RNA can translate the genetic information contained within DNA to form proteins. The information is copied directly from the DNA in a process similar to that which takes place in DNA replication. The double stranded DNA is unzipped using the enzyme Helicase. This allows the single stranded sequence to be read by RNA polymerase, whilst simultaneously synthesising a complementary RNA strand messenger RNA (mRNA), as shown in figure 1.7. The mRNA leaves the nucleus through nuclear pores and migrates into the cytoplasm for next stage of protein synthesis - translation.

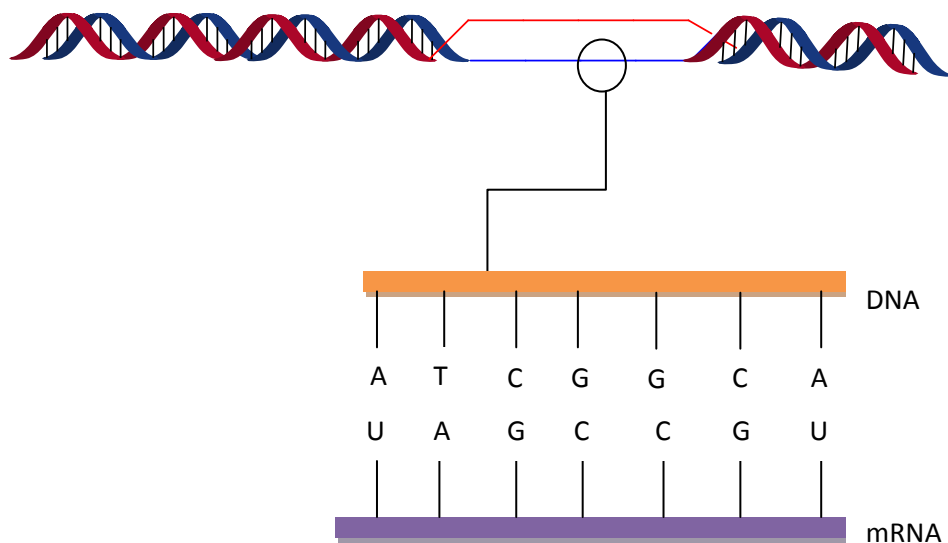


Figure 1.7: Process of transcription, conversion of DNA to mRNA.

## 1.2.2 TRANSLATION

Protein synthesis takes place during the translation stage. This stage is slightly more complicated because there is the conversion from RNA bases to amino acids and protein synthesis occurs on the surface of a ribosome. The main issue when converting RNA into an amino acid is the fact that there are only four bases in DNA and RNA, yet there are 20 amino acids. A molecule called transfer RNA (tRNA) is implemented: this molecule bridges the gap between the DNA and proteins. tRNA contains a three letter nucleotide sequence called an anticodon - situated at one end of this molecule - which relates to the 3 letter sequence of mRNA translated from the DNA sequence called a codon. Each anti-codon sequence relates to a specific amino acid, which is covalently attached to the other end of the tRNA. However, as three nucleotides bases code for one amino acid, that would mean there is the possibility of 64 different codons, therefore several sets of trio of bases code for the same amino acid. The process of matching the codon and anti-codon occurs in the ribosome once the mRNA molecule enters the ribosome. The matching tRNA molecule will associate with this molecule. The covalently linked amino acid is freed from the tRNA by proteins which catalyse the bond called aminocyl tRNA syntheses; liberating the amino acid into the growing polypeptide chain, as shown in figure 1.7. The process is repeated until the primary sequence of the protein is translated.

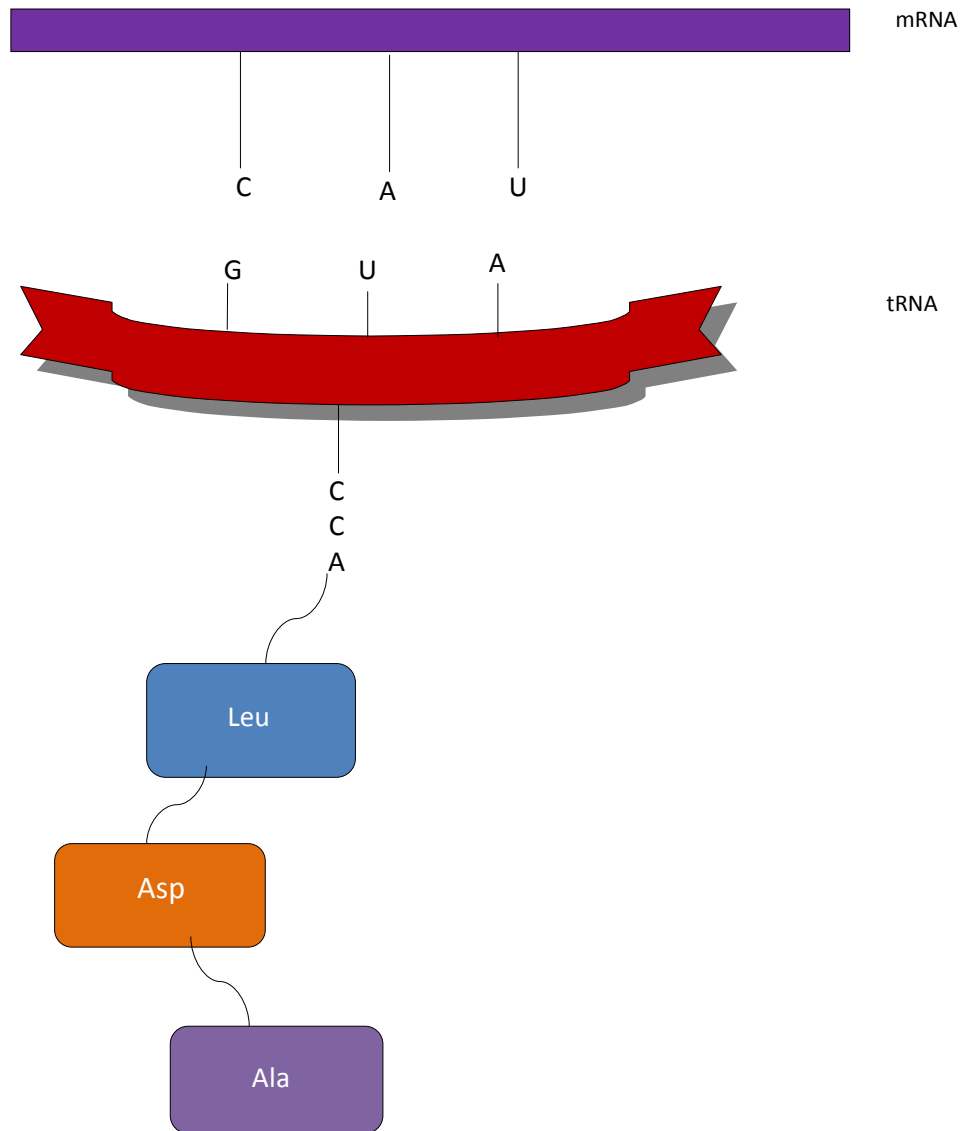


Figure 1.8: Schematic of the translation process which occurs on the surface of the ribosome. Once translation has been carried out, the completed protein contains a sequence of amino acids called signal sequences, which dictate where the protein is to be transposed to. The final location of a protein could be the cytosol of the cell, whereby the protein will be taken up into either the nucleus or other cellular components, or the translation could have finished in the ER, whereby the likelihood is that a protein would be transported to the outside of the cell to perform the required duties. The roles which these proteins play are essential to the functioning and health of every cell.

## 1.3 PROTEIN FUNCTIONS

The term protein is commonly used; however, it covers a broad range of molecules differing in composition, structure and function. They can be classed in a variety of different ways (fibrous, globular, degrees of aggregation, size etc.). One of the most common ways to class proteins is through their function. Examples of such classes are as follows: enzymes, receptors and regulatory proteins and are outlined in sections below. All are considered crucial to cellular function and by extension in the progression of disease states. Biomarkers are classed as substances that are used as an indication of a biological state and can encompass a variety of forms, including genes, proteins and metabolites. Certain proteins can be expressed in disease states; an example of this is the protein Octamer Binding Transcription Factor 4 (Oct-4) which has been implemented in the formation of tumours in adult germ cells. The ability to identify biomarkers responsible for causing diseases, allows for early diagnosis and thus offers the potential of better treatment options.<sup>12</sup>

There have been many debates regarding the prediction of protein function with regard to protein structure. Previously the prediction of function was based upon sequence similarity between proteins of know function and those of unknown. However, this proved to provide poor correlation as proteins with similar primary structure were found to have diverse functions. The general consensus now is to group proteins according to function with numerous classes emerging, which are discussed below.

- *Enzymes*

Emil Fischer, in 1894, was first to hypothesise that enzyme action was a very specific process. *'I could say that the enzyme and substrate must fit each other like a lock and key...'* In a synthetic environment, an enzyme is a synthetic, chemical compound which lowers the activation barrier of a chemical reaction. In this same way, proteins act as biological enzymes which catalyse the chemical reactions within the body and are classified in relation to the substrate which they act upon. Famous examples are: kinases, which catalyse the transfer of phosphate from ATP to hydroxyl side chains on proteins causing changes in function; and transferases, which catalyse the transfer of a functional group from one molecule to another.

- *Hormones*

Hormones are essential to the health of the cells within the human body as they regulate many processes. A hormone is essentially a chemical messenger that transports signals from one cell to another. These molecules initiate signal transduction mechanisms which lead to specific responses within the cell. A prime example is insulin; this protein is responsible for the reduction of glucose levels in the blood stream. The presence of high levels of glucose in the blood stream stimulates cells in the pancreas to increase the amount of insulin secreted into the blood stream, this in turn, activates muscle cells and the liver to take up the excess glucose. These types of proteins are relatively small and tend to be classed as peptides for this reason.

- *Transport*

This class of proteins have the task of transporting or storing other chemical compounds or ions, which are essential to the human body. Haemoglobin-present in red blood cells-is a famous example in its transport of oxygen around the human body. Another example is the protein albumin which transports fatty acids in the blood stream.

- *Antibodies*

These proteins are important as they form the basis of the defence of the immune system. Antibodies are used by the immune system to neutralise foreign objects which enter cells such as bacteria and viruses. It is a specific interaction that occurs between the antibody and a molecule expressed by the foreign object called an antigen. The antibodies are generated by B-cells which have received signals from T-cells, detailing the nature of the foreign object so that the correct antibodies can be generated.

- *Structural*

As the name suggests, this class of proteins are responsible for the maintenance of structural attributes of other biological components, such as cells and tissues. Such proteins include collagen and  $\alpha$ -Keratin.

- *Motor*

These proteins are difficult to separate from structural proteins, due to the similarity in the roles which they perform. These proteins store chemical energy and convert this energy into mechanical energy. An example of this is actin, which is involved in muscular motion.

- *Receptors*

Receptors are important molecules within a cell and are associated with signal detection and translation from various parts of the cell. Many receptor proteins are situated within the cellular membrane and they are of particular importance as they control which components can pass through the membrane and ultimately enter the cell. By attachment to the receptor a conformational change is activated allowing the molecule into the cell. An example of a receptor is a G-protein, which is part of a large family of transmembrane receptors.

- *Signalling*

Signalling proteins relay the instructions between different parts of the cell to ensure smooth functioning. Typically these proteins cause a significant conformational change in presence of signal molecules such as GPTases.

- *Storage*

These proteins are important for releasing stored energy during a metabolism process in the organism.

- *Regulatory*

Most proteins are regulatory proteins in that they participate in a cascade of events within the body. It is through the interaction of one protein with another in a particular pathway which causes a domino effect between the proteins within the pathway. This activates each following protein until the end goal is reached. Such as the Ras-Raf complex which initiates the Mitogen Activated Protein Kinase (MAPK) pathway. This pathway is important in the role of transmitting proliferative signals generated by cell surface receptors and cytoplasmic signalling elements to the nucleus, without the initial binding of Raf-1 to Ras this process would not occur.<sup>13</sup>

## 1.4 PROTEIN-PROTEIN INTERACTIONS

Proteins play a vital role within the cell, often involving complex pathways and an intricate network of protein–protein interactions.<sup>14</sup> Protein-protein interactions can be classed into two groups: stable; and transient. Stable interactions are those which are associated with proteins that have a multi-subunit complex. The multiple units can be identical or different and examples include Haemoglobin and RNA polymerase. Transient interactions are the interactions that control the cellular processes. These intrinsic interactions take part and control virtually every process in cells, such as DNA replication, signal transduction and metabolism. Proteins bind to one another through a variety of interactions namely; hydrogen bonds, Van der Waals and salt bridges.<sup>15</sup> Developing a greater understanding of such interactions has been the focus of a large amount of research and has led to vital discoveries in disease detection and of the easing of symptoms of diseases such as Alzheimer’s disease. It is through the study and understanding of these interactions, and in particular the possible sources and causes of disruptions in cascade pathways, which will prove invaluable in the quest to prevent and cure numerous diseases.

### 1.4.1 STUDY OF PROTEIN-PROTEIN INTERACTIONS<sup>16, 17</sup>

Protein-protein interactions have been analysed using a variety of different methods, which includes co-immunoprecipitation. This method uses an antibody that targets a known protein, which is part of a larger network of unknown proteins. Through targeting of the known protein using the antibody, the larger complex can be captured and identification can occur. Crosslinking protein interaction analysis - as the name suggests - involves the use of crosslinking agents, which covalently bind proteins as they interact to allow for analysis. Far Western Blot Analysis is a modification of the traditional Western Blot Analysis, instead of using an antibody to detect a specific protein, this technique uses a non-antibody approach to allow for a large range of protein interactions to be analysed. Light scattering techniques can be used to assess the size of proteins and the binding affinity of such interactions, using techniques such as Surface Plasmon Resonance (SPR). Fluorescence spectroscopy is one of the most popular methods for the characterisation of protein-protein

interactions. This method is based upon the polarisation of fluorescence. The value that is obtained indicates the extent to which the molecule retains its orientation of the exciting light in its emission. Small molecules lose the orientation or polarisation, whereas larger molecules are the opposite.

#### 1.4.1.1 FLUORESCENCE MICROSCOPY

Fluorescence is the process whereby a molecule -commonly referred to as a fluorophore- absorbs light energy which promotes the molecule into the highest excited state<sup>18</sup>. This excited state is unstable and consequently the molecule relaxes into the lowest excited state, which is slightly more stable. This lower excited state does not last for very long (between  $10^{-15}$  - $10^{-9}$  seconds) and is known as the fluorescent lifetime. Upon relaxation to the ground state, the excess energy is released and emitted as light.<sup>19</sup> The light is emitted at a longer wavelength as it is lower energy. This process is outlined in figure 1.9.

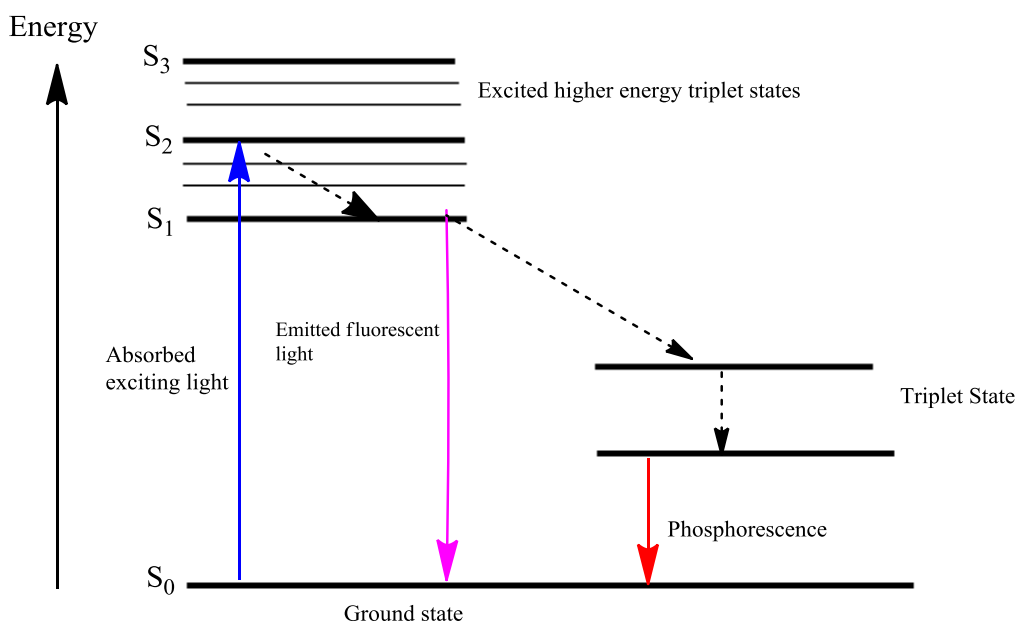


Figure 1.9: Jablonski diagram representing the possible processes that occur upon the absorption of a photon of light.

Fluorescence is the most commonly used detection method in the biological field.<sup>20</sup>  
<sup>21</sup> The main reasons for this are: compatibility with aqueous environments; capability of identifying specific protein interactions (against a background of over 30,000

other proteins within a living cell); and the availability of a vast range of commercial fluorescent tags, that can be used in conjunction with biological macromolecules.<sup>22, 23</sup> Traditional fluorescence microscopy is known as epifluorescence. Recently there has been resurgence in publications concerning fluorescence.<sup>24</sup> This is most likely due to the rise in the use of confocal microscopy which is capable of reducing the background signal of the sample in a way that epifluorescence cannot.<sup>25</sup> In addition a 3D image of the sample can be constructed to produce a more accurate representation of the cellular environment. The benefit of fluorescence is the ease with which biological components can be combined with synthetic fluorophores. Furthermore, fluorescence microscopy can distinguish fluorescently labelled molecules with a high degree of specificity, from non-fluorescent material - highly advantageous in the complex cellular environment.

Although a proven technique and used ubiquitously, there are associated disadvantages with this technique which include problems with photobleaching, resulting in the destruction of the fluorophore. However, the most crucial limitation is the inability to multiplex fluorophores efficiently. Although it is possible to multiplex fluorescence techniques, it can be very challenging. The information obtained from this technique is limited due to the resulting broad spectrum which is characteristic of fluorescence spectroscopy. Information relating to excitation and emission wavelengths of the substrate<sup>26</sup> is elucidated, meaning care must be taken when multiplexing, to ensure that fluorophores do not overlap in the excitation/emission range. Furthermore, Förster resonance energy transfer (FRET) can be an issue; emitting energy that corresponds to the excitation of the multiplexed fluorophore. FRET is where two fluorophores are used, that have overlapping excitation and emission profiles.<sup>27</sup> The process involves the excitation of the first fluorophore which upon emission causes excitation of the second fluorophore. This process is distance dependant, with the requirement of the fluorophores having to be within 10 nm of each other.<sup>19, 28</sup>

## 1.4.2 Quantum Dots<sup>29,30</sup>

One method of addressing the lack of robustness of organic fluorophores has been the development of semiconductor nanocrystals known as quantum dots (QD).

Quantum dots typically fall within the 2-10 nm size range, however larger quantum dots have been synthesised it is generally dependent upon the material used to synthesis and the intended application, a schematic is shown in figure 1.10.

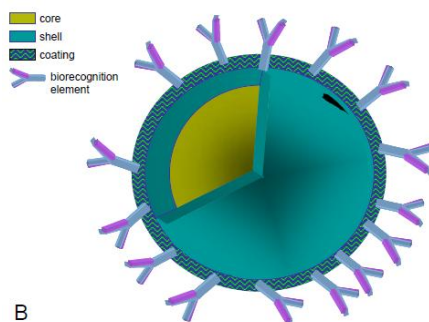


Figure 1.10: Schematic of a quantum dot showing the semi conductor core and protective shell, upon which a biomolecule has been conjugated.<sup>30</sup>

The popularity of quantum dots has stemmed from the improved optical qualities which are tuneable through the manipulation of size and the material used to synthesis the quantum dots. As shown in figure 1.10 the quantum dots are comprised of a core and a shell. Both are comprised of a semi-conductor material. First synthesised by Bawendi *et al.* the core is typically synthesised from cadmium selenide or lead selenide which is pacified by a coating or shell that is also of semi conductor nature, normally zinc sulphide or zinc selenide.<sup>31</sup>

Quantum dots have been in a variety of applications, which can be divided into two distinct groupings; biosensing and biological imaging. When used in biosensing, quantum dots can be functionalized with biomolecules through attachment to the shell coating, after which point these molecules can be employed in typical fluorescent based assays, for example adenosine-triphosphate was detected using a QD tagged aptamer.

As a consequence of their improved brightness and photostability QDs have been used extensively for biological imaging. Many researchers have visualised QDs

under in vivo conditions in many different types of organelles, as demonstrated by figure 1. 11.



Figure 1.11: Taken from reference X: six different QDs imaged using one excitation source.<sup>29</sup>

Although used extensively QDs do have several disadvantages associated with their use. QDs are synthesised from elements which are toxic to cells, cadmium ions have been shown to bind sulfur atoms which can have a knock on effect and cause stress within the cell and ultimately lead to cell death. In addition QDs have been shown to cause damage to DNA which can disrupt normal cell operation.

## 1.5 FLUORESCENT PROTEINS

Fluorescent proteins found their niche in fluorescent microscopy. First discovered in the late 1950s by Shimomura, the use of fluorescent proteins has gathered pace over the last two decades.<sup>32</sup> The original fluorescent protein was named, Green Florescent Protein (GFP). This protein was discovered in the jelly fish *Aqueoria Victoria*.<sup>33</sup> It transpired that the fluorophore was contained within the centre of the cylindrical structure of the 238 amino acid macromolecule, as shown in figure 1.12.<sup>34</sup> The unique aspect of this fluorescence was the lack of co-factors required to produce the fluorescence. It is an intrinsic property of protein, as the protein folds into the natural conformation the fluorescence is emitted.<sup>35</sup>

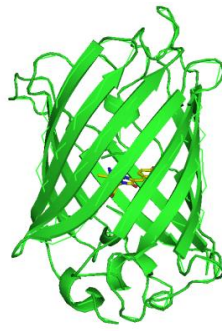


Figure 1.12: Structure of GFP, beta barrel structure with the chromophore residing in the centre of the cylindrical structure

From there the combination of Martin Chalfie's research on expressing GFP in *Escherichia coli* (E-coli)<sup>36</sup> and Roger Tsien's research into the production of synthetic fluorescent proteins with varying excitation and emission profiles, has led to the exponential growth in the field of fluorescent proteins and their use in cellular biology.<sup>37</sup> The culmination of the discovery and development of GFP resulted in the award of the Nobel Prize for Chemistry in 2008, being bestowed upon Shimomura, Chalfie and Tsien.<sup>38</sup> EGFP and its variants are used extensively as biological markers for other proteins of interest. This can be attributed to the fact that they are biological components themselves, thus making the process of attaching a protein to a fluorophore relatively easy.<sup>39</sup> Martin Chalfie initially showed that GFP could be expressed within E-Coli, paving the way for FP chimera development. This circumvented the need for complex protein modification as protein fusion could be achieved by incorporating a fluorescent moiety through the use of chimeras.

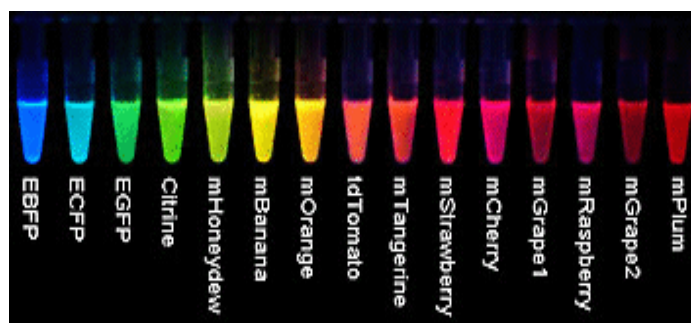


Figure 1.13: Range of FPs available commercially.<sup>28</sup>

Fluorescence spectroscopy shed light on the cellular environment and the components therein. It has progressed our understanding of cell based processes

greatly and is still the current method of choice. However, as mentioned previously, photobleaching is an issue with this technique. Photobleaching results after repeated analysis of the fluorophore. The intensity of the exciting light causes a change in the structure, resulting loss of fluorescing ability of the molecule. Another limitation is the inefficiency of multiplexing: the dynamic nature of the biological environment means it would be advantageous to observe more than one biological molecule at any one time. In fluorescence (due to the overlapping excitation and emission profiles) there are only a finite number of fluorophores that can be used. Raman based spectroscopy has been shown to overcome these limitations.<sup>40, 41</sup> Raman scattering is a vibrational technique and the characteristic narrow band present on a spectrum means multiplexing is possible - paving the way for multiplexed analysis. Due to the observation of enhancement factors of up to  $10^{15}$  Raman based techniques have been shown to rival the sensitivity of fluorescence, which is discussed further in section 1.8.<sup>42</sup> The major component of this technique is the use of a gold or silver surface. This surface exists in a variety of forms: the most common surface used is that of nanoparticles. Synthesised in a colloidal format, the ease of synthesis combined with the ability to tailor the spectroscopic properties of these nanoparticles contribute to the popular use of this surface.

## 1.6 NANOPARTICLES

The use of nanoparticles in biotechnology type sensor applications has grown exponentially over the last twenty years. There are many different types of nanoparticles available, ranging from noble metals to magnetic cores. However, the first example of synthesis was of gold nanoparticles dating back to the 4<sup>th</sup> or 5<sup>th</sup> century BC<sup>43</sup> discovered from specimens in China and Egypt.<sup>44, 45</sup> Perhaps the most famous example of the exploitation of the optical properties of nanoparticles is the Lycurgus cup: when held in the light the colour of the object changes. The glass contained within the cup scatters green light and transmits red light. This cup is housed in the British Museum, where a study commissioned revealed that there was a mixture of both silver and gold nanoparticles within the glass. There have been several scientists who have explored the interaction between light and nanoparticles. In 1857, Michael Faraday carried out the first reported scientific study on the

preparation of gold nanoparticles; publishing in the Journal of Philosophical Transactions of the Royal Society of London.<sup>46</sup> This paper reported the phenomenon of light interacting with gold leaf, with the main observation being the transmission of green light. From this experiment he hypothesised '*Light has a relation with the matter it meets with in its course, and is affected by it, being reflected, deflected, transmitted, refracted and absorbed by particles very minute in their dimensions.*' This led him to synthesise the now characteristic ruby coloured gold nanoparticles that are used so commonly today. Maxwell Garnet followed Faraday's pioneering work from 1904-1905, lead to the development of the Effective Medium Theory, which gave rise to the expression dielectric constant. The dielectric constant is defined as the ratio of the permittivity of a substance to the permittivity of free space, within a matrix containing small metallic spheres.<sup>47</sup> A few years later, Debye attempted to rationalise the interaction of light with matter by regarding light as exerting a mechanical pressure on the nanoparticles, however this explanation was weak. In 1908 Gustav Mie published a ground breaking paper, where he calculated the excitation, scattering and adsorption cross-sections of Au nanoparticles. Mie's theory is arguably the most popular theory used due to the remarkable accuracy with which he predicted the trends in spectroscopic properties observed with increasing particle size.<sup>48</sup>

In this seminal paper, Mie described the interaction of light with nanoparticles in terms of a collective oscillation of the metal's free electrons. In order to fully understand the theory, nanoparticles should be considered as spherical metallic objects containing a cationic network with a cloud of free electrons. Once the incident electromagnetic radiation (or incident light) interacts with the nanoparticle, there is a displacement of this electron cloud which leads to the creation of surface charges. These are positive where the electron cloud is absent and negative where the cloud is concentrated. All the electrons move collectively while under the effect of the electromagnetic field.<sup>49</sup> This oscillation leads to a Surface Plasmon Band (SPB), which for Au and Ag is a strong and broad band seen as absorption in the visible spectrum, 520 nm for 13 nm diameter Au nanoparticles and 400 nm for 35 nm diameter Ag nanoparticles. Consequently this is known as Surface Plasmon Resonance (SPR), (see figure 1.14). The frequency at which the SPB is observed is

dependent on many factors such as: the size and shape of the nanoparticles; the inter-nanoparticle distance; and the dielectric constant of the surrounding medium. This all combines to produce unique tuneable optical properties. In addition to the ability to optically tune nanoparticles to specific uses, their ease of synthesis has been an attractive advantage.<sup>50</sup>

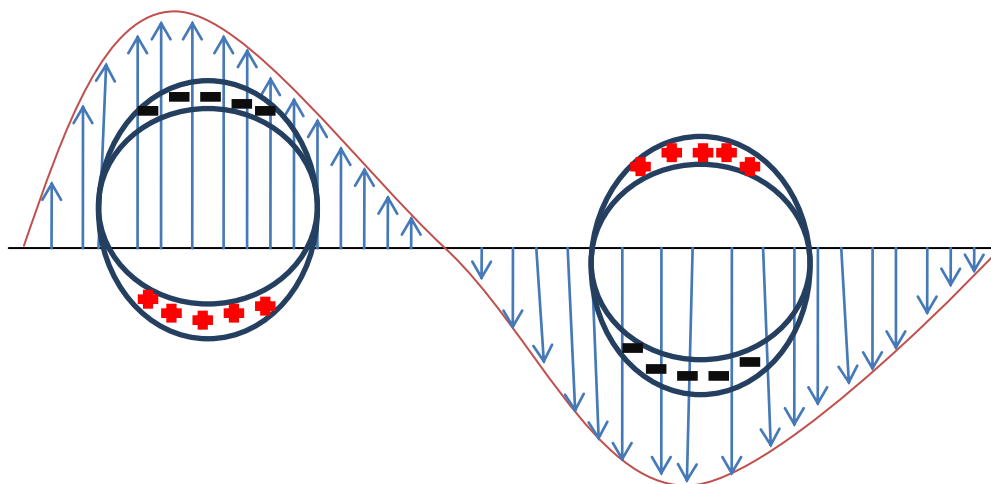


Figure 1.14: Schematic of the oscillation of electron cloud

For Au nanoparticles, the most commonly used method is known as the Turkevitch method. This synthesis involves the reduction of  $\text{HAuCl}_4$  using sodium tricitrate. The  $\text{Au}^{3+}$  ions are reduced to  $\text{Au}^0$  by the use of sodium citrate which acts both as a reducing agent and as a stabilising agent to ensure the production of uniform nanoparticles. It is this method that was used in the work carried out in this Thesis. However, this method was slightly adjusted in 1973 by Frens.<sup>51</sup> Known as the Turkevitch method it produced nanoparticles that had a diameter of around 20 nm. Frens showed that by varying the ratio of gold: citrate the diameter of the nanoparticles could be manipulated, (ranging from 16 to 147 nm).

Ag nanoparticles have a very similar synthesis path. The Lee-Meisel method is a variation on the Turkevitch method, whereby  $\text{AgNO}_3$  is used as the metal source.<sup>52</sup> Sodium tricitrate is used once more as a reducing and stabilising agent, however there has to be precise temperature control in this method and a range of particle diameters are obtained. An additional method that precludes the vast range of diameter size obtained in the Lee-Meisel method is now commonly referred as,

Creighton method; this synthesis yields particles with an average diameter of 10 nm.<sup>53</sup>

The surface area to volume ratio of nanoparticles is one of the most fundamental properties and directly affects the functionality and uses of such particles. For example, nanoparticles with a 70 nm diameter and at a concentration of 0.01 mg/mL have a total surface area of 0.8 m<sup>2</sup>/L whereas a larger particle with a diameter of 200 nm with the same concentration have a total surface area of 0.3 m<sup>2</sup>/L.<sup>54</sup>

### 1.6.1 CHARACTERISATION OF NANOPARTICLES.<sup>55</sup>

UV-Visible spectroscopy is one of the main methods for nanoparticle characterisation. This is due to the sensitivity of the SPB, which varies with nanoparticle size and nanoparticle morphology. Typically, for silver citrate nanoparticles between 10-35 nm in size, the SPB is located at 400 nm: with 13 nm gold citrate nanoparticles this band is located at 520 nm. In order to determine the nanoparticle morphology: scanning and transmission electronic microscopy (SEM and TEM respectively) are the most commonly used methods, as shown in figure 1.15. These techniques involve examining whether or not a nanoparticle colloidal solution is monodisperse and of the desired shape

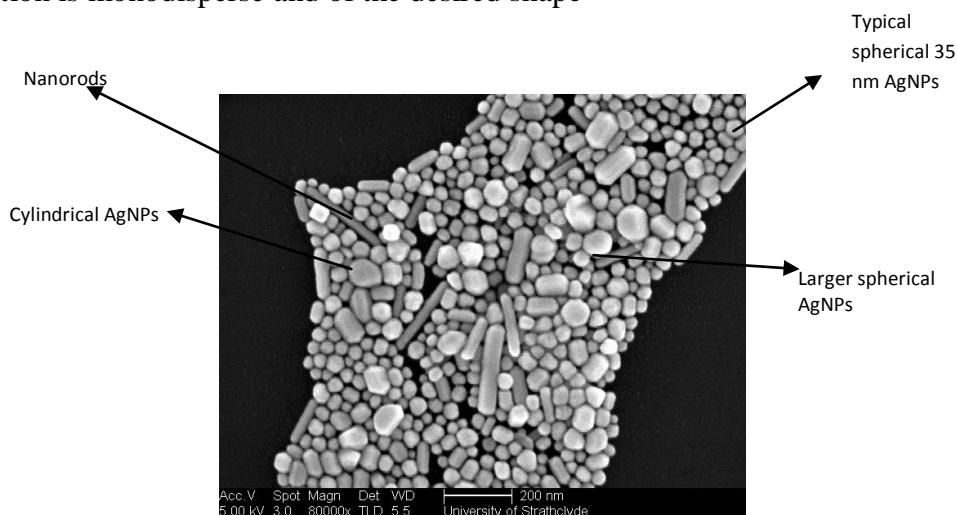


Figure 1.15: SEM image of silver citrate nanoparticles, typically the synthesis of silver citrate yields a variety of shapes of nanoparticles. SEM imaged by Dr Iain Larmour, University of Strathclyde.

## 1.7 PROTEIN AND NANOPARTICLES

Nanoparticles have been used in biological applications and have led to the creation of the so-called bionanotechnology field. In the early research stages, the main purpose of nanoparticles was to provide a passive label, a label that did not react to their environment and simply highlighted the area. Immunostaining was also a very popular methodology for gold nanoparticles. The concept behind this technique relies on an immunogenic response of the cell of interest. In general, gold nanoparticles were labelled with antibodies that bind to the antigen released by the cell in a certain disease state. Through molecular recognition the antibody, bound to the nanoparticle, will seek out the antigen and bind through specific chemistries. The presence of the nanoparticles provides a contrast to the cellular environment which could be visualised. Despite the development in this technology, there has now been a shift towards active nanoparticle labels, to use these conjugates as active sensors.

It has been the endeavour of many scientists to use nanoparticles as a probe within the cellular environment. We can learn a great deal from the cellular environment which carries out complicated processes in a nanoscale environment on a daily basis.

<sup>56</sup> Due to the small dimensions of nanoparticles they are compatible with biological molecules; typically proteins are around 5 nm. Therefore, it is possible to incorporate nanoparticles into a biological environment without steric hindrance disrupting the native interactions. This allows the possibility of nanoparticle to be used as reporter molecules to gain insight into interactions at the cellular level.<sup>57</sup> Nanotechnology is the study of science on the nanoscale. Essentially biology has already beaten scientists to the goal of performing reactions on a nanoscale. Biology has the ability to self assemble macromolecules with immense precision and detail; it will be through the ability to understand biology at this level that will enhance and further develop the field the workings of nanoscience.<sup>58</sup> This branch of science, which requires an understanding in all life sciences, is concerned with studying objects within the dimensions of 100 nm.<sup>59</sup> The field has truly become a multi-disciplinary area, allowing for a new era of science creating the way for new opportunities in fields such as biomedicine and materials science. Nanoparticles have the ability to enter cells via receptor mediated endocytosis and therefore provide an ideal transport vehicle to be used as a probe in the cellular environment. The attachment of

nanoparticles to proteins has led to a broad range of applications including imaging, catalysis and understanding structure in protein folding.<sup>60</sup> These type of conjugates have even been used in the areas of materials science and physics. Lynch *et al.* have published several papers detailing the benefit of using nanoparticles to probe the protein-protein interactions.<sup>54</sup> One of the more challenging issues with respect to the conjugation of proteins to nanoparticles is the ability to produce such conjugates successfully and reproducibly. Aubin-Tam *et al.* have proposed four main strategies for successful preparation of conjugates, shown in figure 1.16<sup>61</sup>:

- I. Electrostatically
- II. Conjugation via a linker to NP surface
- III. Conjugation of co-factor
- IV. Direct linkage

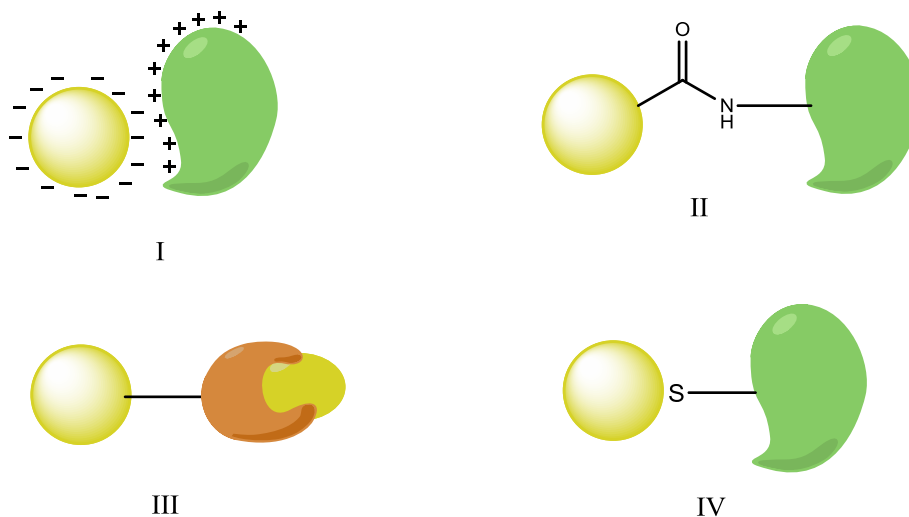


Figure 1.16: Schematic of the four commonly used methods for the attachment of proteins to nanoparticles. I- electrostatic attachment, II- attachment using a linker, III- attachment via co-factor conjugation and IV- direct attachment.

The use of electrostatics is the most widely used method. It is simple and requires no formal bond formation. The manipulation of charge can be carried out through modification of pH.

The use of a linker creates a formal bond between the nanoparticle surface and protein. Amino acids contain primary amine groups which are available for interaction via activated esters. Controlling the number of proteins attached to nanoparticles can be achieved via this method. Hainfield *et al.* demonstrated this

control through the isolation of AuNPs with a single protein molecule present on each nanoparticle.<sup>62</sup> Maleimide groups are known to interact with thiol containing cysteine groups within proteins. Douglas *et al.* demonstrated that a 1:1 protein: synthetic label ratio could be achieved via this approach. The protein contained one cysteine group which meant a 1:1 ratio could be achieved.<sup>63</sup> This control cannot be achieved with the electrostatic method.

The use of a co-factor involves conjugating a component that binds the protein, such as an antibody. This concept has been exploited with the biotin-streptavidin interaction. This interaction is one of the strongest interactions known within the biological community, providing a strong anchor between the nanoparticle and the protein. The use of this interaction has now been expanded with the introduction of organic linkers, modified with biotin to enable the conjugation to occur, yet it also provides a point for protein attachment.

Finally proteins can be directly conjugated to the nanoparticle surface by exploiting the inherent affinity of sulfur for gold and silver. This method can be used for any protein containing cysteine residues available at the surface of the protein, once in its final confirmation.

### 1.7.1. PROTEIN – NANOPARTICLE CONJUGATES

Protein-nanoparticle conjugates have been utilised in a variety of applications. Thousands of papers have been published on the use of protein-nanoparticle conjugates. Sivanesan *et al.*, have demonstrated the use of silver nanoparticles in the formation of Self Assembled Monolayer (SAMs) followed by functionalisation with Cytochrome c. It was shown through precise tuning of the plasmonic properties that it was possible to detect specific protein co-factors in the nanomolar concentration.<sup>64</sup> Zhao *et al.* have demonstrated the use of nanoparticles in an Enzyme linked immunosorbent assay (ELISA).<sup>65</sup> This is a commonly used method for the detection of antibodies or antigens in a sample based on antibody-antigen immunoreactions.<sup>64</sup><sup>65</sup> The cancer marker p53 was detected with the incorporation of gold nanoparticles, acting as a carrier and amplifier, producing an assay with a detection limit of 5 pg mL<sup>-1</sup>. This was much lower than the previously reported detection limit of 0.1 ng-1 µg mL<sup>-1</sup>.<sup>66</sup> De *et al.* have also shown that through the implementation of gold

nanoparticles and cationic linker's, serum proteins were detected. This was achieved through a competitive binding process. A fluorescent protein (GFP) was displaced - upon successful binding of a serum protein with greater affinity for the nanoparticle- which generated a fluorescent signal. The development of this system provided a highly selective array-based sensor system.<sup>67</sup> Onoda *et al.* developed a novel strategy for the development of a programmed assembly system using Heme-immobilised gold nanoparticles prepared using a disulfide linkage. It was found that these conjugates could be used as electron transfer mediators.<sup>68</sup> The examples detailed above illustrate the wide variety of applications where protein-nanoparticle conjugates have been implemented successfully and demonstrated the ease with which these conjugates can be prepared. However, prior to implementing these conjugates in a given sensor-type application, it is necessary to confirm that successful conjugation of protein to nanoparticle has occurred. This can be done using several different methods, outlined in the subsequent section.

#### 1.7.1.1 ANALYSIS OF PROTEIN NANOPARTICLE CONJUGATES

Yan *et al.* state that upon binding of a protein to the nanoparticle surface, there are several indicators that can monitor this binding effect. These indicators include: electron or energy transfer; spectroscopic changes; and size & shape changes.<sup>24</sup> Optical spectroscopy can be used to interrogate protein nanoparticle conjugates. Due to the highly sensitive nature of the surface plasmon the  $\lambda$  max of unmodified gold and silver nanoparticles occurs at 520 nm and 400 nm respectively. SPR is highly sensitive to changes in the nanoparticle environment and thus a shift and broadening of the SPR can be indicative of the formation of a bond or presence of protein. Therefore UV-VIS analysis is often used when studying protein-nanoparticle conjugates. The changes exhibited by the plasmon can be used to evaluate the degree of binding. Cannistraro *et al.* have shown that the shift and broadening of the UV-Vis spectral profile of azurin-gold NP conjugates was dependent upon the concentration of azurin.<sup>69</sup> Dynamic light scattering (DLS) is used to determine the average particle size of a solution. Upon protein binding, the size of the particle will increase, which will be seen through the use of DLS. However, DLS can also be used to establish the binding ratio. Niemeyer *et al.* have determined the molar ratio of

Cytochrome P450 to quantum dots to be between 5 and 6.<sup>70</sup> Finally another popular method for the analysis of protein nanoparticle conjugates is through the use of Raman scattering. This vibrational spectroscopy can identify bands of the amino acid chains which comprise the protein.<sup>71</sup> Through the assignment of these bands it is possible to determine the orientation of the protein on the nanoparticle surface.<sup>72, 73</sup>

## 1.8 RAMAN SCATTERING

When light interacts with matter, one of two processes can occur: absorption; or scattering. In absorption, the photon interacts with matter and causes the electrons to be promoted into an excited state. This occurs when the wavelength of the incident light corresponds to an energy gap between the ground state and an excited state within the matter. There are two types of scattering: elastic; and inelastic and are often referred to as Rayleigh and Raman scattering respectively. Inelastic light scattering was first observed in 1928 by C.V Raman, thus giving rise to the term Raman scattering<sup>74</sup> He was awarded the Nobel Prize for Physics in 1930. In the succeeding years, many scientists have harnessed the analytical potential of this technique and have further developed techniques to yield pioneering breakthroughs. Raman spectroscopy is an inherently weak process, with only 1 in every million photons scattering. The process can be further broken down into Stokes and Anti-Stokes. Stokes scattering occurs when the molecule is in the ground state prior to interaction with a photon. The emitted photons are, therefore, of lower energy than that of the incident photons. Anti-Stokes scattering occurs when the molecule is in a higher vibrational level (i.e. in its excited state at the point of contact with a photon). This means that the emitted scattered photons are of higher energy than the incident photons (as shown in figure 1.17). However, it should be noted that at room temperature most molecules are in their ground state and consequently most Raman scattering consists of Stokes scattering.<sup>75</sup>

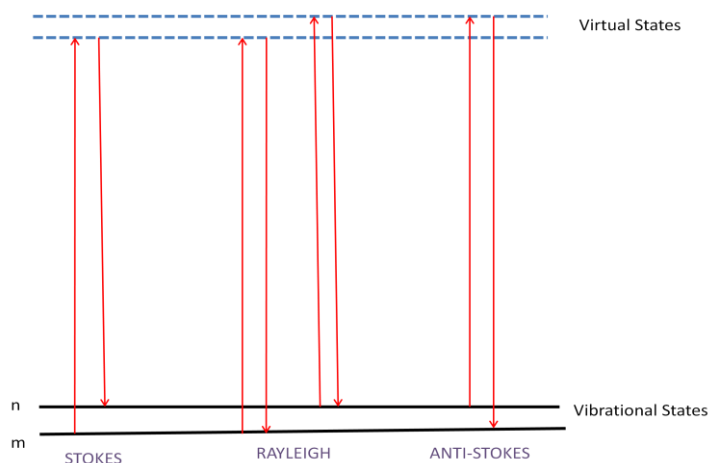


Figure 1.17: Energy level diagram of different forms of scattering that can be observed when a photon is scattered

### 1.8.1 RESONANCE RAMAN

The first variation in Raman scattering came in the form of Resonance Raman Scattering (RRS). In this technique, the wavelength of laser light is selected specifically such that it overlaps with an electronic transition within the molecule. This allowed for incorporation of coloured compounds previously excluded for use in Raman scattering due to sample degradation and fluorescence issues. This methodology has been shown to enhance Raman scattering by up to  $10^6$  - making the technique much more sensitive and selective.

### 1.8.2 SURFACE ENHANCED RAMAN SCATTERING<sup>76, 77</sup>

Surface Enhanced Raman Scattering (SERS) involves the use of a roughened metal surface to enhance the Raman scattering process, with reported enhancements of  $10^6$  being observed.

SERS was first observed by Fleischman *et al.* in 1974, where pyridine was adsorbed on silver electrodes, electrochemically roughened in potassium chloride aqueous electrolyte.<sup>78</sup> Fleischmann *et al.* surmised that the intensity difference between each set of signals must be a product of increasing the surface area on the electrode through various cycles of oxidation and reduction. However in 1977 two independent research groups simultaneously published papers stating the enhancement observed

could not be solely due to the increased surface area. Creighton *et al.*<sup>79</sup> and Van Duyne and Jeanmarie<sup>80</sup> showed that the enhancement factor from the level of increased surface area (between 20-30%) would only produce a signal enhancement of a factor of ten - inconsistent with the observed factor of  $10^5$ . The source of the enhancement in SERS has been the subject of much debate, with controversy still surrounding issue today - thirty years since its discovery. There are two proposed mechanisms for the enhancement of Raman when using a roughened surface namely: electromagnetic enhancement; and chemical enhancement. There are clear arguments for both but they may not be mutually exclusive. Indeed, many scientists believe it is a combination between the two mechanisms that produces such vast enhancements.

#### 1.8.2.1 ELECTROMAGNETIC ENHANCEMENT

This mechanism is considered to be the bigger contributing factor in the signal enhancement process. Many models have been theorised to demonstrate this effect which are based upon the observation of a single metallic particle and the effect the surrounding field exerts on such a particle. It is the aggregation of these small metallic nanoparticles that produces the strongest enhancement, therefore in reality, these models will not be accurate but can provide some insight into the ideal conditions to achieve optimal SERS. This type of enhancement is a result of the excitation of the surface plasmon which induces a strong electromagnetic field at the metal dielectric interface of a metallic nanoparticle. It has been shown that the greatest enhancement is seen when the molecule is absorbed onto a surface and polarised perpendicular to it.

#### 1.8.2.2 CHEMICAL ENHANCEMENT<sup>81</sup>

Chemical enhancement is the less favoured mechanism within the scientific community. It involves a physical bond between the substrate and the metal surface and upon formation, a new sub-species emerges allowing access to the electrons in the metal and the substrate. The polarisation that occurs is further increased due to the fact the substrate has a greater interaction with the electrons of the metal.

### 1.8.2.3 SURFACES<sup>82</sup>

A variety of metals have been used as an amplifier for signal enhancement, including noble metals, Li, Na, Ga and Cd. Noble metals have found popularity in this field, as they have been shown to provide the greatest enhancement factors in the visible region. Commonly SERS involves the use of a colloidal solution of nanoparticles. The ease of synthesis is one of the most attractive features of such solutions. This type of synthesis generally yields nanoparticles that are spherical in nature with diameters in the region between 5-40 nm. However, there has been a shift towards the use of non-spherical particles due to the ability to gain even greater enhancements - a phenomenon known as the lightning rod effect. This effect occurs when the effective curvature of the feature is smaller than the wavelength of incident light of interest. The shapes which exhibit this effect tend to be cubes or triangular plates.<sup>83</sup>

However SERS is not just achievable with colloidal solutions - the use of engineered surfaces has been implemented. Indeed, the discovery of this technique was through the adsorption of analytes onto the surface of a silver coated electrode. Surfaces suitable for SERS are synthesised through the deposition of the chosen metal, gold or silver. These surfaces are required to be roughened for the enhancement of the electromagnetic field and can be achieved using a variety of methods. These include repeated electromagnetic cycling of a metal electrode or through the creation of thin metal islands, roughened via a splutter coating process.<sup>84, 85</sup> However, several problems are associated with the use of surfaces as silver (the better enhancer) which oxidises easily. On a surface there are a limited number of analyte molecules, which can lead to non-uniform results.

### 1.8.3 SURFACE ENHANCED RESONANCE RAMAN SCATTERING (SERRS<sup>86, 87</sup>)

This technique combines both the resonance dye and roughened metal contributions. It is an emerging field within biodiagnostics, with the main focal point driving research being the significant potential enhancement it offers over Raman -up to  $10^{14}$  have been reported. However, these enhancements are not always reliable and

therefore research in this area continues. This transforms Raman scattering into a very sensitive technique, thereby unlocking potential for use bio-nanoscale applications.

### 1.8.3.1 AGGREGATION- THE ON/OFF EFFECT

SER(R) S is often described as possessing an ON/OFF element, which is controlled by the formation of “hotspots”. Hotspot is a term relating to the aggregation of plasmon coupling to one another, providing greater enhancement of the electromagnetic field. Kneipp *et al.* showed that when analysing single gold nanoparticles of 60 nm in diameter, an enhancement factor of  $10^3$  was observed when the excitation wavelength was tuned to the surface plasmon of the single nanoparticle.<sup>88</sup> However, when these single 60 nm gold nanoparticles were aggregated into clusters of 250 nm or more, the enhancement factor observed increased to  $10^{14}$ .<sup>89</sup> Additionally the clusters were excited in the near infrared region corresponding to the shifted plasmon of the nanoparticles. This phenomenon is not observed with single nanoparticles of the same size as these clusters, thus, it is at the junction of these aggregates where the highest enhancement factor - and by extension the most intense SERS signal - is observed, demonstrated in figure 1.18.<sup>90,91</sup>

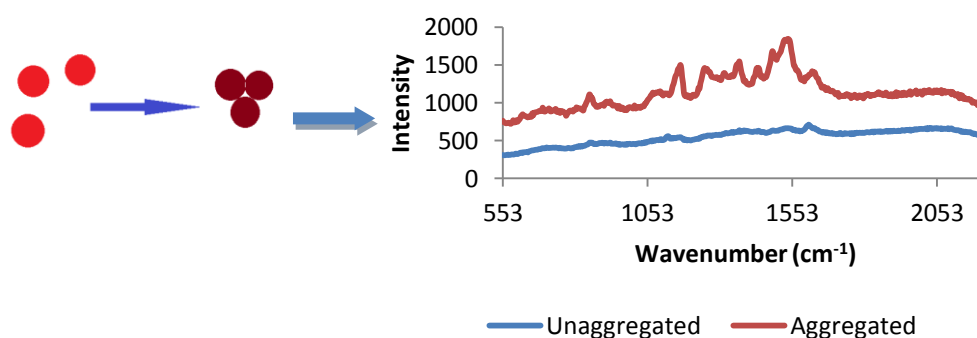


Figure 1.18: The effect of aggregation on signal intensity. The left image demonstrates the process of aggregation from single nanoparticles to a collection of nanoparticles forming a hotspot at the junction of the nanoparticles. The graph on the right shows overlaid SER(R) S spectra of this effect, with the blue line showing the spectrum of EGFP before aggregation and the red line showing the spectrum after aggregation.

## 1.9 SERS IN BIO-NANOTECHNOLOGY

SERS has been used in vast range of applications, due to its ability to uniquely identify molecules through the vibrational information that is obtained. These applications include: *in vitro* bio-sensing; chemical warfare detection; and identification of environmental pollutants.<sup>57, 92-95</sup> The detection of DNA and proteins has traditionally relied upon fluorescence.<sup>96</sup> However, this technique lacks specific molecular information and in addition multiplexing with this technique is very difficult. Although possible, the fact that many fluorophores absorb and emit light in the same wavelength range, means there are only a finite number of fluorescent probes can be used simultaneously. SERS provides the ability to multiplex by using unique vibrational peaks associated with each molecule to identify different biomolecules.<sup>97, 98</sup> Furthermore it is the long term mission for this technique to be used in the study of *in vivo* analysis of the cellular environment. Cellular studies have been carried out using a variety of different techniques other than fluorescence including IR, Coherent anti-Stokes Raman spectroscopy (CARS) and SERS.<sup>99-101</sup> The main drawback associated with the use of IR spectroscopic analysis is that water can cause interference as it absorbs in the 1300-1900 nm region. However, no such issue is present in Raman based techniques as water has a relatively small Raman cross-section and therefore does not cause interference in Raman spectra. Finally, photobleaching can cause problems when using fluorescence as this phenomenon is irreversible, causing the dye to lose its fluorescent characteristics thus rendering the analytical tool redundant. SERS overcomes this problem and therefore time dependant processes can be monitored within the cell. With the advantages outlined above and the constant advancements being made, the use of SERS in the detection of biomolecules and for cellular investigation has grown in the last decade.

### 1.9.1 SERS IN THE DETECTION OF DNA

The use of SER(R)S for the detection and analysis of DNA has grown in recent years and has led to sensitive and low limits of detection in the sub picomolar region.<sup>102</sup> DNA does not alone meet the stipulations required for successful SERS to be observed. The four bases that constitute this molecule do not provide unique

chromophores. Another challenging aspect of DNA detection using nanoparticles is the repulsion from the negatively charged backbone and the citrate stabilised colloid. In order to overcome this disfavoured electrostatic environment, it is necessary to introduce a stabilising group. This is commonly in the form of a surface seeking group that acts as an anchor to the nanoparticle surface and as a distinct label for identification.<sup>103</sup> SE(R)RS spectroscopy is an analytical tool offering information-rich spectra and distinctive narrow bands allowing for the identification of multiple sequences of DNA simultaneously.<sup>104</sup> The most common method for attachment of DNA to gold or silver nanoparticles is through a thiol modification of the DNA sequence. The inclusion of an appropriate dye label exploits the resonance enhancement contribution to the Raman Effect and allows for multiplexed detection. As fluorescence is the main tool for the detection of biological molecules, there is a plethora of commercially available fluorophore-labelled DNA sequences. Due to the ability of gold and silver nanoparticles to quench fluorophores, such dye labelled sequences can be successfully incorporated into SERRS based assays. However, fluorescent dyes are not a pre-requisite for SERRS analysis and thus non-fluorescent dyes can also be used, such as benzotriazole dyes. The labelling of DNA sequences is carried out through various different methods. One common method is to synthesise the DNA sequence using a dye labelled phosphoramidite, to incorporate the label into the sequence directly.<sup>105</sup> Fluorescent probes can be used with this technique as the presence of the nanoparticles quenches the fluorescent background revealing the vibrational information. However other methods have been used successfully with Steven *et al.* demonstrating the use of the Diels Alder reaction to attach a Raman active dye to a selected DNA sequence.<sup>104</sup> This progress has led to publications detailing the multiplexing ability of SERRS. Faulds *et al.*, have shown the detection of five DNA sequences simultaneously with a detection limit of  $10^{-12}$  M, as shown in figure 1.19.<sup>98</sup>

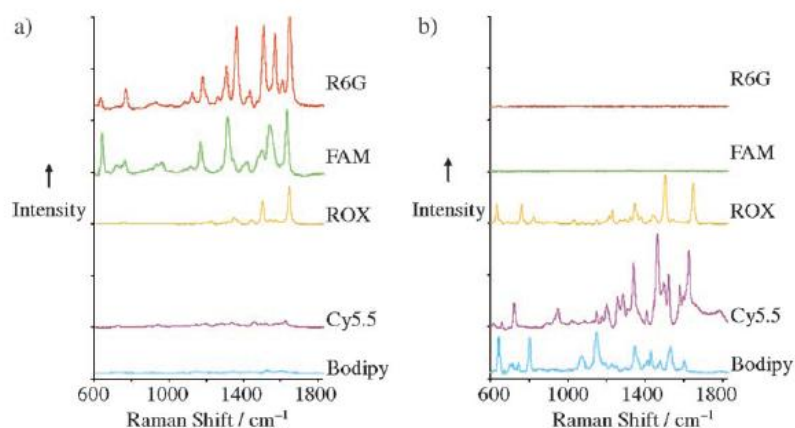


Figure 1.19: SERS spectra of five different dyes, used in multiplexing of DNA

Further to this Sun *et al.* have demonstrated the detection of an 8-plex DNA sequence via a mixed monolayer strategy.<sup>106</sup> Many groups have demonstrated pioneering research using this technique in the detection of DNA.<sup>106</sup> Cao *et al.* has detected disease-coding sequences such as Human Immunodeficiency Virus (HIV), Ebola virus and the smallpox virus, variola. Vo Dinh *et al.* has reported the use of SERRS DNA detection in the analysis of the breast cancer gene, BRCA1.<sup>77</sup> In addition, Stokes *et al.* produced information on a variety of dye labelled oligonucleotide, analysed at three different wavelengths on both gold and silver nanoparticles detailing detection limits of each dye and providing a starting point for multiplexing experiments.<sup>107</sup> One of the most recent breakthroughs was the ability to fabricate hotspots using DNA to direct the hotspot formation. Thompson *et al.* labelled two sets of silver nanoparticles: firstly with dye; then followed by DNA functionalisation with thiol modified DNA. In absence of the complementary target the SERRS intensity was low, yet upon hybridisation the intensity of the signal was enhanced due to the formation of the hotspots.<sup>108</sup> The detection of DNA using SERRS has been well studied and implemented in a variety of applications<sup>109-112</sup>. Although there are challenges that remain, it is the detection of proteins using a Raman based technique which still requires further investigation.

### 1.9.2 SERS IN PROTEIN DETECTION

When compared to DNA based SERRS applications, the detection of protein using SERRS analysis is a relatively new technology. This can be part explained by the

increased complexity in protein systems compared to those of DNA. The zwitterionic nature of the protein, a consequence of the side chains of amino acids which create the primary structure, creates a charged environment which can be difficult to control. This has implications in the aggregation state of nanoparticles as it can cause uncontrollable aggregation of the nanoparticles, eventually leading to the nanoparticle cluster becoming so large it precipitates out of solution. In addition, adsorption of protein onto a surface of any type has the potential to cause denaturation, thus rendering the analytical method ineffective.

Raman Spectroscopy has been utilised in the investigation of protein structure for over 30 years and consequently the vibrational spectra of the 20 essential amino acids have been identified and well studied.<sup>113</sup> Raman spectroscopy (discussed in section 1.8) is an inherently weak process and therefore SERS can be used to enhance this process. Dyes are often used as Raman reporters due to their high molar extinction co-efficient. When conjugated to proteins, low concentrations can be detected by conjugating Raman reporters to the biomolecules and using SERS as the analytical detection method. This has been demonstrated by many research groups - in particular the detection of proteins using SERS has been extensively used in the field of immunoassays.<sup>92, 114-116</sup> In this type of study a step by step protein-antigen interaction is constructed upon the nanoparticle surface, with a Raman reported molecule present, as indicated in figure 1.20.

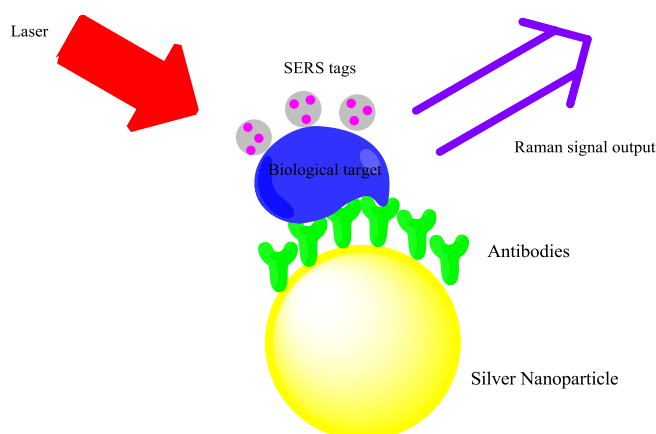


Figure 1.20: A schematic of an immunoassay using SERS. Antibodies are absorbed onto nanoparticles using one of the previously mentioned techniques. The protein targeted by the chosen antibody is labelled with a SERS target and therefore upon interaction the label is brought close enough to the nanoparticle surface allow detection and therefore confirming the interaction.

In addition to the sensitive nature of this technique ( $10^{-11}$ ,  $10^{-12}$  M), good selectivity is also achievable.<sup>108, 117</sup> Benzotriazole dyes have an affinity to silver surfaces due to the presence of a triazole ring.<sup>118, 119</sup> Douglas *et al.* used maleimide chemistry to conjugate a benzotriazole dye to Cytochrome c. This protein contains one free cysteine residue capable of reacting with maleimide in the presence of amines at physiological pH, demonstrating the importance of labelling a protein at a specific site. This led to the ability to label one protein molecule with one label. Furthermore, they demonstrated the possibility of using the dye both as a SERRS label and an anchor for attachment to the nanoparticle surface.<sup>63</sup> However, label free detection of proteins using SERS has been carried out successfully by Han *et al.*, where pre-aggregation of the colloidal solution allowed for sensitive detection of lysozyme.<sup>120-122</sup> Label free detection is of interest when using SERS, due to the goal to expand the use this technique in cellular environments. Such environments are complex and for direct visualisation of such samples, the ability to use synthetic labels to identify proteins may not be possible and could introduce further issues.

## 1.10 USE OF DYES IN RAMAN SCATTERING<sup>123-125</sup>

The incorporation of a resonance component within Raman Scattering opened a plethora of potential applications in the analytical detection field. Coloured compound could be incorporated into such analysis and the synthesis and selection of dyes became a prominent feature of SERRS investigations. The variety of dyes that can be used in Raman Scattering is phenomenal. The majority of dyes that are used are also fluorescent - a result of the extended conjugation present in the structure of these dyes. Raman Scattering, however, does not have this limitation as non-fluorescent dyes can be Raman active.

When using SERRS one can match the laser wavelength to the absorption maximum of the label to gain the biggest enhancement factors. Stokes *et al.* published an extensive table detailing the optimum combination of dye, nanoparticle type and laser wavelength.<sup>107</sup> This re-enforces one of the greatest advantage of SER(R)S - its multiplexing capability. This is not a readily available option with fluorescence based analysis due to the broad spectral profile resulting from such techniques.

Table 1: Taken from reference 106, whereby a range of dye labelled oligonucleotide were conjugated to both gold and silver nanoparticles and analysed over a range of wavelengths to determine multiplexing ability

Dye label	$\lambda_{\max}$ [nm]	$\lambda_{\text{ex}}: 514.5 \text{ nm}$	$\lambda_{\text{ex}}: 632.8 \text{ nm}$		$\lambda_{\text{ex}}: 785 \text{ nm}$
		Silver [mol dm <sup>-3</sup> ]	Silver [mol dm <sup>-3</sup> ]	Gold [mol dm <sup>-3</sup> ]	Silver [mol dm <sup>-3</sup> ]
FAM	492	$2.7 \times 10^{-12}$	$2.0 \times 10^{-9}$	–	–
TET	521	$1.6 \times 10^{-11}$	$2.0 \times 10^{-9}$	–	–
R6G	524	$1.2 \times 10^{-12}$	$1.1 \times 10^{-10}$	–	–
Yakima Yellow	526	$1.7 \times 10^{-11}$	–	–	–
HEX	535	$7.8 \times 10^{-12}$	$1.2 \times 10^{-9}$	–	–
Cy3	552	$2.6 \times 10^{-10}$	$1.5 \times 10^{-10}$	–	–
TAMRA	565	$3.5 \times 10^{-12}$	$1.8 \times 10^{-10}$	–	–
Cy3.5	581	$2.5 \times 10^{-11}$	$7.5 \times 10^{-13}$	$2.5 \times 10^{-10}$	–
ROX	585	$8.1 \times 10^{-11}$	$3.3 \times 10^{-11}$	$1.1 \times 10^{-9}$	–
BODIPY TR-X	588	$1.3 \times 10^{-10}$	$7.9 \times 10^{-12}$	$4.9 \times 10^{-10}$	–
Cy5	643	–	$8.3 \times 10^{-11}$	$1.7 \times 10^{-9}$	–
Cy5.5	683	–	$5.2 \times 10^{-12}$	$7.3 \times 10^{-11}$	–
Cy7	748	–	–	–	$5.8 \times 10^{-11}$

Whereas with Raman Scattering because it is a vibrational technique, the spectra that are obtained provides information about the molecular structure of the substrate and the spectrum for each molecule is unique to it because of this factor. Therefore multiplexing with more than one dye is a realistic and achievable goal. The cellular environment is complex and dynamic; featuring numerous intertwined interactions, meaning the ability to study several interactions simultaneously and in real time is key to advancing cell based research. Consequently, the monitoring of a single label is not sufficient. This is, by far, the greatest obstacle facing the progression of study within the field. There are several ways in which a dye can be employed in SE(R)RS analysis. There are dyes that have an affinity for the nanoparticle surface, for example benzotriazole dyes will form a monolayer on silver nanoparticles due to the presence of the tri-nitrogen group within this dye (see figure 1.21).<sup>119</sup> Another class of dyes in common use is enzyme activated dyes.<sup>105, 126</sup>

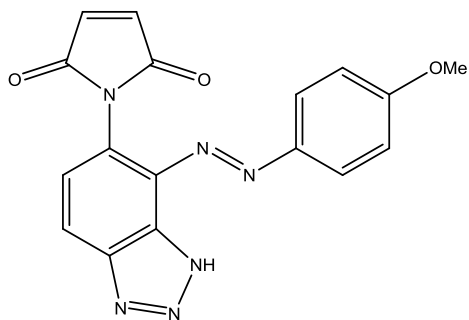


Figure 1.21: Structure of a benzotriazole dye

These molecules are synthesised to incorporate a mask, which when cleaved by the desired enzyme, will reveal the dye which is then SER(R)S active. The majority of dyes that are used are incorporated into the biomolecule, which can be achieved through either direct or indirect attachment. In the direct route, the dye is incorporated into a biomolecule through a direct modification on that particular biomolecule. Integration of these synthetic molecules has been carried out routinely and with relative ease using DNA. It has been well documented that DNA can be modified through several different routes on a reliable basis. However this process becomes more difficult with respect to proteins. This is due to the absence of easy modification routes which are open to DNA. Although, it is possible through the use of specific chemistry, the indirect method is through the use of synthetic linkers. These are functional groups that have affinity to both gold and silver nanoparticles, such as nitrogen and sulphur. This affinity can be exploited to enable successful absorption on to the nanoparticle. In addition, linkers have been synthesised to act as an anchor to the nanoparticle surface, while also providing a site for biomolecule conjugation. The use of simple amide-coupling chemistry has shown dye-coupling to be a robust method.<sup>127</sup> Finally, dyes have been used in a mixed monolayer approach, whereby the dye is absorbed onto the chosen surface together with the molecule that is being investigated.

The type of dye that is used depends upon the desired function. There has been an interest in synthesising dyes that have a compatibility with laser wavelengths towards the Infra-Red (IR) region of the light spectrum. Cellular components such as plasma and blood emit strong fluorescence at lower wavelengths especially 532 nm. Therefore using a laser at a longer wavelength extinguishes this effect and focuses on the dye which will indicate the presence of the substrate.

It is hoped that Raman spectroscopy can be implemented in the same breadth that it has been in the genomic field.<sup>103</sup> The detection of DNA through the use of Raman spectroscopy has grown and developed over the last twenty years. It is a well-established analytical tool that is used in the bio-diagnostic applications of DNA.<sup>60, 128</sup> However with proteins, their much greater complexity creates much larger problems. Which includes the effect of adsorption onto the nanoparticle surface (which has been documented to cause protein deactivation<sup>129</sup>) and Raman spectroscopy where detection of proteins and their interactions are much more in their infancy. It is for that reason that research within this area is extremely important. Investigations into suitable Raman reporters and conditions for protein detection using SERS were carried out to aid in the development of this field.

## CHAPTER 2: AIMS

- To prepare fluorescent protein nanoparticle conjugates and investigate their potential as biosensors.
  - Achieve solution based SERS detection of EGFP and RFP conjugates
  - Develop a successful and stable method for the conjugation of EGFP and RFP to silver nanoparticles
  - Optimise the conditions to obtain consistent SERS
  - Determine a LOD for solution based detection of FPs by SERS
  - Investigate the possibility of multiplexing potential of EGFP and RFP using SERS
- To conjugate the cell penetration peptide, TAT, to silver nanoparticles and investigate their uptake using HeLa cells.
  - Visualise these nanoparticles using SERS to identify the Raman label of TAT
  - Investigate stability of these conjugates under cellular conditions
- To synthesis novel linker molecules for the detection of protein-protein interactions
  - Compare the success of various synthetic procedures
  - Investigate the use of the linker molecule as a Raman reporter
  - Investigate the linkers as sensors for the analysis of protein-protein interactions through a use of a protein assay.

# CHAPTER 3: DETECTION OF FLUORESCENT PROTEINS VIA SERS

## 3.1 INTRODUCTION

The Nobel Prize for chemistry 2008 was awarded to three scientists: Osamu Shimomura; Martin Chalfie and Roger Tsien for the discovery and development of Green Fluorescent Protein (GFP). This discovery and development of fluorescent proteins (FPs) revolutionised the cellular biology field.

GFP was discovered in the early 1960s by Osamu Shimomura. This protein was discovered during the research of the bioluminescence of the jellyfish *Aequorea Victoria*.<sup>36</sup> Through this research it was found that the bioluminescence of this jellyfish was due to a protein, which was named Aequorea. It was found that this protein emitted light in the presence of calcium ions and was situated around the outside of the umbrella of the jellyfish shown in figure 3.1.



Figure 3.1: Bioluminescence of *Aequorea Victoria* jellyfish.<sup>35</sup>

During the course of purification of the protein Aequorea, it was seen that there was another protein - a by-product - which exhibited green fluorescence. Shimomura *et al.*<sup>32</sup> purified this by-product, gaining a trace amount which they named 'green protein'. This protein was later renamed by Morin and Hastings as the infamous protein which is so well known today – Green Fluorescent Protein.<sup>130</sup> GFP is a Förster Resonance Energy Transfer (FRET) partner to the Aequorea protein. The energy of the blue light emitted from this protein overlaps with the excitation maximum of GFP and therefore GFP is excited - consequently emitting green light. Research into

this protein was difficult due to the small amounts isolated of the protein Aequorea. From 10,000 jellyfish around 5 mg of the Aequorea protein was obtained, consequently an even smaller amount of GFP was obtained.

This created an issue when trying to gain a sufficient amount of GFP to enable a study into the chromophore and mechanism of GFP. This chromophore was discovered in the 1970s as shown in figure 3.2.

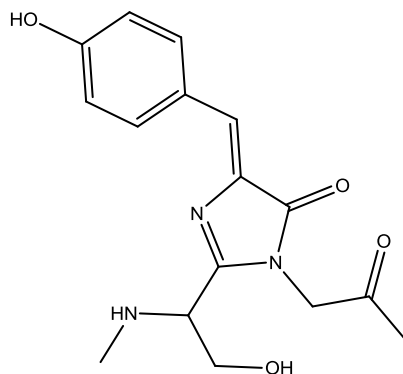


Figure 3.2: The structure of the GFP chromophore as discovered by Osamu Shimomura

The chromophore is contained within the centre structure of the protein. This is a property unique to GFP. When compared to traditional proteins which are fluorescent; the fluorescence is a result of complex of protein with a fluorescent compound.<sup>131</sup> Three amino acids which comprise the chromophore are serine, glycine and tyrosine. The initiation of the formation of the chromophore occurs upon cyclisation between serine and glycine to form the imidazolin-5-one intermediate. Followed by dehydration of the  $\alpha$ ,  $\beta$  bond of tyrosine it forms the complete chromophore<sup>132</sup>, shown in figure 3.3.

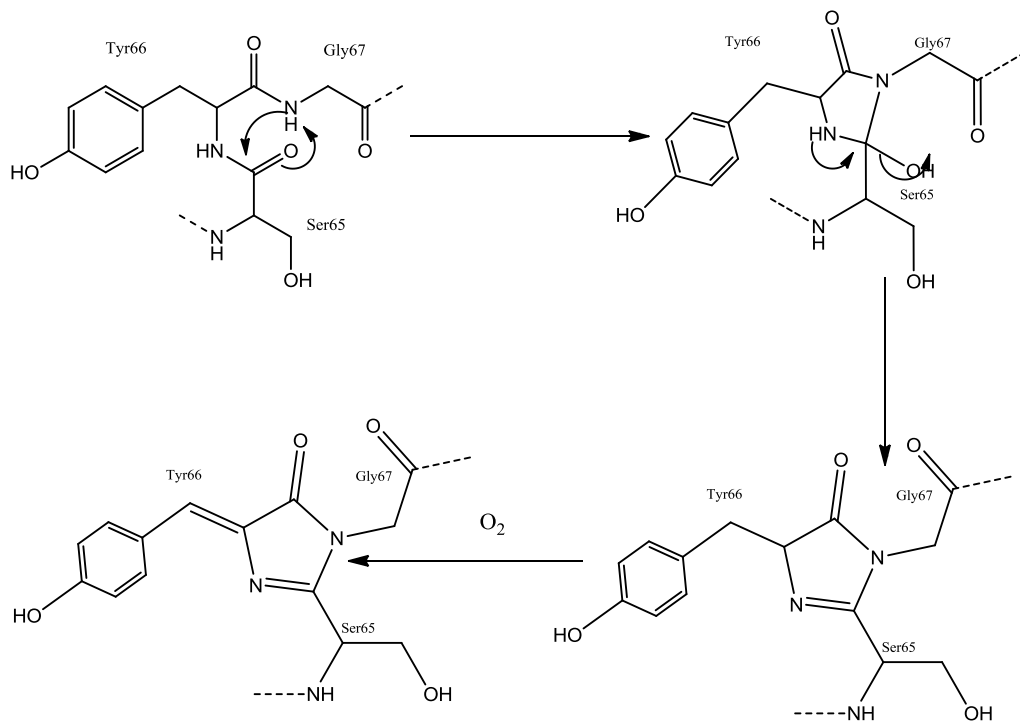


Figure 3.3: The proposed mechanism of the formation of the GFP chromophore.

Martin Chalfie's role in this development began when he was working on the gene expression of *C.elegans*. Chalfie's group produced GFP expressed in *E.coli* producing *E.coli* that fluoresced green. From this work, Chalfie could then express GFP in *C.elegans* which meant for the first time touch receptor neurons of this species could be visualised. In addition to this, the most ground breaking advantage of this molecule was in fact discovered by Chalfie's wife, Tulle Hazelrigg. Hazelrigg discovered that this protein could in fact be fused with another protein forming an active probe. This probe could be used to follow the course of the original protein due to the fluorescence and it was shown that this fusion did not prevent the action of the original protein.<sup>36</sup>

Roger Tsien's contribution was through the development of various different fluorescent proteins. Tsien's interest in GFP came from his work in the development of FRET-based sensors for the study of cAMP. Tsien demonstrated that GFP could be expressed within yeast cells; however, this observation revealed that the signal from cell to cell varied dramatically confirming that GFP was variable and that a suitable FRET partner was required. These observations allowed Tsien to begin work on mutating the sequence of the protein to vary its optical properties hence altering

the colours obtained. Through further investigation the amino acid serine was replaced with threonine which by UV-vis showed that the blue band became 5 or 6 times higher. It was found that this improved the performance of GFP in yeast cells.<sup>133</sup> In a further development Cormack *et al.* mutated the protein even further - replacing the phenylalanine with leucine with which a new GFP protein was born. This mutant was called Enhanced Green Fluorescent Protein (EGFP) and is now commercially available.<sup>134</sup> The benefits over the original GFP were faster maturation at higher temperatures and brighter fluorescence. This mutation and others led to the generation of Cyan FP and Yellow FP which began the creation of a palette of FPs that are now commercially available.<sup>34, 135, 136</sup>

Without the combined research of each of these three scientists, cellular biology research would be completely different and perhaps be 'in the dark' without the knowledge that has been provided by GFP. The advantages of this protein are clear: they are a class of relatively small proteins; they are excited by blue or ultraviolet light; are a set of stable proteins that have high quantum efficiency and do not photobleach easily; and finally there is no external cofactor required for the protein to fluoresce, proving why these proteins are widely used within this field.<sup>35</sup> FPs have a unique property discovered by Chalfie, in that as the fluorophore is part of the sequence of the protein the vector which codes for FPs can be inserted into the gene encoding for a protein of interest. Upon expression of this protein it will be fluorescent and this ability enables the monitoring of a protein, via fluorescence, without affecting the activity of the protein.

Fluorescence microscopy is the predominant analytical method of choice for the cellular biology community, however there are a number of disadvantages associated with this technique. Broad emission bands are not molecularly specific, resulting in overlapping of bands and loss of the potential to multiplex. While multiplexing is possible with fluorescence, it is limited due to the issue of overlapping excitation and emission wavelengths, as well as the risk of photobleaching of the fluorophore. Surface Enhanced Resonance Raman Scattering (SERRS) and Surface Enhanced Raman Scattering (SERS) have the ability to minimise the problems associated with fluorescence microscopy. This is a vibrational spectroscopy technique which identifies stretches in the chosen

chromophore and provides the prospect of multiplexing. The fingerprint spectra obtained can overcome the broad emission bands in fluorescence without the risk of photo bleaching of the substrate. The enhancement factor of these processes is attributed partly to the use of roughened metallic surfaces such as gold and silver. Nanoparticles have been utilised in the detection of biomolecules as biosensors, in bio-imaging and in cancer therapeutics. The attraction of using these nanoparticles is a result of the variety of attributes that they possess: such as their size; the high surface to volume ratio; and the ability to be taken up by cells with relative ease. The bioconjugation of nanoparticles has been well documented, enabling SER(R)S to be used as a method of biomolecule detection. For example, this technique has been used extensively for the detection of DNA. This methodology requires the oligonucleotide or surface to be labelled with a SE(R)RS active dye - these dyes are also fluorescent. When compared to detection of DNA via fluorescence, SERRS can demonstrate a lower limit of detection. The detection of proteins by SERS is slightly more challenging owing to the fact that protein activity can be compromised when absorbed onto nanoparticles, therefore care must be taken to determine what surface to use. It has been shown that use of citrate reduced colloidal gold and silver retain the native protein on adsorption and denaturing does not occur. Reasoning for this is denaturing of proteins occurs when the protein is bound directly to the metal, however the presence of the citrate layer provides a barrier between the metal surface and the protein, preventing such action.<sup>86</sup> The biggest priority for protein conjugates to be used in SERS is that the activity remains; this is an important factor when it comes to monitoring proteins. They must be able to activate and control the pathways within the cell and show researchers what causes malfunctions that lead to disease. Therefore the surface chemistry of the nanoparticles has to be taken into careful consideration. Many methods involve the use of a linker, in order to prevent direct contact of protein and the nanoparticle. This is a popular method owing to the fact that the linker can be tailored to bind the protein to the nanoparticle surface irreversibly through covalent interactions. Rotello *et al.* have shown the use of various linkers on nanoparticle surfaces; creating functional groups capable of electrostatic

interactions with EGFP. This work showed the ability to use the protein as a sensor rather than a specific biomarker. The research presented in this document worked towards the long term goal of employing SERS as a detection technique of FPs as a comparative to fluorescence. Although linker methodology is commonly used for protein attachment to the surface of a nanoparticle, in this case it would not be suitable as the addition of a linker would not be able to be reproduced by a gene and the fusion would fail. Therefore alternative methods of detection were sought.

## 3.2 PREVIOUS WORK

Research using fluorescent proteins has focused upon its fundamental use as a marker in the field of cellular biology. There have been numerous publications documenting the results from these papers. However this document will predominately focus upon the research which has developed the study of fluorescent proteins using Raman spectroscopic based techniques. EGFP has been used in other methods apart from as a biomarker: The Rotello group have published several papers using EGFP as a sensor molecule. Gold nanoparticles were incorporated with a linker to electrostatically bind EGFP. When the sensor molecule interacted with other proteins, a competitive binding process took place resulting in either a positive or negative fluorescence response depending on the displacement or retainment of EGFP. This technique used a fluorescent analytical read out.<sup>137-139</sup> The number of publications regarding the detection of EGFP using SERS is limited with a search using Web of Knowledge returning only two publications in 2003.<sup>140, 141</sup> Before designing an experiment for SERS detection it was important to study the Raman profile of the protein to identify which peaks related to the protein and to identify the peaks which would be enhanced.

### 3.2.1 RAMAN OF EGFP

There are many more papers in the literature detailing the use of Raman spectroscopy and EGFP. The majority of these papers use the technique to investigate the two forms of the chromophore present in the wild type GFP. Wild

type GFP refers to the original protein discovered by Shimomura in 1960. The UV-visible absorption spectrum of wild type GFP contains two main bands at 395 nm and 475 nm which are associated with the neutral and anionic form respectively. The anionic and neutral forms have similar fluorescence profiles. Tsien developed a mutant of wild type GFP known as the S65T mutant, closely followed by Cormack developing Enhanced Green Fluorescent Protein (EGFP) which contains the S65T mutation as well as the F64L mutation. Both these derivatives lose the secondary peak in the absorption profile when analysed. Researchers have also used Raman spectroscopy to study model chromophore structures - which mimic the chromophore of the protein - to determine if the Raman peaks obtained were from the chromophore of the fluorescent protein rather than the other amino acids comprising this protein. It was shown that this was indeed the case.

In a paper published by Bell *et al.* Raman spectra was obtained from wild type GFP and the corresponding S65T mutant.<sup>142</sup> The spectra were collected using an acquisition time of 8 minutes and a protein concentration of 60  $\mu$ M. In this paper, model chromophores were synthesised and Raman spectroscopy was carried out on these compounds. The aim was to determine if the chromophore dominated the spectrum when compared to the rest of the protein. It was found that this was indeed the case. The spectra that was obtained directly related to the chromophore with additional vibrational peaks associated to the other amino acids present in the protein. There is a difference within the chromophore of wild type GFP and S65T. In wild type GFP at position 65, there is the amino acid serine whereas, as the naming suggests, in the S65T mutant threonine is in the 65 position. Due to this situation there would be an expectation that the spectra between the wild type and S65T would differ slightly. Bell *at al.* demonstrated this within the published paper - it was these results that were used to compare the results obtained for EGFP. EGFP contains the same mutation as the S65T mutant. In addition to this there is a mutation at position 64 where phenylalanine has been replaced with lysine, however it was not expected that the results should vary significantly as this mutation is not part of the chromophore.

### 3.2.1.1 INVESTIGATION OF RAMAN PARAMETERS OF EGFP

The conditions used by Bell *et al.* were repeated using EGFP, however, the small volumes of protein available meant a solution with the concentration of 60  $\mu\text{M}$  could not be used, therefore a 10  $\mu\text{M}$  solution was used and analysed. The results that were obtained were disappointing: no signal was produced when following Bell's conditions; and increasing the acquisition time did not improve the system. It was important to gain Raman spectrum of EGFP to identify the components from the protein. A different approach was required, as the main obstacle seemed to be the concentration of the protein, as Raman is a weak process with only 1 in every  $10^6$  photon being Raman scattered.

A 1  $\mu\text{L}$  sample, at a concentration of  $3.4 \times 10^{-5}$  M, was pipetted onto a glass coverslip as well as as a control, the buffer which the protein resided in (1 $\times$ PBS), followed by drying under dark conditions. Each spot was analysed using 3 different wavelengths: 532 nm; 633 nm; and 785 nm. The spectra obtained at 532 nm was essentially redundant due to the high fluorescence background. This was to be expected at this wavelength due to the excitation of EGFP which produces the fluorescence signal. The longer wavelength analysis produced encouraging results as these laser wavelengths are red-shifted, thus there was a stark reduction of the fluorescence background, revealing the detectable peaks.

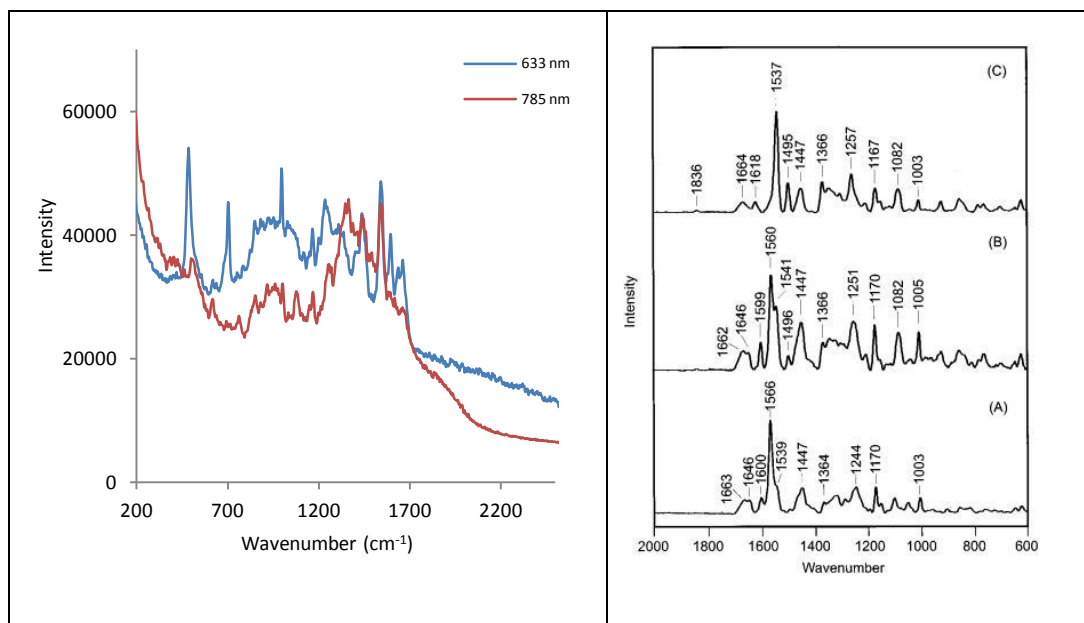


Figure 3.4: On the left is the Raman spectra of EGFP at 785 nm (red line) and 633 nm (blue line) obtained using the conditions outlined above. On the right is the results obtained by Bell *et al.*, when using a protein concentration of 60  $\mu\text{M}$  and acquiring the spectra for 8 minutes. **A** represents the wild type GFP in Tris buffer (pH 8.0), **B** represents the S65T mutant of GFP in sodium acetate buffer (pH 5.0) and **C** represents the S65T mutant in Tris buffer (pH 8.0).<sup>142</sup>

Figure 3.4 shows the Raman spectra recorded at 633 nm (blue line) and 785 nm (red line) of EGFP. There are slight differences between these spectra due to different laser wavelength, which can enhance slightly different bands.

The bands obtained, at 785 nm of EGFP, are detailed in table 3.1 and were compared to the vibrational bands obtained by Bell *et al.* when analysing the S65T mutant of GFP at 752 nm. It was shown there was good agreement between each set of spectra, however the results do vary slightly; most likely a consequence of pH. The Raman spectrum of EGFP was taken at pH 7.2, however when comparing the Raman spectra taken by Bell *et al.*, of the S65T mutant at pH 5 and pH 8 differences in peaks are observed. Another observation made from comparing these spectra was the Raman spectrum of EGFP (which contains the S65T mutation and a F64L mutation) and the Raman spectrum of the S65T mutant was not significantly different. This indicated the Raman spectrum of EGFP was predominately from the chromophore, which was confirmed through the absence of any vibrational peaks from the second mutation, F64L.

TABLE 3.1: Results from EGFP Raman measured at 785 nm, compared to results published by Bell *et al.* also measured at 752nm. Units:Wavenumber (cm<sup>-1</sup>)

Results obtained by Bell <i>et al.</i> , when examing S65T mutant in Tris buffer (pH 8.0) <sup>142</sup>	Results obtained using the technique outlined in this thesis.
1003	764
1082	1079
1167	1176
1257	1257
1366	
1447	1440
1495	
1537	1557
1618	1620
1664	

### 3.2.2 SERS OF EGFP

Unlike the publications describing the Raman and Resonance Raman of EGFP, there are a limited number of publications detailing the detection of EGFP by SERS, with only two papers published in 2003 by Habuchi *et al.*<sup>140</sup> and Tozzini *et al.* The conclusion of the Habuchi *et al.*, paper was SERS could be used as a method to gain structural evidence for the photophysical processes of fluorescent proteins. Whereas the paper published by Tozzini *et al.* focussed upon the low vibrational region of Raman spectroscopy.

The work published by Habuchi *et al.* achieved this by creating a 1 mM solution of NaCl and silver citrate colloid containing EGFP and then depositing a sample onto a poly-L-lysine coated slide.

Locating a signal on a surface can be easier due the fact that the sample is static, i.e. the section which is being studied will always remain constant, whereas in solution based circumstances the product that ‘floats’ past the laser beam is what is examined and it becomes impossible to relocate the specific area. The static nature of this method is a disadvantage in the long term; the ability to tranpose this into cellular situations would be difficult and lengthy. In additon to this, the surface that Habuchi *et al.* chose was a poly-l-lysine slide. This could have caused interference during the experiment, as the silver nanoparticles are coated

on to this slide, which could have resulted in a background signal of poly-l-lysine. Therefore detection of EGFP via solution-based methods would be advantageous for *in vivo* work.

### 3.2.2.1 SURFACE BASED DETECTION OF EGFP

The work carried out by Habuchi *et al.* was repeated to determine if the method developed by the group could be repeated reproducibly and therefore determine a measure robustness for the technique. The supplementary information provided by Habuchi *et al.* did not supply the specific ratios of NaCl and EGFP, therefore a range of conjugates were synthesised, as outlined by table 3.2.

Table 3.2: Ratio of NaCl:EGFP used for repetition of work published by Habuchi *et al.*

Sample/Ratio of NaCl:EGFP	Volume of Ag	Volume of NaCl (1 mM)	EGFP Volume ( $2 \times 10^{-8}$ M)
One/1:1	250 $\mu$ L	625 $\mu$ L	625 $\mu$ L
Two/2:1	250 $\mu$ L	833 $\mu$ L	416 $\mu$ L
Three/3:1	250 $\mu$ L	937.5 $\mu$ L	312.5 $\mu$ L
Four/4:1	250 $\mu$ L	1000 $\mu$ L	250 $\mu$ L
Five/5:1	250 $\mu$ L	1042 $\mu$ L	208 $\mu$ L
Six/6:1	250 $\mu$ L	1071 $\mu$ L	179 $\mu$ L
Seven/7:1	250 $\mu$ L	1094 $\mu$ L	156 $\mu$ L
Eight/8:1	250 $\mu$ L	1111 $\mu$ L	139 $\mu$ L
Nine/9:1	250 $\mu$ L	1125 $\mu$ L	125 $\mu$ L
Ten/10:1	250 $\mu$ L	1136 $\mu$ L	114 $\mu$ L

Sodium chloride and EGFP were incubated in each specific ratio (outlined in table 3.2) for 1 hour, followed by the addition of AgNPs. This solution was incubated for a further hour after which point 1  $\mu$ L of the conjugate was spotted onto a Poly-l-lysine coated glass slide. Following air drying of the spots, the slide was analysed at 532 nm; mapping 10  $\mu$ m x 10  $\mu$ m sections of the slide. A low laser power was used due to the issue of burning of the slide and therefore degrading the sample. The laser power was determined to be 1 mW.

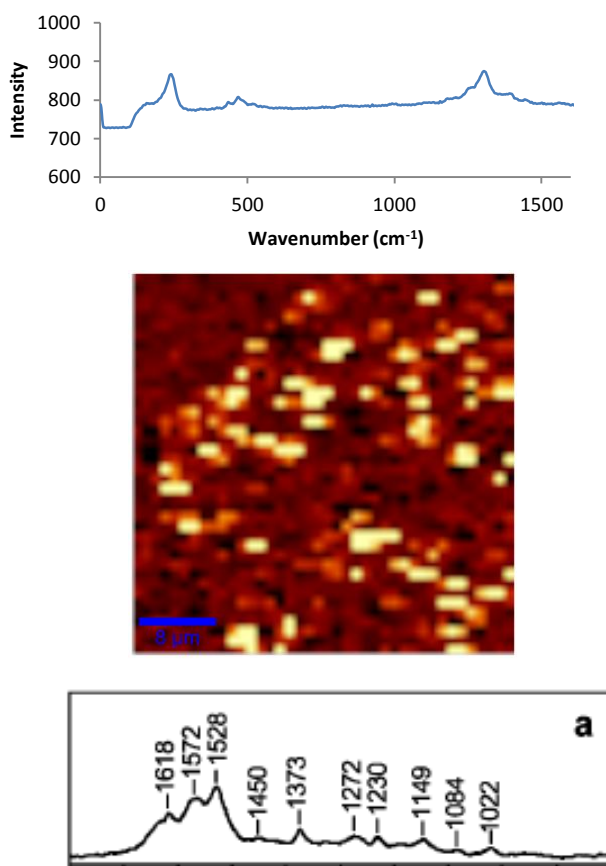


Figure 3.5: False colour SERS intensity map of conjugate 5 on poy-l-lysine coated coverslip, map created by focussing on area between 0-1600  $\text{cm}^{-1}$ . The yellow colours indicate areas of high intensity. It was found many of these areas did not represent EGFP but poly-L-lysine. Spectrum above represents the average spectrum from this area. Below the false colour map is the averaged SERS spectrum obtained by Habuchi et al., built up from 80 individual EGFP molecules.

It was found that signal was predominately located at the edges of the spots; typical of the coffee ring effect often found when drying samples. It was found that the signal was sporadic in each of the spots analysed regardless of the ratio of aggregating agent to protein. Figure 3.5 demonstrated the sporadic nature of this technique; the yellow sections indicate where the most intense signal is present. The signal is not uniform the spectra shown in figure 3.5 was obtained predominately. When comparing these results to the spectrum obtained by Habuchi et al., it was shown there appeared to be no correlation.

In addition to this there were areas where fluorescence was obtained, which obscured any signal. Another concerning issue was in the absence of protein: a

high background signal was observed and it was hypothesised this signal was a consequence of the coating of poly-l-lysine. Overall this method was found to be lacking in reproducibility and reliability. It was hoped this is where solution based detection would be more beneficial.

Another paper published in the same year as Habuchi *et al.*, examined the low vibrational modes of GFP using SERS. Tozzini *et al.* achieved SERS spectra by the addition of 70  $\mu\text{M}$  aliquot of EGFP to silver citrate colloid and analysed with a 623.8 nm laser.<sup>141</sup> Encouraging results were obtained detailing the low vibrational sector of the protein, however, in the spectra, they obtained a very high fluorescence background signal which made analysis difficult. This was most likely due to the high protein concentration - a final protein concentration of 5  $\mu\text{M}$  was used. This quenching is distance dependant - the further away the molecule is from the nanoparticle the process of fluorescence quenching becomes less efficient. The presence of a high level of protein would 'swamp' the nanoparticle, creating layers upon layers of fluorescent protein, thus increasing the distance between nanoparticle and the protein. Due to the high level of fluorescence exhibited by fluorescent proteins, it was essential to bring the molecule as close to the surface of the nanoparticle as possible to gain the most efficient quenching effect.

SERS has been predominately used in conjunction with a strong Raman reporter, such as synthetic dyes, e.g. TAMRA or fluorescein. These dyes are normally conjugated to the biomolecule of interest and through the presence of the dye signals, there is a positive confirmation that the biomolecule is present.<sup>143, 144</sup> However, a more direct approach was required to visualise the peaks resonating from the biomolecule, therefore the detection of EGFP had to be label-free. Label-free detection using Raman spectrometry has been carried out previously: McGuinness *et al.* published a paper detailing the detection of the fluorescent protein, allophycocyanin (APC).<sup>145</sup> In this paper, the conditions that were used were as follows: 100  $\mu\text{L}$  of APC was added to 200  $\mu\text{L}$  of silver colloid before the solution was analysed 20  $\mu\text{L}$  of NaCl was added. This solution was then analysed using a 532 nm laser. Using this technique single molecule detection was obtained. The results published in this paper were encouraging and it was

hypothesised that as EGFP was also a fluorescent protein the method would yield similarly good results. A solution of EGFP, 100  $\mu\text{L}$  of a  $1 \times 10^{-8}$  M solution was added to 200  $\mu\text{L}$  of silver colloid. On this addition, the conjugate was unstable and led to irreversible aggregation. It was surmised that this method would not be beneficial for the detection of EGFP.

Another method was published in a paper by Han *et al.* which detailed the label-free detection of proteins using SERS.<sup>120</sup> Within this paper, the method involved pre-aggregation of the colloid before the addition of the desired protein. In an attempt to obtain solution-based SERS of EGFP the method from this paper was adapted. To a 300  $\mu\text{L}$  aliquot of silver colloid, sodium sulfate was added and incubated for 30 minutes before 50  $\mu\text{L}$  of EGFP - at a concentration of  $1 \times 10^{-7}$  M - was added. The samples were analysed at 514.5 nm with the results shown in figure 3.6. As it can be seen, the results are poor. The signal obtained did not provide any vibrational information: once more this method was deemed not to suit the detection of EGFP.

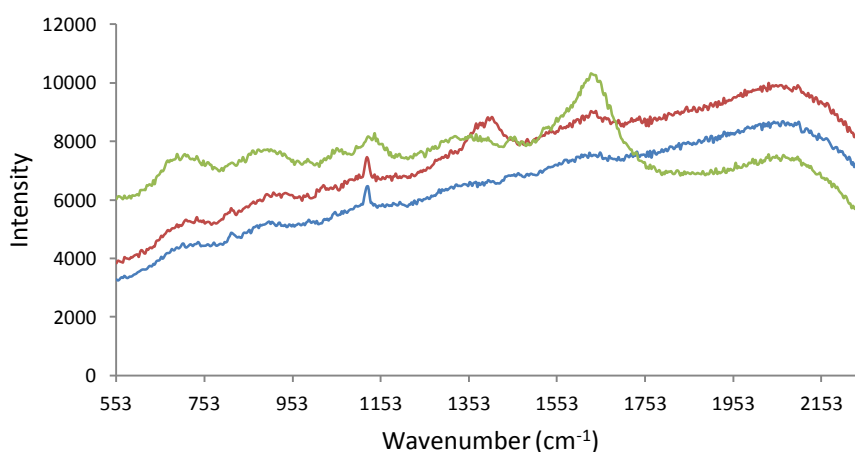


Figure 3.6: SERS spectra of EGFP using three different types of silver citrate colloid, using the method detailed by Han *et al.*(reference 115)

### 3.3 ELECTROSTATIC METHODOLOGY

In search of a new method, inspiration came from De *et al.* who have used electrostatics in the detection of proteins; using fluorescence as the analytical method. In these papers, De *et al.* used cationic linkers, covalently linked to gold

nanoparticles, to create an electrostatic connection between gold nanoparticles and EGFP.<sup>139</sup> The electrostatic nature of the protein can be manipulated through pH. The isoelectric point (pI) of a protein is the pH at which the protein carries no net electrical charge, i.e where the positive and negative charges residing on each of the side chains of the amino acids are equal. At a pH that is below the pI of the molecule, this molecule will be net positively charged and consequently at a pH above the pI the molecule will be net negatively charged. The pI of EGFP was investigated and was found to be 5.92.<sup>146, 147</sup> Therefore at a pH below pH 6, the protein that has an overall charge on the protein will be positive, whereas at a pH above pH 6, the protein has a net negative charge.

Silver citrate colloid has a pH of 7. This type of colloid was stabilised using citrate groups which are negatively charged to prevent aggregation of unmodified nanoparticles at this pH through the repulsion of this negative charge. Therefore, if the protein had a net positive charge, it could create an attraction between the negatively charged colloid and the positively charged protein; forming the conjugate electrostatically. This concept is shown in figure 3.7.

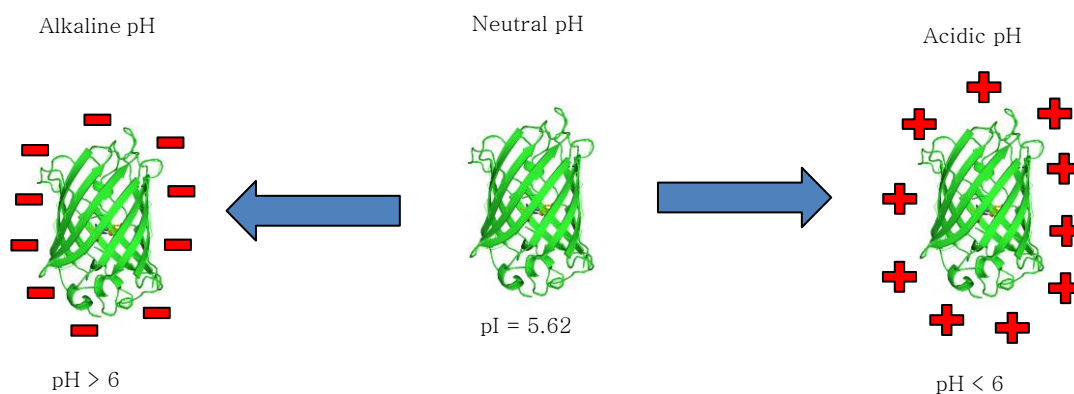


Figure 3.7: Concept for manipulation of pI to form charged protein, neutral pH indicates a neutral charge on the protein at pH 6

By lowering the pH of the colloid, a net positive charge would exist on the protein and thus aggregation between the protein and negatively charged nanoparticles could be induced. The SERS effect could be 'switched on', as illustrated in figure 3.8; leading to significant signal enhancement.

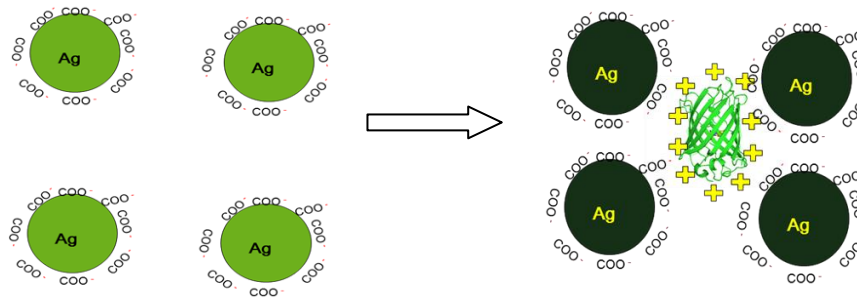


Figure 3.8: Aggregation caused by electrostatics interactions between the protein and Ag nanoparticles

### 3.4 INVESTIGATION OF pH MODIFICATION OF COLLOID

In order to lower the pH of silver citrate colloid (which had a pH 7), several acidic solutions were investigated. Table 3.3 details such acids and the resulting pH of the silver citrate colloid after addition of each acid in various volumes.

Table 3.3: pH values of colloid solutions after addition of each acid.

Acidic Solution	pH value of Ag citrate
Ascorbic acid	3.87; 4.36
Citric acid	3.06; 3.62; 5.46; 6.17
Hydrochloric acid	1.99; 2.36; 5.65
Nitric Acid	2.56; 4.43; 6.93
Sulfuric Acid	1.88; 2.93; 4.68

The role of the acidic solution was to lower the pH of the colloid in a stable manner, i.e. avoid aggregation of the bare nanoparticles. To confer net positive charge on EGFP the pH had to be reduced to pH 6. Therefore it was decided to trial three different pHs for each acid – pH 2, pH 4 and pH 6.

The solutions using ascorbic and citric acid could only lower the pH of the colloid to around pH 3 without causing irreversible aggregation. At the pH range of pH 1.8 – 2.3, the colloid was unstable and irreversibly aggregated the conjugates after only a few hours, regardless of the type of acid used, shown by the spectra in figure 3.9.

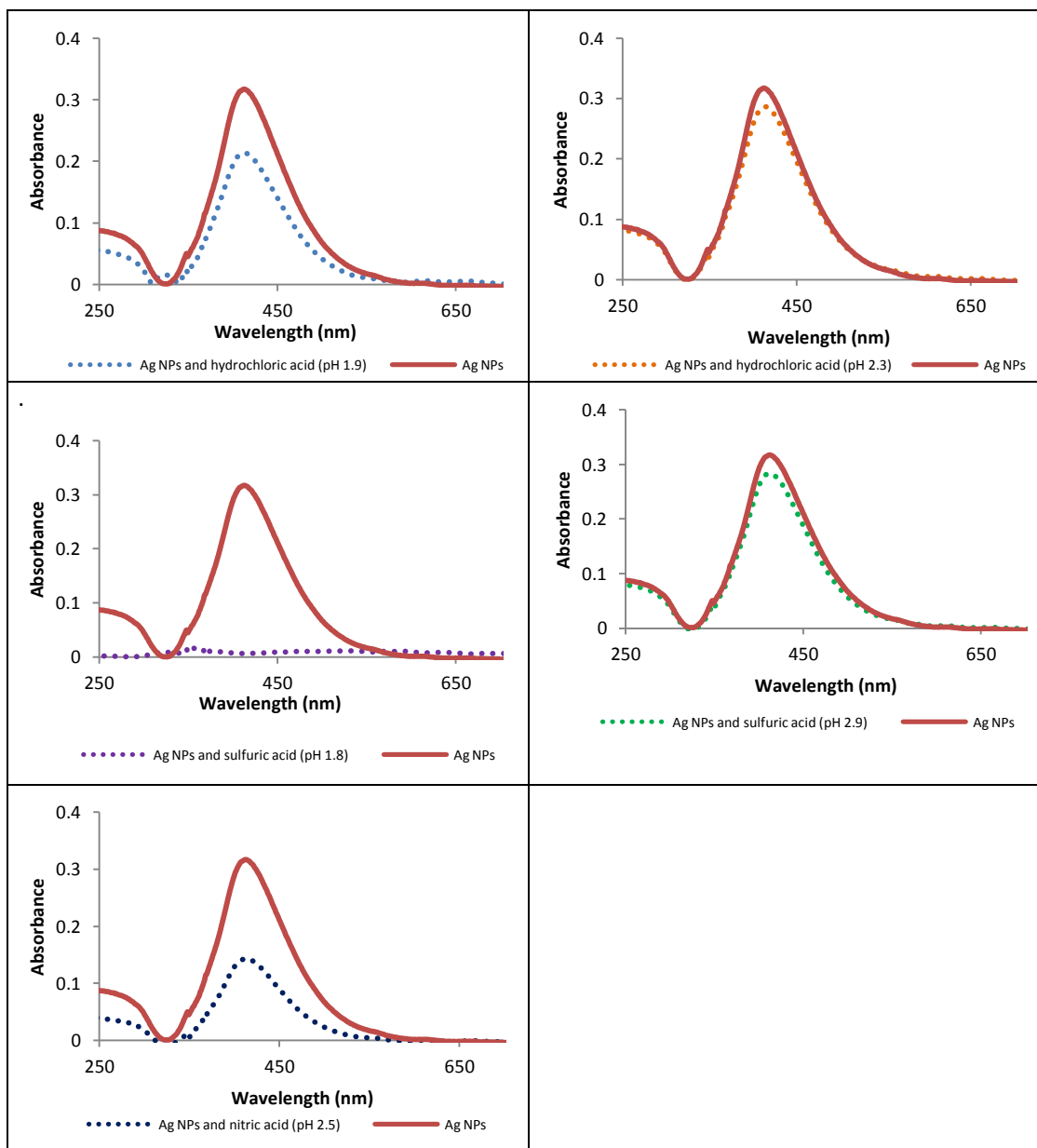


Figure 3.9: UV-visible spectra of Ag citrate colloid, pH modified with low pH acidic solutions.

From figure 3.9, it can be seen that the colloid adjusted with sulfuric acid to pH 1.8 crashed out immediately, with the absence of a peak at 400 nm. The other three colloidal suspensions show signs of early aggregation with a drop in absorbance when compared to the bare colloid. Over the course of two hours this led to complete and irreversible aggregation rendering these acidic solutions as non useable for stability reasons. Likewise, the higher pH colloidal solutions were analysed for their effect on the  $\lambda$  maximum of silver citrate colloid: figure 3.10

shows the various solutions and their effect. All but one solution showed that silver citrate colloid remained stable: this was determined from the  $\lambda$  maximum which remained unshifted. Normally if there has been a significant change at the surface of the nanoparticles this would be reflected in the  $\lambda$  maximum. Therefore, it was a good indication that the pH could be altered without a significant effect on the stability of the colloidal suspension.

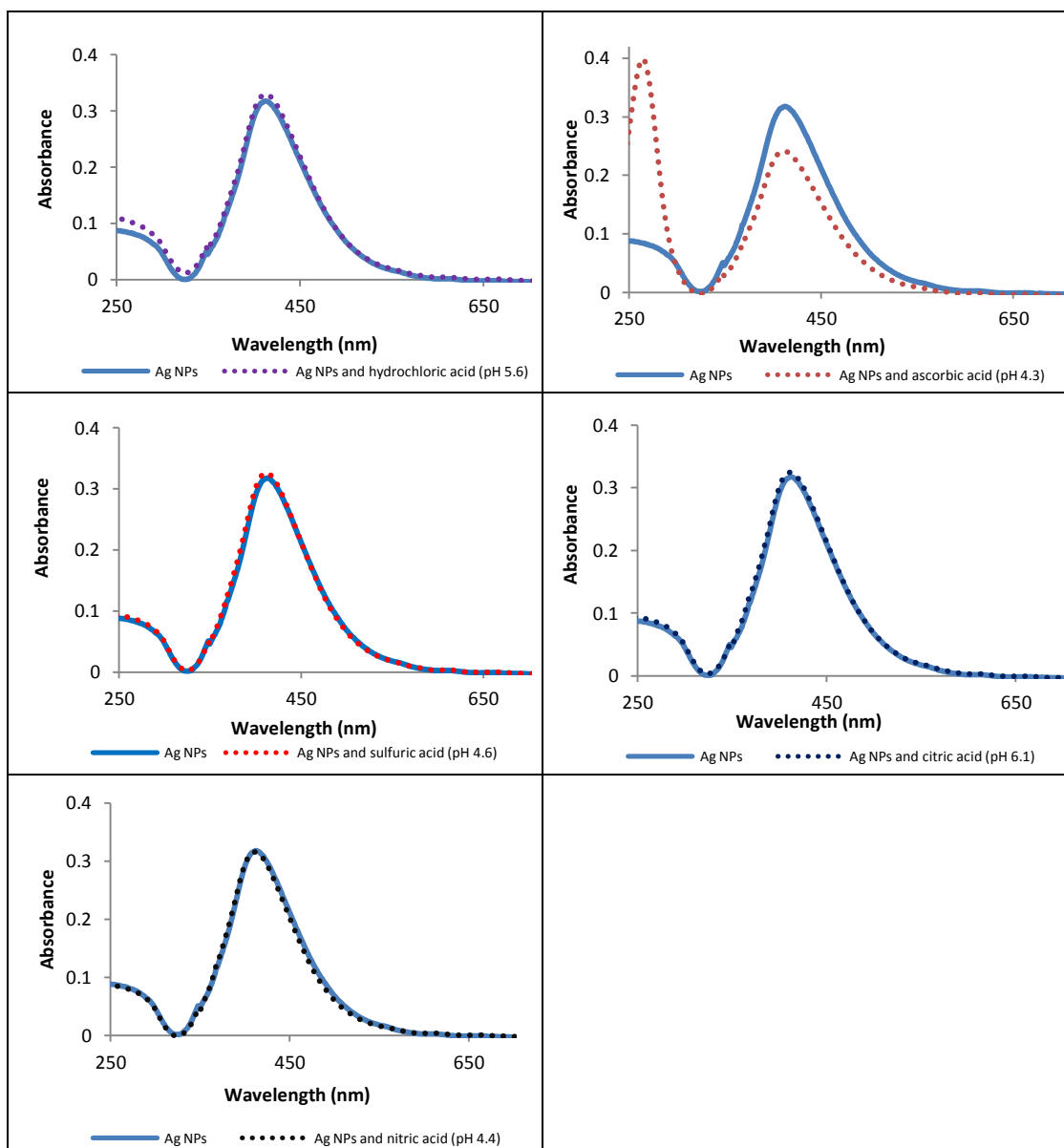


Figure 3.10: Uv-visible spectra of colloidal suspensions pH adjusted with higher range acidic solutions.

The results shown in figure 3.10 were encouraging, showing that the stability of the pH adjusted silver citrate was not affected. Therefore, the next stage was to investigate whether the addition of the acidic solutions affected the SERS profile of silver citrate colloid.

The colloidal solutions were analysed using SERS to ensure no significant background signal was observed from the addition of these acidic solutions. This also served as a negative control as it could be directly compared to EGFP functionalised nanoparticles, shown in figure 3.11.

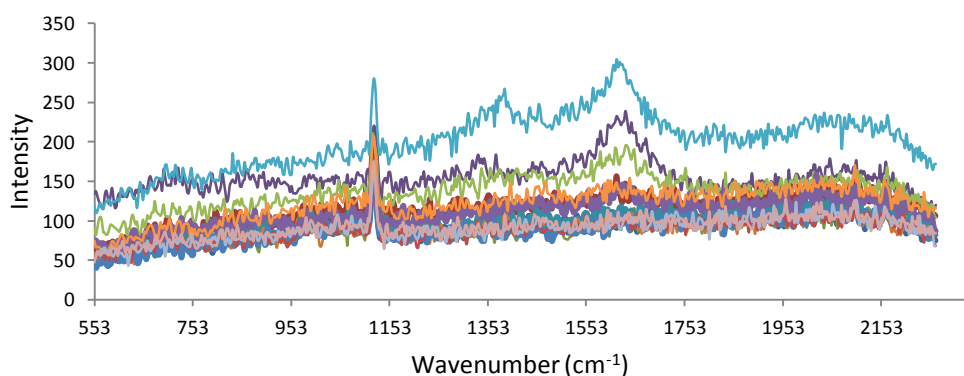


Figure 3.11: SERS obtained from pH adjusted colloid pH ranged from 2 -7

Figure 3.11 shows the signal obtained from unmodified silver citrate colloid, after pH adjustment. There was no observable effect on the background and allowed for the progression into the investigation of EGFP detection. The next step was to determine the best solution to use: initially to do this the interaction between the control sample, 1×PBS, and the pH modified colloidal suspension was investigated. The control was 1×PBS buffer - the buffer that was used for the dilutions of EGFP throughout the experiments carried out in this work. The spectra was aquired for 30 seconds and 5 aquisitions collected, the results are shown in figure 3.12 and figure 3.13.

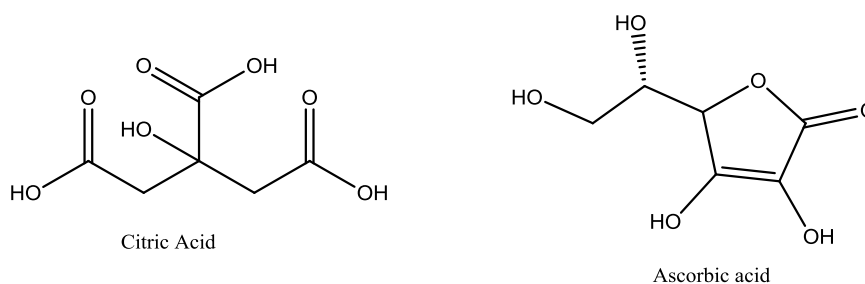
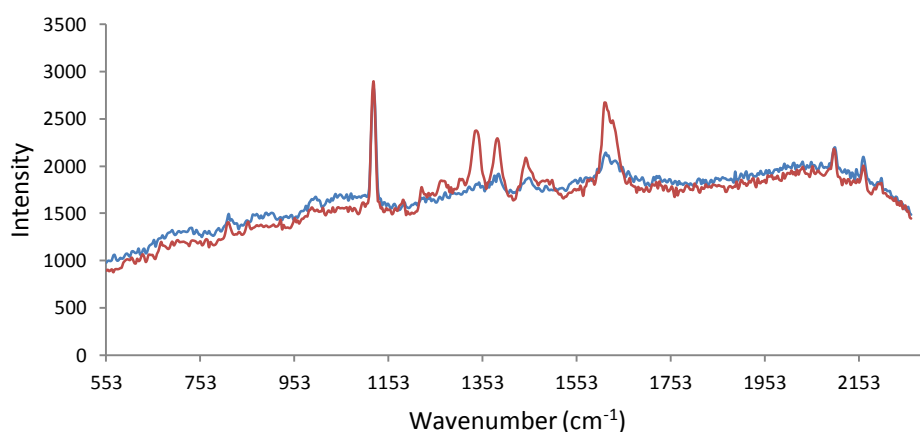


Figure 3.12: SERS spectra of ascorbic and citric acid adjusted colloidal solutions incubated with 1xPBS and structures of these acids. Spectra collected using 514 nm for 20 sec acquisition time. Blue line is ascorbic acid and red line is citric acid.

The SERS spectra shown in figure 3.12 ruled out the use of either ascorbic or citric acid. When 1xPBS was incubated with citric acid, modified silver citrate colloid intense vibrational peaks were obtained. This could be explained by the complex structure of the acid, shown in figure 3.13. The structure contains three carboxylic acid groups which are Raman active. This result led to the decision to avoid using ascorbic acid. Although such intense peaks were not displayed in the SERS spectrum it was decided to keep away from this acid due to the similar complicated structure as citric acid. In addition, it was found when adjusting the pH of the colloidal solution that large volumes of these acids were required to reach the desired pH which consequently diluted the colloidal solution.

Such groups are absent in nitric and sulfuric acid and consequently the SERS spectra obtained when the modified colloidal solution (of each acid) was incubated with 1xPBS, displayed very little interference, as demonstrated in figure 3.13.

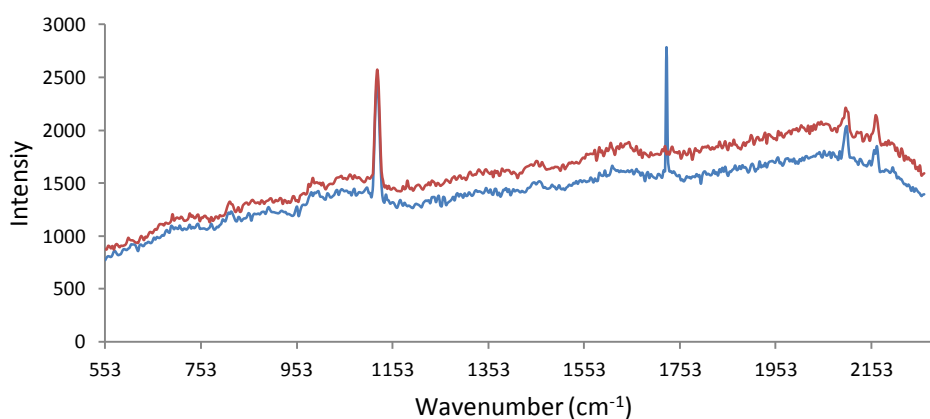


Figure 3.13: SERS Spectra obtained from incubation of 1xPBS with nitric acid modified colloid (blue line) and sulfuric acid modified colloid (red line).

From initial testing, nitric and sulfuric acid were deemed suitable solutions for the pH modification of colloidal solutions. It was then necessary to investigate the compatibility each type of modified colloid in the preparation of EGFP functionalised nanoparticles.

To bare colloidal solution, one batch was modified with nitric acid and a separate batch with sulfuric acid. EGFP was added at a  $1 \times 10^{-7} \text{M}$  concentration and incubated for 5 minutes before analysis at 514 nm. The results are shown in figure 3.14.

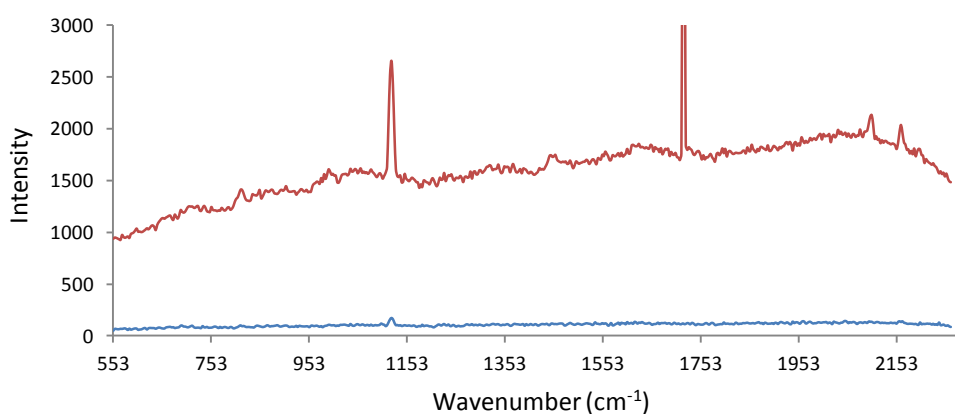


Figure 3.14: SERS Spectra of EGFP after a 5 minute incubation, with nitric acid modified colloid (blue line) and sulfuric acid modified colloid (red line).

When compared to the control spectra, there is no difference indicating that the conjugation through electrostatics had been unsuccessful. It was hypothesised that this could have been due to the incubation time. The formation of the overall positive charge on the 238 amino acid protein would not have been instantaneous. With this notion, the conjugate was incubated over a period of 54 hours and re-analysed; the result is shown in figure 3.15.

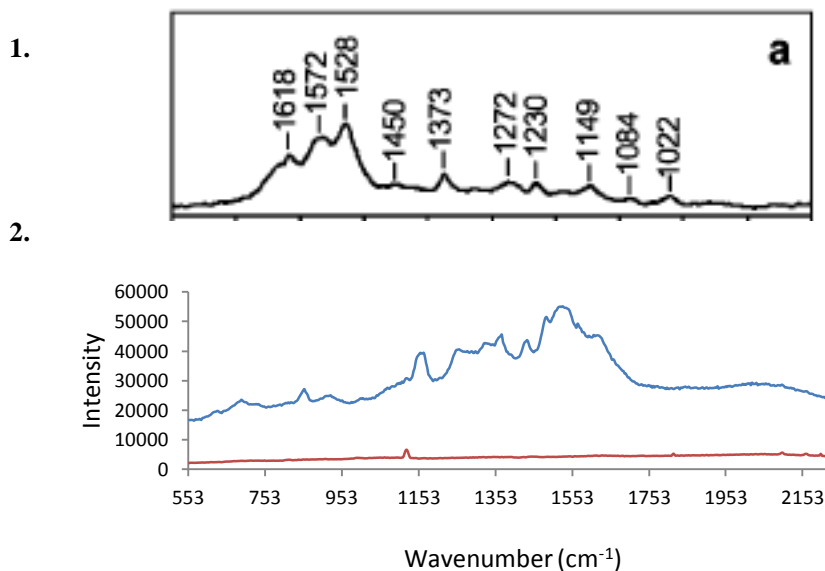


Figure 3.15: The results obtained by Habuchi *et al* are shown by spectrum **1** which are compared to the SERS spectrum of EGFP-NP conjugates obtained using the newly developed electrostatic technique, **2**. Silver conjugate pH adjusted with nitric acid (blue line) and sulfuric acid (red line) and analysed using a 514.5 nm laser after a 54 Hr incubation.

The signal was observed from the colloidal solution modified by the nitric acid solution. The signal that was obtained was compared to the results published by Habuchi *et al*. and are shown in table 3.4.

Table 3.4: Assignment and comparison of vibrational peaks between Habuchi published results (left hand column) and the results obtained using nitric acid modified colloid (middle column).

<b>Habuchi Results<sup>140</sup></b>	<b>Results obtained using the technique outlined in this thesis.</b>	<b>Assignment</b>
1560		Phenol
1536	1536	Imidazolinone C=C mode
1493	1527	Phenol
	1485	Phenol C-H deformation
1448	1430	C=N stretch
1364	1369	
1300	1341	Phenol
	1272	
1254	1253	
1166	1161	Phenol C-H deformation
1079	1069	Imidazolinone C-C stretch and C=O bend
1001	1003	Amide I mode

It was clear that the optimal solution for the modification and successful formation of conjugation was nitric acid at a pH between pH 4 – 6. When compared to the results obtained by Habuchi *et al.*, it can be seen that there was good agreement between each set of results. Evidentially there are differences, however this could be explained through the difference of techniques used to gain the results. This was, at the time of writing, the first record of solution based, label-free SERS of EGFP.

It was important to determine whether the manipulation of the pI point was responsible for allowing successful conjugation of EGFP to the nanoparticles. To test this theory, conjugates were synthesised (as detailed in section 8.4) however using a batch of acidic, basic and neutral colloids. The acidic batch was pH adjusted using 0.01% v/v nitric acid to a pH of 4.1, the basic batch was adjusted with 10 mM NaOH to pH 10 and unmodified colloid which has a neutral pH of pH 7.4. The samples were incubated for 50 hours and analysed at 514.5 nm. The results are shown in figure 3.16.

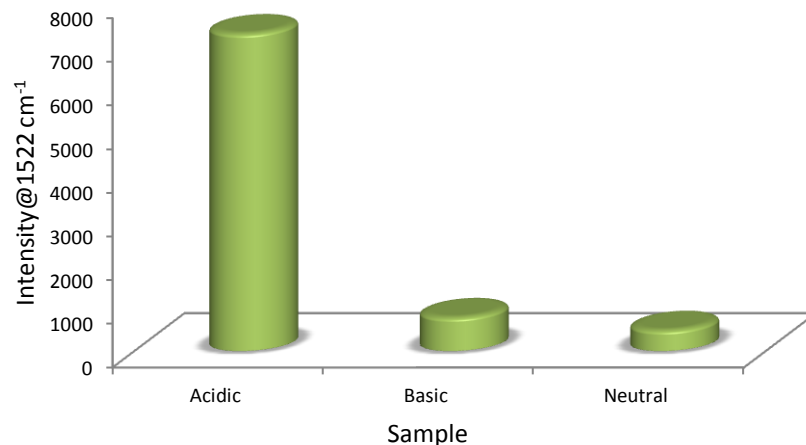


Figure 3.16: The SERS signal intensity of peak 1522 cm<sup>-1</sup> of EGFP-NP conjugate at different pHs: Acidic pH 4.1; Basic pH 10; and unmodified silver citrate colloid (neutral) pH 7.4.

The results show that the acidic pH was responsible for the intensity of signal that was obtained. This proved that through careful manipulation of pH, the charge properties of EGFP could be controlled to ensure successful conjugation to silver nanoparticles.

To ensure the pH modification had not caused a shift in the overall charge of the colloid, zeta potential measurements – which measure the stability and charge of nanoparticle suspensions – were taken on: native colloid, immediate modification colloid; and month old modification colloid. The results are shown in figure 3.17.

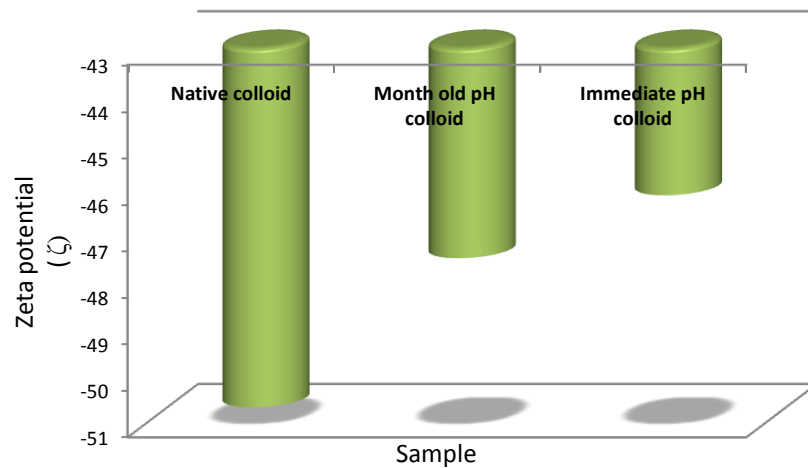


Figure 3.17: Comparison of zeta potentials of unmodified colloid and colloid modified with 0.01% nitric acid after different incubation periods.

Figure 3.17 shows that post modification with nitric acid, the overall charge on the colloid remains negative, thus ensuring the colloid remained overall negatively charged, which proposed the method would still work.

A comparison between the Raman and the SERS spectra was carried out - this was to ensure that the spectra that was obtained was from the chromophore of EGFP. Figure 3.18 shows this comparison. It shows that there is enhancement of the bands at  $1166$  and  $1538\text{ cm}^{-1}$ , providing evidence that the spectra obtained in SERS experiments was that of the EGFP chromophore.

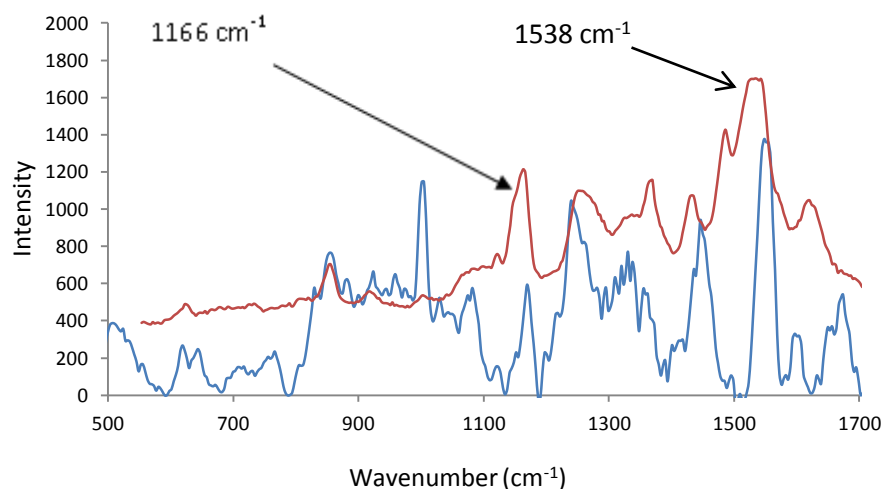


Figure 3.18: Comparison of Raman (blue line @ 633 nm) and SERS of EGFP (red line @ 514 nm)

This was significant in itself as the creation of solution based SER(R)S assays are notoriously difficult. It was necessary to test the robustness of the preparation method to ensure conjugates could be synthesised reproducibly. Three different conjugates were synthesised and analysed in triplicate as can be seen by the results shown in figure 3.19.

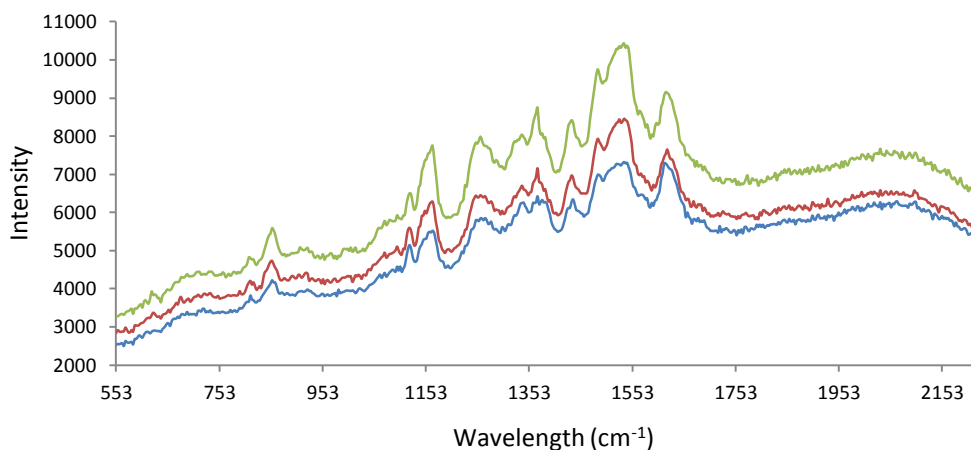


Figure 3.19: SERS spectra of three different EGFP-NP conjugates, measured at 514.5 nm, acquired for 20 secs.

Figure 3.19 illustrated the similarity in all three conjugates with respect to SERS

behaviour and demonstrated the success of the conjugation technique developed thus far. Consequently, it was necessary to optimise the SERS conditions to obtain maximum signal intensity, with a view to determining a limit of detection for this system.

### 3.5 OPTIMISATION OF SERS CONDITIONS

In order to optimise the SERS conditions, a number of parameters were investigated including: volume of protein added; the incubation time; acquisition time; and method of pH control. In all previous work, a protein concentration of  $1 \times 10^{-7}$  M was used. When using SERS as an analytical technique, it is ideal to have monolayer coverage of the nanoparticle (typically achieved by using a concentration of  $1 \times 10^{-6}$  M of small molecule Raman reporters). However, as proteins are larger than the average dye molecule it was surmised a slightly lower concentration of  $1 \times 10^{-7}$  M was required.

Acquisition time was the first parameter to be studied and samples were analysed using 1, 10 and 20 second acquisitions. Figure 3.20 shows the results from this experiment, although as the signal was obtainable at 1 second, it was weak and therefore it was determined that the best acquisition time was 20 seconds.

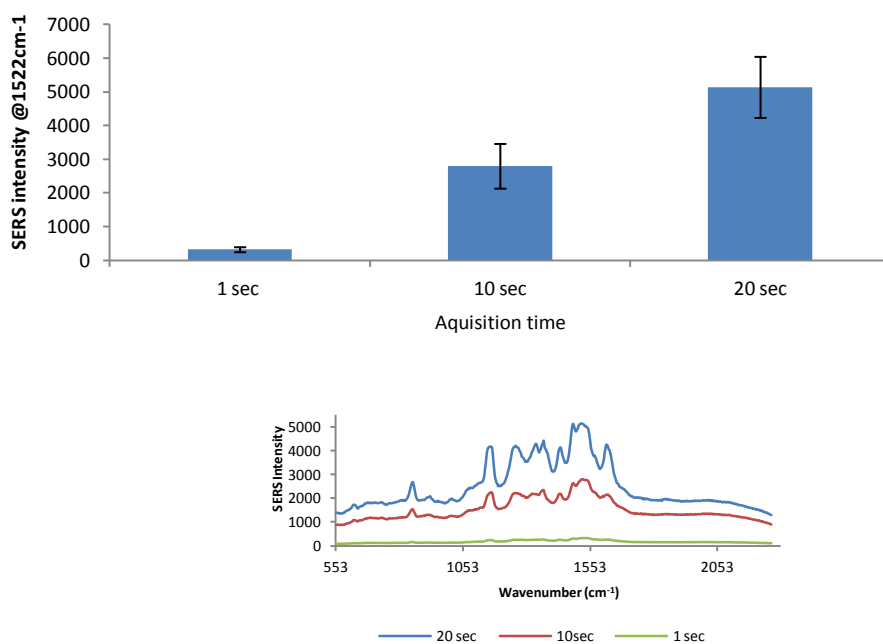


Figure 3.20: Optimisation of acquisition time for SERS of EGFP-NP conjugates, analysed using the peak at 1522 cm<sup>-1</sup>.

Following from this, the length of incubation was investigated: a conjugate was synthesised; and a spectrum was taken every 30 minutes over the course of 53 hours.

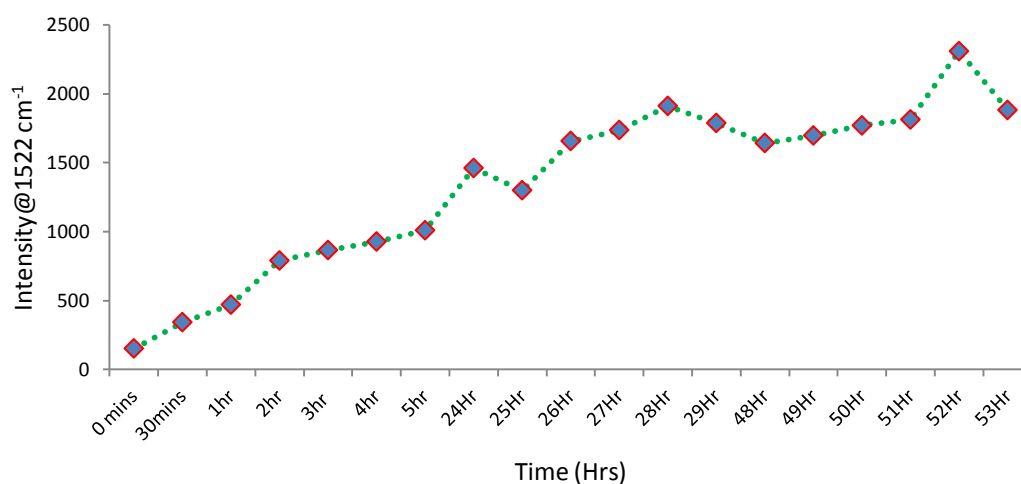


Figure 3.21: Optimisation of incubation time of EGFP-NP conjugates, analysed at 514.5 nm recorded every 30 minutes over the course of 53 hours.

As it can be seen from the data in figure 3.21 the signal increases gradually until it reaches a plateau at around 28 hours. It was determined that this was the optimum time for the best signal. Therefore, the samples were incubated in excess of 28 hours before analysis was carried out. The high cost associated with EGFP meant sample usage had to be strictly controlled. The volume of GFP was altered from a minimum of 10  $\mu\text{L}$  to 60  $\mu\text{L}$ . Introducing a protein volume greater than 60  $\mu\text{L}$  caused the conjugate to aggregate after only a few minutes. The samples were synthesised and analysed in triplicate.

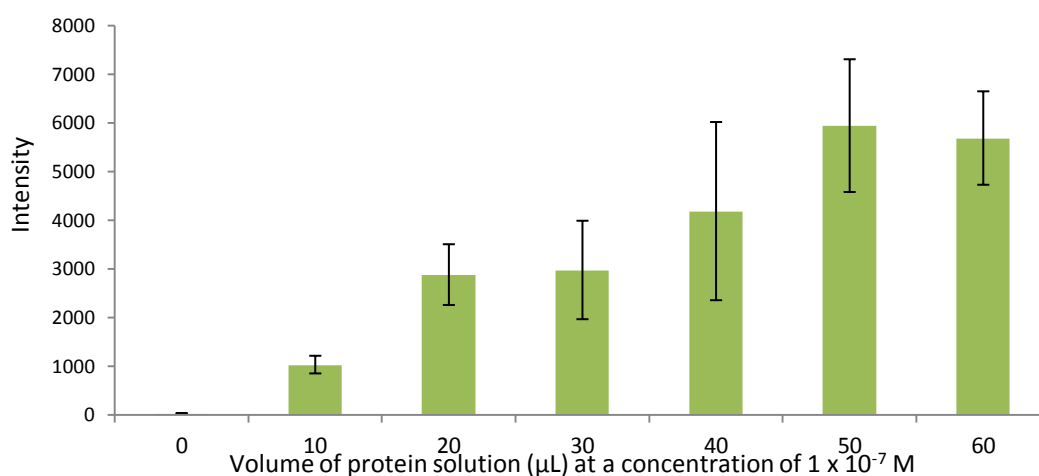


Figure 3.22: Optimisation of volume addition of EGFP added to silver citrate colloid, determined by analysing the peak at  $1522\text{ cm}^{-1}$

The results shown in figure 3.22 indicated the optimum volume of EGFP in the colloidal system was 50  $\mu\text{L}$ . Following successful solution based detection and optimisation of EGFP using electrostatic interactions, the next stage was to obtain a limit of detection for this system.

### 3.6 LIMIT OF DETECTION STUDY

Fluorescence spectroscopy has typical detection limits in the region of  $10^{-12}\text{ M}$ . It was therefore necessary to investigate the limit of detection of the current system developed, in order to determine whether the solution based detection of EGFP

could compete with the commercial techniques used in this field.

Initially this was carried out using serial dilutions from a starting concentration of  $1 \times 10^{-7}$  M until a concentration of  $1 \times 10^{-10}$  M solution was reached; dilutions were carried out using  $1 \times$ PBS. As a control  $1 \times$ PBS was used and added to the colloid in the same ratio as the sample. At each concentration and control, the samples were analysed in triplicate.

Figure 3.23 shows the results that were obtained were very disappointing. It appeared that the signal disappeared after the highest concentration of  $1 \times 10^{-7}$  M (equating to a final protein concentration of  $1.1 \times 10^{-8}$  M).

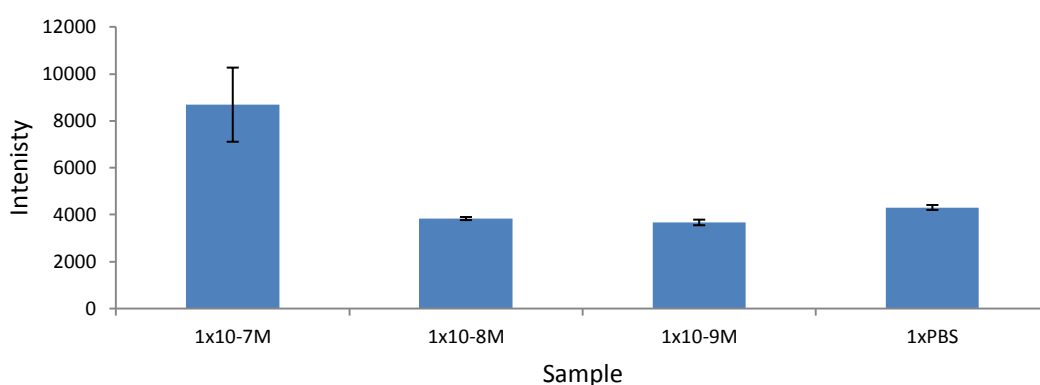


Figure 3.23: Initial LOD study of solution based detection of EGFP. Analysed at 514.5 nm using the peak at  $1522 \text{ cm}^{-1}$ .

Whilst these results were disappointing, they were also surprising. It appeared that below the final protein concentration of  $1.25 \times 10^{-8}$  M the conjugates were not forming successfully. In order to identify a true LOD of the system, an in depth concentration profile was required. Once more the concentration points were determined using serial dilutions. The concentration points used are shown in table 3.5.

Table 3.5: Concentrations used in second LOD study.

Original protein concentration	Final protein concentration in conjugate
$1 \times 10^{-6}$ M	$1.1 \times 10^{-7}$ M
$7 \times 10^{-7}$ M	$7.7 \times 10^{-8}$ M
$5 \times 10^{-7}$ M	$5.5 \times 10^{-8}$ M
$3 \times 10^{-7}$ M	$3.3 \times 10^{-8}$ M
$1 \times 10^{-7}$ M	$1.1 \times 10^{-8}$ M
$7 \times 10^{-8}$ M	$7.7 \times 10^{-9}$ M
$5 \times 10^{-8}$ M	$5.5 \times 10^{-9}$ M
$3 \times 10^{-8}$ M	$3.3 \times 10^{-9}$ M
$1 \times 10^{-8}$ M	$1.1 \times 10^{-9}$ M
$7 \times 10^{-9}$ M	$7.7 \times 10^{-10}$ M

The conjugates were synthesised, as detailed in section 8.4. At each concentration, the samples were prepared in triplicate and analysed as such using a 514.5 nm laser. In figure 3.24 the results can be observed; the greatest intensity can be seen when a protein concentration of  $3 \times 10^{-7}$  M was used. This can be most likely attributed to the formation of a monolayer of EGFP around the nanoparticle surface. When analysing the data and using the 3xsignal/noise ratio - which compares the analyte signal to the noise measured on the blank - it was found that the limit of detection for the system was when a protein concentration of  $3 \times 10^{-8}$  M was used.

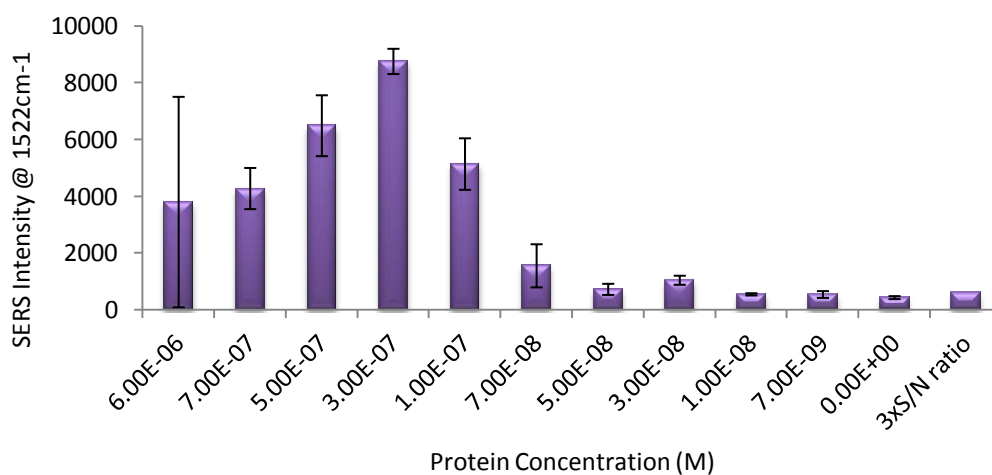


Figure 3.24: Limit of detection study with additional concentration points. Compared to the signal to noise ratio.

The spectra at concentration below  $3 \times 10^{-8}$  M are shown in figure 3.25 which demonstrates the LOD was indeed at  $3 \times 10^{-8}$  M. The drop in intensity observed at a protein concentration of  $5 \times 10^{-8}$  M which could be explained by interference caused by enhancement of different vibrational bands. However, it can be clearly seen there was a distinct signal assigned to EGFP. Such signals are absent in the spectra of the concentrations below  $3 \times 10^{-8}$  M.

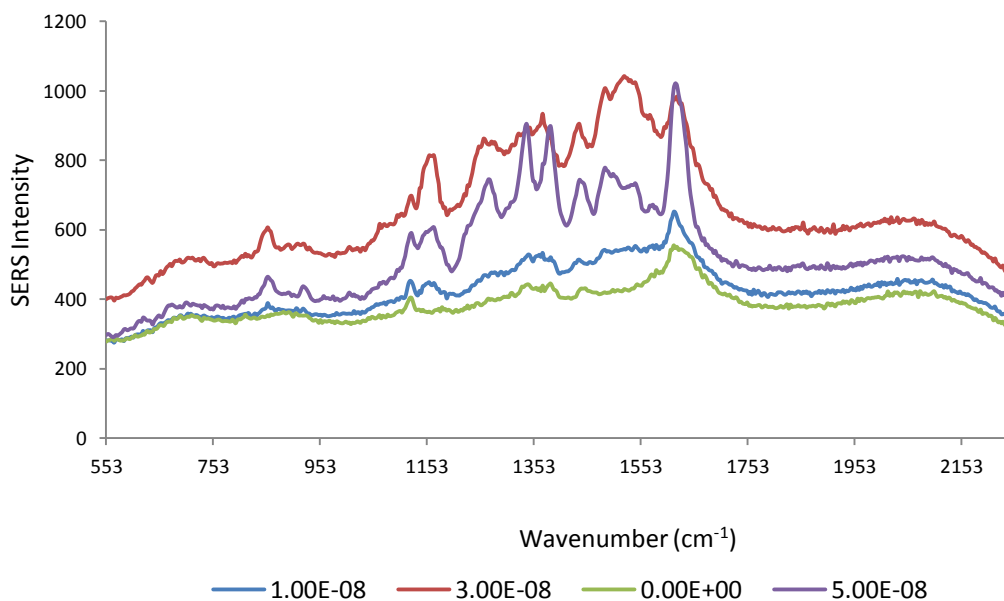


Figure 3.25: SERS spectra of EGFP conjugates from LOD study.

The results for the highest protein concentration are highly varied as indicated by the large error bars. This could be attributed to ‘overloading’ the nanoparticle surface with protein, thus inhibiting the inherent fluorescence quenching property of the nanoparticles. At the time of writing, this is the first limit of detection profile of solution based SERS detection of EGFP. The limit is within the nanomolar range which is a respectable limit of detection. However, it was surmised that inefficient aggregation could be occurring in the colloidal system and by increasing the aggregation, greater signal intensity could be achieved leading to lower detection limits. UV-vis analysis was used to investigate the aggregation process of the conjugates at different stages of incubation.

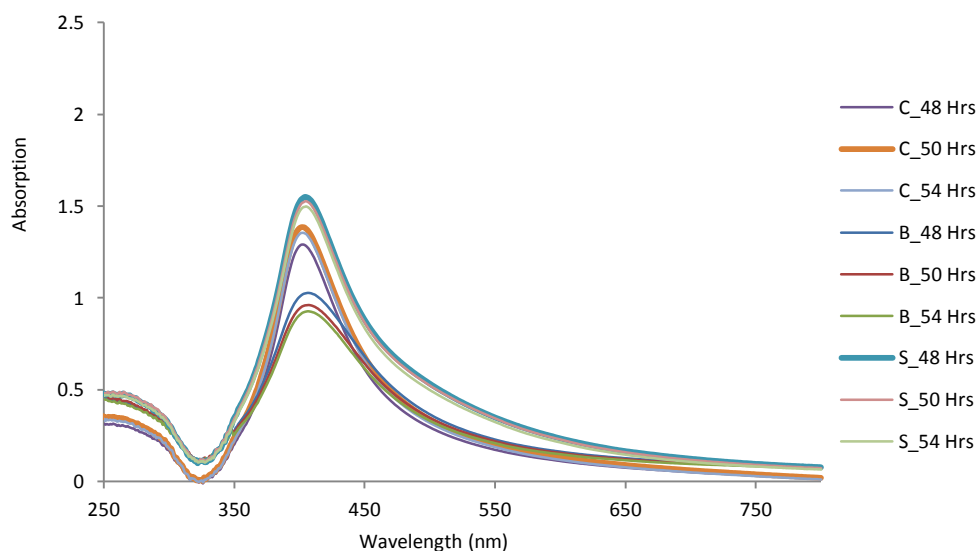


Figure 3.26: UV-Vis spectra of EGFP conjugate at various times of incubation

The data shown in figure 3.26, suggested that the extent of aggregation did not have an overwhelming effect on the system. It was therefore surmised that the introduction of aggregation to the system would improve the LOD. The choice of aggregating agent is important as the dynamic nanoparticle environment is delicate and the introduction of an external aggregating agent could have an adverse effect on the sample.<sup>87, 148</sup> Four common aggregating agents were investigated:  $MgSO_4$ ; NaCl; spermine; and poly-L-lysine.  $MgSO_4$  and NaCl are common salts that are often used to investigate the interactions at the nanoparticle surface, whereas spermine and poly-L-lysine have been used ubiquitously in SERS detection of DNA due to their ability to be able to ‘bring’ DNA onto the nanoparticle surface (arising from their positive charge).

Conjugates were prepared as detailed previously and to each conjugate an equivalent volume of aggregating agent was added. SERS results are shown in figure 3.27.

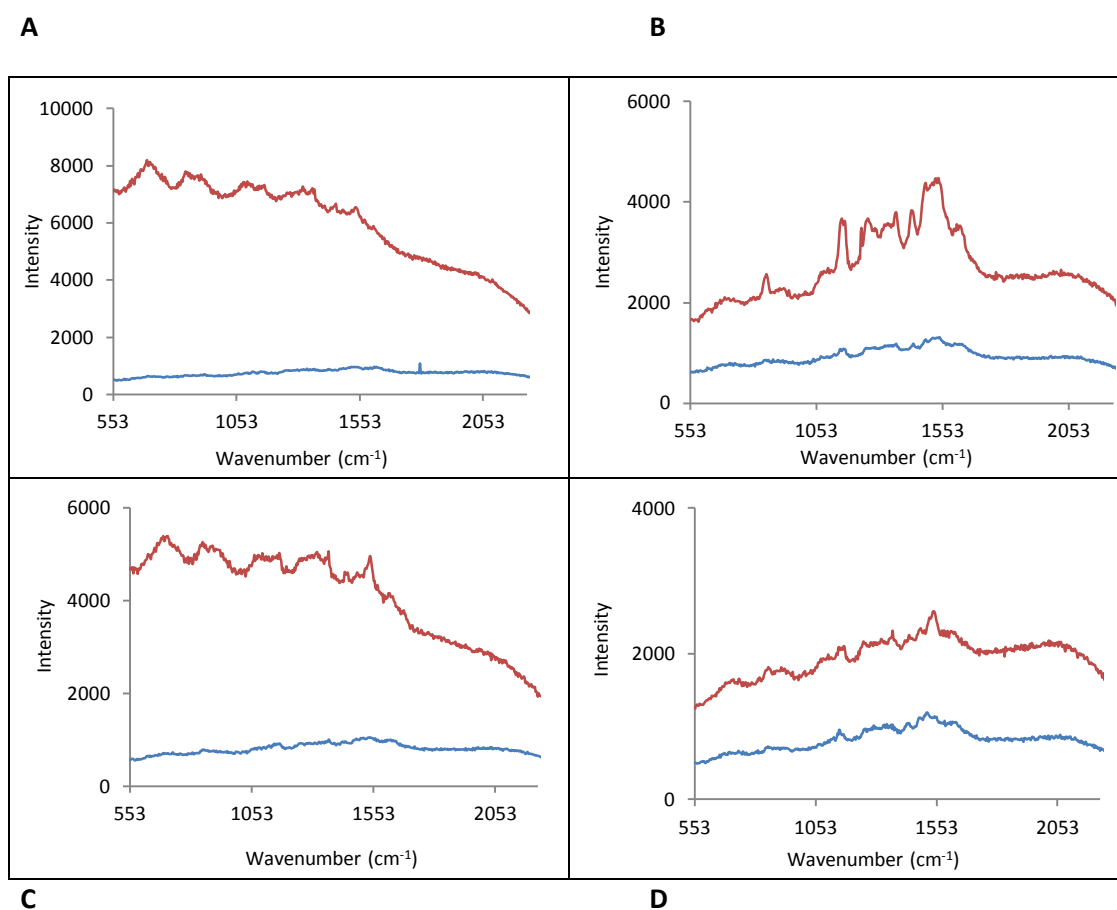


Figure 3.27: SERS spectra showing pre and post-aggregation of EGFP-NP conjugates with four common aggregating agents. **A:** 0.1 % spermine **B:** 10 mM MgSO<sub>4</sub> **C:** 0.01 % Poly-L-lysine **D:** 1 M NaCl. Blue lines are spectra pre aggregation and red lines are post aggregation. Spectra analysed at 514 nm and acquired for 20 sec.

It was found that the use of MgSO<sub>4</sub> produced the greatest enhancement and clarity of signal - this was not unexpected. NaCl and MgSO<sub>4</sub> produced much better results when compared to spermine and poly-L-lysine. Spermine and poly-L-lysine are both positively charged (making them ideal aggregating agent for negatively charged DNA) but not suitable for use with positively charged protein species such as EGFP i.e. both positive charges would repel each other thus preventing aggregation from occurring. To ensure that the signal remained from the chromophore and was not affected by the aggregation agent, a negative control sample was analysed. This consisted of addition of 50  $\mu$ L of 1 $\times$ PBS to the AgNPs. The spectrum obtained displayed no definitive peaks as shown in figure 3.28.

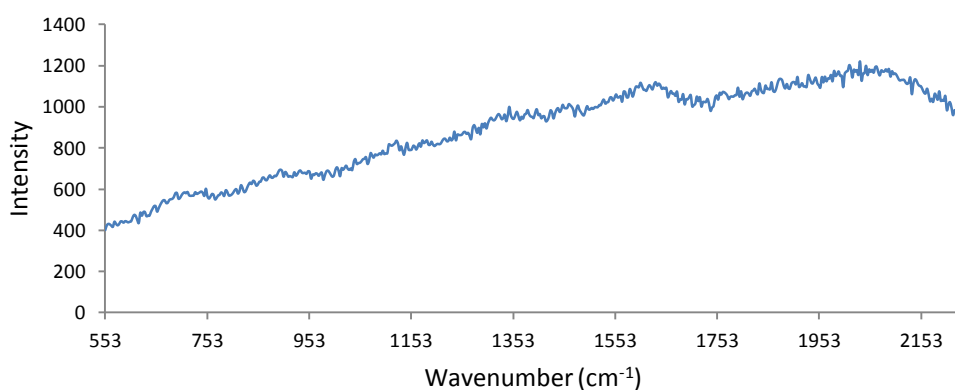


Figure 3.28: 1xPBS conjugate aggregated with MgSO<sub>4</sub>, analysed at 514 nm with a 20 sec acquisition time.

After confirming MgSO<sub>4</sub> as the most suitable aggregation agent, it is necessary to optimise the volume added to the system. Various volumes of 10 mM MgSO<sub>4</sub> were added to conjugate containing a final protein concentration of  $3.3 \times 10^{-8}$  M (equivalent to monolayer coverage). The results of this optimisation study are shown in figure 3.29. The signal was recorded pre-aggregation and post-aggregation. The best volume to use appeared to be 40  $\mu$ L, however the difference in increased signal between 20-50  $\mu$ L was minimal.

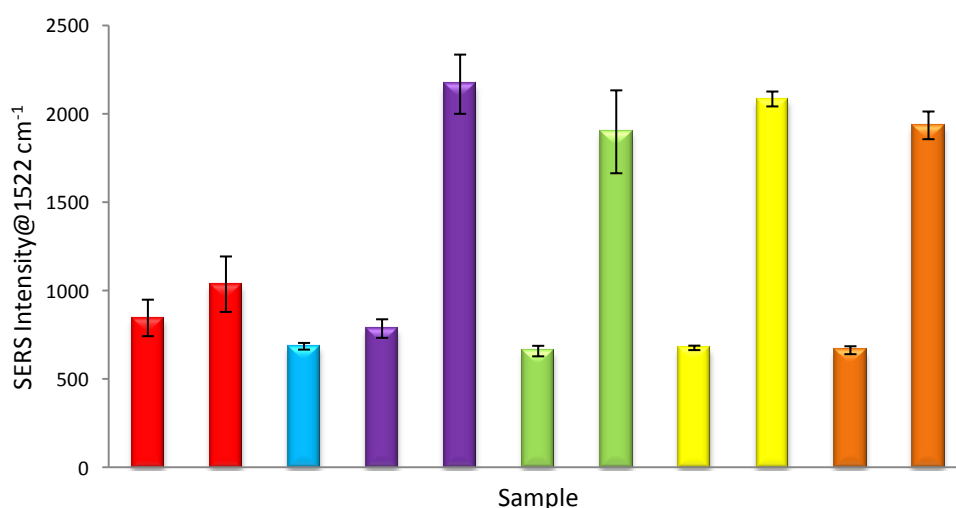


Figure 3.29: Optimisation of MgSO<sub>4</sub> addition, various volumes were added: Red - 1  $\mu$ L; Blue - 10  $\mu$ L; Purple - 20  $\mu$ L; Green- 30  $\mu$ L; Yellow- 40  $\mu$ L; and Orange- 50  $\mu$ L

The limit of detection study was repeated. The protocol was modified slightly by

the addition of  $\text{MgSO}_4$  (20  $\mu\text{L}$ , 10 mM) after a 50 hour incubation period. SERS analysis was carried out, before and after the addition of aggregating agent. As shown in figure 3.30 there is a slight improvement in the LOD. Once more when using the 3x signal/noise ratio as the baseline, it can be seen the LOD was when a protein concentration of  $1 \times 10^{-8}$  M was added. This was vastly improved upon  $3 \times 10^{-8}$  M for the system prior to aggregation, shown by figure 3.30.

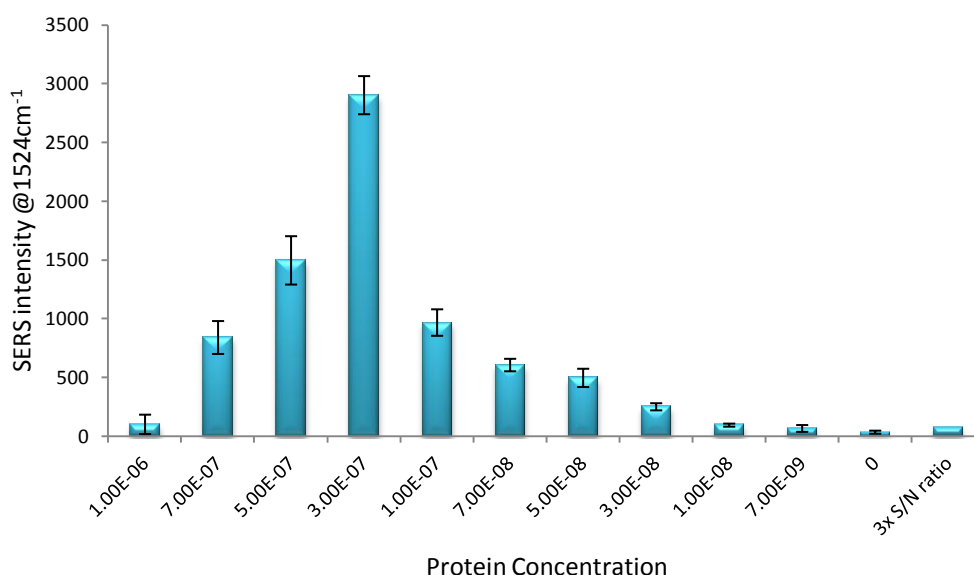


Figure 3.30: LOD introducing aggregation to the EGFP samples using 10 mM  $\text{MgSO}_4$ . The chart is based on analysis of the  $1524 \text{ cm}^{-1}$  peak of EGFP

The lower detection limit could be linked to the reduction in fluorescent background observed when using an aggregating agent. The limit of detection is competitive, however it was hypothesised that a more direct method of pH modification could further lower the limit of detection.

### 3.7 ALTERNATIVE ROUTES OF DETECTION

The electrostatic method outlined previously had been successful and reliable at providing a good limit of detection. However it was decided to investigate different methods in an attempt to lower the limit of detection. The first method was an investigation into the process to induce the positively charged EGFP. It was decided to re-suspend the EGFP in citrate buffer. Citrate buffer has a pH

range of 3 - 6.2. As the pI of the protein is 5.62 it produced the net positively charged EGFP, consequently removing the requirement to pH adjust the silver citrate colloid. To test this hypothesis, 2.9  $\mu\text{L}$  of the stock EGFP solution in 1 $\times$ PBS was diluted to  $3\times 10^{-7}$  M with 10 mM citrate buffer. The samples were then incubated with unmodified silver citrate colloid for 50 hours. The results obtained are shown in figure 3.31.

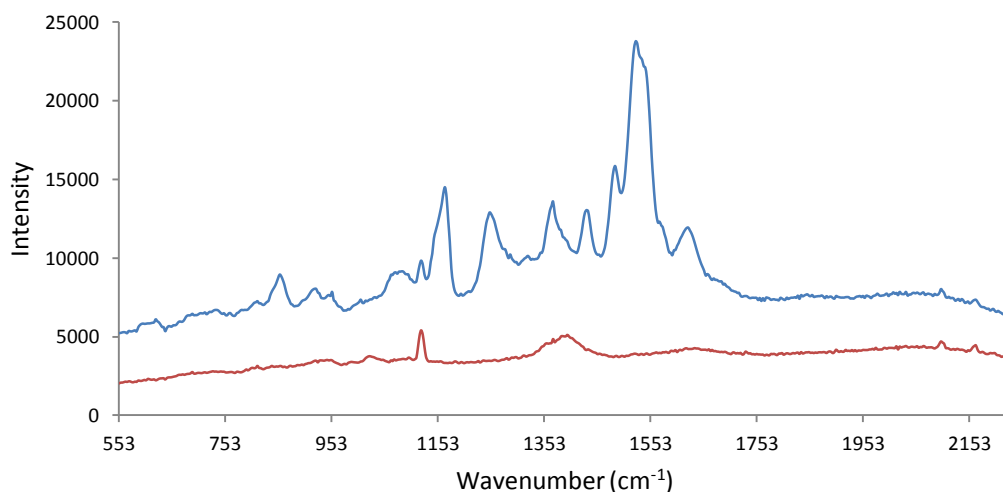


Figure 3.31: Representative SERS spectrum of EGFP using citrate buffer method. SERS obtained using 514 nm, 20 second acquisition time.

Figure 3.31 shows that it was possible to detect EGFP using this method. However, when both colloid pH adjustment and protein pH adjustment protocols were compared, spectral differences were observed, as shown in figure 3.32.

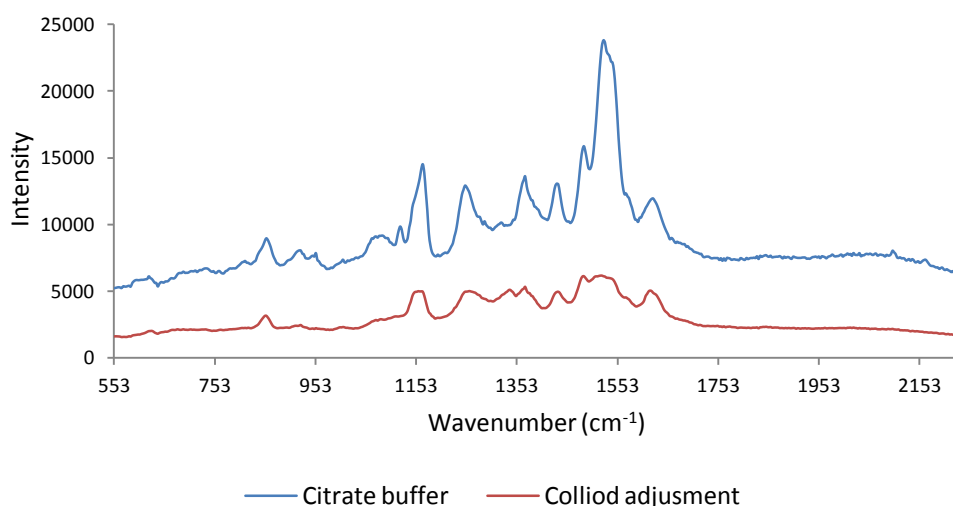


Figure: 3.32 Comparison of vibrational peaks between the two different methods of SERS detection of EGFP. Red line represents EGFP detection using pH adjusted colloid and blue line was obtained from the citrate buffer method.

Although the characteristic peaks were coincident between the two spectra, greater enhancement was observed for the electrostatic method. In order to assess the suitability of this method for SERS detection of EGFP, a limit of detection study was carried out. The same concentrations as before were used in this study; the only difference being the buffer that these samples were suspended in. The samples were incubated for 50 hours and the analysed at 514.5 nm for 20 seconds. As before the samples were synthesised and analysed in triplicate (figure 3.33).

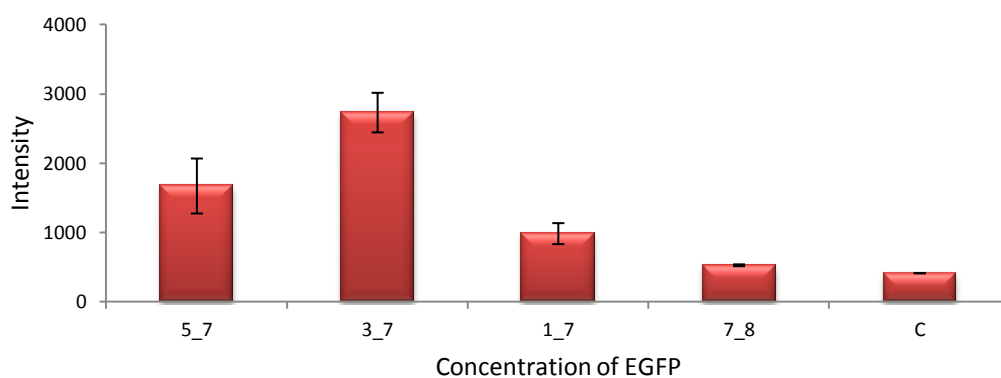


Figure 3.33: LOD using citrate buffer method for detection of EGFP by SERS. Based upon vibration peak at 1525 cm<sup>-1</sup> in spectrum. SERS obtained using 514 nm and 20 secs.

It can be seen by the graph that the limit of detection for this method is much higher than that of the colloid pH adjustment. The highest concentration of protein ( $1 \times 10^{-6}$  M and  $7 \times 10^{-7}$  M) could not be analysed as these samples aggregated irreversibly before analysis could take place. This indicated that this system was unreliable and would not serve as a replacement to the colloid pH adjustment.

In a second attempt to gain a more sensitive LOD, positively charged nanoparticles were investigated. Positively charged species are able to pass through the cell membrane more easily and thus the pursuit of positively charged particles could allow for the use of EGFP functionalised nanoparticles in cell based experiments.

It has been shown that polyelectrolytes have been utilised with metallic nanoparticles, by using a technique called layer by layer absorption (LbL). LbL is essentially a collection of electrostatic interactions holding the system together. A paper published by Kahraman *et al.* demonstrated the use of positively charged polyelectrolytes to form stable silver nanoparticles.<sup>149</sup> It has been noted in literature that coating nanoparticles with polyelectrolytes protects them from aggregation and increases the general stability of the system. Due to the negatively charged silver citrate colloid used in this work a positive polyelectrolyte was chosen, namely Poly(diallyl ammonium chloride) (PDAA), as shown in figure 3.34.

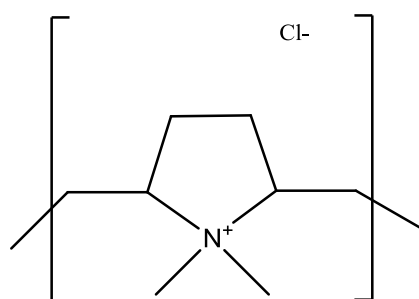


Figure 3.34: Structure of PDAA

Caruso *et al.* demonstrated the benefit of carrying out the LbL technique using nanoparticles, namely the ability to monitor the growth progression and layer

build up on the nanoparticles (by observing in changes in the surface plasmon).<sup>150</sup> The first step in the formation of positive silver nanoparticles was to determine what concentration of PDDA solution should be used. Typically, a 10 mg/mL polyelectrolyte solution is used.<sup>151</sup> Consequently, three different solutions of PDDA were tested; 1, 5 and 10 mg/mL. The presence of NaCl in the system is vital to enable the correct formation of layers and it was found that a 1 mM solution of NaCl provided the stability for the formation of the layer, without cause aggregating of the bare silver citrate colloid.

For the synthesis of the positive colloidal solutions, typically 8 mL of bare AgCit was added to 40 mL of 1 mM NaCl. A 1 mL aliquot of this nanoparticle solution was taken and 100  $\mu$ L of the polyelectrolyte was added. Each concentration of PDDA was investigated at this stage. Each solution was incubated for 45 minutes, after which the conjugate was centrifuged at 5000 rpm for 20 minutes. The supernatant was removed and the pellet was re-suspended in 1 mM NaCl. The success of this conjugation was monitored using the surface plasmon. The results are shown in figure 3.35.

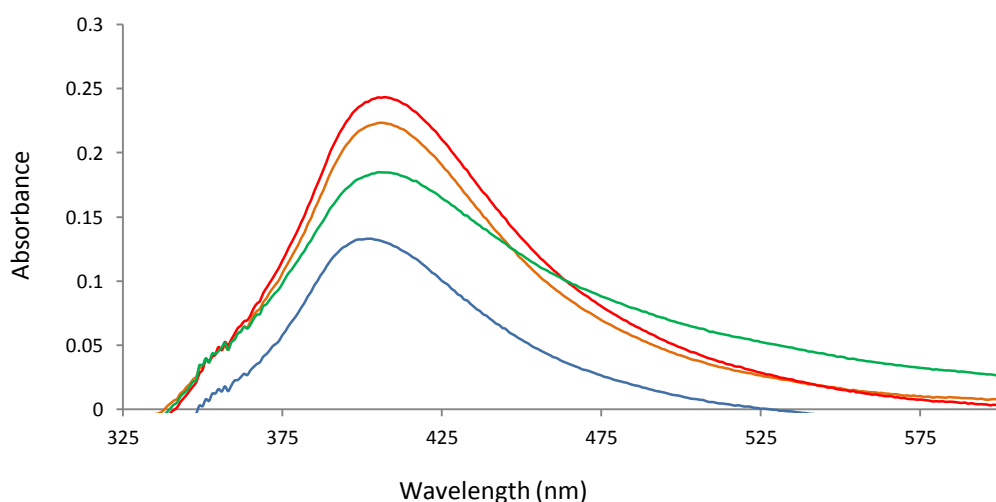


Figure 3.35: Uv-Vis spectra of PDDA AgNPs: Bare AgNPs (blue line); 10 mg/mL PDDA coated AgNPs; 5 mg/mL PDDA coated AgNPs (green line); and 1 mg/mL PDDA coated AgNPs (orange line)

The results showed that the optimum concentration of PDDA to use was 10 mg/mL. To ensure that the colloidal solution was indeed positively charged, zeta

potential measurements were taken. The results are shown in figure 3.36.

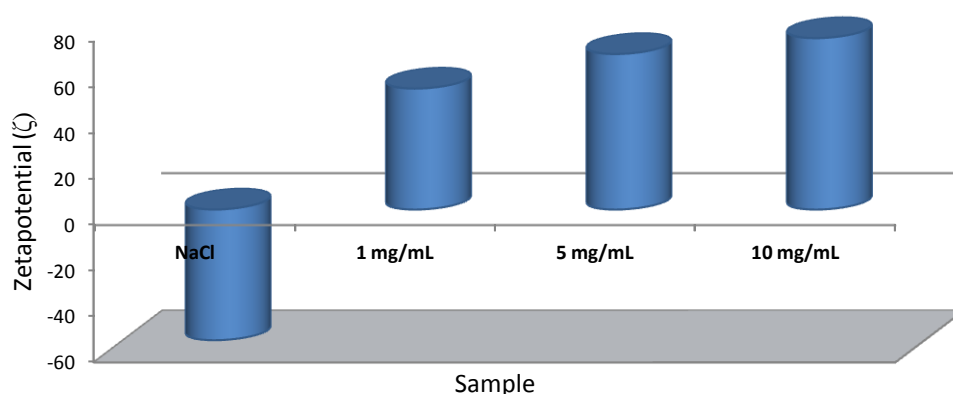


Figure 3.36: Zeta potential measurements of PDDA nanoparticles. From L to R: Bare silver citrate nanoparticles suspended in 1 mM NaCl; silver nanoparticles coated with 1 mg/mL PDDA; AgNPs coated with 5 mg/mL; and AgNPs coated with 10 mg/mL PDDA

Stable nanoparticle suspensions have a zeta potential of around  $\pm 40 \zeta$ . It can be seen from the figure that the bare unmodified nanoparticles in 1 mM NaCl have a zeta potential of -57.1. On conjugation of the PDDA, the charge on the nanoparticles becomes positive, as shown in figure 3.37. With increasing PDDA concentration the nanoparticle suspension charge increases. This data confirmed that the formation of the PDDA layer to AgNPs had been successful.

After confirming the successful formation of the PDDA layer, it was necessary to test the compatibility of these positively charged particles with EGFP. As the zeta potential shows, the PDDA conjugates were not particularly stable on addition of both PBS and EGFP which caused immediate aggregation. Due to this, the samples were analysed immediately instead of incubating for 50 hours. The spectra were analysed using a 514.5 nm laser and the results are shown in figure 3.37.

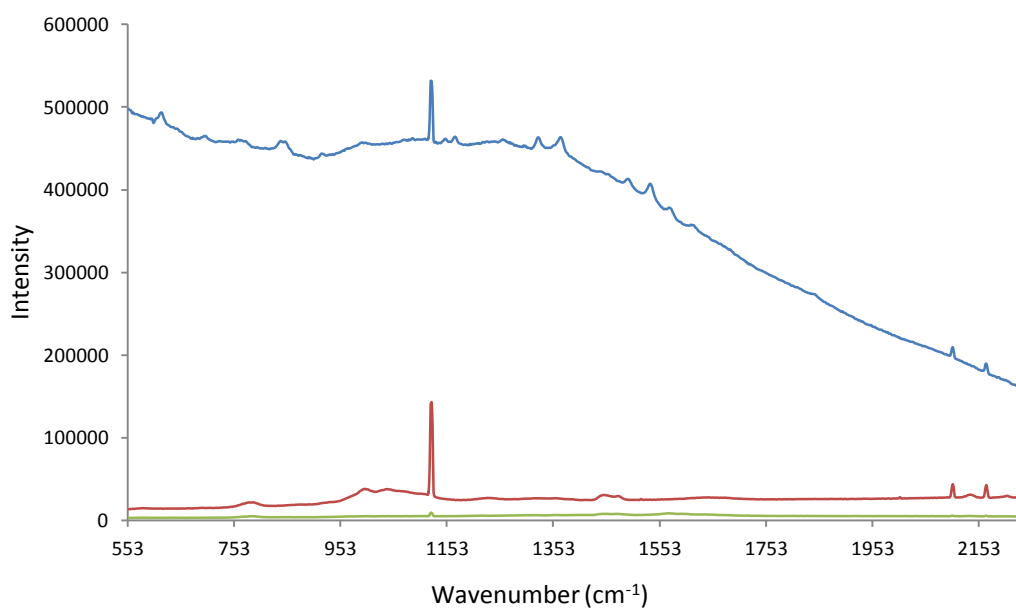


Figure 3.37: SERS of PDDA NPs analysed at 514 nm, 20 second acquisition time: Bare PDDA nanoparticles (red line); PDDA nanoparticles and 1xPBS (green line); and EGFP and PDDA nanoparticles (blue line)

The figure shows a signal from the EGFP which correlated to the results previously obtained. It can be seen that the peaks are not present in either controls: bare PDDA; and PDDA NPs in PBS (thus indicating the signal originates from the chromophore of EGFP). The results were encouraging, though it should be noted that there was a high fluorescent background from the EGFP sample indicating that the AgNP was not quenching the protein effectively. This could be due to the presence of the polyelectrolyte layer acting as a barrier between the protein and the nanoparticle thus inhibiting the ability to quench the fluorescence. Although signal was obtained, it was evident that this system was not a stable one. This was further reinforced by the difficulty in synthesising the PDDA nanoparticles reproducibly. Due to the success of earlier methods, the decision was taken to end this line of investigation and revert back to use the original method which was more reliable and reproducible.

### 3.8 RED FLUORESCENT PROTEIN (RFP)<sup>20, 135, 152</sup>

The term fluorescent proteins (FP), covers a wide range of proteins. GFP was the pioneer which enabled the development of many more FPs. Every FP is derived from

a form of GFP. As discussed previously there are slight differences namely colour and physical properties, such as brightness and maturation time. All modifications are a result of slight mutations in the amino acid sequence. When this modification occurs at the chromophore, it was proposed that as SERS is a vibrational spectroscopy, this technique could be used to identify the differences between FPs, therefore opening the way to multiplexing FPs.

Red Fluorescent Protein (RFP) is a protein in common use but which possess a different chromophore to EGFP. Also known as DsRed, the protein was first isolated from coral by Yarbrough *et al.*<sup>153</sup> This protein differs in quaternary structure compared to EGFP: RFP is a tetramer; whereas EGFP is a monomer. Another difference between the two proteins is the UV-vis emission profile of the corresponding chromophore. The maximum absorbance of GFP occurs at 509 nm compared to the 589 nm for RFP. The longer wavelength of the emission of RFP is thought to be linked to the mechanism of the formation of the chromophore. The generation of such a protein sparked intense interest within the scientific community as the development of this protein could lead to the generation of a more efficient FRET partner for EGFP.<sup>27</sup>

RFP is a 28 kDa protein with a broad excitation and emission bands, occurring at 558 nm and 583 nm. It has been noted in literature that all of the fluorescent proteins fold into the same conformation - RFP is no different. The confirmation contains an 11-stranded  $\beta$ -barrel with a coaxial central helix. The chromophore of RFP differs slightly from the chromophore of EGFP due to the greater degree of conjugation present in RFP and consequently, such a difference could be detected using SERS analysis. These chromophores are shown in figure 3.38.

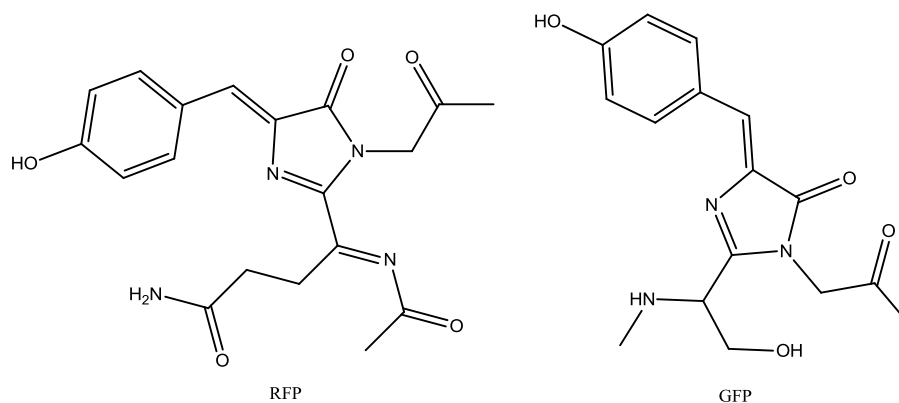


Figure 3.38: Structural comparison between chromophores of RFP (left) and EGFP (right).

As illustrated in figure 3.38 it is the presence of an imine group within RFP which accounts for the structural difference. The success of the electrostatic method for generating EGFP conjugated silver nanoparticles allowed the developed protocol to be tested for generating RFP conjugates. The pI had to be first identified to determine what modification - if any - had to be carried out on the colloidal solution to promote absorption of the protein. The pI of RFP was found to be 8, therefore indicating that at pH 7 (corresponding to the native pH of unmodified silver citrate), RFP would be net positively charged showing there was no requirement for the modification of the pH of the colloid that was used with RFP.<sup>152</sup> However, as carried out previously, the Raman of RFP was recorded at 785 nm, as with EGFP. The results are shown in figure 3.39

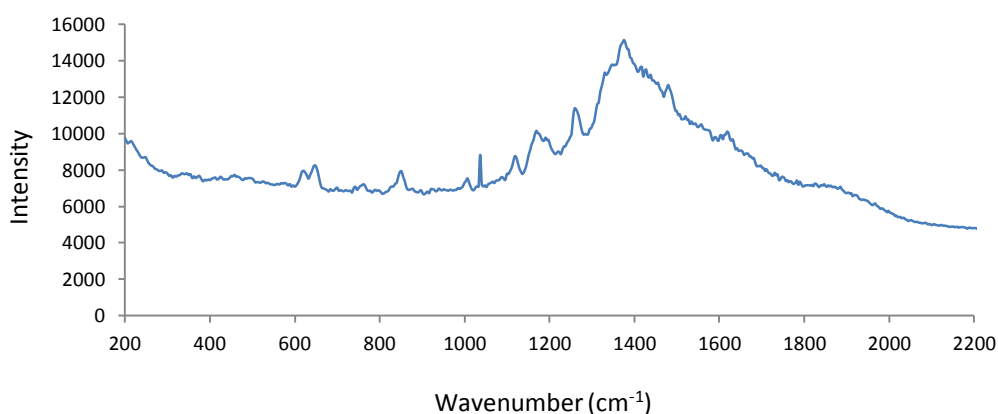


Figure 3.39: Raman of RFP analysed at 785 nm

Following on from this, RFP was incubated in 50  $\mu\text{L}$  aliquot at an initial concentration of  $1 \times 10^{-7}$  M with unmodified silver citrate colloid for 50 hours. It was then analysed at both 514.5 and 633 nm. It was not possible to predict which laser wavelength would lead to the greatest signal enhancement. The results are shown in figure 3.40.

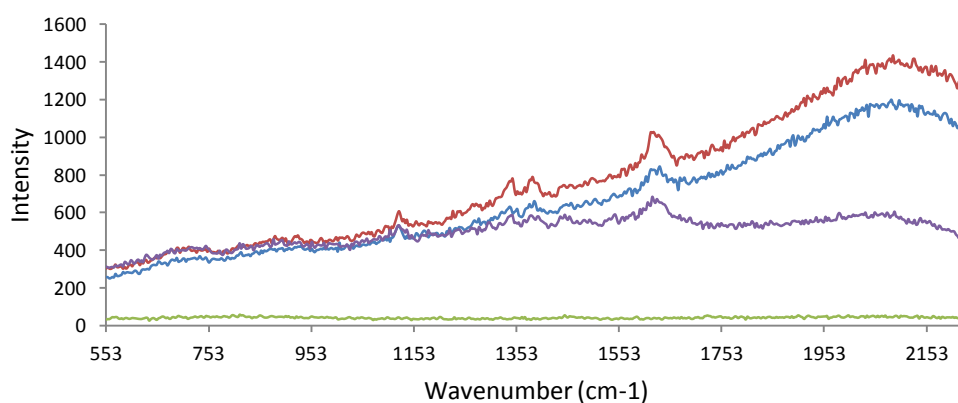


Figure 3.40: SERS spectra of RFP-NP conjugates using the electrostatic method. Red, blue and green line depict RFP samples, while the purple line depicts the control sample.

As shown in in figure 3.40, no observable peaks were present at either of the two wavelengths. This can be seen from the comparison of the two positive RFP conjugate samples (red and blue lines) with the control line (purple line). Unlike the equivalent work with EGFP, the RFP conjugates did not display similar results. There could have been a number of reasons, for example: protein concentration; incubation time; or the pH of the colloid. Even though the pH of

the colloid was 7 and should of ensured a net positive charge, it was decided that to ensure RFP was in a positive state the pH of the colloid was lowered. This was achieved by using was 0.01% nitirc acid as before. Once more they failed to produce a positive result after SERS analysis. It has been noted in literature that RFP does have several disadvantages over EGFP: including slower maturation; and as a tetramer it is a much weaker FP. It was therefore decided that the use of electrostatics attachment to the nanoparticle surface was insufficient when using this protein and thus, another method was sought. In order to increase the robustness of nanoparticle attachment, a chemical method was investigated, in the hope that it would transform the relatively weak electrostatic interactions into a stronger one based on covalent bonding.

Thioctic acid is a small disulfide containing organic acid, as structure shown in figure 3.41. It has been used in a variety of applications in conjunction with gold and silver nanoparticles, including conjugates which have been used to probe the nanoparticle surface by using nitroxide modified thioctic ester spin labelled probes.<sup>154</sup> This commercially available organic compound has found popularity with gold nanoparticles due to the nature of the thiol gold interaction. Dougan et al. have shown thioctic acid modified oligonucleotide gold conjugates possess a greater stability when compared to monothiol modified oligonucleotide gold conjugates. It was found when these conjugates were exposed to DTT, the monothiol conjugates had aggregated completely within a minute, whereas the thioctic acid conjugates had half-lives between 140 - 245 minutes.

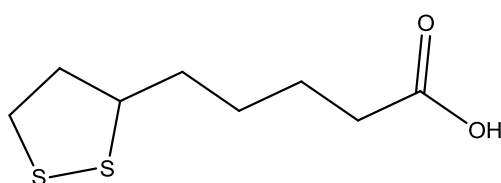


Figure 3.41: Structure of thioctic acid

The enhanced stability has been attributed simply to the presence of the disulfide. It is proposed the disulfide bond is broken and a covalent bond is formed from each sulfur to the gold surface. As the electrostatic method had not yielded successful RFP conjugates, it was decided that the protein should be anchored

onto the nanoparticle surface using thioctic acid. This was chosen due to its high stability and its small size which would not disrupt the distant dependant enhancement factor. Amide chemistry was employed once more between the carboxylic acid of thioctic acid and an available primary amine of RFP.

Maya *et al.* had demonstrated the successful formation of thioctic acid conjugates, whereby the pH of the colloidal solution was altered using a weak sodium hydroxide solution to bring the pH within a range of 9 -11 - this was achieved with the addition of 10 mM NaOH. The thioctic acid nanoparticles (TA-NPs) were prepared as discussed in section 8.4

The now thioctic acid functionalised nanoparticles were suspended in carbonate buffer. This buffer was used due to the pH requirements for amide couplings. Alkali pH is essential and the buffering range of carbonate solution is pH 9.2 – 10.8, making this ideal for amide formation. EDC and NHS were added to the conjugate and incubated for 30 minutes followed by the addition of RFP; the mechanism for this activation is shown in figure 3.42.

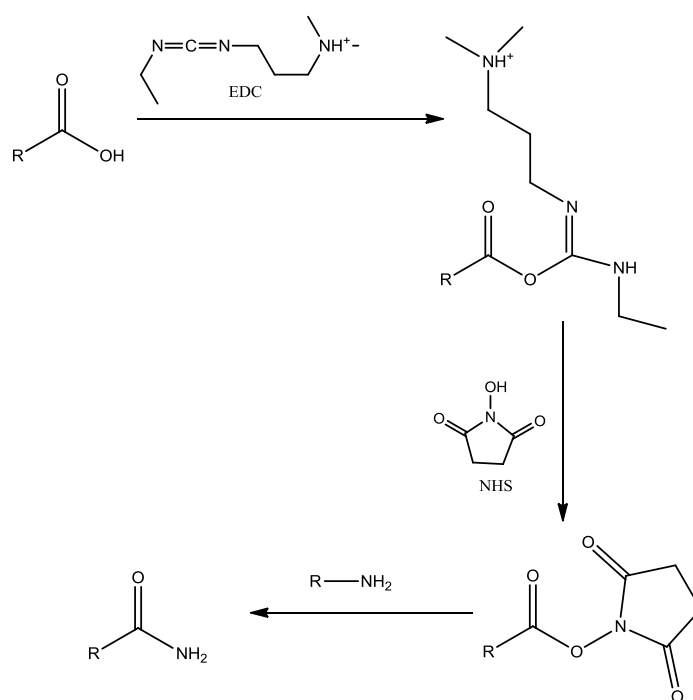


Figure 3.42: Mechanism of EDC and NHS in the formation of an amide.

Following successful conjugation of the RFP-TA@AgNPs the next step was to

analyse the conjugates using SERS. Due to the red shift in the chromophore of RFP (582 nm, compared to 509 nm of EGFP) it was decided to exam these conjugates at both 514.5 nm and 633 nm. The results shown in figure 3.43 were promising, however out of ten identical conjugates, only one remained stable enough to allow for analysis.

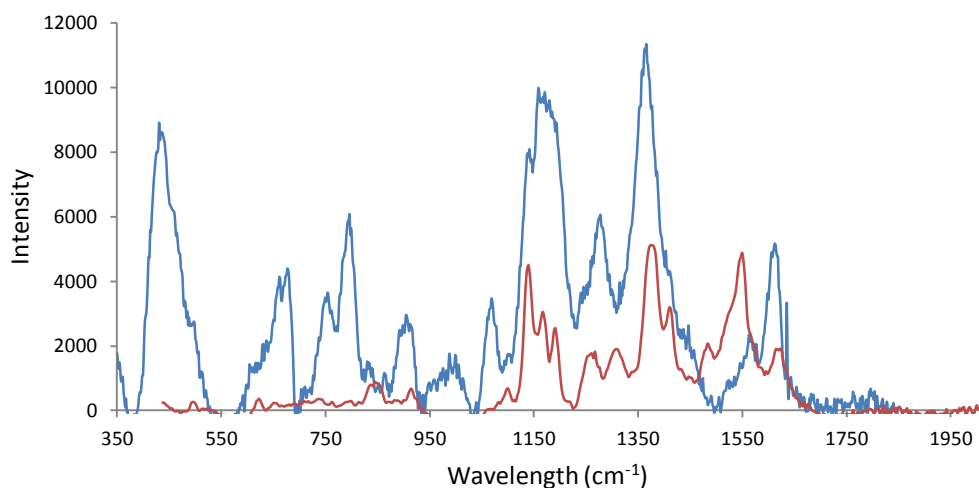


Figure 3.43: SERS spectra of RFP conjugates at 514 nm (red line) and 633 nm (blue line)

Due to the poor reproducibility of the synthesis method, the use of a lower concentration of RFP was attempted.

RFP was diluted to make a concentration of  $1 \times 10^{-7}$  M and once again RFP-TA@AgNPs were synthesised.

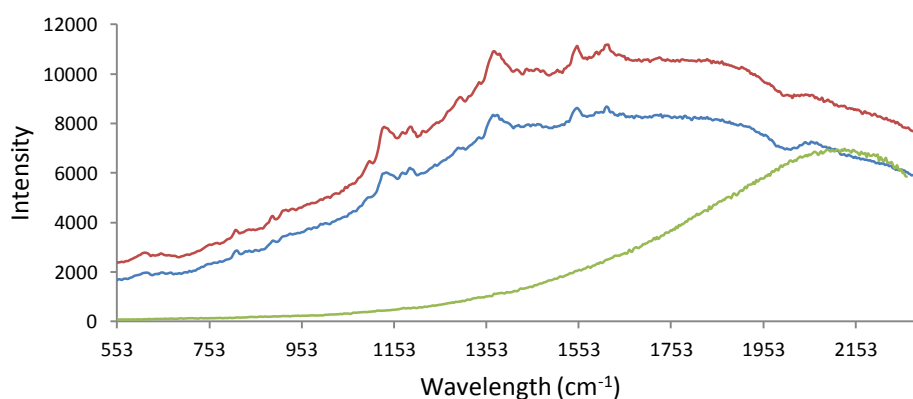


Figure 3.44: SERS spectra of RFP-TA@AgNP conjugates and the effect of dilution on the spectra: No dilution (green line); dilution of sample with water by half volume (blue line); and dilution by water by 100%.

Initial analysis with a 514.5 nm laser caused high fluorescent backgrounds to be observed (shown in figure 3.44). However, upon dilution of the sample it was shown vibrational signals began to emerge from the fluorescent background. The concept of dilution vs signal intensity is not a new one, with Faulds *et al.* demonstrating through strategic dilutions, an optimum colloid concentration can be elucidated and good signal enhancement achieved, where previously only fluorescence was observed.<sup>111</sup> This set of results has shown that through subtle modifications of the SERS analysis method, detection of RFP has been achieved. At the date of writing this the first reported solution based SERS detection of RFP.

However, additional work would be required to further develop this line of research, which has been detailed in section 7.

At the outset of this work, one of the main aims was to explore the possibility of designing a multiplex system using several different types of fluorescent proteins, whereby the proteins could be detected simultaneously using SERS analysis.

### 3.9 MULTIPLEXING

The initial investigation of determining whether or not EGFP and RFP were suitable multiplexing partners involved analysis of their respective SERS spectra. Although RFP conjugates gave positive SERS results when interrogated with both 633 and 514.5 nm wavelengths, EGFP conjugates could only be analysed at 514.5 nm and thus it was the latter wavelength that was selected for initial comparison work between the two conjugates. Figure 3.45 shows the overlaid spectra obtained when SERS analysis was carried out on the conjugates individually.

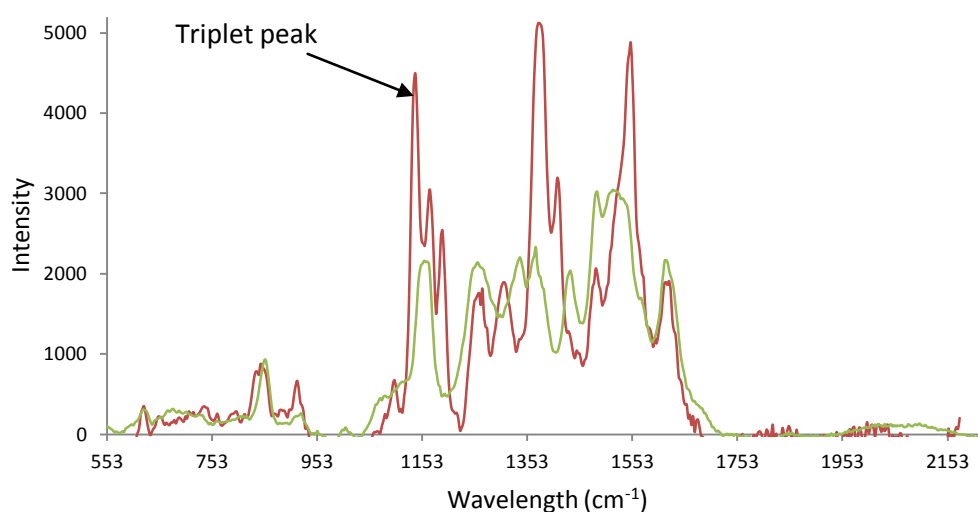


Figure 3.45: Overlaid SERS spectra of EGFP conjugate (green line) and RFP conjugate (red line) analysed at 514 nm and aquired for 20 seconds.

It appeared that there were several distinct peaks in each protein between the region of 1140 - 1191 cm<sup>-1</sup>. RFP exhibited a triplet peak whereas EGFP showed only a single peak at 1166 cm<sup>-1</sup>. This could be used as a defining peak between each protein. These initial results were very promising - indicating the potential for multiplexing. The next step would be to carry out SERS of a mixed solution of each type conjugate, as discussed in section 7 – Future Work.

# CHAPTER 4: THE DETECTION OF NANOPARTICLES IN CELLS THROUGH THE USE OF TAT PEPTIDE.

## 4.1 INTRODUCTION

Cellular membranes are the gateway to the cell and its components. They are composed of layers of phospholipids, which form a hydrophobic inner layer and a hydrophilic outer layer, as shown in figure 4.1. This layer is formed and sustained by forces such as, Van der Waals, non-covalent, electrostatics and Hydrogen bonds. It is very difficult to deliver macromolecules into cells as these molecules are polar due to the components which construct the macromolecule. The difficulty arises because of the hydrophobic layer.<sup>155</sup>

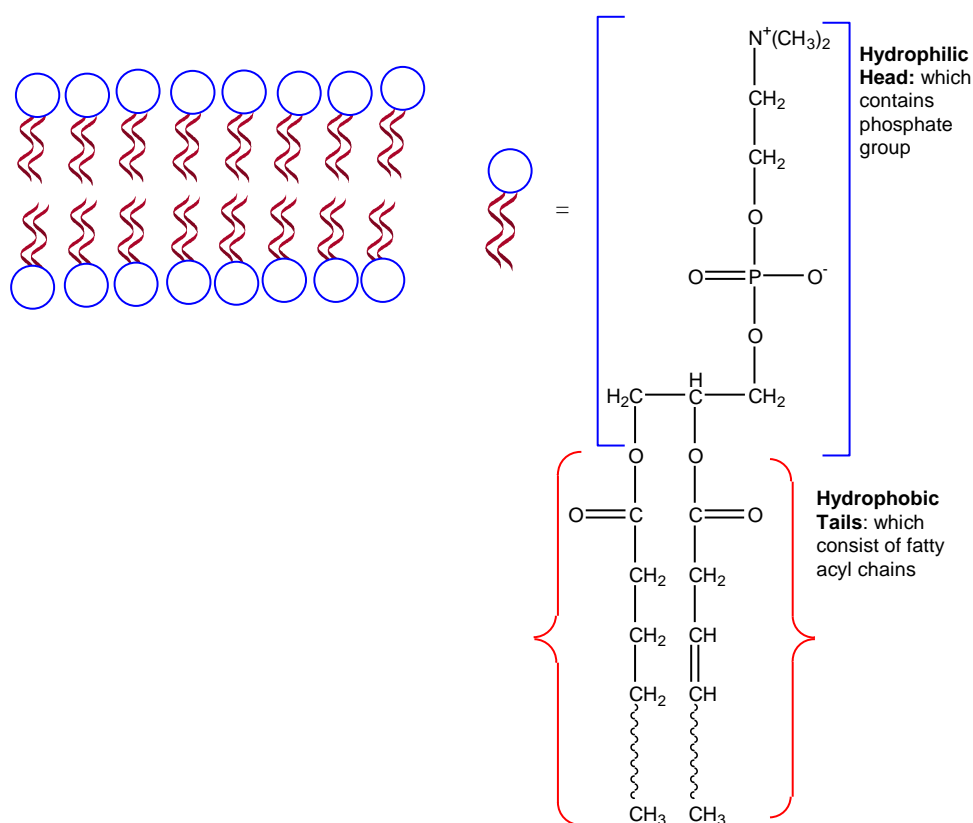


Figure 4.1: Arrangement of the phospholipid groups forming the cellular membrane which is composed of bipolar molecules: the hydrophobic tails which are comprised of fatty acids and the hydrophilic head which contains the phosphate group.

The membrane is constructed from a variety of proteins, which act as receptors and can guide specific molecules across the membrane. Membranes operate on a selective permeability basis: it allows some substances to cross it more easily than others. In general, biological membranes allow only small molecular weight uncharged drugs or biomolecules with the appropriate ligand to enter. However, there are other methods to cross the cell membrane. These methods are collectively grouped under the term endocytosis and generally the process involves engulfing the macromolecule.

There are several types of endocytosis, with two of these being: Receptor-mediated endocytosis (also known as clathrin-dependant endocytosis) and Pinocytosis. Receptor-mediated endocytosis is where the cell will internalise the molecule on the basis of a specific interaction, budding of the membrane occurs creating a vesicle which contains sites for a specific interaction of the molecule that has been internalised, however this method can only be employed if the appropriate receptors are present. Pinocytosis is where absorption occurs via a non-specific pathway for molecular uptake.

Regardless of these methods, cellular membranes have shown to have extremely poor permeability to substances such as drugs, DNA and proteins. Not only do membranes have poor permeability to such molecules, but even if they do successfully cross the membrane, they can be 'lost in transit' and fail to reach their target.

#### 4.1.1 Cell Penetrating Peptides

The discovery of Cell Penetrating Peptides (CPP) revolutionised the process of membrane crossing. Additionally, it was found that this type of peptides were internalised by most cell types. CPPs originated from research concerning the HIV-1 TAT *trans*-activating factor.<sup>156</sup> It was discovered that full biological activity remained when this protein was incubated with cell cultures, suggesting that the protein remained intact and that it had crossed the cellular membrane. Lebleu *et al.* assigned the ability to cross the membrane to the short sequence of basic amino acid-rich peptides.<sup>157</sup> From this initial research a variety of CPPs were discovered which are classified into two different groups, which are defined by the source of these short peptides. The first group contains peptides which have been sourced from a

protein's Protein Transduction Domain (PTDs) - such as TAT. The second group contains peptides, which are chimera proteins, in that they contain sections from two or more other proteins. An example of this is Transportan, which is derived from mastoparan and galanin.

The discovery of these unique attributes - allowing of membrane translocation and cellular localisation - propelled this research to the forefront of the cellular biology field.<sup>158, 159</sup> TAT was one of the first CPPs to be discovered.

#### 4.1.2 TAT Peptide

Labelled as the first cell penetrating peptide - discovered in the 1980s during research into AIDS - TAT consists of 86 amino acids. It was during research into the structural and functional components of TAT, that scientists discovered that it could be internalised by HeLa cells. The primary sequence of this peptide is shown in figure 4.2.

Arg-Arg-Arg-Gln-Arg-Arg-Lys-Lys-Arg-Gly-Tyr

Figure 4.2: Primary sequence of Tat Peptide

More remarkably, TAT was able to deliver its target to the nucleus, which is a notoriously difficult task.<sup>160</sup> A review by Eric Vives showed that in 50% of cases studied using CPPs; TAT peptide was the peptide of choice.<sup>161</sup> Reasons for the enduring popularity of TAT include: the efficiency of the peptide to cross and deliver substrates into a range of different cellular compartments; and the ease with which it can be attached to other molecules.<sup>162</sup> It has been shown that TAT has been attached to and allows the uptake of many different molecules. Nie *et al.* showed that TAT can be attached to quantum dots (QDs) and the cellular uptake & transportation of these TAT labelled QDs, could be monitored through the fluorescence of the QDs.<sup>163</sup> CPPs have been used to insert drug molecules, proteins and oligonucleotides into cells for *in vivo* studies.<sup>164-166</sup> In recent years, there has been an interest in combining nanoparticles with these CPPs. This interest has been sparked by the development of using Raman based techniques for cellular detection as the particles can be tailored to the investigator's requirements. In addition, the similar size of nanoparticles to biomolecules means the insertion of nanoparticles does not disturb the cellular

environment. Nanoparticles are often used - although not exclusively - in the technique Surface Enhanced Resonance Raman Scattering (SERRS). This vibrational technique has been used to study the localisation and factors that affect cellular uptake of nanoparticles.

Metallic nanoparticles have been implemented in the study of TAT. In 2005, De la Fuente *et al.* demonstrated that gold nanoparticles coated with tiopronin followed by conjugation of TAT peptide, crossed the cellular membrane and could enter the cell nucleus and accumulate.<sup>167</sup> Tiopronin was used to allow an EDC/NHS coupling of TAT to the nanoparticle and used Transmission Electron Microscopy (TEM) to view the nanoparticles in the cells. More recently, Steven *et al.* published a paper detailing the conjugation of TAT peptide to a DNA sequence to facilitate the conjugate in crossing the cellular membrane.<sup>162</sup> The most recent publication in this area came from Gregas *et al.* who have shown that nanoparticles are more readily taken up by cells when TAT peptide is attached, compared to nanoparticles not functionalised with TAT peptide.<sup>168</sup> SERS was used in this technique also, through the formation of a mixed monolayer on hydroxylamine stabilised silver nanoparticles.

## 4.2 RESULTS AND DISCUSSION

The ultimate aim of this work was to visualise the nanoparticles within the cellular environment using SERS. Research by Chithrani *et al.* has investigated the factors which affect the rate of cellular uptake of gold nanoparticles of different sizes and shapes.<sup>169</sup> In this research it was shown that 50 nm nanoparticles were the optimum sized nanoparticles to be used. This size of nanoparticles was taken up by mammalian cells which are faster and at a higher concentration rate when compared to the other sizes.<sup>50, 170, 171</sup> Chithrani *et al.* hypothesised that bare gold nanoparticles entered the cell using receptor mediated endocytosis, through non-specific adsorption of serum proteins onto the surface of the nanoparticles.<sup>172</sup> However, there are several known pathways that enable nanomaterials to enter cells.<sup>14, 173</sup> These include; non-specific endocytosis; direct microinjection; electroporation and targeted uptake.<sup>170</sup>

This information would suggest that there is no further requirement to modify the nanoparticle for entry into the cell, however with non-specific endocytosis, there is a risk that the nanoparticles will not get to their ultimate target site within the cell. It has been reported that the methods of direct microinjection and electroporation are not suitable: they are harsh techniques that cause the disruption of the cellular membrane, to get the desired product into the cell. Additionally, only a certain number of cells can be used meaning the volume of experiments is limited. Therefore the use of TAT would increase the chance of the nanoparticles entering the cell and localisation. Fluorescein is a commonly used dye for conjunction to biomolecules; the TAT peptide was purchased from CSS Albachem with a fluorescein label attached which was achieved via the formation of an amide bond, as shown in figure 4.3.

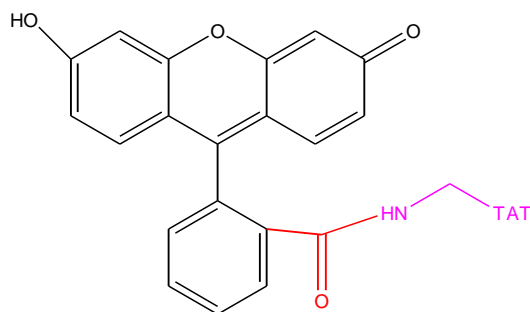


Figure 4.3: Fluorescein labelled TAT peptide, the red coloured functional group is from the fluorescein and the pink from the TAT peptide.

However, to be used in conjunction with nanoparticles, an intermediary linker was required to connect the peptide with the nanoparticle surface. It was important, however, to not create a large distance, >10 nm, such that there would be a loss of SERS enhancement. For the formation of the linker several factors had to be considered. There was the requirement for a surface seeking group for attachment to the nanoparticle surface. Sulfur interaction with gold and silver has been documented in literature. This bond is strong and there is a natural attractiveness.<sup>174</sup> It has been shown that when disulfides have been used to anchor molecules to the nanoparticle surface, they provide greater stability of the nanoparticle conjugate avoiding uncontrolled aggregation, when compared to a monothiols.

One of these disulfides is the compound thiocetic acid which has been shown to produce enhanced stability compared to monothiol modifications. This is also the case in harsh conditions such as high salt concentration which normally causes nanoparticle aggregation. This compound has an additional benefit, containing a carboxylic acid. This molecule provides an efficient method for modification through the formation of an amide bond. For these reasons it was decided thiocetic acid should be used as an anchor compound to the nanoparticle surface thus ensuring the carboxylic acid is free for further reaction.

TAT peptide is rich in arginine residues. As such there are a number of primary amines available for reaction, which can once more be exploited for the formation of an amide. To enable Raman detection of the eventual conjugate the TAT peptide was conjugated via an amine group to the dye fluorescein.

With the view that this nanoparticle capable conjugate of thiocetic acid and TAT peptide linker would be incorporated into cells it was surmised that a stabilising group was required to ensure the conjugate did not aggregate under cellular

conditions, if aggregation did occur this would have an adverse effect for cellular uptake. Polyethylene glycol (PEG) groups have long been used in conjunction with polypeptides and proteins.<sup>175, 176</sup> The popular use of this polymer is attributed to its ability to provide stability to a system. It has been shown that this stability is far reaching, with colloids having been reported to be stable for more than six months after the original synthesis.<sup>177</sup> In addition, PEG molecules have been shown to improve bio-availability when in the cell.<sup>178-180</sup> Brown *et al.* published a paper on the synthesis of a linker, which incorporated all of the desired components: thioctic acid and a PEG linker. This particular linker was used to complex anti-cancer drugs to nanoparticles.<sup>181</sup> This linker used thioctic acid to tether the drug to the nanoparticle surface and a PEG compound with a free amine, to be used as a point of further reaction. It was decided to synthesise the linker used by Brown *et al.* as shown in figure 4.4, which had used a PEG<sub>41</sub> compound. The PEG group had a dual functionality of stability and providing a free amine, to be used as a point of further reaction.

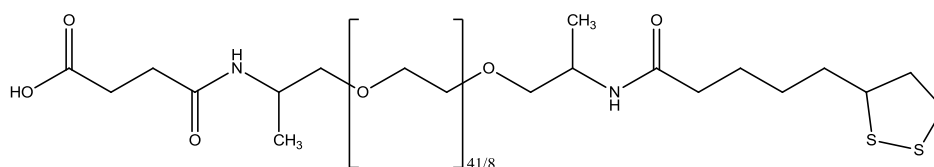
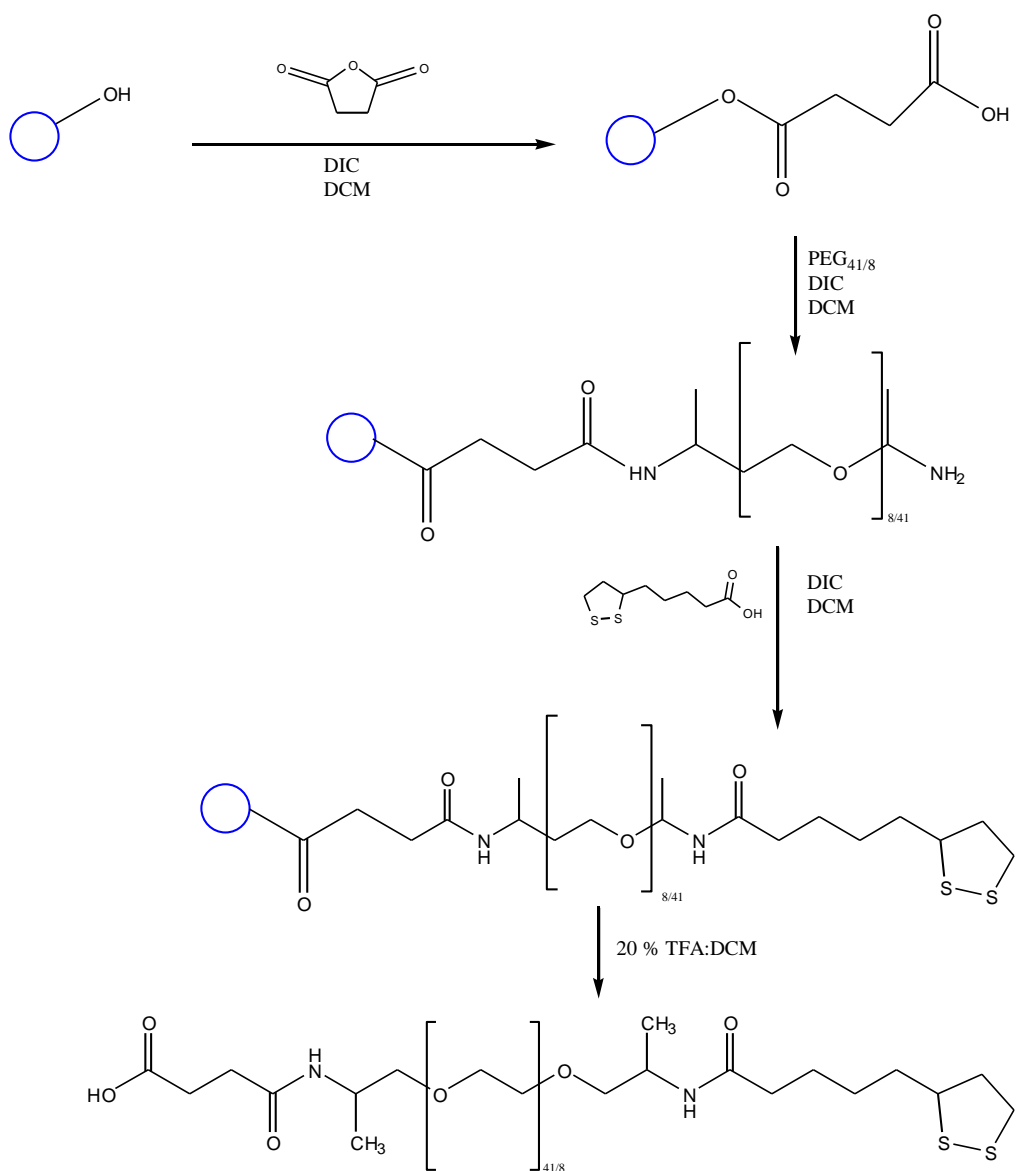


Figure 4.4: Structure of PEG<sub>41</sub> and PEG<sub>8</sub> linker.

There were several factors to consider for the synthesis of this linker as thioctic acid is extremely delicate: decomposition occurs above 30 °C and when exposed to light. PEG molecules compounds have the additional consideration that they are polymers and as such purification is difficult. Another factor that had to be considered was the length of PEG to use. Previous work had also shown that use of PEG<sub>3</sub> proved to be too unstable, forming irreversible aggregation of the nanoparticles.<sup>218</sup> Therefore two lengths of PEG were chosen, the first; PEG<sub>41</sub>, had great stability potential, however, there was apprehension over the eventual distance between the nanoparticle and the absorbed material; and so PEG<sub>8</sub> was chosen as the second length.

### 4.3 LINKER SYNTHESIS

To avoid a difficult and lengthy purification process, the linker was synthesised using a solid support: Wang resin. Solid phase synthesis solves the problem of purification: reagents are added in excess and the unused material is washed away, therefore avoiding the need to separate the desired product and any unwanted by-products. Wang resin has an alcohol group as an end terminus, which was incompatible with the commercially available PEG compounds, which have two terminal primary amino groups. To enable successful coupling, the alcohol group was converted to a carboxylic acid. This was easily achieved using established succinic anhydride chemistry. The PEG<sub>8</sub> and PEG<sub>41</sub> linkers were synthesised in the same manner, as shown by scheme 4.1.



Scheme 4.1: Synthesis of PEG-thioctic acid linker

Wang resin was suspended in dichloromethane (DCM), succinic anhydride was added and the reaction mixture was refluxed for 6 hours. The resin was then captured by filtration then washed with DCM and methanol three times respectively, before drying the resin under vacuum.

One disadvantage of solid phase synthesis is the inability to monitor the success of reactions with traditional techniques such as NMR, therefore colorimetric resin tests were used to estimate the success of the reactions. Malachite green oxalate is used to test for the presence of acid groups. A sample of dried resin was added to a malachite

green oxalate solution, dissolved in ethanol, followed by addition of triethylamine. After a 5 minute incubation period, the resin was filtered and washed with DCM. The result of the test is shown in figure 4.5. The colourless resin remained green, indicating successful modification of the resin.



Figure 4.5: Acid group test, positive result (left) compared to negative result (right).

Following confirmation of successful conversion, the resin was suspended back into DCM, before the addition of the PEG group (41 or 8) with a coupling agent, such as diisopropylcarbodiimide (DIC). The reaction mixture was agitated at room temperature for 18 hours and once more, the resin was filtered and washed with DCM and methanol. The success of the reaction was determined using another colour test. Ninhydrin is a popular stain for the visualisation of TLC plates; it indicates the presence of both primary and secondary amines through a blue and purple colour respectively. A sample of the resin was suspended in a ninhydrin solution and heated to reflux, whereby the resin changed from colourless to a blue colour, as shown in figure 4.6.



Figure 4.6 Ninhydrin test: free amine containing resin (left); and negative resin (right)

The penultimate step was the attachment of thioctic acid. The resin was suspended in DCM and to this suspension; thioctic acid and DIC were added and agitated for 18

hours at room temperature. Filtration, DCM/methanol washing and finally vacuum drying were carried out. As before, the resin was tested using Ninhydrin to confirm successful coupling. In this instance, the resin remained colourless - indicating no free amine groups remained.

The final step involved the cleavage of the linker from the resin; trifluoroacetic acid (TFA) is a commonly used cleavage reagent. The resin was suspended in DCM for the final time, to which 6 mL of TFA was added to create a 20 % solution. This reaction solution was agitated at room temperature for 6 hours, before carrying out a final filtration. The filtrate was retained and the resin was discarded. The excess TFA was neutralised through the addition of triethylamine,  $^1\text{H}$  NMR and MALDI mass spectrometry confirmed the successful synthesis of these linkers.

## 4.4 CONJUGATE SYNTHESIS

With the successful synthesis of two linkers, the next step was to investigate the conjugation of the linkers with nanoparticles. Traditional synthesis of gold nanoparticles yields 13 nm gold nanoparticles. It was surmised that these nanoparticles should be used initially. The gold nanoparticles were synthesised via the Turkevitch method using sodium tricitrate as the stabilising agent. This method produced gold nanoparticles with a  $\lambda$  maximum of 520 nm. The  $\lambda$  maximum of gold nanoparticles is an indicator of the dynamics at the nanoparticle surface, if there is a change at the nanoparticle surface, a shift in the  $\lambda$  maximum is observed due to the sensitivity of the SPB to its local environment. Likewise, the surface plasmon of silver nanoparticles can be used in the same manner to detect surface changes and provide confirmation of attachment of substrates to the nanoparticle surface. Silver citrate nanoparticles are synthesised using a modified Lee and Meisel method, which typically produces 35 nm diameter nanoparticles with a  $\lambda$  maximum of 400 nm.

#### 4.4.1 PEG<sub>41</sub>-AUNP INVESTIGATIONS

The PEG<sub>41</sub> linker was used initially as it was surmised that the larger PEG group would provide enhanced stability to the nanoparticle conjugate, which could prove to be an advantage when exposed to a cellular environment.

##### 4.4.1.1 GOLD NANOPARTICLES AND PEG<sub>41</sub>

The linker was dissolved in MeOH to a final concentration of  $10^{-5}$  M. In each sample, 1 mL of 17 nm AuNPs was added to varying volumes of linker. Between 10  $\mu$ L - 100  $\mu$ L of linker was added to the colloidal solution and the samples were left to incubate for 15 hours, followed by centrifugation. Thereafter, the supernatant was removed and the conjugates were re-suspended in distilled H<sub>2</sub>O (dH<sub>2</sub>O) and underwent a further round of centrifugation. This cycle was repeated three times to remove excess linker before suspending the conjugate in 10 mM phosphate buffer. Upon analysis using UV-vis spectroscopy, the conjugates exhibited a slight red shift of 2 nm to 525 nm, which indicated that there had been a change at the surface of the nanoparticle, as shown in figure 4.7.

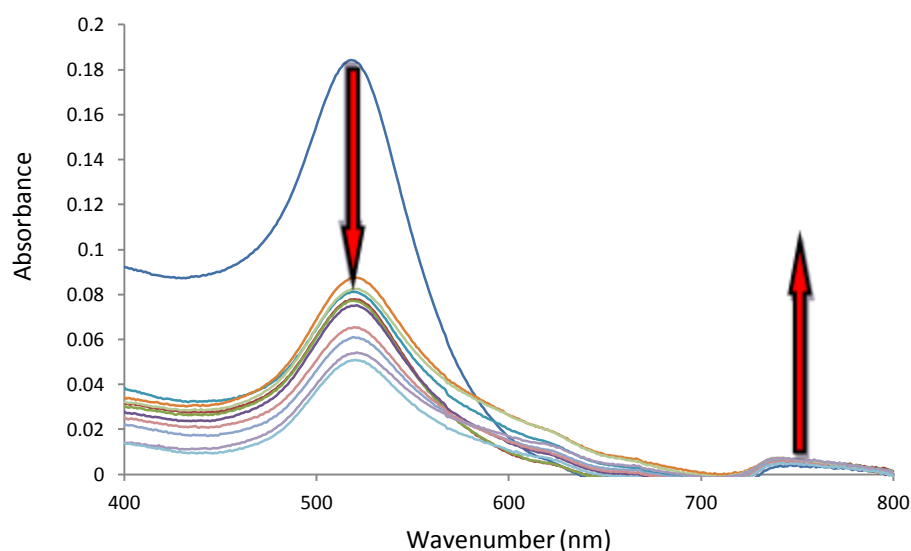


Figure 4.7: UV-vis spectra of PEG<sub>41</sub>-AuNPs conjugates, bare AuNPs (blue line) compared to conjugates synthesised with varying volumes of PEG<sub>41</sub> linker.

The figure shows there was a large drop in absorption and the emergence of a peak in the 700-800 nm range, indicative of aggregation. Although no colour change was

evident by eye - typically associated with aggregation of nanoparticles - it still demonstrated that the nanoparticles were not stable. As such, an alternative method was sought.

A paper published by Qian *et al.*<sup>182</sup> demonstrated that optimum monolayer coverage of 60 nm gold nanoparticles with PEG occurred using a solution which contained approximately 30,000 PEG molecules. When equating this number of molecules to a 13 nm gold nanoparticle, the linker was added to the colloidal solution at a concentration of  $10^{-3}$  M in a 100  $\mu$ L aliquot. This concentration and volume of linker correlated well with the experimental detail used by Brown *et al.* where a similar linker was used in the research of anti cancer drugs. Figure 4.8 shows the results from the addition of increased linker to 13 nm gold nanoparticles.

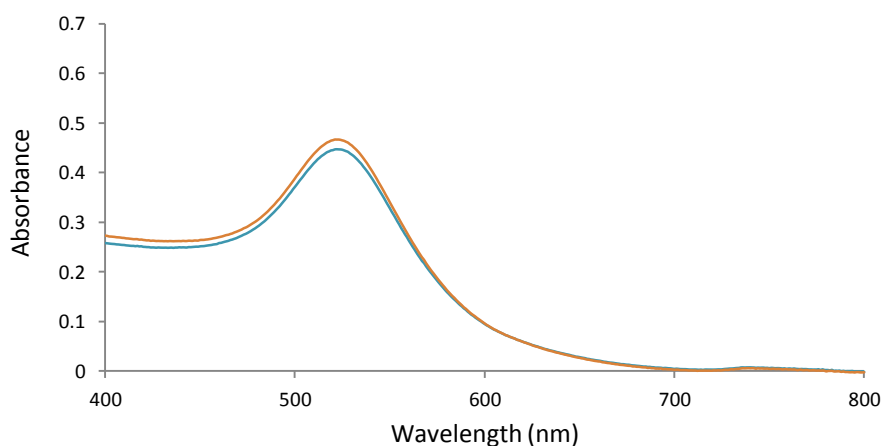


Figure 4.8: UV-visible spectrum of 13 nm of 17 nM AuNPs conjugated with PEG<sub>41</sub> linker (blue line) compared with spectrum of bare 13 nm AuNPs (orange line)

The results illustrated in figure 4.8 showed that there was no drop in absorbance, coupled with the lack of a peak in the 650-800 nm range; this indicated the formation of stable conjugates. Following this successful conjugation, the next step was to conjugate TAT to the remaining free amine of the PEG group.

#### 4.4.1.2 SILVER NANOPARTICLES AND PEG<sub>41</sub>

Silver nanoparticles were also investigated as a possible surface to be used in conjugation with SERS, as it has been reported the enhancement factors with this surface are greater than that of gold nanoparticles. The PEG<sub>41</sub> linker was used in a  $10^{-3}$  M concentration and a 100  $\mu$ L and was added to a solution of 0.4 nM silver citrate nanoparticles. The conjugates were prepared as discussed in section 8.4.

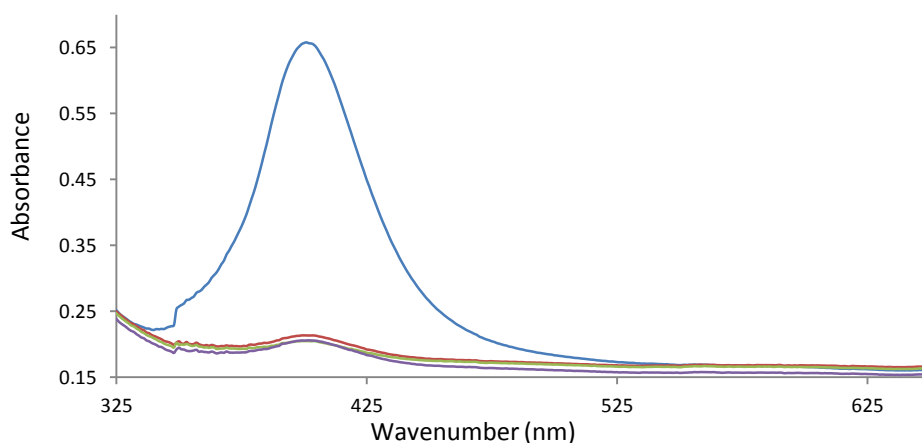


Figure 4.9: Representative UV-vis spectra of PEG<sub>41</sub>-AgNP conjugates, comparison between bare AgNPs (blue line) and PEG<sub>41</sub>-AgNPs conjugates (red, purple and green lines)

Figure 4.9 demonstrates the effect of the PEG<sub>41</sub> linker on the stability of AgNPs. It can be seen that there was a dramatic drop in absorbance in the  $\lambda$  maximum of the AgNPs; bare AgNPs had a  $\lambda$  maximum of 401 nm at an absorbance of 0.65. Upon interaction with the PEG<sub>41</sub> linker, the  $\lambda$  maximum is shifted to 405 nm and the absorbance dropped to 0.2. This showed that this system was not stable and could not be used in conjunction with silver nanoparticles. It was essential for this initial step in the process of the conjugate synthesis to form a stable foundation before the addition of the biomolecule.

#### 4.4.2 TAT CONJUGATION TO PEG<sub>41</sub>-AUNPS

Following the successful conjugation of the PEG<sub>41</sub> linker to AuNPs, the next step was to investigate the feasibility of TAT conjugation to the PEG<sub>41</sub>-AuNPs conjugate. It was proposed the conjugation of TAT to the linker would proceed through the formation of an amide bond - using well established amide chemistry - between the carboxylic acid group of the linker and a primary amine in the peptide. Ethyldiisopropylcarbodiimide (EDC) and N-hydroxysuccinimide (NHS) were used as a coupling reagent and as an activator, respectively, to promote amide formation. EDC and NHS were added to the linker nanoparticle conjugate in 20 $\mu$ L aliquots at a concentration of 2 mg/mL. The solution was then incubated for 30 minutes, followed by the addition of the fluorescein labelled TAT. The peptide was added in varying volumes (10-100  $\mu$ L) at a concentration of  $1 \times 10^{-8}$  M. When comparing the UV-visible data, it is clear that there are shifts in the SPR. This indicates the successful conjugation of the peptide to the linker-nanoparticle conjugate, shown in figure 4.10.

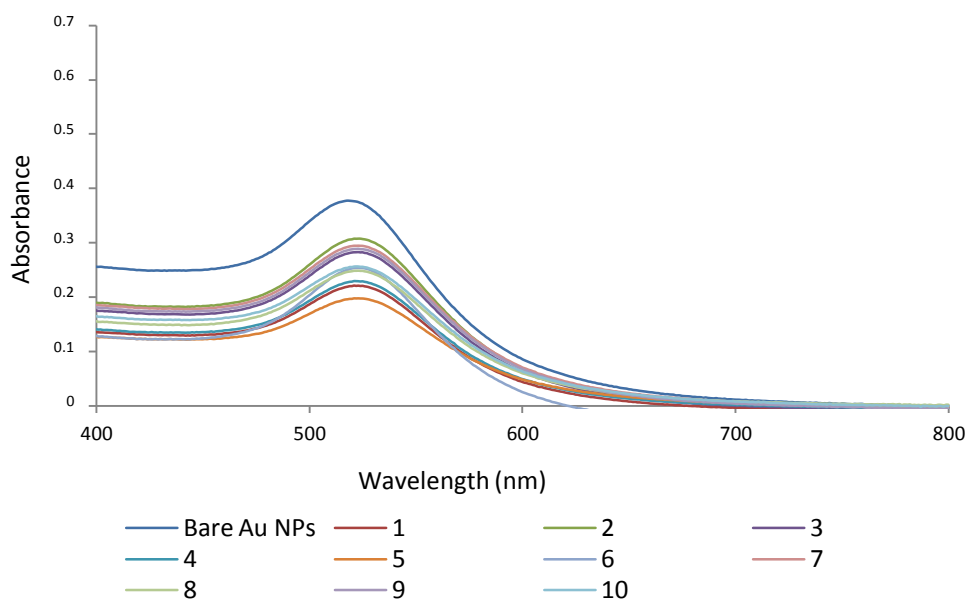


Figure 4.10: UV-visible spectra of 17 nm TAT-PEG<sub>41</sub>-AuNP conjugates, the numbers 1-10 correspond to the volume of TAT peptide added (1 -10  $\mu$ L- 10 – 100  $\mu$ L) increasing in 10  $\mu$ L increments.

Figure 4.10 displays the UV-vis spectra of the conjugated peptide to the PEG<sub>41</sub>-AuNPs. Confirmation of successful conjugation was obtained through the red shift,

of the  $\lambda$  maximum from 521 to 525 nm. The conjugates appeared to be stable; the evidence being the absence in drop of absorbance and lack of peak indicative of aggregation. The slight drop in absorption witnessed was surmised to be due to the losses from the conjugate concentration during the washing cycles. This theory was supported by the absence of a peak around 700 nm.

The samples were then analysed using a 633 nm laser. Initial results were poor, as there was no identifiable signal from the conjugates. It was suggested that the reason was due to the low addition concentration of the peptide, therefore the experiment was repeated with the peptide at a concentration of  $1 \times 10^{-3}$  M. Due to the higher concentrations, the volume added was reduced to between 1-19  $\mu$ L. This was to avoid overloading of the nanoparticle which could have resulted in instability and aggregation.

The new conjugates were once more analysed using a 633 nm laser with varying exposure times ranging from 10 seconds to 120 seconds. Figure 4.11 presents the SERS results.

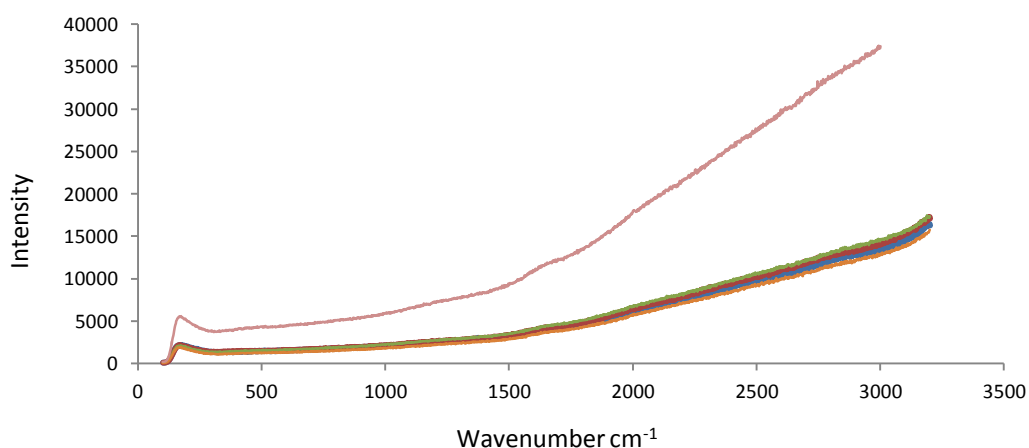


Figure 4.11: SERS spectra of TAT-PEG<sub>41</sub>-AuNP conjugates. Blue thick line represents the PEG<sub>41</sub>-AuNPs unconjugated to TAT, TAT-PEG<sub>41</sub>-AuNPs aggregated with 10 mM MgSO<sub>4</sub> (pink line); TAT-PEG<sub>41</sub>-AuNPs aggregated with 1 M NaCl (green line); TAT-PEG<sub>41</sub>-AuNPs aggregated with 0.01 % of poly-L-lysine (orange line) and TAT-PEG<sub>41</sub>-AuNPs aggregated with 0.1 % spermine (red line) analysed at 633 nm, centred at 1450 cm<sup>-1</sup> and acquired for 10 seconds.

Once again the results were very poor. There appeared to be no difference between the control samples (PEG<sub>41</sub>-AuNPs) and the TAT-PEG<sub>41</sub>-AuNPs samples. Aggregation was carried out in an attempt to observe the signal from the conjugate samples; aggregation of nanoparticles creates hotspots - as discussed in section 1.8.3.1 - which can provide additional enhancements to the system. Several different types of aggregating agents were used, however all failed to induce aggregation and signals were still absent.

The poor results could have been attributed to a number of factors: the coupling between the linker and TAT peptide could have been unsuccessful; and the laser wavelength of 633 nm was not an ideal match with fluorescein. The dye has an emission of 520 nm and thus a shorter laser wavelength, such as 514.5 nm, would have been more desirable.

#### 4.4.3. CHARACTERISATION OF TAT-PEG<sub>41</sub>AUNP COUPLING

To determine the limiting factor in the detection of TAT peptide, several parameters were investigated.

The coupling between the linker and TAT peptide was the first parameter examined. The coupling reaction was performed off the nanoparticle surface, this allowed investigation of the coupling reaction by high performance liquid chromatography (HPLC).

The linker and peptide were conjugated, as detailed in section 8.4. In addition to the linker-TAT, control samples were necessary to enable assignment of the different peaks from the chromatograph and definitively determine the success of the reaction. The three controls were: COOH-PEG<sub>41</sub>- thioctic acid; COOH-PEG<sub>41</sub>- thioctic acid mixed with EDC and NHS; and finally TAT peptide.

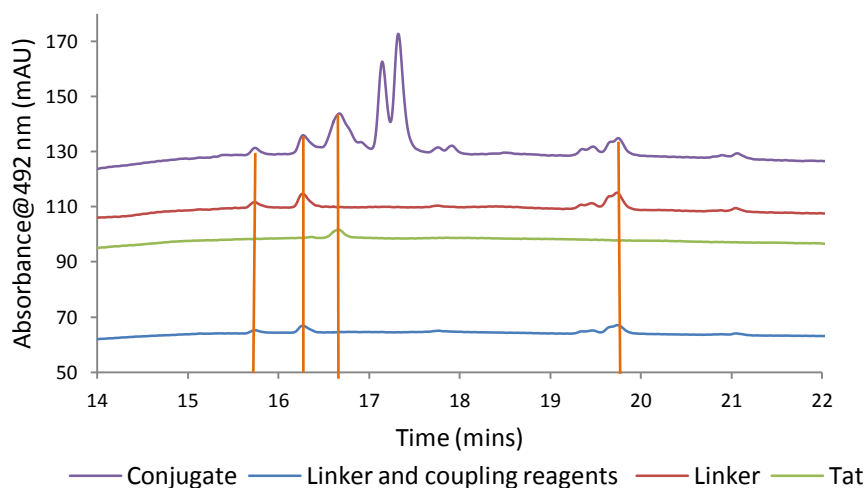


Figure 4.12: HPLC chromatogram of conjugation sample and its corresponding controls.

Figure 4.12 shows the HPLC trace recorded at 492 nm. Each chromatograph was offset to allow for easy comparison. The simplest chromatograph is from the TAT peptide alone. There is one peak at 16.8 minutes, which indicates the peptide was pure and still retained the fluorescein label. The red chromatograph is from the COOH-PEG<sub>41</sub>-thioctic acid linker. There were four different peaks, which was unexpected. As the linker was synthesised using solid phase techniques it was assumed upon cleavage of the resin that the only product obtained would be the desired product. The column that was used was a hydrophobic C<sub>18</sub> Jupiter Phenomex column. It works on the basis that the most hydrophilic components of a mixture will elute from the column first. This would suggest that the peaks at 15.8 and 16.2 minutes are a by-product involving the thioctic acid, due to the fact these peaks elute before the peak for the TAT peptide – reasoning that TAT would be more hydrophobic. It is assumed the group of peaks between 19.2 and 19.8 minutes are related to the fully formed COOH-PEG<sub>41</sub>-thioctic acid linker. The addition of the long chain PEG compound would increase the hydrophobicity and therefore would be retained in the column for a longer period of time. The peak at 19.2 is most likely a degradation product of the COOH-PEG<sub>41</sub>-thioctic acid linker, perhaps with less PEG groups, which could indicate the slightly less retention time coupled with the small nature of the peak. The blue line which represents the COOH-PEG<sub>41</sub>-thioctic

acid linker and the coupling reagents (EDC and NHS) does not show any additional peaks. This was expected as the coupling reagents are not conjugated there would not show any peaks when monitored at 492 nm. Finally the most interesting chromatograph - purple line - related to the reaction between the COOH-PEG<sub>41</sub>-thioctic acid linker and TAT peptide. As expected the reaction mixture was not purified prior to the HPLC analysis, therefore the peaks at 15.6 16.2, 19.2 and 19.8 minutes all relating to the COOH-PEG<sub>41</sub>-thioctic acid linker are present. There is also a peak at 16.5 minutes, which from previous interpretation, belongs to the TAT peptide, this indicated the coupling reaction is not proceeding at a yield of 100%. However a double peak at 17.2 minutes appeared in the conjugate trace which did not appear in any of the other traces, therefore it was assumed this is the formation of the linker-TAT conjugate. To support this view a hydrophobicity calculator was used to estimate the interaction of the peptide with HPLC column. It was found that of the percentage of hydrophilic residues was 83%. Therefore the peptide was predominately hydrophilic in nature. This was confirmed when analysing the TAT alone chromatograph where the peptide eluted at 16.5 minutes before that of the COOH-PEG<sub>41</sub>-thioctic acid linker. Therefore it was surmised upon conjugation of TAT peptide to the COOH-PEG<sub>41</sub>-thioctic acid linker, the peak for this new species would elute somewhere in-between, incorporating the properties of both molecules. Upon confirmation that the coupling was proceeding successfully, the next step was to analyse the conjugate on the nanoparticle surface. This characterisation involved analysis of the TAT conjugates using gel electrophoresis. Gel electrophoresis has been successfully employed, predominately in the characterisation of DNA fragments. The principle of this method is that it separates DNA fragments on the basis of increasing charge with respect to increasing size of the DNA fragment i.e. the smaller fragments travelling the furthest down the gel as they have a smaller collective charge when compared with the larger DNA fragments, which have a larger negative charge and are therefore retarded by the gel. More recently, this type of gel electrophoresis has been used to separate nanoparticles. Hanauer *et al.* demonstrated the separation of silver nanoparticles based upon size and shape. This principle was used with the gold nanoparticle conjugates as it was hypothesised there would be a difference between bare AuNPs,

PEG<sub>41</sub>AuNPs and TAT-PEG<sub>41</sub>-AuNPs, confirming that the coupling had been successful. Following the procedures outlined by Hanauer *et al*, a 1% agarose gel was used. 2μL of each sample was mixed with 20 μL of loading buffer, which can be seen as the blue and yellow bands in the figure 4.13 below.<sup>183</sup>

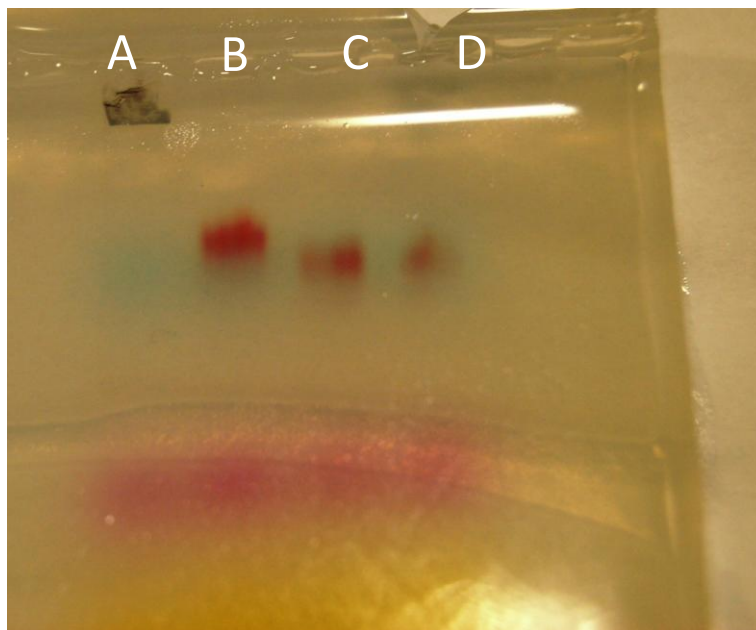


Figure 4.13: Gel of conjugates and controls. A contained bare AuNPs which crashed out upon introduction to gel, B contained PEG<sub>41</sub>-AuNPs and C and D contained TAT-PEG<sub>41</sub>-AuNP conjugates. Blue, pink and yellow bands were from the loading buffer used.

Figure 4.13 shows that Well A contained bare AuNPs which aggregated upon addition to the gel. This was attributed to reagents used to make the gel, which cause aggregation and therefore the nanoparticles become too large to enter the gel. Well B contained the COOH-PEG<sub>41</sub>-thioctic acid linker. Wells C and D contained the complete PEG<sub>41</sub>AuNPTAT conjugate.

It was seen that there was a difference between the PEG<sub>41</sub>AuNPs and the TAT-PEG<sub>41</sub>-AuNP, with TAT-PEG<sub>41</sub>-AuNP conjugates travelling further through the gel than the PEG<sub>41</sub>-AuNPs. This was unexpected. With the addition of the TAT peptide, it would be expected that this would increase the diameter of the conjugate when compared to the PEG<sub>41</sub>AuNPs. This abnormality could be explained by the effect of charge. Traditionally when using gel electrophoresis, the fragments are driven by

charge, i.e. as negatively charged molecules the DNA fragment will gravitate towards the positive electrode situated at the opposite end of the wells within the gel. Therefore, the TAT peptide had to be considered. This peptide consisted of a majority of positively charged amino acids and as such at physiological pH carries a net positive charge. As such this conjugate would want to migrate towards the negative electrode therefore appearing to be retarded within the gel when compared to the COOH-PEG<sub>41</sub>-thioctic acid linker. The difference in behaviours between the PEG<sub>41</sub>AuNPs and the TAT-PEG<sub>41</sub>-AuNP within the gel, was an encouraging result indicating that each set of conjugates were different and consequently would indicate that TAT attachment was successful, further proving the successful formation of the TAT-PEG<sub>41</sub>-AuNP conjugate. Consequently the next stage was to investigate the conjugates at a lower wavelength of 514.5 nm, which was in resonance with the emission of the fluorescein label.

#### 4.4.4 SERRS Analysis of TAT-PEG<sub>41</sub>AuNP Conjugates at 514.5 nm

The conjugates were synthesised as discussed in section 8.4 and analysed using a 514.5 nm laser.

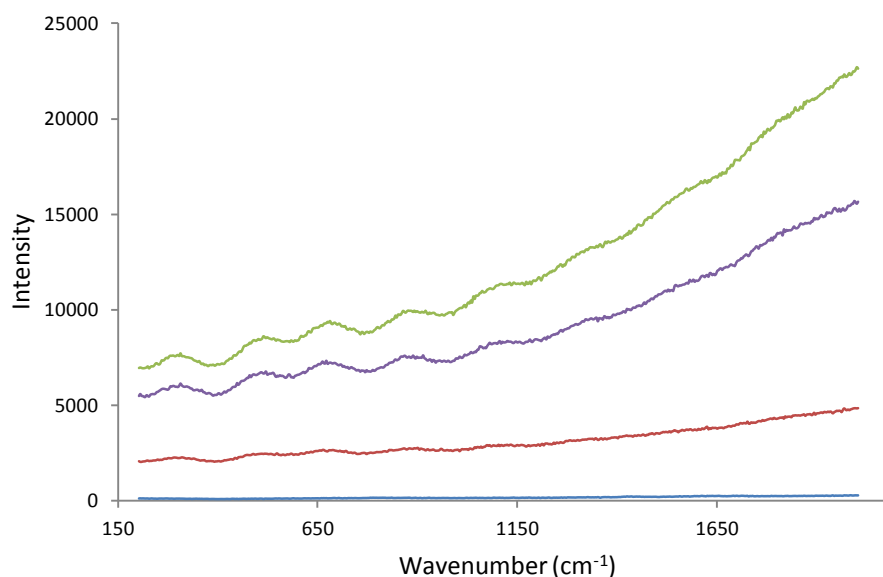


Figure 4.14: SERS spectra of TAT-PEG<sub>41</sub>-AuNP conjugates, PEG<sub>41</sub>-AuNPs (blue line), TAT-PEG<sub>41</sub>-AuNP aggregated with 10 mM MgSO<sub>4</sub> (green line, 5  $\mu$ L of TAT), TAT-PEG<sub>41</sub>-AuNP aggregated with 1 M NaCl (purple line, 10  $\mu$ L of TAT), TAT-PEG<sub>41</sub>-AuNP aggregated with 0.01% poly-L-lysine (red line 1  $\mu$ L of TAT) analysed at 514 nm, centred at 1450  $\text{cm}^{-1}$  and acquired for 10sec.

Figure 4.14 shows the results when analysed using a 514.5 nm laser. Once more poor results were obtained with no identifiable peaks relating to the fluorescein label. This was extremely disappointing and was due to the presence of a high fluorescence background. Once more, this was a positive indication of the success of the coupling step; however this would suggest that the nanoparticle was not efficiently quenching the fluorescence of the fluorescent label. In an effort to gain a positive result, aggregation was used. Extensively documented within literature, the aggregation of nanoparticles ‘turns on’ the SERS effect: it allows the nanoparticles to come closer to one another, creating hotspots which provide the greatest enhancement factor. The fluorescent background that was observed was due to inefficient quenching by the AuNPs. Therefore it was surmised that with aggregation, this action would bring the

nanoparticles together; providing a greater ability to quench the fluorescent background and revealing the vibrational peaks of the conjugate. However - as can be seen from figure 4.15 -regardless of the type and volume of aggregating agent used, the conjugate samples showed no visible signs of aggregation.



Figure 4.15: Conjugate (left), bare nanoparticles (right) after treatment with  $\text{MgSO}_4$

This stability seen from figure 4.15: on the left hand side of the figure is the  $\text{COOH-PEG}_{41}$ -thioctic acid linker conjugate which contained  $360 \mu\text{L}$  of  $10 \text{ mM MgSO}_4$ ; and on the right is the same volume of aggregating agent applied to bare Au nanoparticles. The effect of aggregation can be seen in the bare nanoparticles, as the distinctive ruby wine colour of the nanoparticles has changed to the purple colour shown. This colour change resulted in a red shift from  $525 \text{ nm}$  to over  $600 \text{ nm}$ . However, the  $\text{PEG}_{41}$  linker has stabilised the conjugate - even under high salt concentrations. Although this stability would be an attribute desired for cellular investigations - with the absence of signal, this system has become redundant.

Another concern was the use of gold nanoparticles. This type of nanoparticle performs best at  $633 \text{ nm}$ . Due to the effect of aggregation, the plasmon band is red shifted towards the  $600 \text{ nm}$  region of the spectrum; consequently at  $514.5 \text{ nm}$  these nanoparticles perform weakly. Nevertheless, a paper published by Li *et al.* in 2008 demonstrated that by using larger gold nanoparticles instead of standard  $13 \text{ nm}$ ; signals from fluorescein were obtained at  $514.5 \text{ nm}$  excitation. Li *et al.* used  $60 \text{ nm}$  gold nanoparticles. In an attempt to synthesise conjugates which were SERS active, it was decided to synthesise  $60 \text{ nm}$  gold nanoparticles.<sup>219</sup>

As the diameter of nanoparticles are increased, the properties of the nanoparticles change: the  $\lambda$  maximum of  $60 \text{ nm}$  diameter gold nanoparticles is further red shifted than the smaller gold nanoparticles, presenting a  $\lambda$  maximum of  $530 \text{ nm}$ . The

methodology used for the smaller gold nanoparticles and PEG<sub>41</sub> linker were employed for the larger gold nanoparticles. The PEG<sub>41</sub> linker was added in a 100  $\mu\text{L}$  volume at a concentration of  $1 \times 10^{-3}$  M. TAT peptide was added in a 1 mM concentration at a volume of 10  $\mu\text{L}$  to the PEG<sub>41</sub>-AuNP 60 nm conjugates in the same procedure outlined in section 8.4.

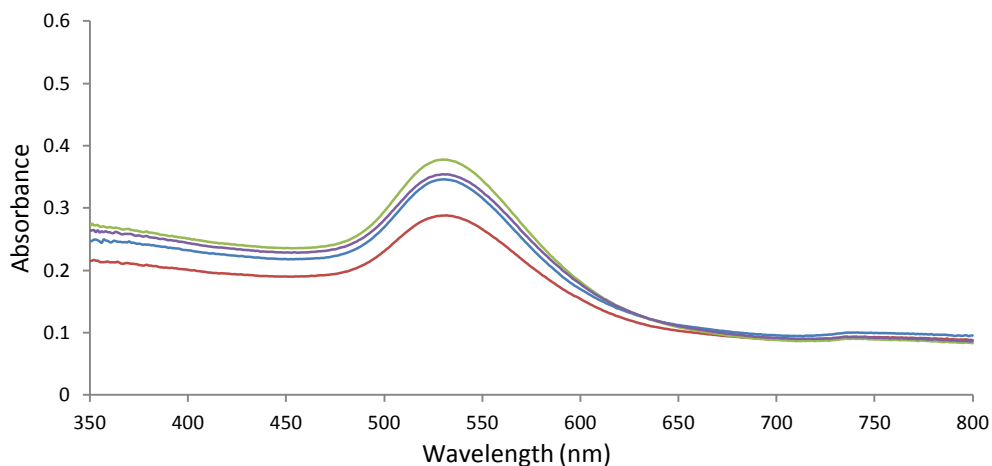


Figure 4.16 UV-vis spectra of 60 nm PEG<sub>41</sub>-AuNP conjugates. Bare 60 nm AuNPs (blue line) and three identical PEG<sub>41</sub>-AuNP conjugates (red, green and purple line)

Figure 4.16 showed that the 60 nm conjugates appeared to be as stable at their 13 nm counterparts.

Once more these conjugates were analysed at 514.5 nm laser - the results are shown in the figure 4.17. No signal was obtained, contradictory to the results of the paper published by Li *et al.*<sup>219</sup>

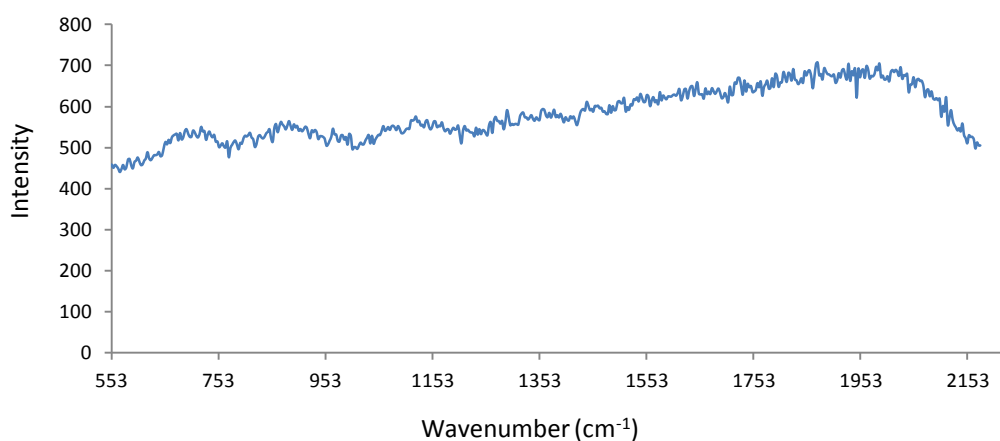


Figure 4.17: Averaged SERS spectrum of PEG<sub>41</sub>- 60 nm AuNP conjugates analysed at 514 nm, centred at 1450 cm<sup>-1</sup> and acquired for 10 seconds.

Once again in an attempt to obtain signal from these conjugations several different aggregating agents were employed to create hotspots to enhance signal and minimise fluorescence. Two salts NaCl (1 M), MgSO<sub>4</sub> (10 mM) and two positively charged aggregation agents spermine (0.1 M) and poly-L-lysine (0.01% w/v) were all trialled over a range of volumes (50 µL- 370 µL), shown in figure 4.18. Nevertheless, aggregation did not occur, as seen from figure 4.18. This data suggests that stability of the PEG<sub>41</sub> linker was in fact having an adverse effect on the sensor ability of these conjugates.



Figure 4.18: 60 nm LinkerAuNP on left, bare 60 nm AuNPs on right both aggregated with 10 mM MgSO<sub>4</sub> (370 µL)

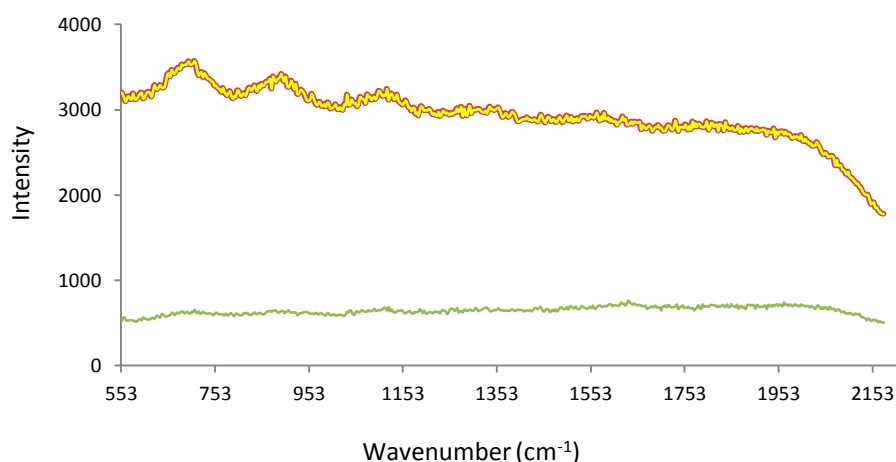
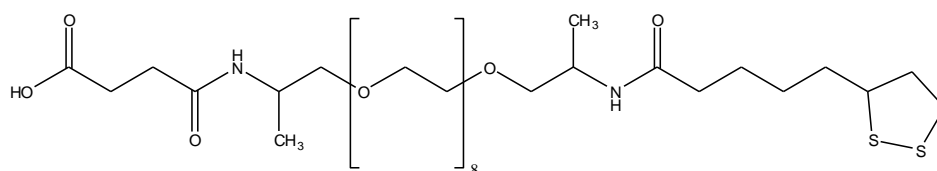


Figure 4.19: SERS spectra of aggregated TAT-PEG<sub>41</sub>-AuNP 60 nm conjugates, PEG<sub>41</sub>-AuNP 60 nm (green line) and TAT-PEG<sub>41</sub>-AuNP 60 nm aggregated with 120  $\mu$ L of 10 mM ascorbic acid (red line) and TAT-PEG<sub>41</sub>-AuNP 60 nm aggregated with 120  $\mu$ L of 10 mM MgSO<sub>4</sub> (yellow line) analysed at 514 nm, centred at 1450  $\text{cm}^{-1}$  with an acquisition time of 10 sec.

The 60 nm conjugates once more failed to produce any signal, as shown in figure 4.19. It was hypothesised that this was due to a stability issue, in that the PEG<sub>41</sub> molecule was encapsulating the nanoparticle thus preventing efficient aggregation. Therefore, with a PEG molecule of a shorter length, stability would be provided, yet aggregation to provide a SERS response could still be achieved. PEG<sub>3</sub> linker compound had been shown to irreversibly aggregate on addition of the peptide, therefore PEG<sub>8</sub> was chosen - as an intermediate length - for the synthesis of the linker.

#### 4.4.5 Investigation of PEG<sub>8</sub> as linker in formation of TAT-NP conjugates.

The new linker was successfully synthesised and confirmed by MALDI-TOF mass spectrometry. This linker (with the structure shown in figure 4.20) was employed using both 13 nm and 60 nm gold nanoparticles.



59

Figure 4.20: PEG<sub>8</sub> linker structure, containing thioctic acid group and free carboxylic acid group.

The COOH-PEG<sub>8</sub>-thioctic acid linker was added in a volume of 100  $\mu$ L at a 1 mM concentration. The UV-vis spectra shown in figures 4.21 and 4.22 indicated that both types of conjugates were stable in 10 mM phosphate buffer. This was shown by the lack of dampening in the  $\lambda$  maximum of each set of conjugates and the absence of an additional peak in the 700 nm region of the spectra.

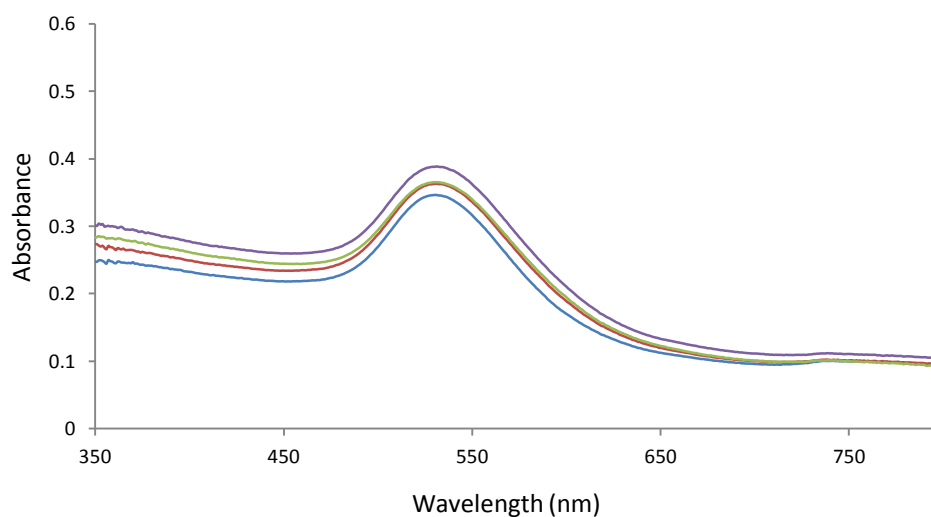


Figure 4.21: UV-vis spectra of TAT-PEG<sub>8</sub>-AuNP 60 nm conjugates (green, red and purple lines) when compared to PEG<sub>8</sub>-AuNP 60 nm (blue line)

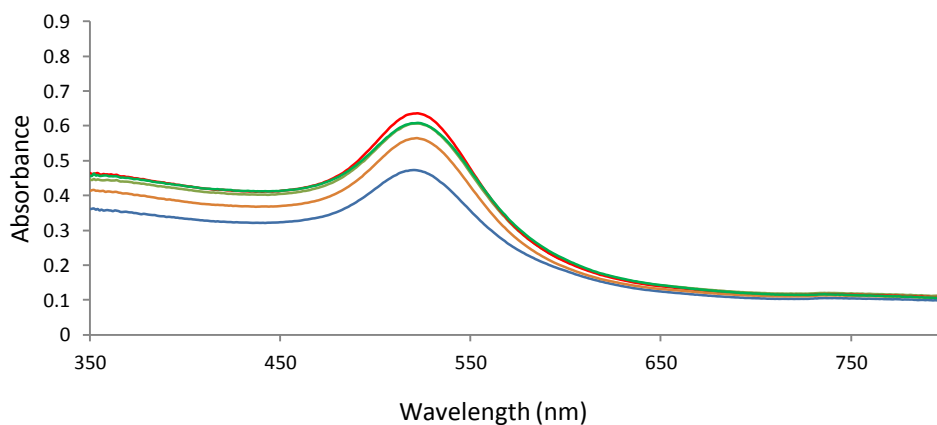


Figure 4.22: UV-vis spectra of 13 nm TAT-PEG<sub>8</sub>-AuNP conjugates (red, green and orange lines), compared with spectrum of PEG<sub>8</sub>-AuNPs 13 nm conjugate (blue line)

Once more the conjugates were analysed using an excitation wavelength of 514.5 nm. The results were disappointing. Aggregation once again failed, perhaps indicating that even the PEG<sub>8</sub> was too stable and aggregation was inhibited. It was surmised this system was not going to work in the detection of TAT peptide using SERS measurements.

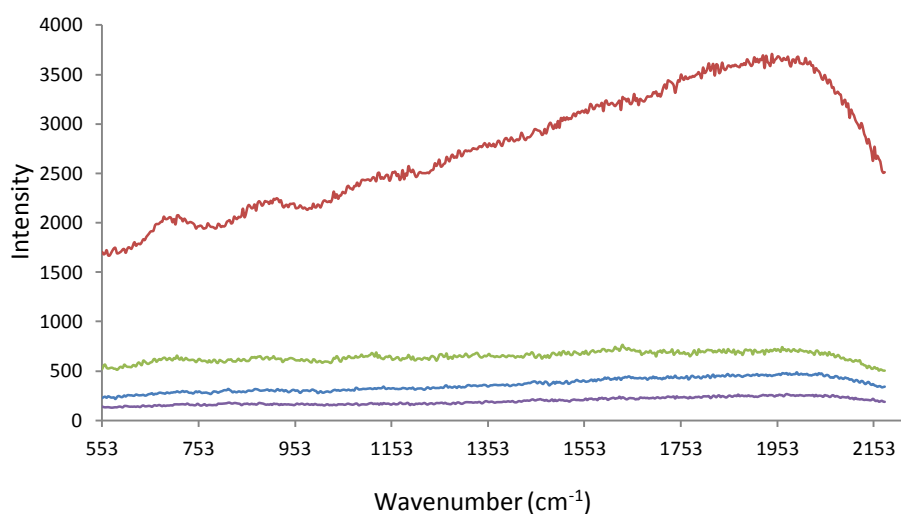


Figure 4.23: SERS spectra of 13 nm TAT-PEG<sub>8</sub>-AuNP conjugates, aggregated with various aggregating agents, Red line – 370  $\mu$ L of 0.1 M spermine; green line – 370  $\mu$ L of 10 mM MgSO<sub>4</sub>; blue line – 120  $\mu$ L of 1 M NaCl; purple line – 370  $\mu$ L of 10 mM ascorbic acid. All analysed at 514 nm, centred at 1450 cm<sup>-1</sup> and an acquisition time of 10 sec.

Figure 4.23 shows the data obtained from the SERS analysis of these conjugations. It was clear that no signal was obtained from these conjugates therefore an alternative method was investigated. The PEG group obviously supplies stability; however it could be hindering the ability to gain a signal. There were factors affecting the lack of signal, of which - predominately - the PEG group was the suspected cause. This group was hindering the ability to 'turn on' the SERS effect due to the failure of aggregation. The aggregation should be controlled, not leading to nanoparticles which aggregate to the degree that the particulates precipitate from solution. On the other hand, lack of aggregation - especially with fluorescent molecules - can minimise the Raman signal and fluorescence can dominate. The secondary problem could be the distance of the fluorescein label to that of the nanoparticle surface. PEG groups could result in a large distance from the surface to the molecule that is being analysed. It has been shown that the intensity of SERS signal drops significantly beyond 5 nm from the surface of the nanoparticle. It was for these reasons that an alternative route was explored which did not involve the use of PEG molecules. Instead, the molecule thioctic acid was investigated and silver nanoparticles used in place of gold. It was theorised that the silver particles would be more suited to this application due to the matching of the laser wavelength and the surface plasmon of the nanoparticles.

#### 4.4.6 ALTERNATIVE METHOD OF FORMATION OF TAT CONJUGATES

A paper by Choi *et al.* showed that the preparation of stable nanoparticles capped with thioctic acid was possible.<sup>184</sup> To 1 mL of 1 nM silver citrate nanoparticles 10  $\mu$ L of 0.1 mM of thioctic acid in ethanol was added and the nanoparticles were shaken overnight at room temperature. An important point to note is that the nanoparticles had to be within the pH range of 9 – 11. This was achieved with the addition of 10 mM NaOH. The thioctic acid nanoparticles (TA-NPs) were centrifuged at 6000 rpm for 20 minutes before removal of the supernatant and re-suspending in 1 mL of dH<sub>2</sub>O, before repeating the process and finally re-suspending the conjugates in 1 mL of sodium bicarbonate buffer at pH 9. Sodium bicarbonate buffer - with an effective

buffering range of pH 9.2 – 10.8 - was chosen as it has been documented that amide couplings have a higher success rate at increasing alkali pH.

Analysis by Uv-vis spectrometry revealed a dramatic red shift in the  $\lambda$  maximum of > 10 nm. Although this is considered a large shift, the conjugates were deemed stable from the lack of an additional peak in the 600 nm range: indicative of aggregation. The next stage was to carry out the coupling between the thioctic acid and the TAT peptide. This was once again carried out through the activation of the carboxylic acid by use of EDC/NHS chemistry as detailed in section 8.4.

The UV-vis spectra in figure 4.24 showed that there has been a red shift of 4 nm from a  $\lambda$  maximum of 418 nm in the TA-NP (red line) to 422 nm in the TAT-TA-NP conjugate (blue line). This indicated that conjugation of the TAT peptide to the thioctic acid capped silver nanoparticles, may have been successful.

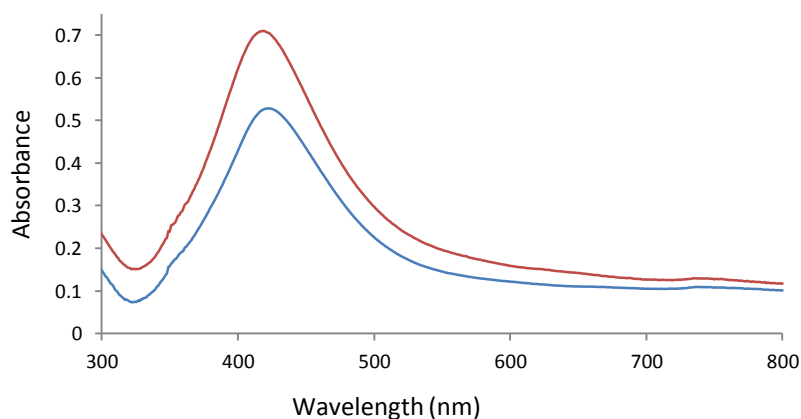


Figure 4.24: Comparison of UV-visible spectra of TA-AgNPs (red line) and TAT-TA-AgNPs (blue line) spectra

The conjugates were then analysed using a 514.5 nm laser. The conjugates were analysed using a sample volume of 400  $\mu$ L, the spectra are shown in figure 4.25.

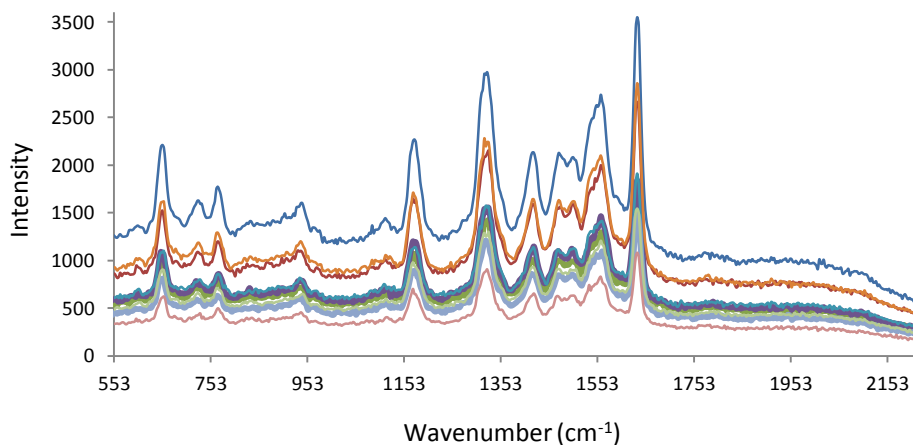


Figure 4.25: SERS spectra of TAT-TA-AgNPs conjugates analysed at 514 nm acquired at 1 sec and centred at  $1450\text{ cm}^{-1}$ . Ten replicates were analysed as shown in the figure.

Figure 4.25 showed the results obtained from the SERS analysis. These results were encouraging as it was the first time signal had been obtained from the TAT peptide thus re affirming the earlier observation the coupling between the functionalised nanoparticle and the peptide was successful. The spectral features shown in figure 4.26 can be assigned as the following: the  $1170\text{ cm}^{-1}$  peaks being attributed to CCH bend;  $1324\text{ cm}^{-1}$  attributed to CC stretch;  $1469\text{ cm}^{-1}$  peak belonging to the CO and CC stretch;  $1556\text{ cm}^{-1}$  attributed to the C=O and CC stretch; and finally the dominate  $1635\text{ cm}^{-1}$  peak attributed to quinine-like stretch.<sup>185</sup> Shown from the above figure, the system is reproducible. Of the ten conjugates synthesised, all ten gave good and consistent signal.

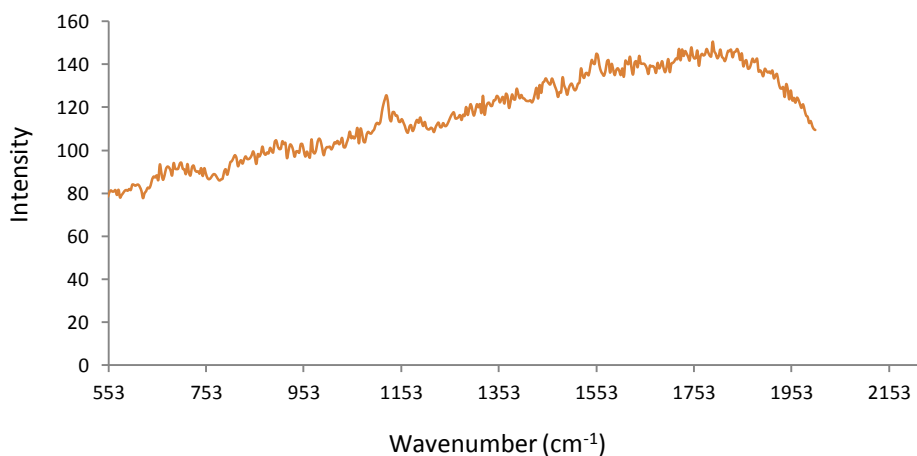


Figure 4.26: SERS spectra of the control conjugate, TA-NP.

To ensure that the signal that was obtained was from fluorescein labelled TAT peptide, SERS analysis was carried out on the control TA-NP. The spectrum that was obtained is shown in figure 4.26. This confirmed that the signal was not originating from the thioctic acid capped nanoparticles, providing detection of the TAT peptide. The next stage was to determine at which volume of  $1 \times 10^{-6}$  M TAT peptide would produce the most intense signal. The volumes 5, 10, 15, 20, 30, 40, 50, 60 and 70  $\mu\text{L}$  were chosen as above 70  $\mu\text{L}$ , the nanoparticles lose stability and begin to aggregate uncontrollably. Figure 4.27 shows the volume optimisation results.

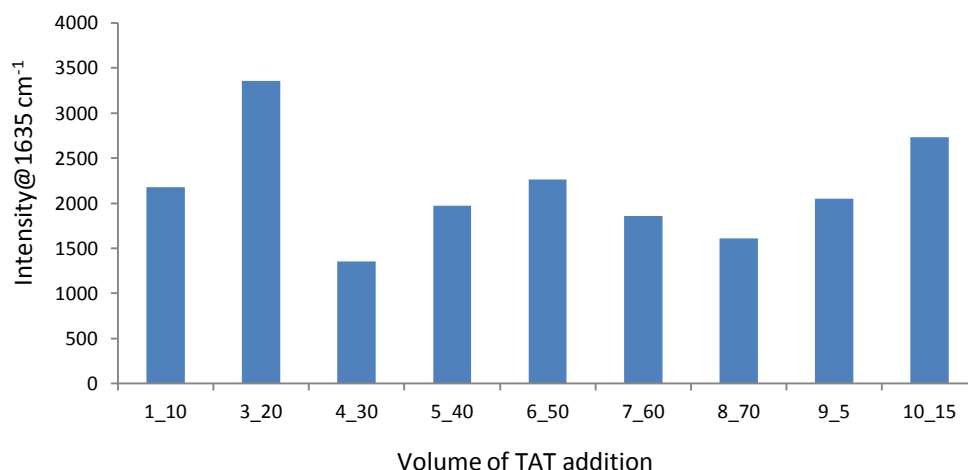


Figure 4.27: Volume optimisation of TAT addition to form TAT-TA-AgNPs conjugates, analysed at 514 nm acquired for 1 sec, centred at 1450 cm<sup>-1</sup> Intensity of SERS spectra determined by peak at 1635 cm<sup>-1</sup>.

The most intense signal occurred upon the addition of 20 µL of TAT peptide at concentration of 10<sup>-6</sup> M, therefore this was the set volume used in future experiments.

This system had proven to be reliable, reproducible and stable. Consequently, the next stage was to incubate the samples with cells and examine the feasibility of these conjugates as cellular reporters.

## 4.5 CELLULAR EXPERIMENTS

It was of crucial importance that before any cellular experiments took place to ascertain the stability of the conjugates in EDEM cell medium. Cell medium contains a high ratio of salts, which can cause instability to nanoparticles.

In order to test the stability of the conjugates, they were suspended in a 1 in 5 dilution, this is the ratio used when the nanoparticles are incubated with cells. The samples were incubated overnight and examined using UV-vis spectrometry and analysed by SERS using a 514.5 nm laser wavelength. Figure 4.28 shows that the stability in cell medium appears very high.

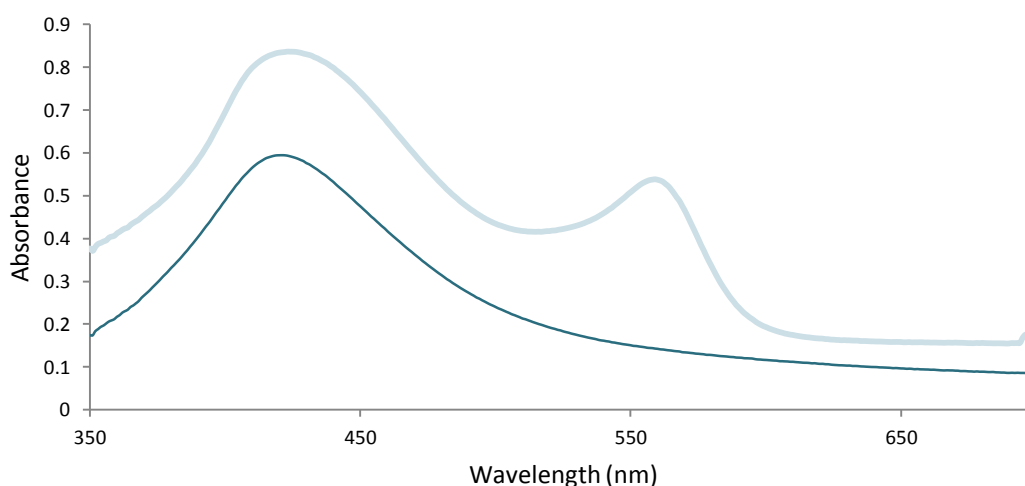


Figure 4.28: Representative UV-vis spectrum of TAT-TA-AgNPs conjugates after 18 hour incubation in cell medium (EMEM buffer) Dark blue line is the spectrum of TAT-TA-AgNPs before incubation with cell medium, light blue line is TAT-TA-AgNPs in cell medium.

When comparing the  $\lambda$  maximum of the conjugates pre and post cell medium, it does not change considerably. Over the ten conjugates examined, the  $\lambda$  maximum remained the same. The peak at 562 nm is not associated with aggregation of the nanoparticles but does originate from the cell medium which is red.

In addition to the UV-vis spectra, analysis by SERS was carried out to ensure that under the conditions required for cellular analysis, the conjugates still gave a Raman signal. From figure 4.29 it can be seen that strong signal was obtained and that the presence of the cell medium did not affect the response of the conjugate.

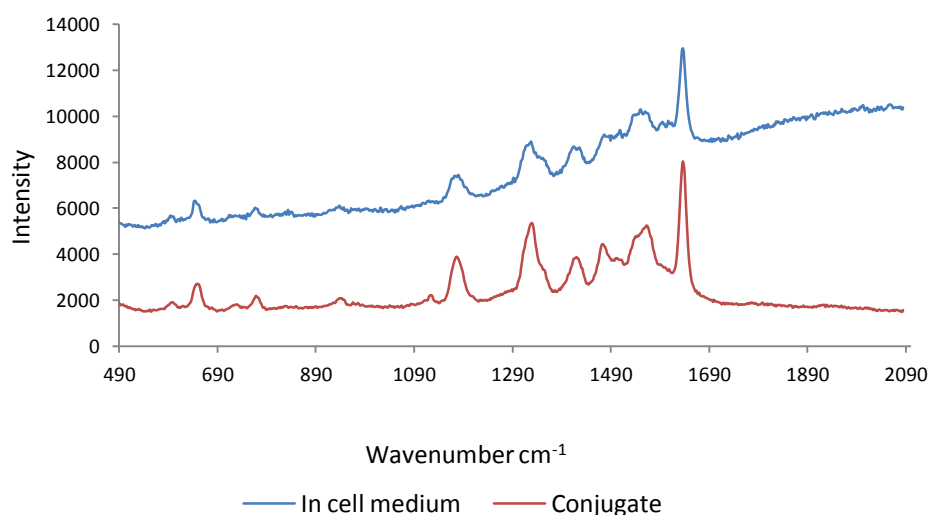


Figure 4.29: SERS of TAT-TA-AgNPs in carbonate buffer diluted in cell medium, analysed at 514.5 nm, acquired for 1 sec, centred at 1450  $\text{cm}^{-1}$  Red line is the SERRS spectrum of the TAT-TA-AgNPs conjugate prior to cell medium incubation and the blue line is the conjugate in cell medium.

From this result, there was now a reason to carry out the cell based experiments. The cells that were chosen for the following experiments were HeLa cells. These cells are derived from the cervical cancer cells taken from Henrietta Lacks shortly before her death from cervical cancer in 1951: chosen, as the cells do not allow for passive uptake, i.e. they would not ingest particles due to concentration effects but would uptake the particles through a specified mechanism.

The cells were incubated with the conjugates, which had an average concentration of 0.3 nM. The incubation was carried out for 6 hours, although other research groups have shown that uptake of functionalised nanoparticles occurs in 2 to 4 hours. It was surmised that 6 hour incubation would provide the greatest chance of uptake. The cells were analysed by using point-by-point mapping at 532 nm. For each measurement, a white light image was taken of the studied area. SERS intensity maps were created using false colour images. The false colour images were created by choosing specific wavelength to study. These maps have been created by concentrating on the region between 500 – 2000  $\text{cm}^{-1}$ . The intensity of the spectra is indicated by the colour: the most intense peaks are shown by the bright yellow colour; and least intense by the dull red regions.

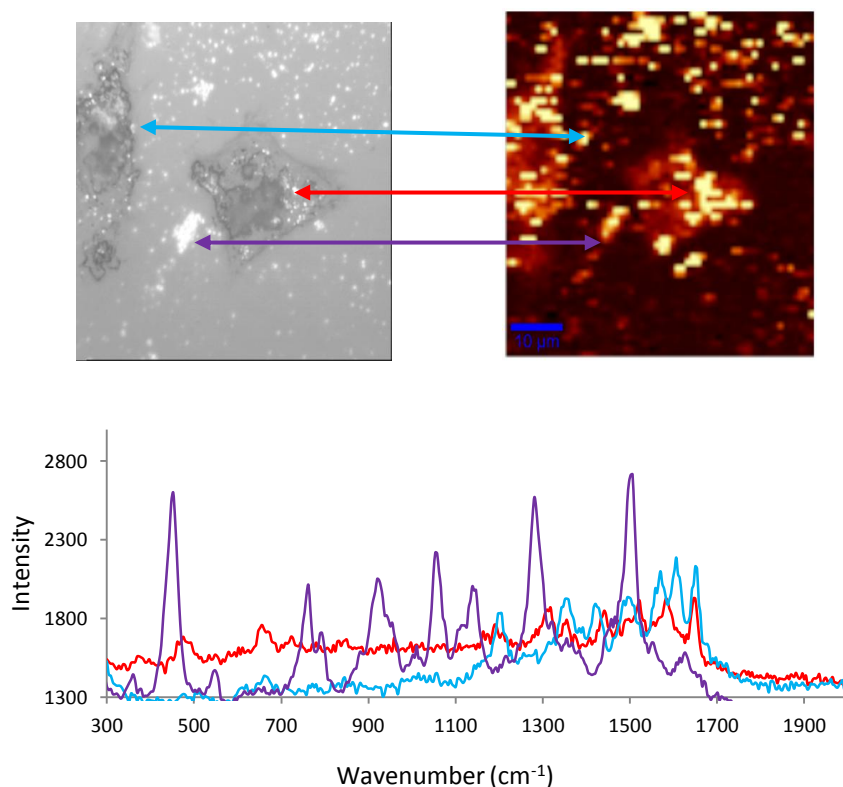


Figure 4.30: White light and false colour images of two cells mapped at 532 nm. 60  $\mu\text{m}$  width x 60  $\mu\text{m}$  map with 0.5 second integration time, spectral centre at 2000  $\text{cm}^{-1}$ . Representative SERS spectra obtained from section of map. The red line indicates nanoparticle cluster in the cell to RHS of diagram with the blue line indicating a cluster of nanoparticles not in cells. Purple line is from nanoparticles approaching the cellular membrane.

Three sets of conjugates were incubated with cells. The three sets of conjugates were all similar and only varied in slight concentration ranges (0.28, 0.30 and 0.31 nM) and were used to demonstrate that the uptake and detection of TAT-TA-NPs was a consistent event. Figure 4.30 is of one conjugate. The white light image shows there to be two cells along with what appears to be several large clusters of nanoparticles. The clusters were confirmed to be of the TAT-TA-AgNPs as shown by the purple spectrum. On the white light image the cluster can be seen as the bright section indicated by the purple arrow. The spectrum obtained was confirmed to be from the fluorescein labelled TAT with the presence of the peaks at 1630, 1453 and 1138  $\text{cm}^{-1}$ . There were additional peaks in the spectrum this could be explained by the fact that anything within a close proximity (approximately 10 nm) to the nanoparticle surface will be enhanced and contribute to the spectrum. The incubation within cell

medium means there will be several complex molecules within this medium. The red spectrum is thought to be from the conjugate within the cell this was - confirmed by the red line. The spectrum correlated well to spectra obtained prior to cell incubation. Peaks were obtained at 1658, 1582, 1425, 1367 and 1193  $\text{cm}^{-1}$ . Once more there were shifts in expected peaks thought to be from cellular interference. This figure demonstrated that Raman signal within cells was possible within cells. It showed that nanoparticles of a certain size could enter the cells, with larger aggregated nanoparticle clusters being unable to cross the cell membrane.

Figure 4.31 is included to show that the ability to detect SERRS conjugates within a cell was a consistent and reliable technique. Figure 4.31 is a white light image and its corresponding false colour image map of another cell incubated with a different set of conjugates.

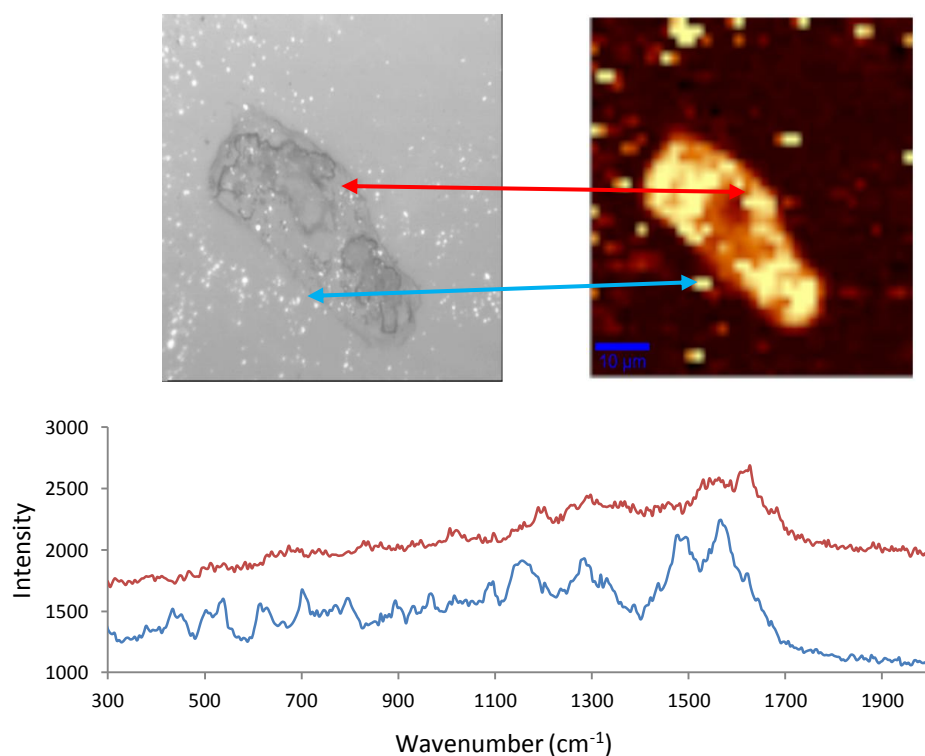


Figure 4.31: White light and false colour images of a cell mapped at 532 nm. 60  $\mu\text{m}$  width x 60  $\mu\text{m}$  map with 0.5 second integration time, spectral centre at 2000  $\text{cm}^{-1}$ . Representative SERS spectra obtained from section of map. The red line indicates nanoparticle cluster in the cell in diagram with the blue line indicating a cluster of nanoparticles not in cells.

What we can see from the cellular experiments is that there has been signal obtained from the cells. When comparing the SERS spectra that were obtained in this experiment to spectra that was obtained out-with cellular conditions it was found that they were slightly different - vibrational peaks were found to have shifted. In the spectrum obtained in figure 4.32, the peak at  $1173\text{ cm}^{-1}$  attributed to the CCH bend appears to be shifted to  $1189\text{ cm}^{-1}$ , however the peak at  $1554\text{ cm}^{-1}$  is consistent with the reported peak at  $1556\text{ cm}^{-1}$  associated with C=O stretch. It was surmised that this observation could be attributed to interference from the cellular components, which would also be Raman active.

The signals obtained appear to have a relatively good match to that obtained under *in vitro* conditions. From this observation it must be concluded that the conjugate was successfully taken up by the cell. From the presence of the fluorescein signal, it can also be concluded that the conjugate has not been broken down or decomposed through entry into the cell. In addition, it can be seen that further work would have to be carried out in this area. TEM images would provide a more in-depth view of the cell and the specific position of the nanoparticles within the cell. This would further confirm the successful uptake of these nanoparticle conjugates.

A paper published by Gregas *et al.* has further developed area following TAT uptake into cells using SERS as the detection method.<sup>168</sup> That paper was published towards the end of this work. The research in the paper published by Gregas *et al.* used multiplex conjugate whereby TAT was used as the entry route into the cell and MHA used as the Raman reporter.

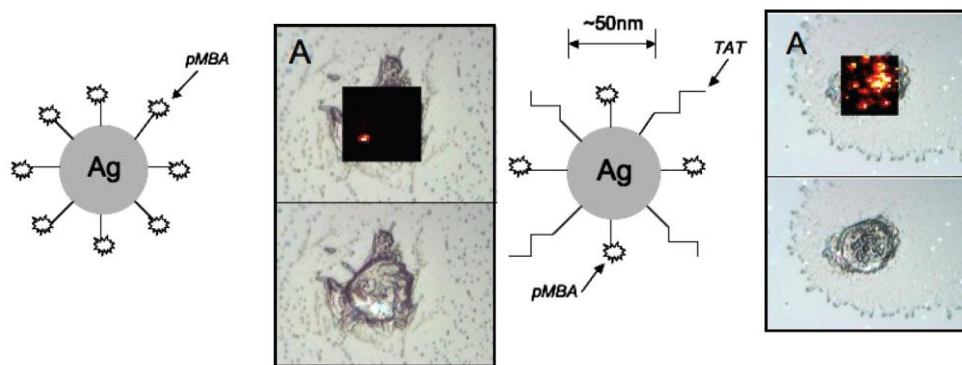


Figure 4.32: Taken from the paper published by Gregas *et al.* This figure shows false colour maps overlaid on the white light image of cells incubated with pMBA alone and then with a mixed monolayer particle contained with pMBA and TAT. It can be seen there was greater uptake when the cells were incubated with the mixed monolayer nanoparticle, leading to the conclusion TAT peptide increases cellular uptake of nanoparticles.

The difference between this work and that of Gregas *et al.* is that this research involves direct labelling of TAT molecule thus removing any doubt of disintegration of the conjugate system. However this paper did demonstrate the addition of TAT peptide increased the nanoparticle cellular uptake which confirmed additional research would be of interest.

The area of intracellular SERS studies has predominately involved the use of gold nanoparticles as the surface. The many reasons for this include the ease of synthesis of these nanoparticles. The toxicity of these nanoparticles have been studied and reviewed, thus the number of publications involving silver nanoparticles and SERS is not as documented in literature. Therefore this research is pushing the boundaries of the use of silver nanoparticles detection in cells.

# CHAPTER 5: SYNTHESIS NOVEL COMPOUNDS TO BE EMPLOYED IN THE DETECTION OF PROTEIN INTERACTIONS.

## 5.1 INTRODUCTION

The combination of dyes and biological macromolecules has been long documented, specifically when fluorescence microscopy has been employed. More recently, however, there has been resurgence in employing these conjugations with Raman spectroscopy. This increase is attributed to the potential to visualise more than one biological component simultaneously, allowing several interactions to be studied at any one time, thus providing a realistic insight into biological pathways.

The aim of this chapter was to prepare dual functioning linkers, for probing protein interactions, with both a Raman active dye and compound with affinity to the nanoparticle surface. This type of conjugate provided the chromophore and the potential for conjugation to different types of nanoparticles, therefore providing the roughened surface and satisfying the conditions necessary for SERS. This concept created several challenges including: dye solubility; dye stability; and ensuring buffering conditions were compatible with the dye, protein and nanoparticle elements of the conjugate system. In addition, protein denaturation was of critical importance i.e. when incorporated into the conjugate system, it was essential that the protein retained its activity to allow specific protein interactions to be observed.

Ultimately, the goal of this research was to employ Raman spectroscopy *in vivo*, as a comparative technique to fluorescence microscopy. Therefore one must consider the effects of wavelength upon the components of the cellular environment. For this reason the wavelengths towards the near IR region ( $> 600$  nm) of the visible spectrum are often used to avoid the interference of intrinsic fluorescence from some aspects of the cell and plasma. In addition, water is Raman active at the lower end of the visible spectrum; consequently it is desirable for the dyes that are commonly employed have a  $\lambda$  maximum  $> 600$  nm.

The dyes synthesised in this research had a  $\lambda$  maximum of 630 nm and originated from a common family - Polymethine.<sup>186</sup> The defining characteristic of these dyes are the bridging carbons that exist within the structure of the dye.<sup>187</sup>

Manipulation of these carbons can alter the  $\lambda$  maximum of the dyes. Additionally the core structure means large libraries of dyes can be synthesised, an attractive quality considering the number of proteins within the human body.

Proteins are composed of amino acids which consist of a plethora of free primary amine groups. Consequently the easiest and most simple reaction to carry out to label the desired proteins was via amide chemistry; therefore the functionality of the dyes had to initially include a carboxylic acid moiety to enable successful reaction. Further to these considerations, the aim was to use these dyes in conjunction with nanoparticles. As such there was the requirement to incorporate a surface seeking group for attachment to the nanoparticle surface. Chemical linkers have been used in the past as a bi-functional protecting group in solid phase chemistry. However, linkers can also provide multi-functionality where several different reactions can be take place using one molecule.<sup>188</sup>

## 5.2 PREVIOUS WORK

For the successful employment in Raman based detection methods, the chosen reporter has to be capable of attachment to the nanoparticle surface, conjugate the biomolecule of interest and provide stability to this new conjugate. The long term goal of Raman based techniques is to incorporate these techniques into cellular environments to act as a comparative technique to the currently used method, fluorescence spectroscopy. Therefore the stability of these conjugates becomes important as cellular environment contains conditions that are harsh to nanoparticles, namely, high salt concentration. A paper published McKenzie *et al.* described the synthesis of a tri-functionalised linker based on the amino acid lysine.<sup>127</sup> Lysine was chosen as it contains two free primary amines and a carboxylic acid, all of which are capable of simple amide forming reactions. McKenzie *et al.* used a PEG group to confer stability to the system and a thioctic acid for attachment to the nanoparticle surface. This work demonstrated successful and stable linker attachment to both gold and silver nanoparticles, proving that the linker had potential to be used for *in vivo*

experiments. It was hypothesised that utilising the PEG/thioctic acid linker in conjunction with the dyes synthesised in this research a stable conjugate to be used for the assessment of these linker molecules as protein markers could be provided as shown in figure 5.1.

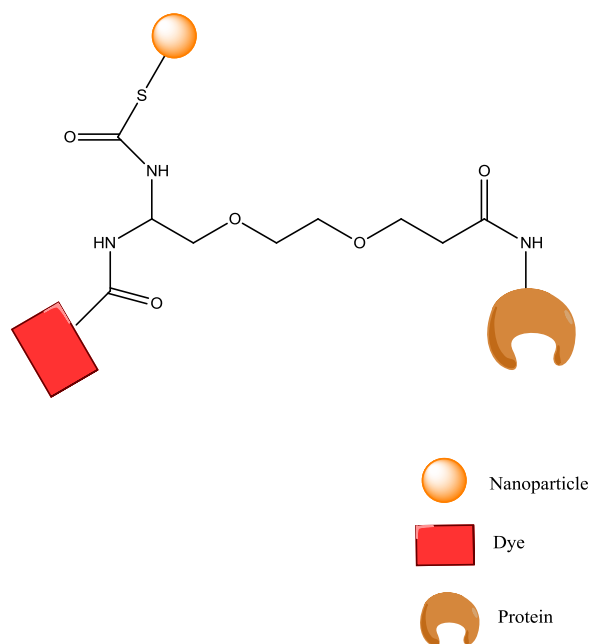


Figure 5.1: Schematic of proposed linker formation showing the planned points of amide formation and the anchor point onto the nanoparticle surface.

Two different dyes were investigated for this purpose: cyanine; and squaraine. Several different methods were implemented in an attempt to synthesise the final linker compounds - including solid phase chemistry. Further investigation into direct modification of proteins with the dyes was carried out, in attempt to compare each method for use in the detection of protein interactions.

### 5.3 CYANINE DYES

Originally synthesised by Williams in 1856, this family of dyes has found use in a variety of fields including: industrial paints; as anti-tumour agents; and in optical disks for recording purposes.<sup>189-191</sup> More specifically, these dyes have been widely used within the biological domain. Fluorescence microscopy is the tool of choice for biologists in the analysis of cells and their components, therefore cyanine dyes have found a use in the field as they possess a high fluorescence quantum yield, thus

providing a strong response when used. Previously these type of dyes have been used to investigate the mechanism of DNA binding due to their ability to interact with DNA through groove-binding and intercalation.<sup>22</sup> The high molar coefficient and the ability to synthesise the dye to tailor the requirements has played a big part in their place in biological labelling. More recently these dyes have been used in conjunction with nanoparticles, allowing for detection by SERS.<sup>192, 193</sup> As a consequence of their high molar extinction coefficient, this also makes these dyes strong Raman reporters. This is an important feature for the applications outlined in this body of work.

The application involves the detection of small biological molecules at very low concentrations (in the picomolar range) therefore utilising molecules that are strong Raman reporters will provide strong and identifiable signals within the low detection limits required. Another advantage of cyanine dyes is that they are synthesised in a step by step method: with the core structure of the dye remaining constant; and the side chains being easily modified to fit the need of the application. This is an advantage for SERS, as it means that several dyes can be synthesised with various different side chains that can be used together to create a multiplex. Vibrational peaks from each separate dye can be indentified and thus identify the biological molecule to which it has been labelled

The general structure of this class of dyes is shown in figure 5.2 consisting of two nitrogen containing heterocyclic linked to one another by an odd numbered polyene chain. In most cases the nitrogen atoms are alkylated, resulting in an overall positive charge in the delocalised system. The heterocycle can be varied between a single benzene ring and a naphthalene type ring attached to the indole ring which is indicated by the numbering system in the nomenclature. CyX (where x =3, 5 or7) denotes a single benzene ring and CyX.5 denotes the presence of the naphthalene ring.

These molecules can be tuned to certain excitation/emission wavelengths by modification of heterocyclic core and the number of carbons within the polyene chain. As the number of carbons are increased the  $\lambda$  maximum of the absorption profile is shifted towards the IR region (a red shift is observed). The longest carbon length that has been employed within biological applications is seven.

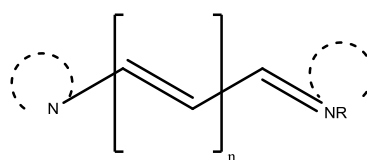
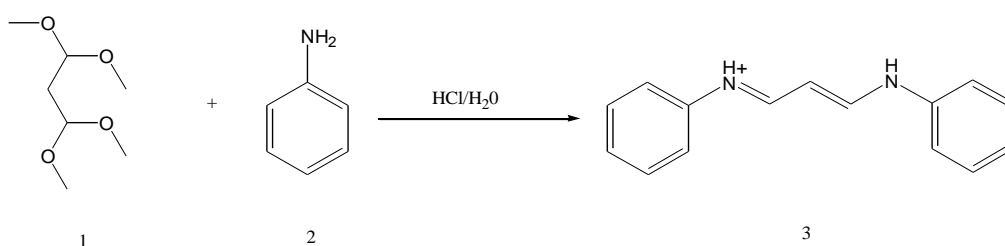


Figure 5.2: General structure of a cyanine dye, where  $n$  = number carbons.

Cyanine dyes are generally synthesised through stepwise addition of nucleophilic compounds. A key intermediate within this synthetic strategy is the polyene chain precursor which determines the length of the chain joining each end of the dye determining whether the Cy dye is Cy3, Cy5 or Cy7. Once the number of carbons had been decided the next step was to consider the functionality of the side groups of the dye - the principle use of these dyes was to react with proteins. As such the functionality used was predominately carboxylic acids to allow for amide formation with primary amines of the protein.

### 5.3.1 SYNTHESIS OF CYANINE DYES

At the core of the dye is the polyene chain which remains constant depending on what CY dye is made, i.e. Cy3, Cy5, or Cy7. The carbon length was chosen as 5 - this enabled the  $\lambda$  maximum to be beyond the 600 nm requirement. The core of the dye is known as an amidine and is synthesised using malondialdehyde bis(dimethylacetal), otherwise known as 1,1,3,3-tetramethoxypropane and aniline, as demonstrated by scheme 5.1.



Scheme 5.1 Formation of amidine using aniline and 1,1,3,3-tetramethoxypropane

This key building block was synthesised with relative ease: a solution of malondialdehyde bis(dimethylacetal) [1] in a mixture of water and hydrochloric acid was added drop wise to a stirring solution of aniline [2], water and hydrochloric acid.

On addition, an orange precipitate was produced. Upon complete addition, the mixture was allowed to stir at room temperature for 4 hours. The orange precipitate was filtered and washed with diethyl ether and allowed to dry under vacuum. This yielded the product in a 48% yield and a purity of ~95%. The next set of building blocks within this synthesis was the heterocyclic side chains of the dye. These side chains were based on the starting material trimethylbenz[e]indole (TMB) (structure shown in figure 5.3). The variation of these building blocks comes from the ability to be able to alkylate the nitrogen with ease.

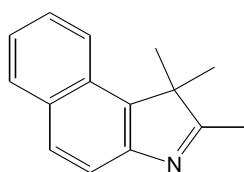
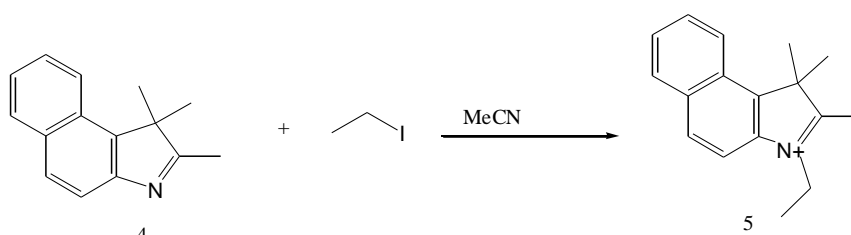


Figure 5.3 Structure of TMB

#### 5.3.1.1 SYNTHESIS OF TMB GROUPS

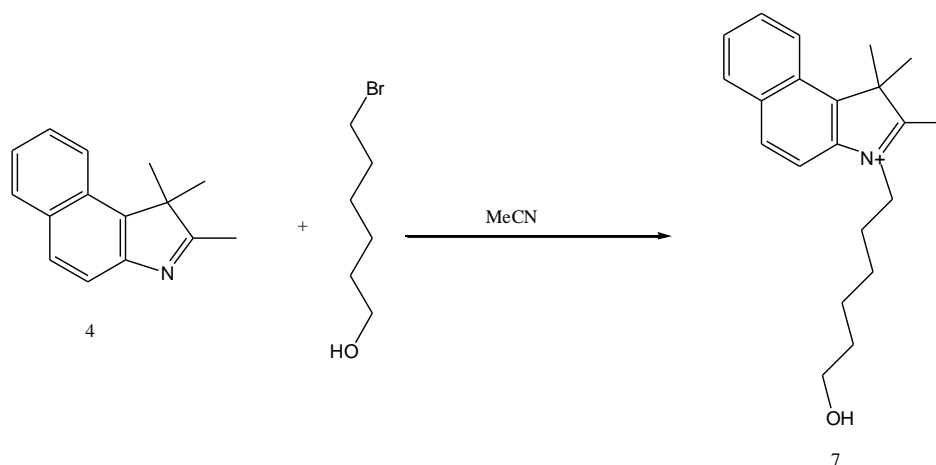
Several different types of functional groups were used in an attempt to provide different anchoring points. The TMB was refluxed between 48-96 hours in acetonitrile with the desired alkyl halide. The reaction mixture was then suspended in 10x volume of diethyl ether for an hour, which caused precipitation of the product. The precipitate was collected by filtration followed by drying over vacuum. This was the standard procedure used for the synthesis of all of the side chains.

Alkyl halides were used to provide the TMB moiety with functionality. These dyes were to be used in the detection of biomolecules and as such require functionality to enable coupling of these dyes to biomolecules, therefore unsymmetrical dyes had to be synthesised to enable selective reactions. Ethyl iodide was used to produce an intermediate for the unsymmetrical dyes that were synthesised to allow for selective reactions to take place, as shown in scheme 5.2.



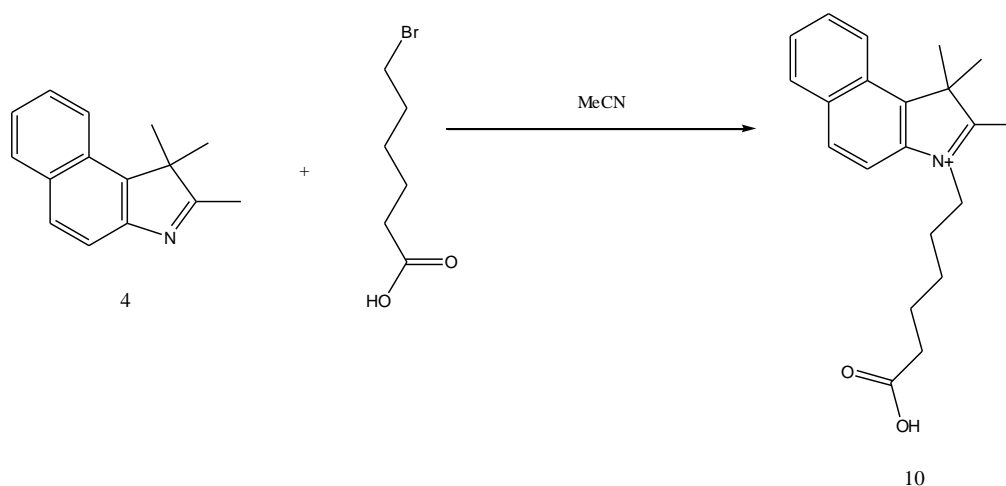
Scheme 5.2: Alkylation of TMB nitrogen with ethyl iodide

TMB was also reacted with 6-Bromohexanol (scheme 5.3) and 6-bromohexanoic acid (scheme 5.4) to allow for further reactions once the final dye had been synthesised.



Scheme 5.3: Alkylation of TMB nitrogen with 6-Bromohexanol

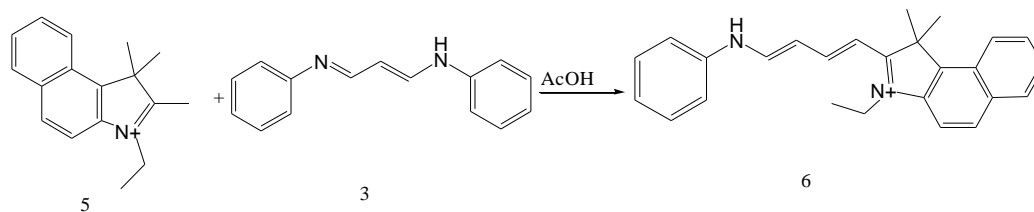
Compound [7] and [10] were synthesised in yields of 80% and 90% respectively.



Scheme 5.4: Alkylation of TMB nitrogen with 6-Bromohexanoic acid

### 5.3.1.2 SYNTHESIS OF INITIAL DYES

Following the successful synthesis of the TMB derivatives, the next stage was to react 3-ethyl-1,1,2-trimethyl-1H-benzo[e]indolium [5] with the amidine [3], shown in scheme 5.5. This was carried out in glacial acetic acid and refluxed for 4 hours.



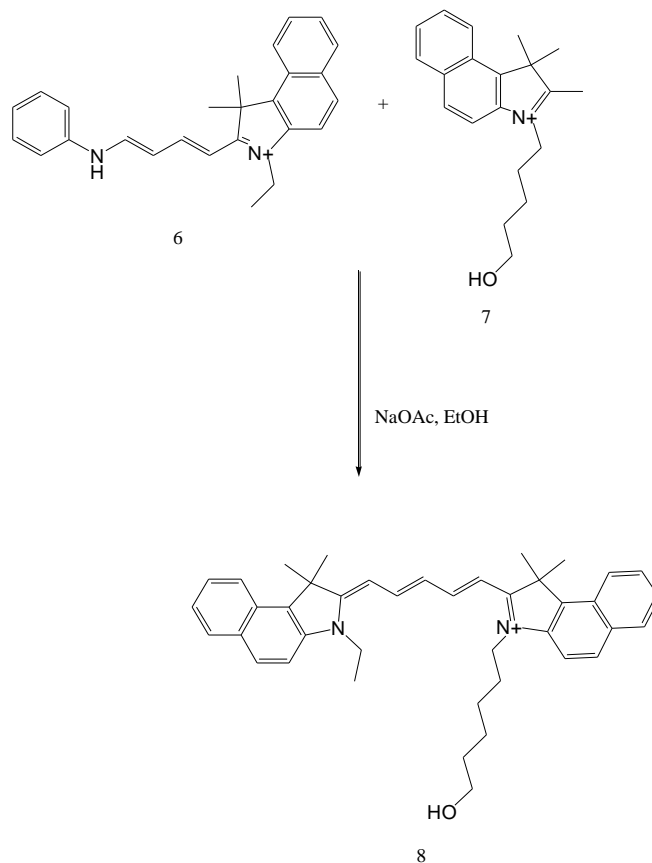
Scheme 5.5: Formation of hemicyanine, using amidine [3] and TMB-Et[5]

Purification of these types of dyes can be very difficult with impurities displaying similar behaviour when visualised by TLC, as in figure 5.4.



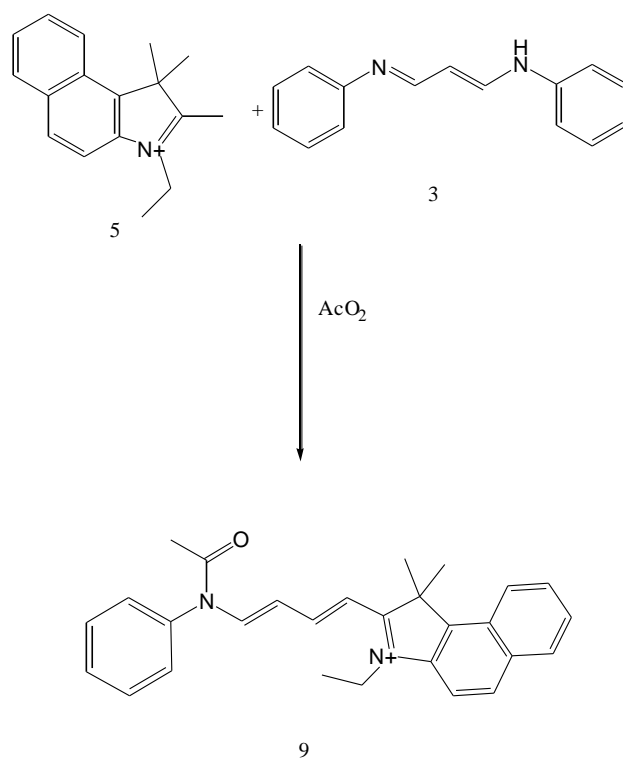
Figure 5.4: TLC of crude mixture from synthesis of dye 1, scheme 5.7, carried out in 9:1 DCM: MeOH

Purification of the hemicyanine was difficult and produced only 5 mg of the desired product. However, it was decided to continue to the last stage of the formation of the dye. A paper published by Jung *et al.*<sup>194</sup> used sodium acetate in ethanol to form the cyanine dye. This method was employed with the hemicyanine [6] and TMB-OH [7] in ethanol with sodium acetate which was refluxed for 4 hours, shown in scheme 5.6.



Scheme 5.6: Formation of cyanine dye 1: between hemicyanine [6] and TMB-OH [7]

A blue coloured solution was obtained upon completion of the reaction; visualisation by TLC showed there to be several different coloured spots. The by-products of the reaction made the separation very difficult through lack of distinct partitioning between the spots when on the silica column. Purification was difficult as only 1 mg was obtained of the pure product which could not be used for further reactions. It appeared the method by Jung *et al.* produced low yields and lack reproducibility. Upon further investigation, a paper published by Mader *et al.* used an alternative method.<sup>195</sup> This method was reported as more successful, in the formation of the hemicyanine intermediate. Acetic anhydride was used in place of acetic acid; yielding a slightly different product.<sup>195</sup> See scheme 5.7.

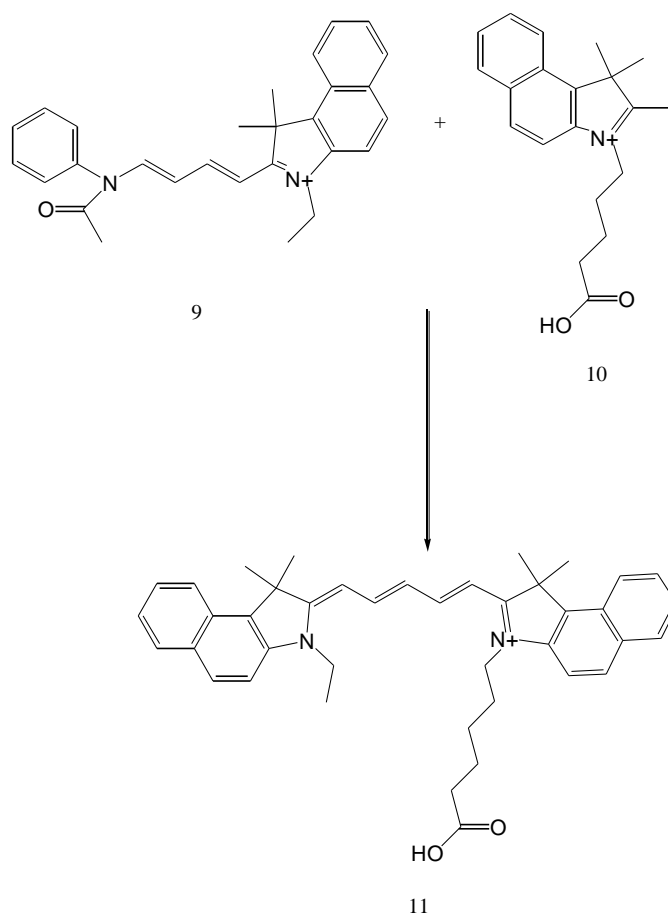


Scheme 5.7: Formation of hemicyanine using TMB-Et [5] and amidine [3] using acetic anhydride as the reaction solvent

Purification by flash column chromatography was readily achieved yielding compound [9]. For the formation of the dye, pyridine was used, as detailed in the paper published by Mader *et al.* Compound [9] was dissolved in pyridine and heated to 50°C for 2 hours producing the desired blue product - compound [8] in a yield of 28% over three steps.

The success of the method served as a validation for the synthesis of a second dye which could be employed in protein labelling, for this compound [10] was used to replace TMB-OH [7].

The TMB-COOH [10] was combined with compound [9] to which pyridine was added before heating at 50 °C for 30 minutes. Producing a blue solution the crude mixture was purified by column chromatography in a 12% yield, producing 5 mg of the desired product (scheme 5.8).



Scheme 5.8: Synthesis of complete dye, compound [11], using hemicyanine [9] and TMB-COOH [10] and pyridine as the reaction solvent.

The successful synthesis of compound [11] meant that this dye could be used in a series of protein labelling experiments to ascertain the viability of this dye in the area of protein detection.

To enable multiplexing scenarios it was decided that it would be beneficial to synthesise a family of dyes which could be used for this purpose. However, with the ongoing purification problems of this class of dye and the low yield that was obtained; this was problematic. The dyes had to be used in further reactions, thus obtaining 2-3 mg of final dye made subsequent reactions more difficult. An alternative route was investigated; Mason *et al.* published a paper detailing the use of solid phase synthesis in the creation of cyanine dyes.<sup>196, 197</sup>

## 5.4 SOLID PHASE SYNTHESIS

Solid phase synthesis (SPP) is an attractive route to use if possible in organic chemistry. The advantages of this type of synthesis are that it can introduce selectivity and purity in the compounds made. Furthermore, there is no requirement to carry out long and difficult columns to purify the compound because in each step the reagents are added in excess and any by-products or unused reactants are simply washed away. Solid-phase organic synthesis has been used largely for the synthesis of peptides and DNA. It is the advantages of solid-phase synthesis that creates the attraction for scientists:

- i. Reactions can be driven to completion through the addition of excess reagent.
- ii. Excess reagents and soluble by-products can be removed by resin washing.
- iii. Physical losses are minimal as the product remains attached to the resin.

However, solid-phase synthesis is not restricted to peptide synthesis and DNA. Many drug and organic compounds have been made via this method. Even in recent times many dyes have been prepared via solid-phase.

In the paper published by Mason *et al.*, the resin of choice was a sulfonyl chloride polystyrene resin, as detailed in figure 5.5.<sup>196</sup> This type of resin has been used in many different types of reactions and is adaptable for many uses.

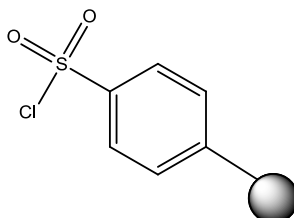


Figure 5.5 Representation of functional group of a sulfonyl chloride polystyrene resin.

The resin was first synthesised by Merrifield in 1963 for peptide synthesis; hoping that it would provide a method for preparing higher molecular weight polypeptide chains.<sup>198</sup> The resin is commercially available and consists of divinylbenzene cross linked polystyrene beads that have been functionalised with chloromethyl groups. A polymer had to be chosen which was insoluble in most common solvents and had a stable physical form. It was found the chloromethylated co-polymer of styrene and divinylbenzene was best suited - the resin composition is shown in figure 5.6.

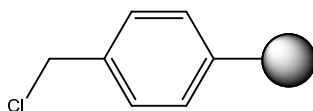
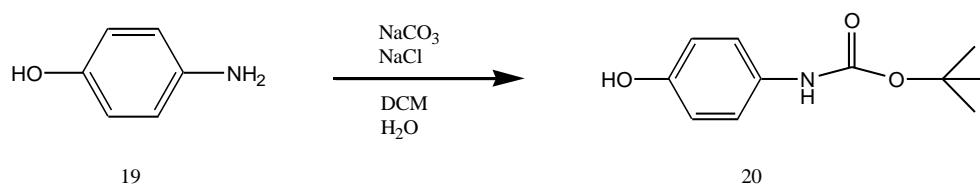


Figure 5.6: Representation of functional group of a Merrifield resin.

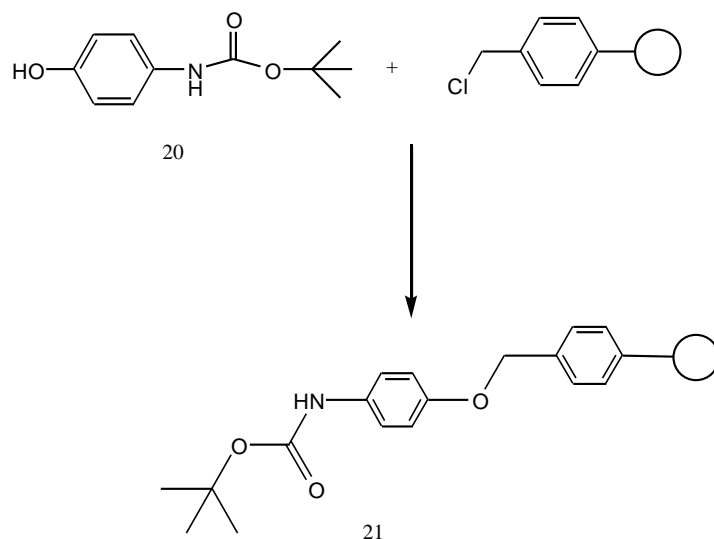
Today, Merrifield resins are used in a variety of organic reactions. These resins are commercially available in a range of Mesh sizes and percentage cross-linked to suit the researcher's requirements. [44], [45]

Mason *et al.* adapted methods already carried out in solution. The first stage of this SPP synthesis involved the protection of 4-aminophenol with the common protecting group, BOC, shown in scheme 5.9.<sup>197</sup>



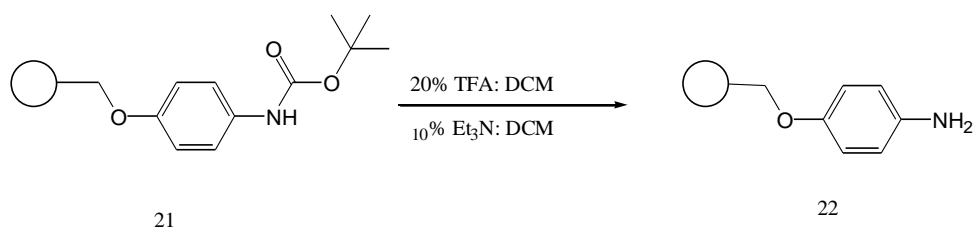
Scheme 5.9: Protection of 4-aminophenol using BOC anhydride

4-aminophenol was dissolved in DCM and H<sub>2</sub>O, to which sodium carbonate and sodium chloride were added. BOC anhydride was dissolved in DCM and added drop wise to this stirring solution. Following stirring at room temperature for 18 hours and removal of excess solvent; compound [20] was isolated. This product was dissolved in DMF and suspended with the Merrifield resin. This suspension was heated at 50 °C for 32 hours - as shown scheme 5.10 – with the modified resin forming through a nucleophilic substitution reaction.



Scheme 5.10 Attachment to the Merrifield resin through a Sn2 reaction.

The crude solution was filtered, removing excess reagents and washed with DCM; producing the product as a beige resin. Deprotection of the resin-bound followed using a 20% TFA:DCM solution, detailed in scheme 5.11. After agitating the solution for 2 hours at room temperature, the resin was filtered and washed with DCM. The resin was then added to a 10% Et<sub>3</sub>N: DCM solution to neutralise excess TFA; producing the product as a beige resin.

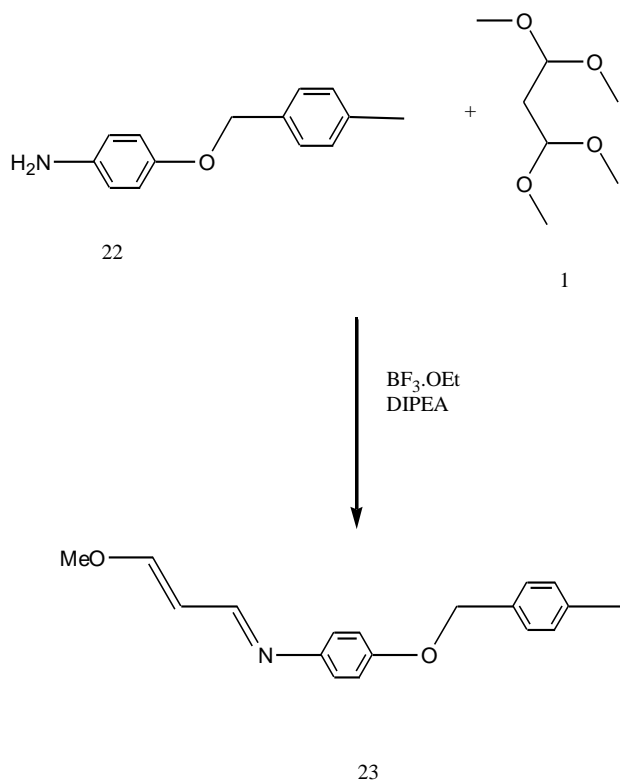


Scheme 5.11: Deprotection of resin bound 4-aminophenol using TFA solution

The Merrifield resin had now been successfully modified for cyanine synthesis. The steps carried out on the resin were not very much different from those carried out in solution phase.

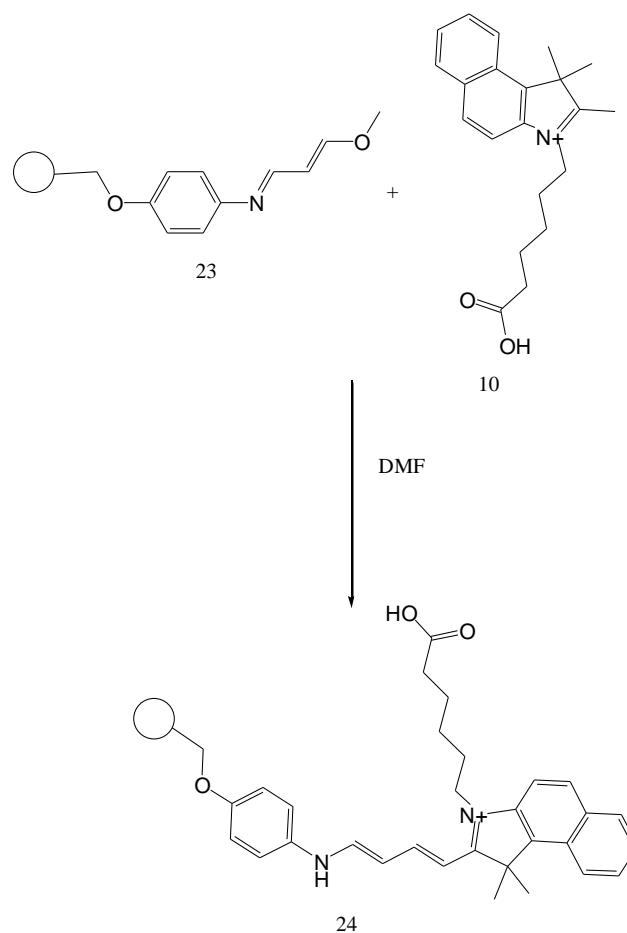
The amidine formed and reacted in the same manner as with the aniline in the solution phase reactions. Malondialdehyde bis(dimethylacetal) [1] the modified resin [21] and boron trifluoride diethyl etherate were suspended in DCM and stirred at room temperature for 6 hours. DIPEA was added and the suspension briefly stirred

for a further 10 minutes before obtaining the beige resin through filtration, shown in scheme 5.12.



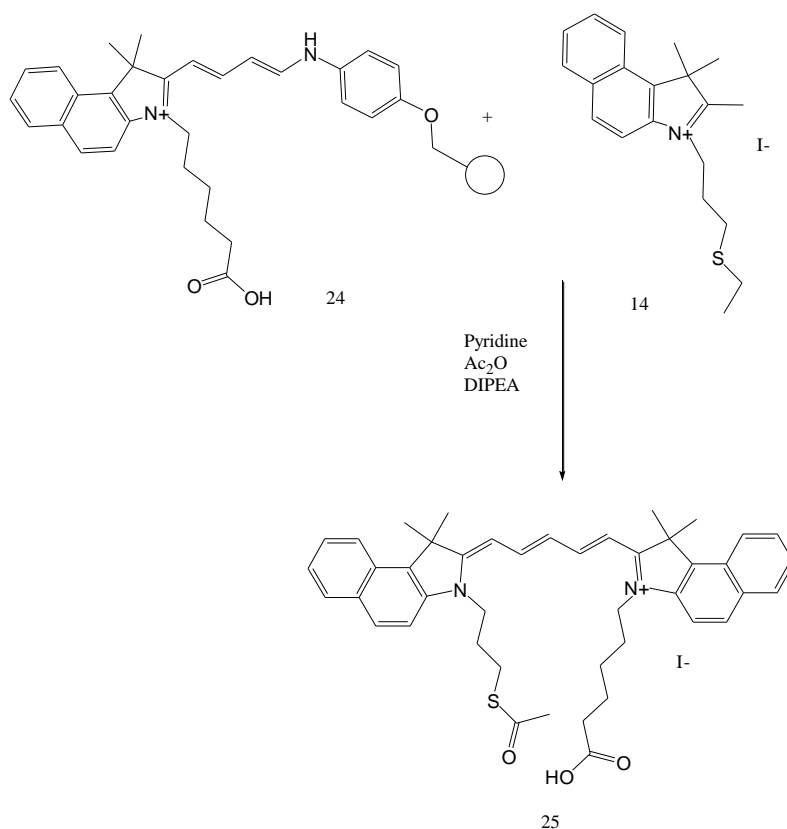
Scheme 5.12: Formation of hemicyanine precursor on Merrifield resin using 1,1,3,3-tetramethoxypropane

The next stage was to form the hemicyanine; the resin-bound amidine was suspended in DMF and 3-(5-carboxypentyl)-1,1,2-trimethyl-1H-benzo[e]indolium was added. The solution was heated at 80°C for 4hrs. The product was isolated by filtration followed by washing with water, DMF and finally DCM – see scheme 5.13.



Scheme 5.13: Formation of hemicyanine on Merrifield resin using TBM-COOH

For formation of the dye TMB-SoAC[14], the modified resin and DIPEA were suspended in acetic anhydride and pyridine was stirred at room temperature for an hour. The action of the formation of the dye causes internal cleavage without the requirement of common resin cleavage agents - such as TFA - which can be detrimental to the final product as scheme 5.14 shows.



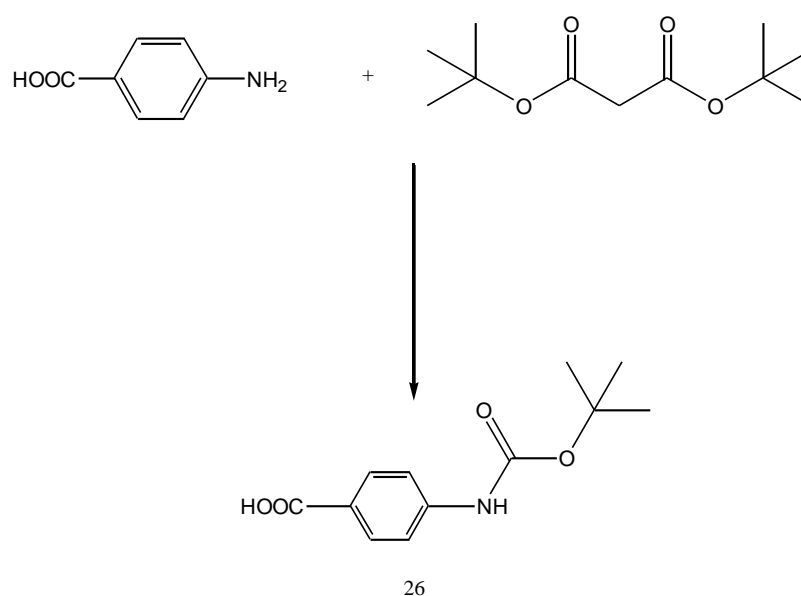
Scheme 5.14: Formation of cyanine dye 3 using TMB-SoAc [14] and hemicyanine [24] attached to Merrifield resin

The reaction mixture was filtered to separate the now redundant resin and the desired product. The excess solvent was removed from the filtrate producing the desired product as a solid in a 15% yield. The yield was lower than expected when compared to the results obtained by Mason *et al.* declaring a yield of 86% for their final product.

One of the disadvantages of solid phase chemistry is the inability to be able to follow the reaction and its efficiency, NMR is typically used to determine the purity and therefore efficiency of chemical reactions. Thus in an attempt to follow the efficiency of the reactions and improve yield; a paper published by Jiang *et al.*, used PEG as a solid phase substrate.<sup>199</sup> PEG groups can be used as solid supports as they are polymers akin to the Merrifield resin; however it is a soluble polymer support. The polymer polyethylene glycol has combined the benefits of solid phase synthesis in

terms of purity of the compound and the fact that as it is a soluble material the reaction can be followed by NMR.

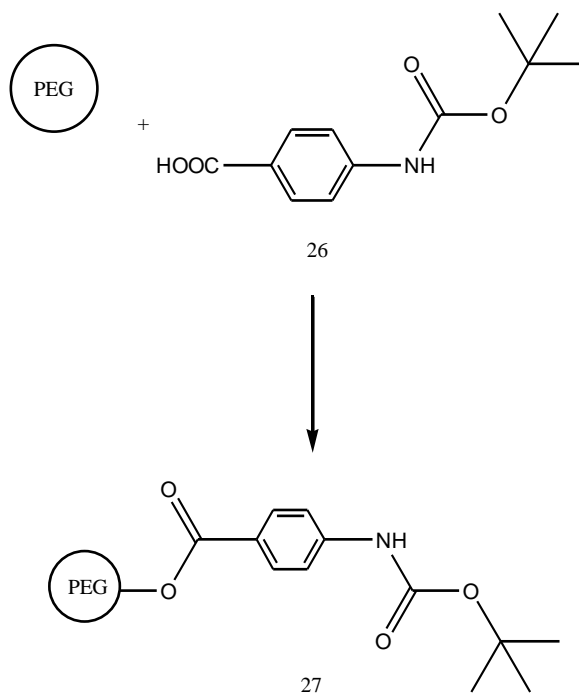
A PEG polymer of a molecular weight of approximately 2000 g was chosen to match that used in research carried out by Jiang *et al.* The synthetic steps were very similar to the steps undertaken by Mason *et al.*, 4-aminobenzoic acid was dissolved in THF. To this solution, tert-butyl dicarbonate, dissolved in THF, was added drop wise to the reaction mixture over the course of 1 hour at 6 °C. The excess solvent was removed and the remaining solid was dissolved in ethyl acetate and washed with 5% HCl and water; the organic layer was dried over MgSO<sub>4</sub> and excess solvent was removed to produce a beige solid, shown in scheme 5.15.



Scheme 5.15: BOC protection of 4-aminobenzoic acid

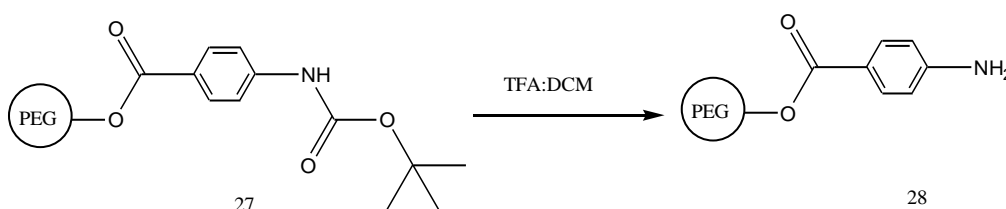
For attachment to the PEG, the protected 4-aminobenzoic acid [26] was dissolved in DCM with 4-diaminopyridine (DMAP) and DCC to which the PEG group was added. DCC was chosen as the coupling reagent, as an advantage of using such agent is that upon successful coupling a precipitate forms; this precipitate is DCU and can be easily filtered from the reaction mixture.

The reaction mixture was stirred at room temperature for 15 hours. Following this, diethyl ether was added which induced precipitation of the PEG polymer support, as scheme 5.16 shows.



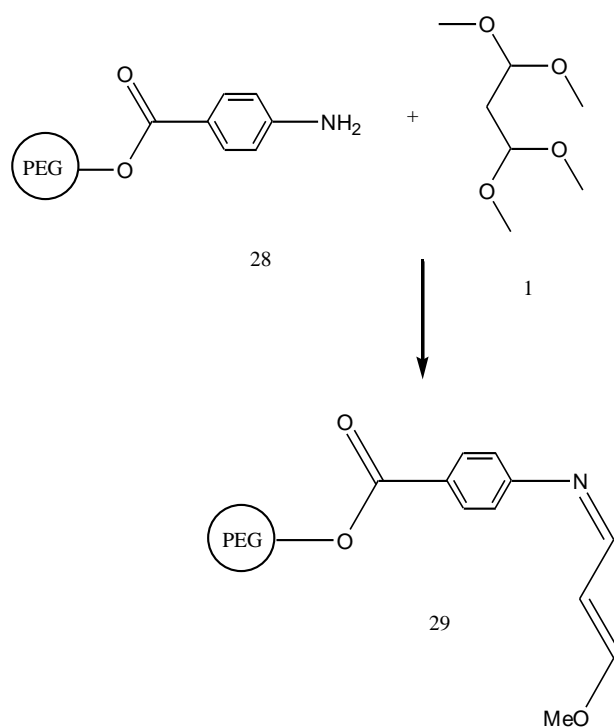
Scheme 5.16: Attachment to PEG group via ester formation with BOC protected 4-aminobenzoic acid

$^1\text{H}$  NMR was used to confirm the success of the coupling. The final step prior to the synthesis of the dye was the deprotection of the amino group. This was carried out following standard procedures; 50% TFA: DCM solution stirred at room temperature for 3 hours, shown in scheme 5.17.



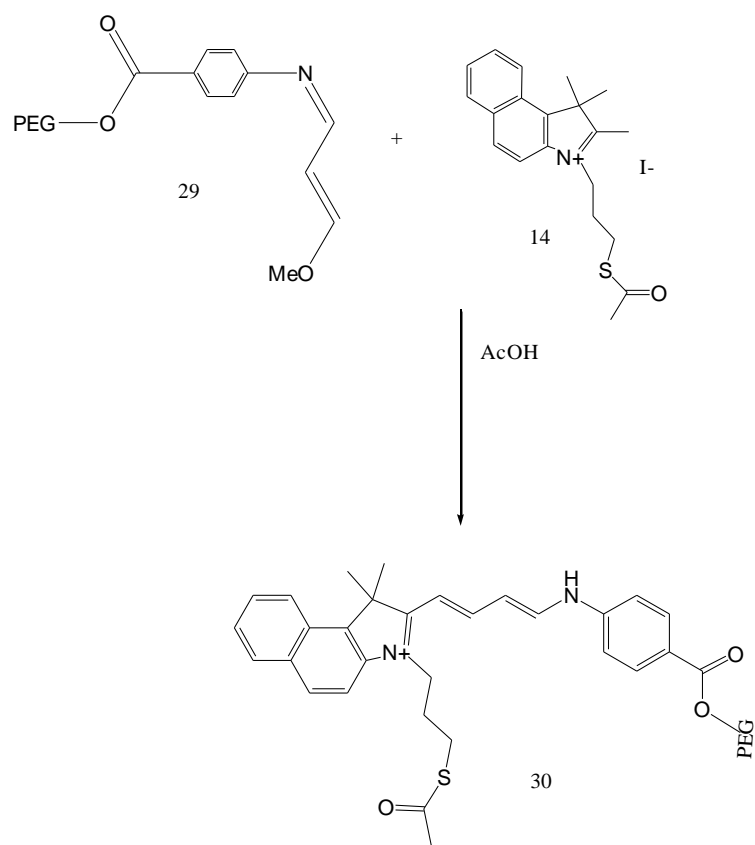
Scheme 5.17: Deprotection of the amino group

For the synthesis of the cyanine dye, the method published by Mason *et al.* was followed. Malondialdehyde bis(dimethylacetal) was added to a suspension of the modified polymer support and glacial acetic acid then heated at 55 °C for 6 hours. Precipitation was facilitated by the addition of diethyl ether; producing the desired product without the need for further purification, as shown in scheme 5.18.



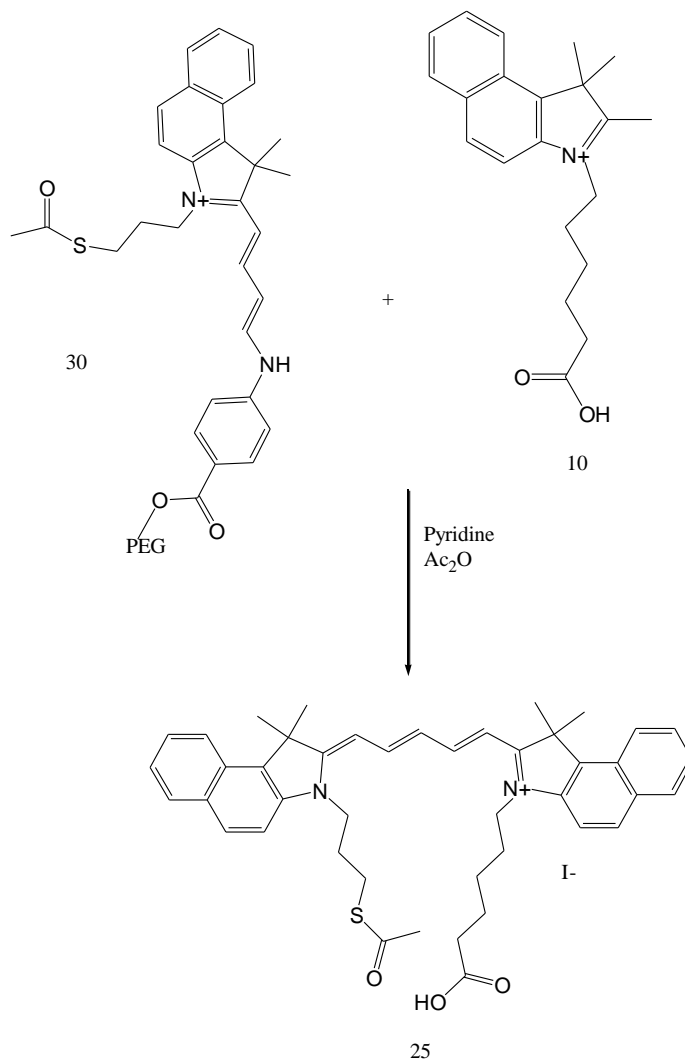
Scheme 5.18: Formation of amidine on polymer support using 1,1,3,3-tetramethoxypropane

Following the success of the resin synthesis of the amidine [29], the formation of the hemicyanine was carried out. The polymer support and compound [14] were dissolved in glacial acetic acid and heated to 80 °C for 1 hour, which can be seen in scheme 5.20. Jiang *et al.* once more used diethyl ether to precipitate the desired product, however, when carried out to produce compound [30], the addition of diethyl ether did not yield a fine precipitate but a slurry. Attempts to purify this slurry using various solvents were unsuccessful; column chromatography was not used due to the difficulties that would undoubtedly be encountered. PEG groups are polymers, therefore have an average molecular weight. As such there were many different side chains which contain the same repeating group, yet differ in the specific number present. Consequently separation on a column would not likely provide adequate separation; as a result the crude product carried forward to the next stage.



Scheme 5.19: Formation of hemicyanine using TMB-SoAC and PEG bound amidine

In the final stage - once more very similar to Mason *et al.* - pyridine and acetic anhydride were used as the solvent system for the formation of the dye as scheme 5.20 explains.



Scheme 5.20: Formation of cyanine dye 4 using PEG bound hemicyanine and TMB-SoAC

Upon completion and removal of excess solvent a black solid was obtained. Further investigation of the <sup>1</sup>H NMR revealed the compound collected did not have the required peaks. It was thought the impurity of the previous stages had caused the failure of the final stage. Therefore it was decided to no longer pursue the solid phase route towards dye synthesis. It was thought that this method would provide a quick and easy route towards a family of dyes that could be implemented in the detection of proteins; however low yields and difficult purifications led to very little success.

## 5.5 SQUARINE DYES-AN INTRODUCTION

Closely related to cyanine dyes the term 'Squaraine dyes', was first coined by Schmidt. However, this class of dyes were first synthesised by Trebs and Jacob in 1965.<sup>200</sup> A number of derivatives of this class of dyes have been reported finding use as: xerographic photoreceptors; cation detectors; long wavelength fluorescence reporters; and in non-linear optics.<sup>201-203</sup> In addition to this squaric acid, the core of these dyes, has been used in the synthesis of chiral ligands which were used in as a catalyst in the formation of ketones and diketones.<sup>204</sup>

The general structure is shown below in figure 5.7. The structure of these dyes is characterised by a central  $C_4O_2$  cyclobutadione bridge comprising an electron deficient Hückel ring. The overall structure can be represented in a number of forms and the charge is considered to be largely delocalised over the molecule.

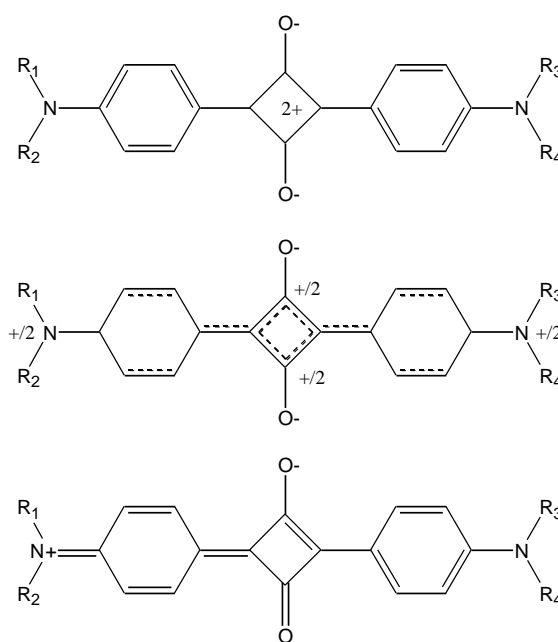


Figure 5.7: Structures for bis(4-alkylaminophenyl)squaraine derived dyes: (a) Fully aromatic, (b) Centrosymmetric partially quinoid form, (c) Non-centrosymmetric form with quinoid and aromatic regions. R = aliphatic hydrocarbons.

This class of dyes has been reported to have excellent photostability and exhibit narrow and intense absorption bands towards the red end of the visible spectrum.<sup>205</sup> This becomes important in the detection of biological components in an *in vivo*

situation as at lower wavelengths the interference from intrinsic fluorescence of the cell would disrupt the results obtained. In recent years there has been a shift from the more traditional applications of use in xerographic devices to more biological orientated and detection type application.<sup>206</sup>

### 5.5.1 PREVIOUS WORK

In 2006 Tatarets *et al.*, followed by Volkova et al., published a paper describing the investigation of a set of squaraine dyes as fluorescent probes and labels.<sup>207, 208</sup> In this paper, it was found that squaraines were shown to have superior properties than the conventional open chained cyanine dyes; providing the ability to be used in fluorescence lifetime based biomedical applications.

Fluorescence spectroscopy is the most commonly used technique for the analysis of biological processes. Although it can be relatively limiting in that the corresponding spectrum obtained is broad and as a consequence the ability to monitor more than one substrate in the real time is intensely difficult. Detailed in section 1.8, Raman spectroscopic techniques produce vibrational spectra, unique to each compound and directly related to the molecular structure. Therefore this property can be used to analyse multiple compounds in real time, i.e. create a multiplex analysis system. With this in mind, the most distinct advantage of this class of dyes becomes apparent. Squaraine dyes have been previously used in Raman spectroscopy. When synthesised as the anilino form, these dyes exhibit a vibrational peak in the  $1700\text{ cm}^{-1}$  region where no other common Raman reporters produced a signal.<sup>97</sup>

It has been reported that this peak originates from the symmetric stretch of the delocalised  $\text{C}_2\text{O}_2$ . It is present regardless of the group present on the nitrogen of the aniline group. It was reasoned that multiplexing would be easier with this unique property, therefore enabling the detection and monitoring of several proteins at one time.

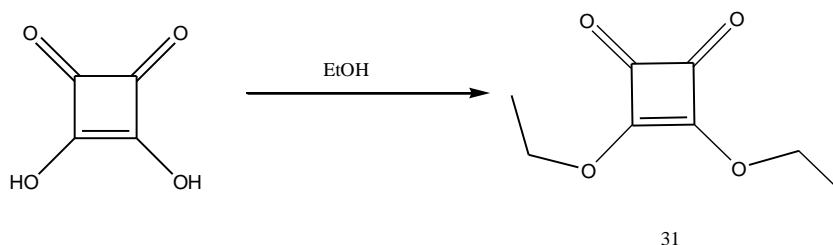
### 5.5.2 SYNTHESIS OF SQUARAIN DYES

The simplest method for the synthesis of this class of dye involves condensation of the side chains of the dye with the core, squaric acid. However, this causes a problem when selectivity is considered. Upon successful synthesis, the subsequent reactions

of these dyes required there to only be one group capable of the formation of an amide bond between the protein, otherwise purification would have been difficult. Therefore asymmetric squaraine dyes were required to be synthesised.

It was important to synthesise groups that were capable of forming amide bonds with primary amines, as with the cyanine dyes, the goal was to conjugate these dyes to proteins and linker molecules. Furthermore, the presence of two free hydroxyl groups on squaric acid meant a protection step was necessary prior to reaction in order to prevent unselective reactions taking place.

Many papers have been published detailing the asymmetric synthesis of this class of dyes and consequently the protection of squaric acid. However, the method that was followed was published by Terpetschinig *et al.* whereby the squaric acid was protected by forming an ester with ethanol, as shown in scheme 5.21.<sup>209</sup>

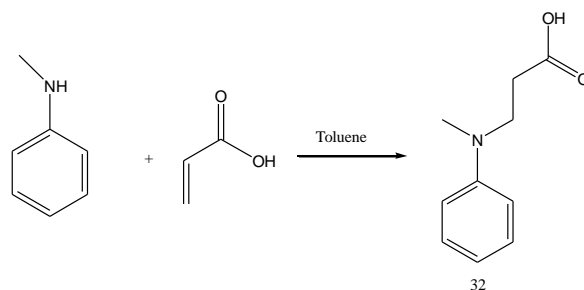


Scheme 5.21: Protection of squaric acid, forming 3,4-diethoxy-3-cyclobutene-1,2-dione

To introduce selectivity in the precursor for subsequent coupling reactions, N-methylaniline was chosen; the presence of the secondary amine allows for selective alkylation and introduction of a reactive group.

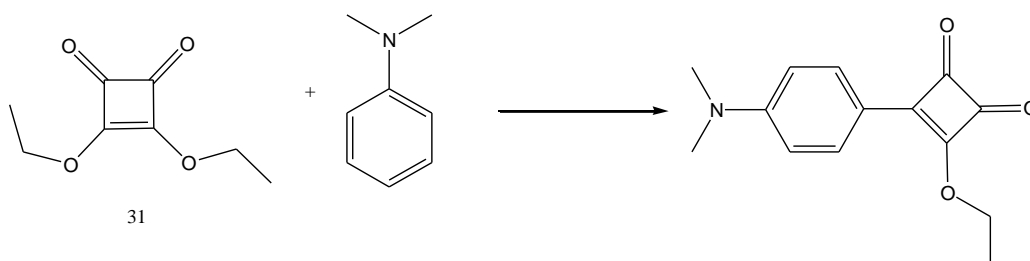
#### 5.5.2.1 SYNTHESIS OF HALF SQUARINE

The Michael addition is an effective and mild way to form carbon-carbon single bonds. This reaction involves a nucleophile and an alpha-beta unsaturated carbonyl compound. N-methylaniline and acrylic acid were dissolved in toluene and refluxed for 48 hours, scheme 5.22.



Scheme 5.22: Michael addition of N-methylaniline and acrylic acid forming compound 32

The crude product was purified using flash column chromatography and produced the desired product [32] as brown oil in a 51% yield. The half squaraine was synthesised with N,N-dimethylaniline (DMA) as it was a commercially available product that was abundant and therefore if the reaction failed there would be no concern in wasting material. Protected squaric acid [31] and N,N-dimethylaniline, were dissolved in ethanol to which triethylamine was added, as scheme 5.23 shows. The reaction mixture was refluxed for 30 minutes.



Scheme 5.23: Synthesis of half-squaraine dye using compound 32 and dimethylaniline

TLC investigation revealed that no new spot had been formed, leading to the conclusion that the reaction had failed. Upon further investigation it was deemed that the reaction had failed due to an impurity present in the protected starting material. Compound [31] was re-synthesised and the reaction detailed in scheme 5.23 was repeated; however it failed once more. In the next attempt to form a half squaraine dye, the reagents were kept the same; however the reaction length was altered to 18 hours to investigate a longer reaction length. Nevertheless once more this reaction failed; in the next attempt the reaction solvent was adjusted.

A paper published by Yagi *et al.* revealed that greater success had been achieved when acetic acid was used as the reaction solvent. Consequently ethanol was replaced with acetic acid and the reaction was refluxed for 3 hours.<sup>210</sup> TLC revealed

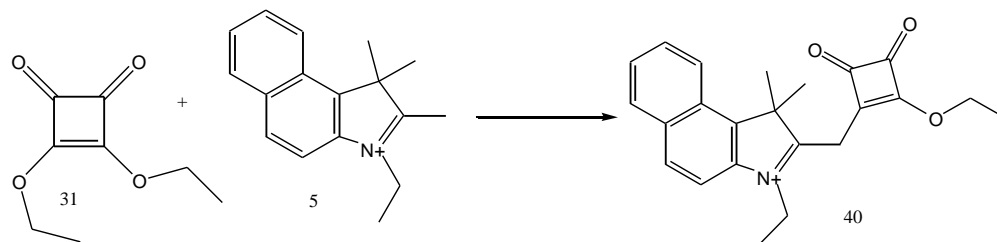
there to be several new spots on the plate, column chromatography was used to purify the crude mixture. The fractions corresponding to the spots on the TLC were collected and NMR analysis revealed that the desired product had once more failed to be synthesised successfully. It was reasoned that this could be down to the use of DMA; perhaps there was a requirement for the aniline to have increased delocalisation to facilitate the formation of the precursor dye. The reaction was once more attempted with compound [32] as the initial aniline to form half squaraine instead of DMA. This reaction was initially attempted using ethanol and then acetic acid as the chosen solvent systems, both reactions failed. In a final attempt to secure success, the choice of base was changed; this however did not bring success.

This step by step reaction mechanism was not progressing with the aniline derivatives. The approach then had to be changed. It was decided that the symmetrical version of the dye would be synthesised with more ease; once synthesised it was surmised selectivity could be introduced using a different approach, as detailed in section 5.6.

However, literature has shown that this step-by-step synthesis of unsymmetrical squaraine dye had been more successful with indole derivatives instead of the aniline version. This hypothesis was tested through the synthesis of indole asymmetric squaraine dyes. It has been reported that the Raman peak in the  $1700\text{ cm}^{-1}$  region obtained with aniline derivatives disappears when the aniline derivative is replaced with the indole version. This has been attributed to the decrease in symmetry in this class of squaraine dyes. Although not ideal, this class of squaraine dye was still a strong Raman reporter consequently increasing the number of dyes available for protein detection.<sup>97,211</sup>

### 5.5.3 INDOLE HALF SQUARAINES SYNTHESIS

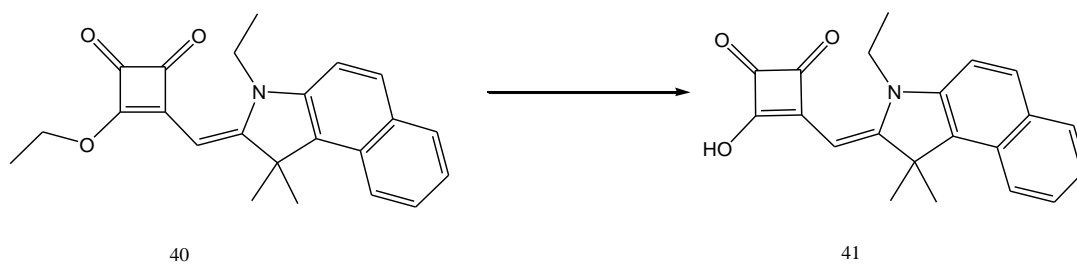
Compound [31] was dissolved in ethanol, to which triethylamine (TEA) and compound [5] was added. The reaction mixture was refluxed for 12 hours, (shown in scheme 5.24).



Scheme 5.24: Synthesis of half squaraine, using TMB-Et and diethyl protected squaric acid

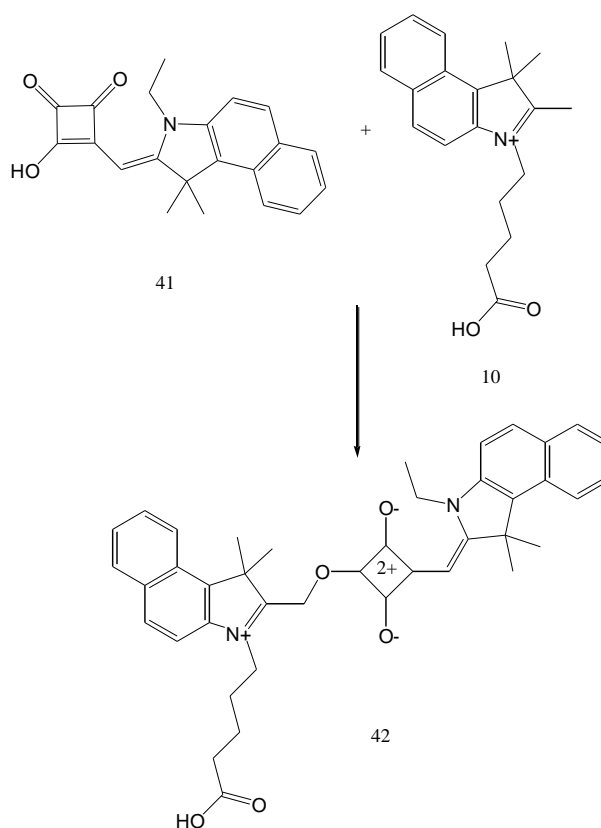
The crude product was purified by column chromatography producing compound [40] as a yellow solid in a 40% yield. Successful synthesis of compound [40] confirmed the theory that this method was best suited to indole substrates.

The next step was to hydrolyse the remaining protected alcohol, this was achieved using 40% (w/v) NaOH and the product was precipitated to avoid the use of column chromatography (Scheme 5.25).



Scheme 5.25: Deprotection of ethyl group using 40% NaOH in EtOH

The final step of the synthesis was to react compound [10] with the deprotected half squaraine product, compound [41]. Compound [10] was dissolved in isopropylalcohol (IPA) to which triethylorthoformate (TEOF) and compound [41] was added; this reaction mixture was refluxed for 18 hours.



Scheme 5.26: Formation of dye 6 using half ethyl squaraine and TMB-COOH

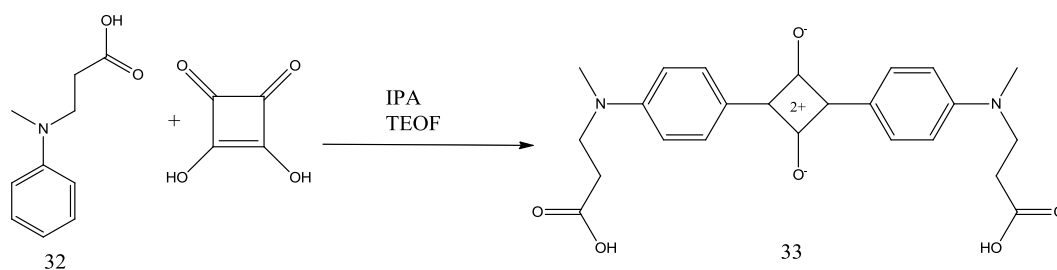
The crude product was purified by flash column chromatography; however on inspection of  $^1\text{H}$  NMR the desired product was not present. It was thought that more aggressive reaction conditions would have to be used.

Squaraine dye synthesis involves the production of water as a by-product. The driving force of the reaction is the removal of this water, hence the requirement of as TEOF as a drying reagent. However, under certain reactions this may not be enough to produce the dye. Dean-Stark apparatus has been used in the past to allow the formation of squaraine dyes. This apparatus was used in the repetition of this reaction, however, the solvent system was replaced - toluene and butanol was used in this attempt. This method successfully produced the product [42] - once purified by column chromatography - as a green solid in a 2.5% yield.

### 5.5.4 SOLID PHASE SYNTHESIS OF SQUARINE DYES - ATTEMPT TO FORM AN ANILINO SQUARINE

Unsuccessful synthesis of an asymmetric anilino squaraine led to the investigation of using SPS to introduce selectivity.

Compound [32] was dissolved in IPA with squaric acid, to which TEOF was added followed by reflux over 24 hours. The reaction mixture changed from a colourless solution to green. This was a positive sign indicating that the reaction had been successful. Upon cooling a precipitate formed and when filtered the product [33] was used without any further purification, which is shown in scheme 5.27.



Scheme 5.27: Formation symmetrical squaraine dye using compound [32] and squaric acid.

With the successful synthesis of product [33], this dye had to be used in subsequent reactions and therefore selectivity was an important property of the dye. It was reasoned that selectivity could be introduced through the use of solid phase chemistry.

Wang resin is a commonly used resin in solid phase synthesis which was inspired by Merrifield. Wang *et al.* designed a hydroxyl functionalised resin originally planned for synthesis of peptide acids using a Fmoc strategy.<sup>212</sup> Commonly used for the immobilisation of acids, these resins consist of chloromethylpolystyrene modified with 4-hydroxybenzyl alcohol (see figure 5.8). It has a free hydroxyl group which can be used as an anchor for modification and attachment to the solid support.

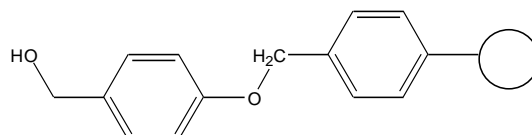
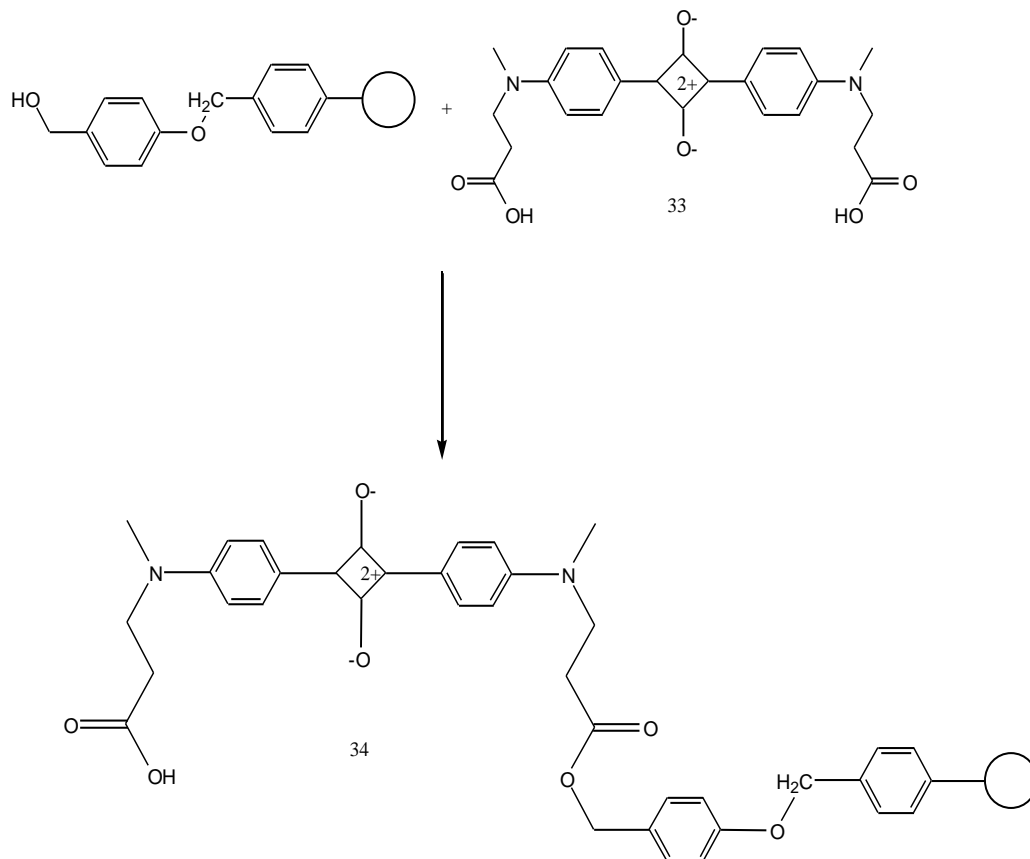


Figure 5.8: Wang resin

The free hydroxyl group on Wang resin was used to form an ester linkage with compound [33] through the carboxylic acid of the dye. The resin was suspended in DCM to which the coupling reagent DCC, DMAP and compound [33] were added; the suspension was agitated at room temperature for 18 hours (See scheme 5.28).



Scheme 5.28: Attachment of dye 5 to Wang resin via the formation of an ester

Traditionally, when using a solid support the reagents are used in a 5 times excess to ensure successful linkage onto the resin. However, the synthesis of the dye yielded very small amounts and consequently the amount of dye available could not be used in such a vast excess. The amount of resin used had to be reduced to allow for an excess ratio to be employed.

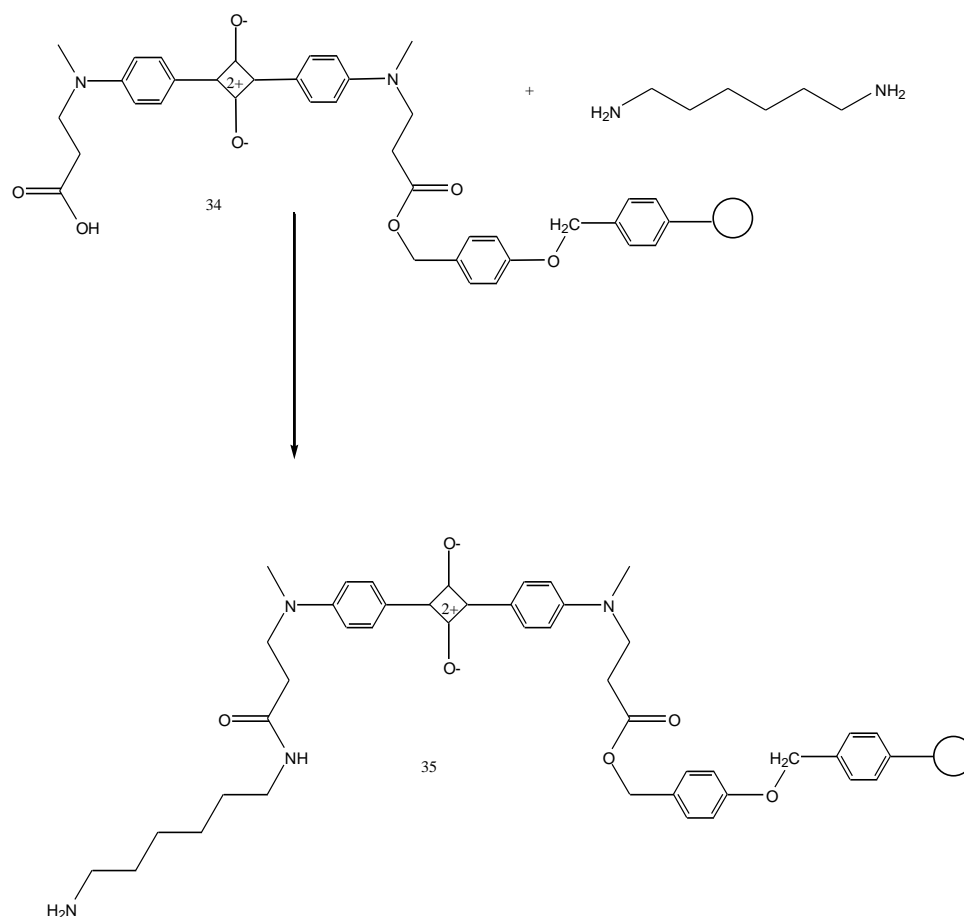
The suspension was filtered and washed with DCM and methanol three times respectively; yielding a resin which was colourless. It was presumed that on addition

to the resin, the dye would alter the colour of the resin indicating adsorption of the dye. Yet upon completion of the reaction the resin remained colourless.

It was hypothesised the failure of this reaction was a consequence of insolubility of the dye. Squaraine dyes have a long published history of the insolubility problems to which they possess. When compound [33] was dissolved in DCM this solubility problem became apparent, it was thought that the issue of poor solubility meant realistically a 5 times excess was not being used in this reaction, which consequently led to the failure of the reaction.

The reaction was repeated once more, however, on this occasion the dye was first dissolved in a mixture of DMF and  $K_2CO_3$ , which improved solubility. In addition to this, DPTS was used to aid the coupling. This led to a blue coloured resin being obtained; leading to the assumption that the reaction had been successful.

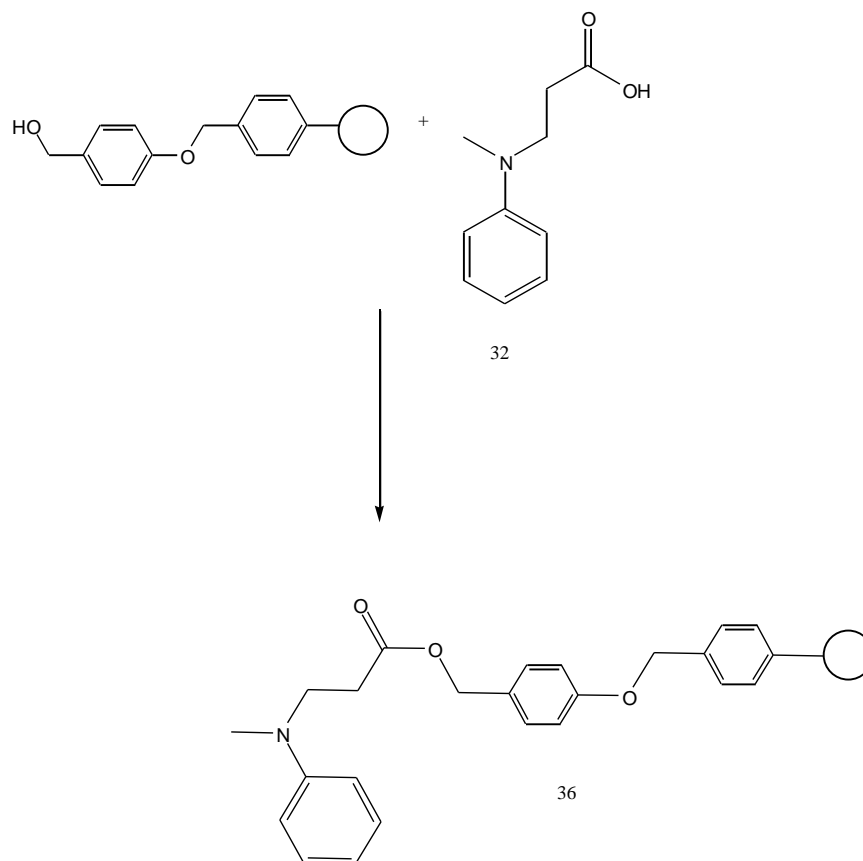
Once conjugated to the resin, the next step was to introduce an amine group to the resin bound dye to introduce selectivity to the dye, as illustrated in scheme 5.29. The modified resin [34] was suspended in DCM to which diamino-hexane and DIC were added; the reaction was agitated at room temperature for 18 hours.



Scheme 5.29: Formation of amide bond between diamino hexane and resin bound squaraine dye

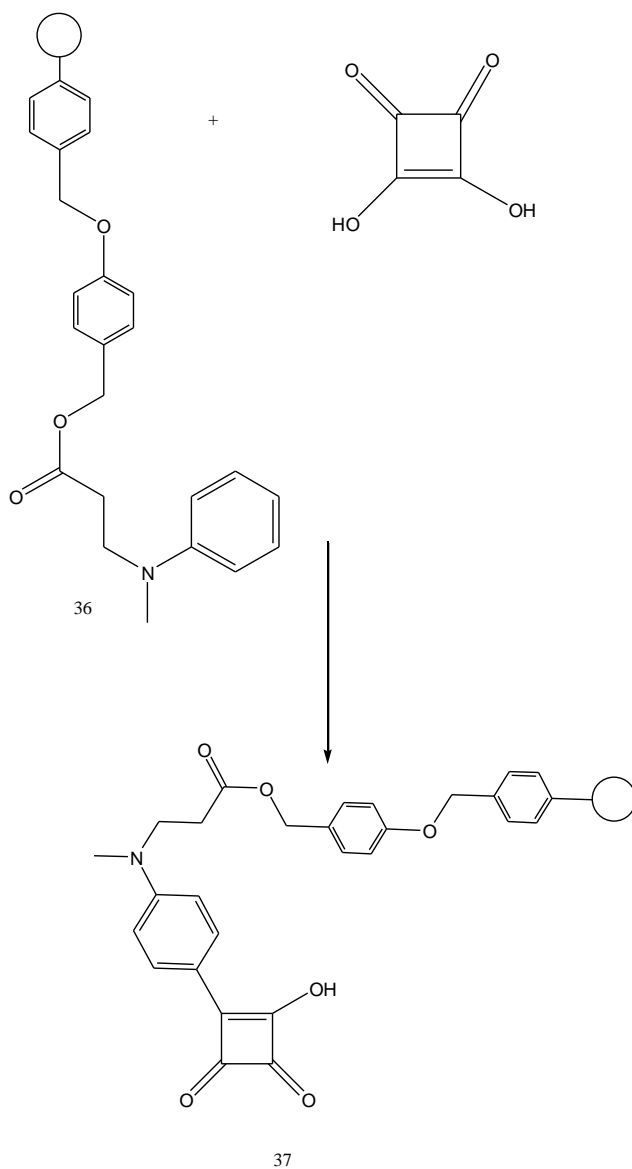
The resin was collected by filtration and washed with DCM and methanol three times respectively - this produced a resin which was now brown in colour. This indicated that the dye had most likely decomposed on the resin. It was unknown why this happened. It was surmised that as only a 1:1 equivalent of dye to Wang resin was used, which may have disfavoured the reaction.

To overcome the lack of dye, it was decided to attempt to form the dye on the resin; synthesising it in a step-by-step fashion. Unmodified Wang resin was suspended in DCM. To this solution, compound [32], DIC and DPTS were added and the reaction was agitated at room temperature for 18 hours, as shown in scheme 5.30.



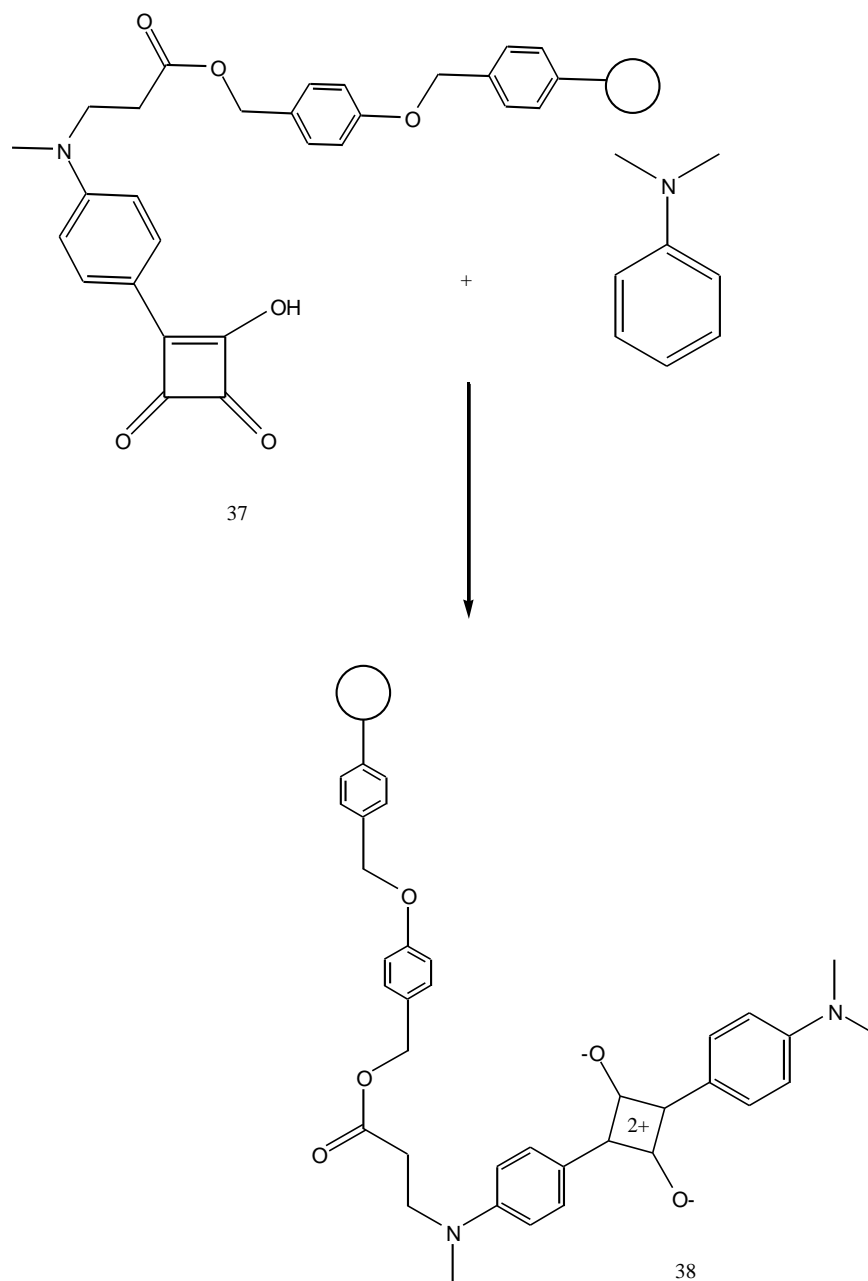
Scheme 5.30: On resin formation of the squaraine dye

The resin was collected by filtration, after washings with DCM and MeOH as before. This methodology had a disadvantage common to solid phase synthesis, namely, the reactions performed on such substrates which cannot be monitored for success or failure. Therefore without confirmation of success of the reaction there had to be an assumption that the reaction had been successful. As a result of this the resin was suspended in IPA, to which squaric acid was added and refluxed for 4 hours as detailed in scheme 5.31.



Scheme 5.31: Reaction between resin bound anilino derivative and squaric acid, forming half squaraine

Once more the resin was collected by filtration and washed with DCM and MeOH, producing the colourless resin. The last stage was to add the DMA to complete the synthesis of the squaraine dye, DMA was added in a 5 times excess and the resin was suspended in IPA and refluxed over 48 hours (see scheme 5.32).



Scheme 5.32: Final step for formation of squaraine dye, between the resin bound half squaraine and DMA.

It was expected that upon formation of the dye, the resin would once more be reflected through the colour of the dye; however this did not happen. Due to the failure in being able to monitor each reaction step, another approach was investigated.

In order to obtain an unsymmetrical version of the anilino squaraine dye (the step-by-step approach had proved unsuccessful) an alternative method to synthesise such dyes involved combining all the reagents and forming the dye in its impure form. The distinct disadvantage using this approach was that three different dyes would be obtained in one crude solution: two symmetrical from each heterocycle group; and the asymmetric product. This caused a problem because purification was very difficult as the separation between each type of dye was not very large, resulting in poor elution from a column. However, Funabik *et al.* have demonstrated success with this methodology. It was hoped that the dye could be purified; yielding enough of the desired product to enable subsequent reactions to take place.

### 5.5.5 ONE POT SYNTHESIS OF SQUARINE

Using the aniline derivatives, N-methylaniline and DMA there were three possible dyes (detailed in figure 5.9) that would have been synthesised and consequently would have to be separated.

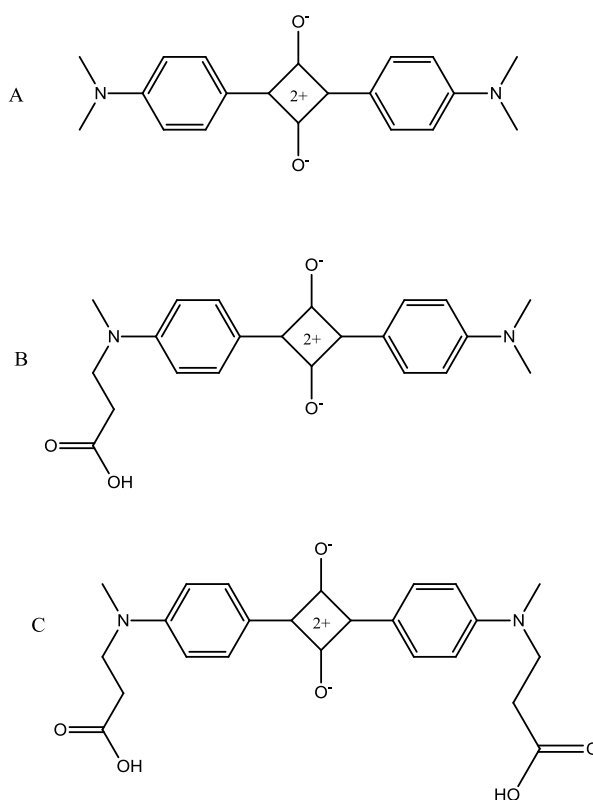
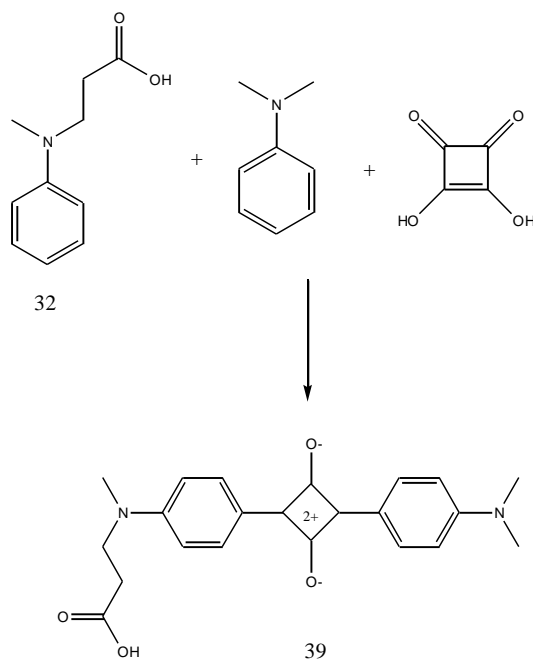


Figure 5.9: Possible dyes

Squaric acid, DMA and compound [32] were dissolved in IPA. To this solution, TEOF was added and the reaction mixture was refluxed for 48 hours. TEOF was used as a drying reagent in this reaction, the by-product of the synthesis of squaraine dyes is the formation of water, and therefore TEOF had to be used to ‘mop’ this up. The excess solvent was removed and the crude product was purified by column chromatography, as shown in scheme 5.33.



Scheme 5.33: One pot synthesis of squaraine dye using N-methylaniline and DMA.

With the successful synthesis of three different dyes, the next stage was to form viable sensing molecules. The synthesis of linker molecules was necessary for the successful attachment of both a nanoparticle and protein to provide stability of the eventual conjugate. Each of the dyes were synthesised with the view to form these sensing molecules,; consequently the source of modification of these dyes were the carboxylic acids which had been incorporated into the structures.

## 5.6 SYNTHESIS OF LINKER MOLECULES

Throughout this work, dyes were synthesised to provide a biomolecular label capable of nanoparticle attachment. This involved the requirement for a linker capable of bridging all of the components. Discussed in section 5.2, McKenzie *et al.*

successfully synthesised a linker with a lysine core. Lysine had been chosen due to the nature of this compound; the amino acid bears two free primary amine groups and one free carboxylic group all available for modification (shown in figure 5.10).

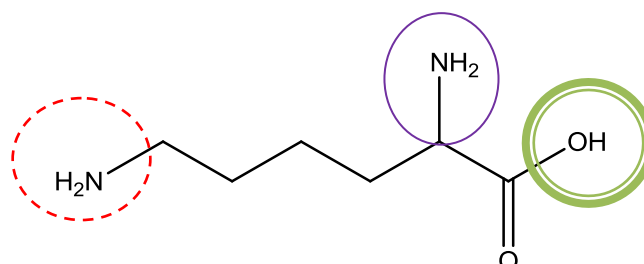


Figure 5.10: Lysine based linker

The trifunctional linker had space for conjugation of three other components: the dye occupied one free amino group; a thiolated compound used for conjugation onto the nanoparticle surface was reacted with the second amino group; and finally a PEG group (used for its stabilising properties) was reacted with the free carboxylic acid. The long term goal was to implement such conjugates in cellular conditions. The stability of nanoparticle conjugates *in vivo* has been documented extensively. In the paper published by McKenzie *et al.*, this type of linker demonstrated good stability in harsh conditions often encountered in cells, i.e. high salt concentrations.

An orthogonal protecting group strategy was employed in the synthesis of this linker to protect the amine groups and prevent intramolecular reaction with the carboxylic acid. The molecule shown in figure 5.11 was the starting material for this synthesis. The lysine group had been BOC and FMOC protected therefore providing the carboxylic acid group for reaction.

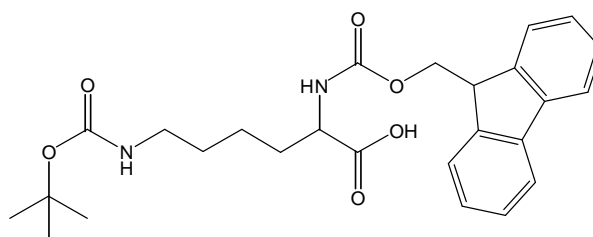


Figure 5.11: Protected lysine

### 5.6.1 CYANINE PEG<sub>3</sub> LINKER SYNTHESIS

The components of the linker are crucial in determining the success of the conjugate preparation and use. The PEG group provides stability to the nanoparticles (a concept discussed in section 5.2). Ultimately, the nanoparticle conjugates were to be used under cellular conditions and the presence of the PEG group was hoped to confer sufficient stability to the system to withstand cellular conditions. The desired PEG group had to be long enough to provide stability, however not too long that the distance between the dye and that of the nanoparticle was too great and lead to a loss of SERS enhancement. It was hypothesised that a PEG polymer consisting of 3 PEG groups would provide the ideal combination of stability and enhancement.

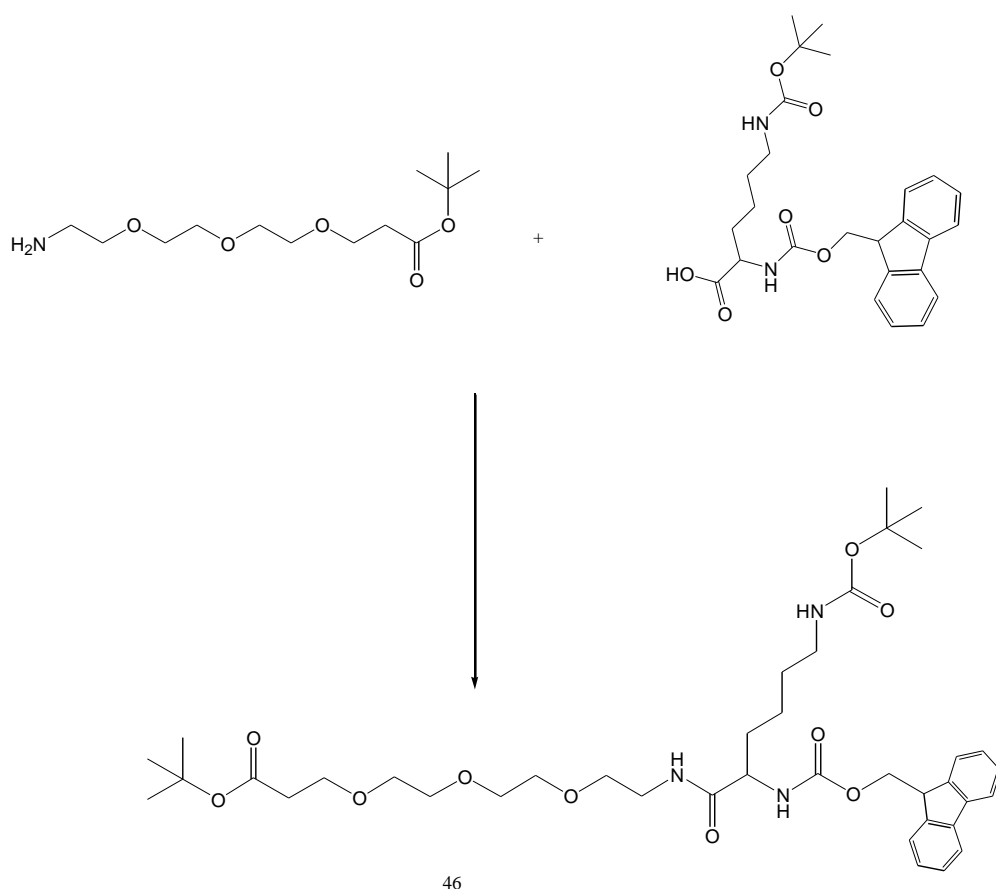


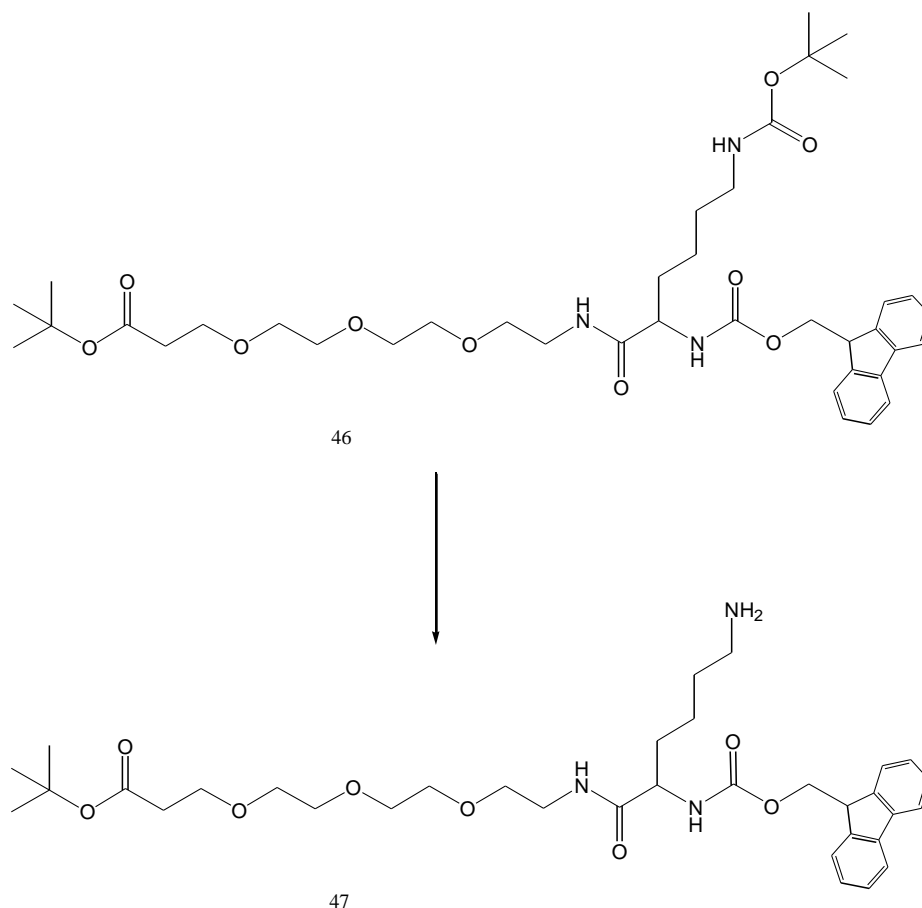
Figure 5.34: Attachment of PEG to carboxylic acid of lysine, forming the core to the linker.

Tert-butyl-12-amino-4,7,10-trioxadecanoate was dissolved in DCM to which Fmoc/BOC lysine and DIC were added and the reaction mixture was stirred at room temperature for 18 hours, as scheme 5.34 shows. DIC was used in this reaction

instead of DCC, as this coupling reagent has been shown to be efficient and there was not the production of a hazardous by-product. The crude product was purified using flash column chromatography producing the desired product [46] in a 31% yield.

Careful consideration had to be taken in the next step; tert-butyl-12-amino-4,7,10-trioxadodecanoate contains a tert-butyl group and this posed a problem. This was because the removal of this group uses the same conditions that are used to remove the amine protecting group BOC. The next stage of the linker involved the removal of the BOC group. Under the traditional conditions this would liberate the primary amine and carboxylic acid which could potentially lead to an intramolecular reaction. In the paper published by McKenzie *et al.* an NHS ester was used to react the amine preferentially, however this is not always successful. To avoid this situation a method was sought to selectively deprotect the BOC group. A paper published by Navath *et al.* detailed the use of BiCl<sub>3</sub> as a selective deprotecting agent. This method was used to deprotect a BOC group in the presence of t-butyl group, Navath *et al.* showed this method produced high yielding results.<sup>213</sup>

Compound [46] was dissolved in a mixture of water and MeCN to which an equivalent of BiCl<sub>3</sub> was added and the reaction mixture was heated at 55 °C for an hour. After this time, another equivalent of BiCl<sub>3</sub> was added. The reaction was heated at temperature for a further two hours before a final equivalent of BiCl<sub>3</sub> was added and heated for an additional three more hours as scheme 5.35 explains.

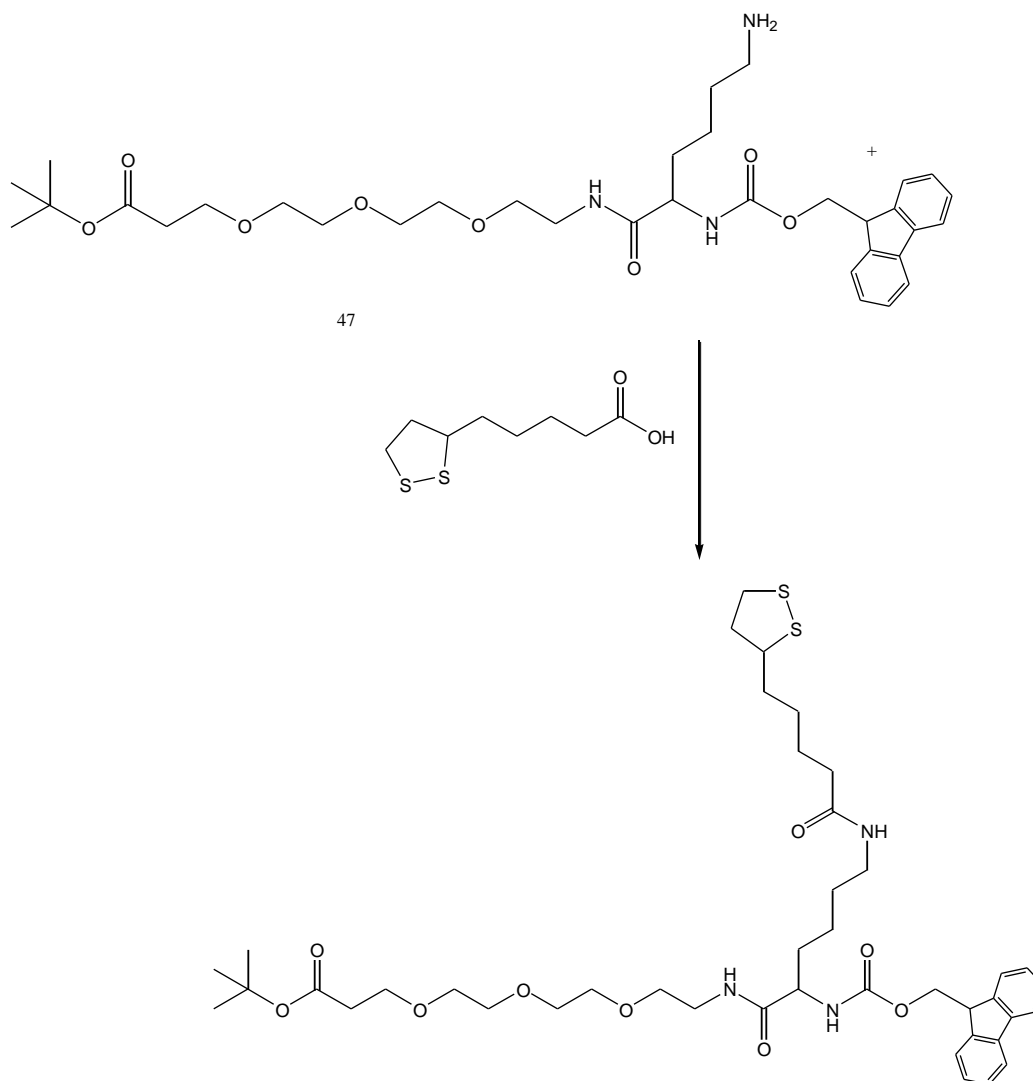


Scheme 5.35: Selective deprotection of BOC group, using  $\text{BiCl}_3$

With the liberation of the amine, the next step was to form the amide bond between compound [47] and thioctic acid. This amide formation was carried out using DIC once more at room temperature. This was particularly beneficial as thioctic acid is both light and temperature sensitive above 30 °C. Upon degradation the compound becomes a jelly like substance that will not dissolve in any common organic solvent - terminating the course of the reaction.

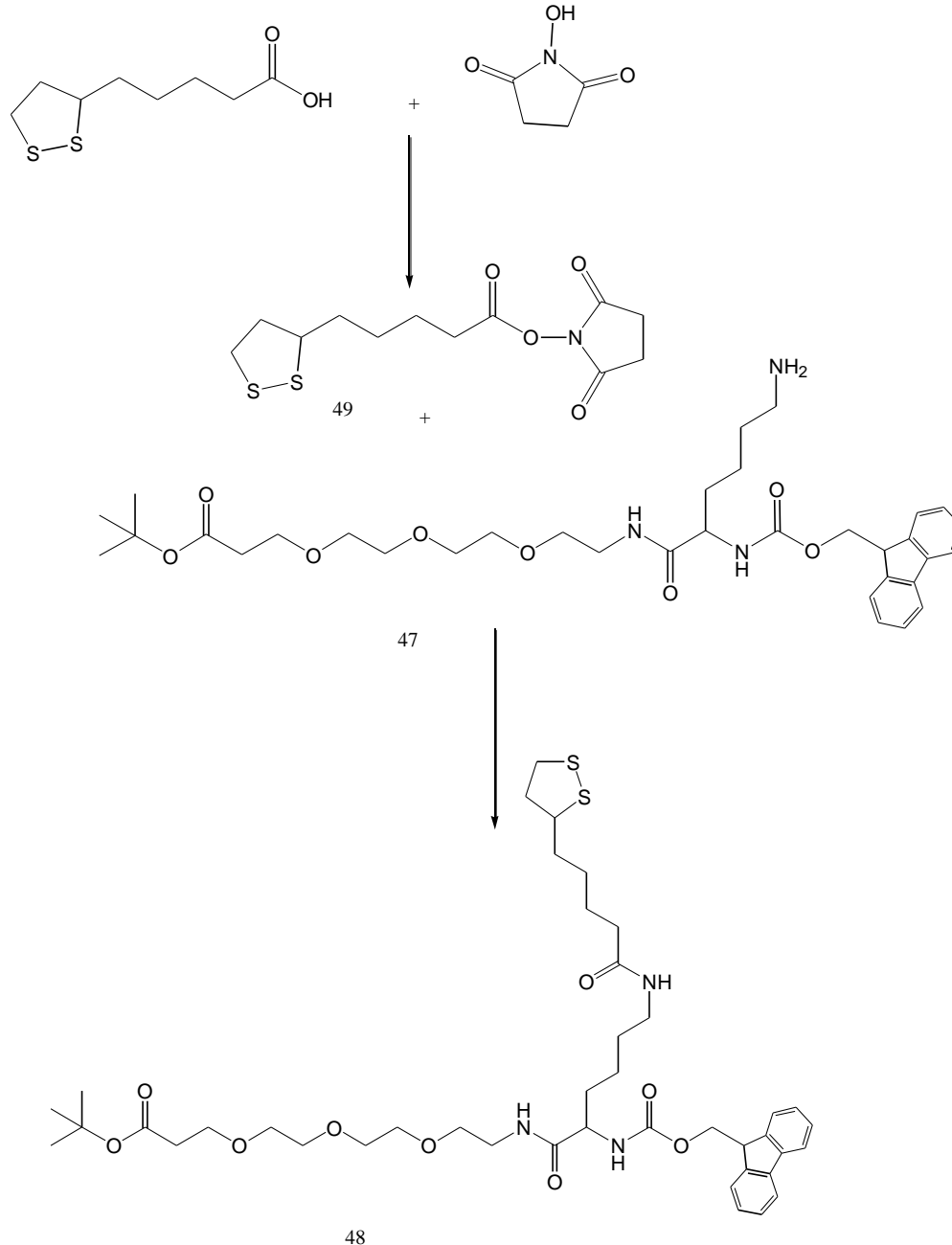
Compound [47] was dissolved in DCM to which DIC and thioctic acid was added and the reaction mixture was stirred for 18 hours at room temperature (see scheme 5.36). TLC analysis identified there to be a new spot - using ninhydrin as a stain which stains spots that are primary amines as purple - therefore the new product spot should not develop any colour as the amine should now be an amide. This was observed and the desired product was purified by flash column chromatography. However, an analysis of mass spectrometry revealed that the desired product had not

been obtained. It was surmised a more active derivative of the thioctic acid should be used to ensure successful coupling.



Scheme 5.36: Thioctic<sup>48</sup> addition to linker 47

N-hydroxyl succinimide (NHS) groups have been well documented in the formation of active esters. This active ester promotes the formation of amides. Thioctic acid was dissolved in DCM; to this solution NHS and DIC were added and the reaction mixture was stirred for 2 hours at room temperature, as detailed in scheme 5.37. Compound [47] and DIPEA were added and the reaction was allowed to stir for 18 hours at room temperature. The crude product was purified by flash column chromatography producing the desired product in 72% yield as yellow oil.



Scheme 5.37: Formation of amide bond between the thioctic acid and lysine

With the successful synthesis of compound [48], the next stage was to remove the Fmoc group. Compound [48] was dissolved in a 20% piperidine in MeCN solution and stirred at RT for 18 hours (shown in scheme 5.38). The excess solvent was removed and the desired product [49] was used without any further purification.

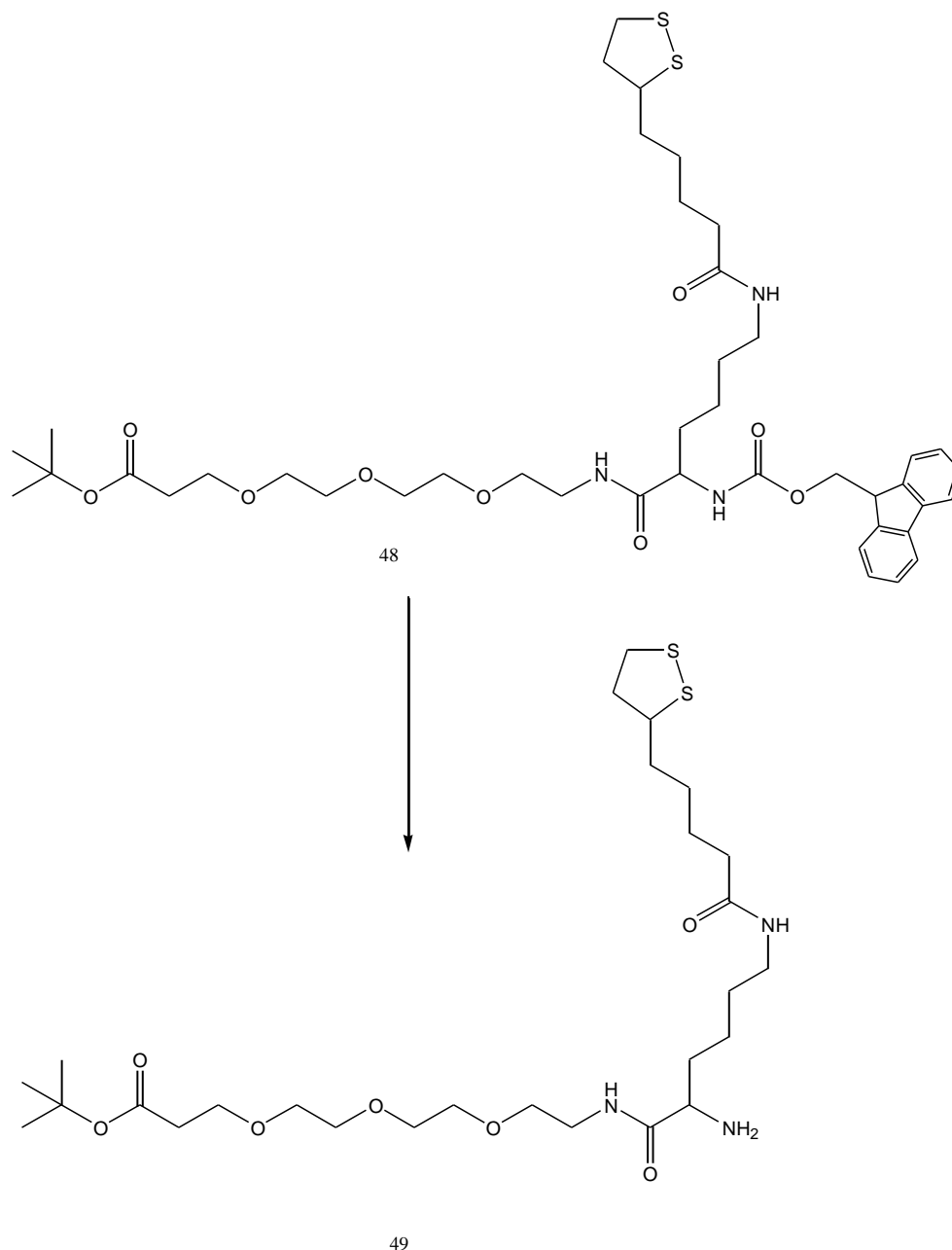


Figure 5.38: Deprotection of Fmoc protecting group on amine of compound [48]

The final coupling stage of the formation of the linker was the attachment of the dye. This was achieved by dissolving compound [49] in DCM to which compound [11] and DIC were added and the reaction mixture was stirred at room temperature for 18 hours. The crude product was purified by column chromatography producing compound [50] in a 4% yield as scheme 5.39 shows.

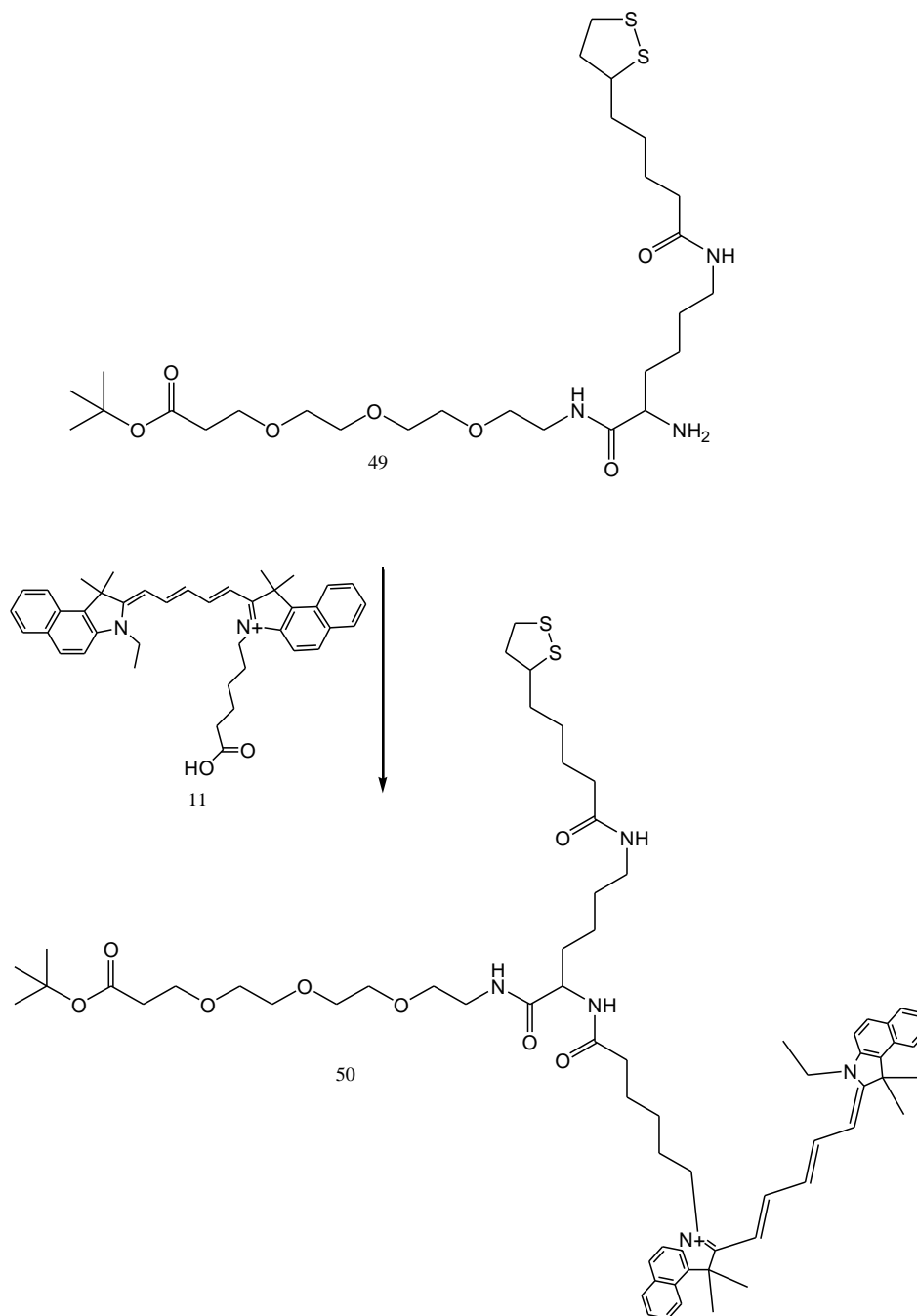


Figure 5.39: Conjugation of cy 5.5 dye to linker compound [49]

With the successful synthesis of the linker compound [50], the final protecting was removed. The tert-butyl group that had protected the carboxylic acid of the PEG<sub>3</sub> group was removed using the traditional method, using a solution of 1:1 TFA:DCM stirred at room temperature for 3 hours, as shown in scheme 5.40. A scavenger resin was used to remove any excess TFA, revealing the final linker compound [51], as a dark solid in a yield of 15%.

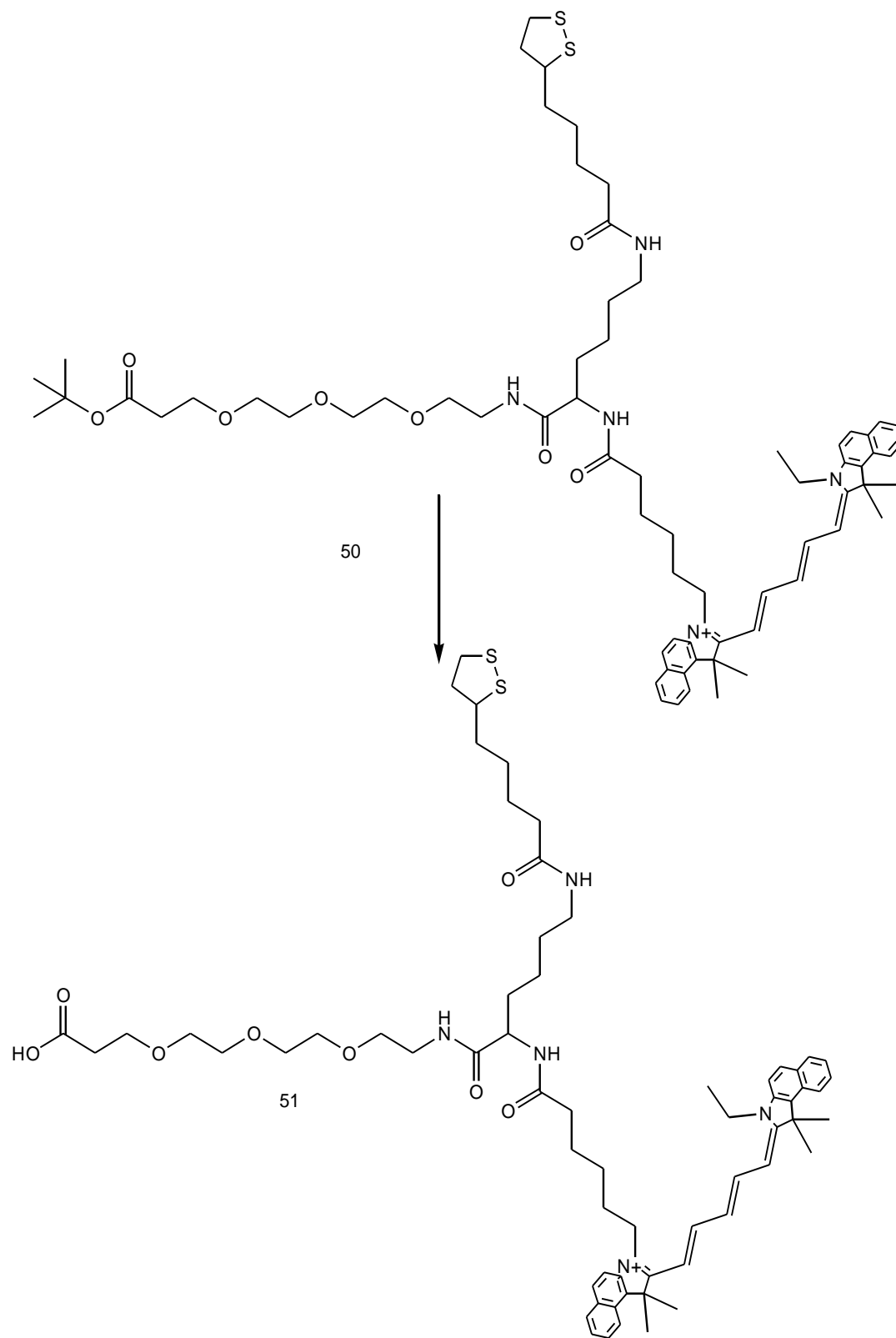
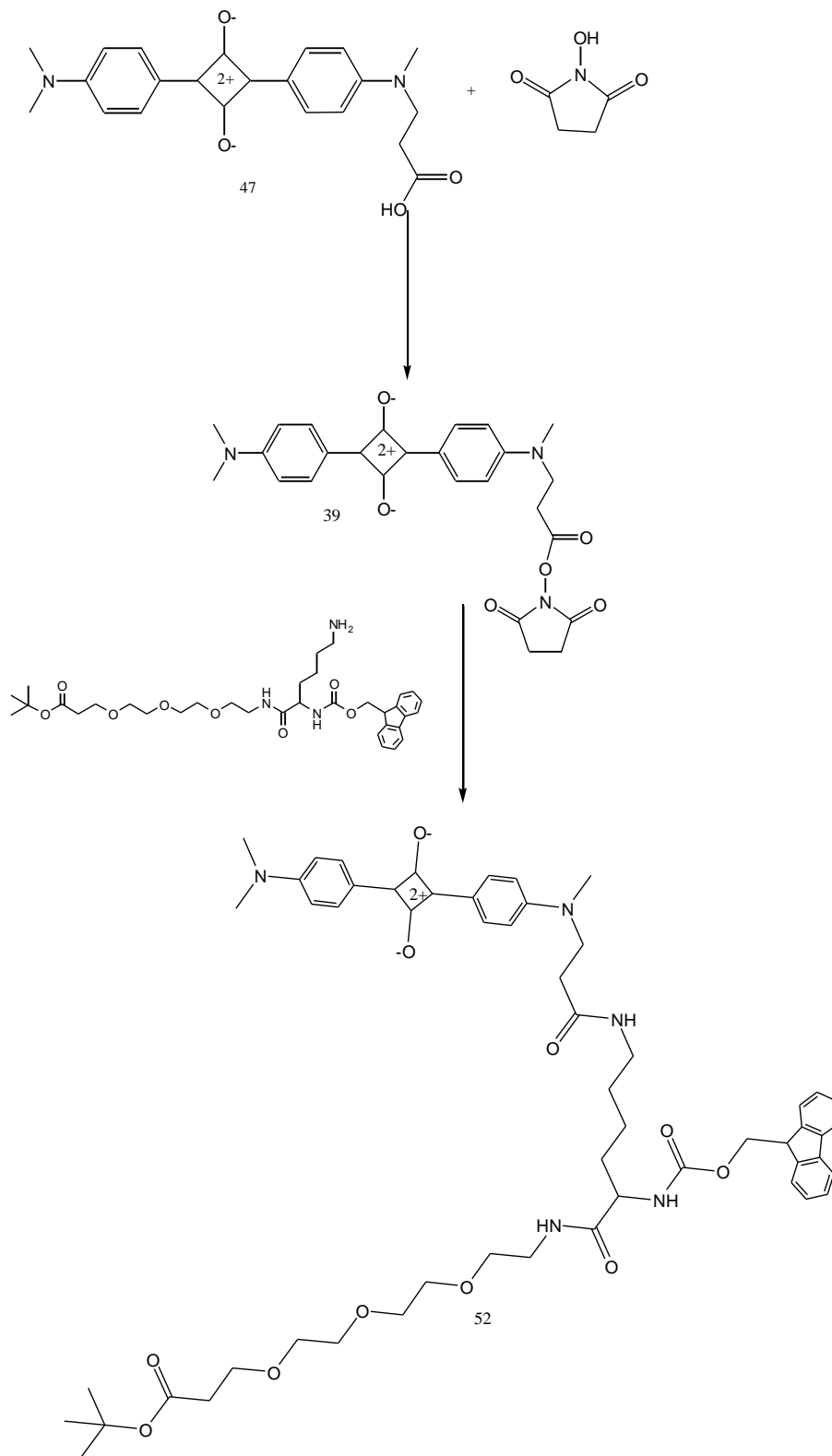


Figure 5.40: Final deprotection step of linker molecule

Following the successful synthesis of linker 1, the process was repeated using the synthesised squaraine, dye B; compound [47].

### 5.6.2 SQUARAININE PEG<sub>3</sub> LINKER SYNTHESIS

Compound [49] was used as the initial building block for this linker, however due to the small quantities of squaraine dye it was surmised that the reaction between the dye and linker had to be promoted as much as possible. NHS has shown to promote the formation of an amide bond through activation of the carboxylic acid, forming the active ester. It was hypothesised that the ester would form in situ under the reaction conditions. Compound [49] was dissolved in DCM to which NHS was added and reacted for 1 hour before compound [47] and DIC and DIPEA was added and the reaction was stirred at room temperature for 18 hours (See scheme 5.41).



Scheme 5.41: Attempted linker formation with squaraine dye through formation of an amide bond

Unfortunately this reaction failed. There were several possibilities for this outcome and the predominant possibility was the repeated solubility issues of this class of dyes. A second problem could have been the excess DIC that was added, which

turned the reaction mixture from green to brown and then yellow by the time the reaction had completed. In an attempt to overcome these issues, the solution of the dye was sonicated to improve solubility and only one equivalent of DIC was added. The dye was suspended in DCM which was then sonicated for 20 minutes after which time NHS and DIC was added and stirred under N<sub>2</sub> for 1 hour at room temperature. After this time, compound [49] was added and the reaction was stirred at room temperature for 18 hours. The crude product was purified by flash column chromatography. Two sets of fractions were collected that were potentially the desired product, however on analysis of the <sup>1</sup>H NMR showed that these products did not correspond to the expected peaks for the desired product indicating the reaction had failed once more. In a final attempt to conjugate the dye to the linker molecule the coupling reagent was changed to CDI. This coupling reagent is more aggressive than DIC - there was no need for NHS in this case - and upon successful coupling there is a release of CO<sub>2</sub> gas. It was important that this reaction was carried out under N<sub>2</sub> due to the air sensitive nature of CDI. In addition to this the solvent of the reaction was altered from DCM to the more polar DMF to aid the solubility of the dye.

The dye was once more dissolved in anhydrous DMF to which CDI was added. This reaction was stirred for 1 hour under N<sub>2</sub> conditions. Compound [49] was then added and the reaction was stirred at room temperature for 18 hours. DMF is very difficult to remove using conventional methods such as rotary evaporation; therefore as DMF is water miscible, it can be washed out of the reaction, provided the desired product remains in the organic layer. The reaction mixture was dissolved in water and diethyl ether. The organic layer was washed repeatedly with water; the product was half in organic layer and half in the aqueous layer, which was indicated by the colour of the dye. To remove the remaining product in the aqueous layer, it was washed with 10% NaOH, followed by addition of more diethyl ether to retrieve the product. The organic layers were combined and washed with saturated NaCl before being dried over MgSO<sub>4</sub>, filtered and concentrated; producing 4 mg of the desired product.

The final stage was to deprotect the remaining protection group. Compound [53] was suspended in a 1:1 TRF:DCM solution. On addition of this solvent system, the blue coloured solution turned pink. This had been previously observed and on complete

removal of TFA the original colour returned. The reaction mixture was stirred at room temperature for 3 hours. In order to remove the TFA, there was a reluctance to use the scavenger resin due to the loss of material that occurred. Therefore Et<sub>3</sub>N was added to neutralise the acid, scheme 5.42.

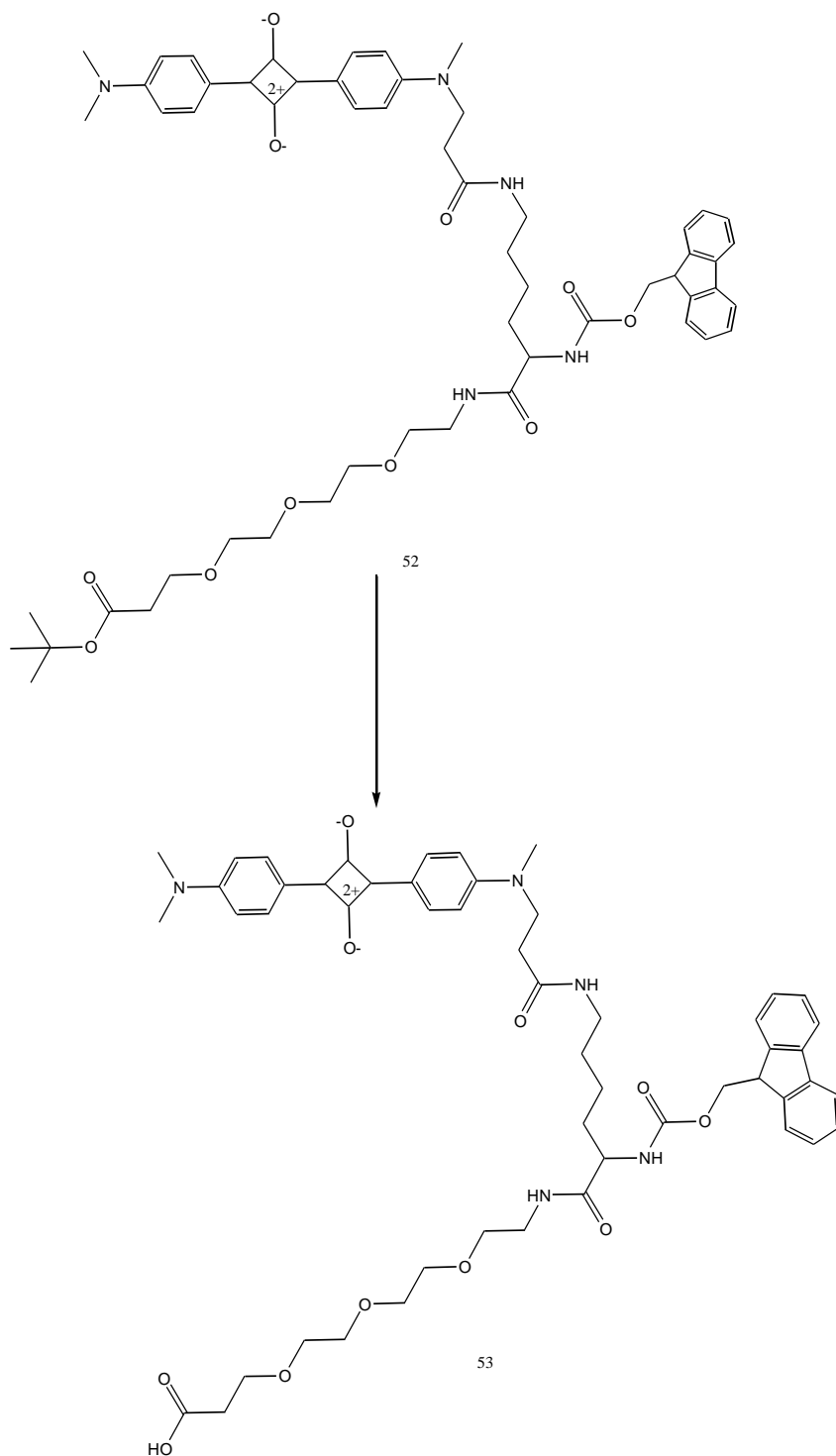


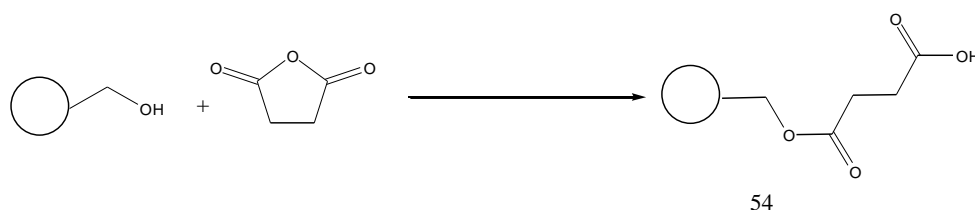
Figure 5.42: Deprotection of t-butyl group of linker molecule

Following final removal of solvent it was found the linker compound had decomposed. It was not clear why this occurred and due to the small quantity the reaction could not be repeated.

The length of PEG molecule used in linkers and their effect in SERS has never been documented. It was therefore decided to investigate the synthetic possibility of synthesising an analogous linker that could be used in protection detection in SERS.

## 5.7 PEG<sub>41</sub> LINKER MOLECULES

During the course of this research it was found that although PEG<sub>3</sub> provided stability when conjugated to nanoparticles, under certain conditions this stability could be compromised and cause uncontrollable and irreversible aggregation. The PEG length that was chosen was PEG<sub>41</sub> as this PEG group had shown enhanced stability over the PEG<sub>3</sub> moiety. Another method for the synthesis of these linkers was investigated. SPOS (mentioned in section 5.4) has many benefits to conventional synthesis; mainly ease of purification. In addition to this longer PEG groups are more difficult to purify. A solid phase synthesis route was devised with Wang resin chosen and the hydroxyl group was converted to a carboxylic acid in order to react with the amine terminated PEG molecule. Wang resin was suspended in DCM to which succinic anhydride was added and the reaction mixture was refluxed for 6 hours, after which time the resin was collected by filtration and washed with DCM and MeOH three times respectively (scheme 5.43 details this).

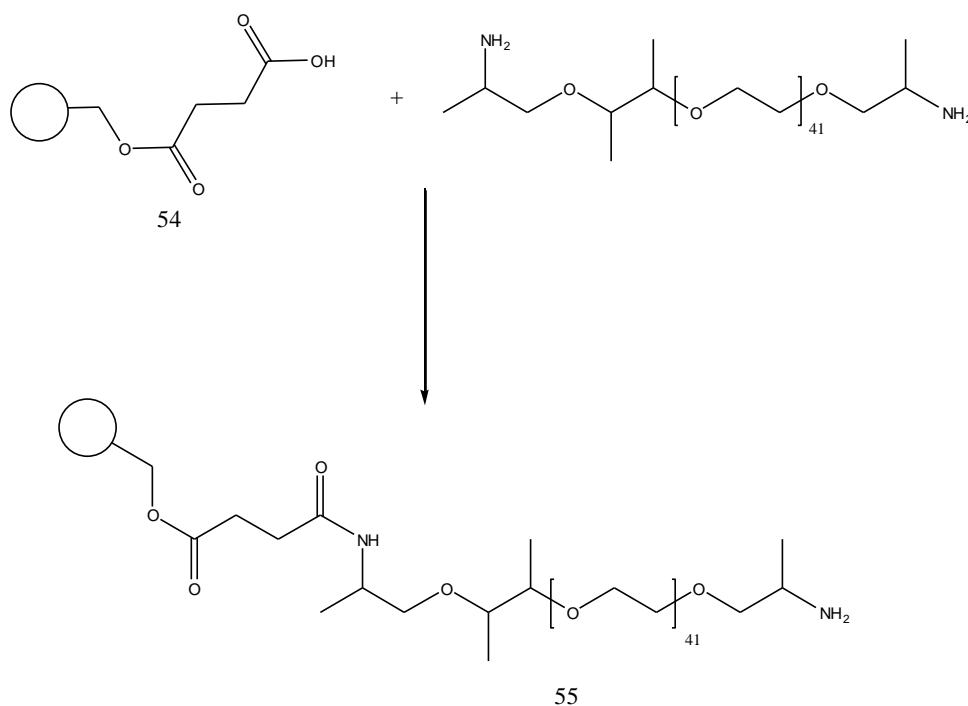


Scheme 5.43: Conversion of functional group on Wang resin

To monitor the course of the reaction a small portion of the resin was tested for the presence of the acid group. This was achieved using malachite green oxalate, which in the presence of carboxylic acid will turn the resin from colourless to green. This resin turned green indicating success; the resin was taken to the next stage of the synthesis.

Compound [54] was resuspended in DCM to which PEG<sub>41</sub> and coupling agent DIC were added - this mixture was agitated at room temperature for 18 hours (see scheme

5.44). The resin was once again collected via filtration and washed with DCM and MeOH respectively three times. To confirm the successful amide coupling between the acid group and the amine group of PEG<sub>41</sub>, a small portion of the dried resin was suspended in ninhydrin stain and heated - the colourless resin turned to purple indicating the presence of a primary amine, therefore confirming the reaction had been successful.



Scheme 5.44: Attachment of PEG to converted Wang resin.

Lysine was added to a suspension of compound [55] and DCM; finally DIC was added and the reaction was agitated at room temperature for 18 hours, as scheme 5.45 shows. The PEG molecule had been successfully attached to the solid support. Terminating with a primary amine, the next stage was to add the lysine to continue the linker formation. The steps that were used to create the linker are almost identical to that of solution phase.

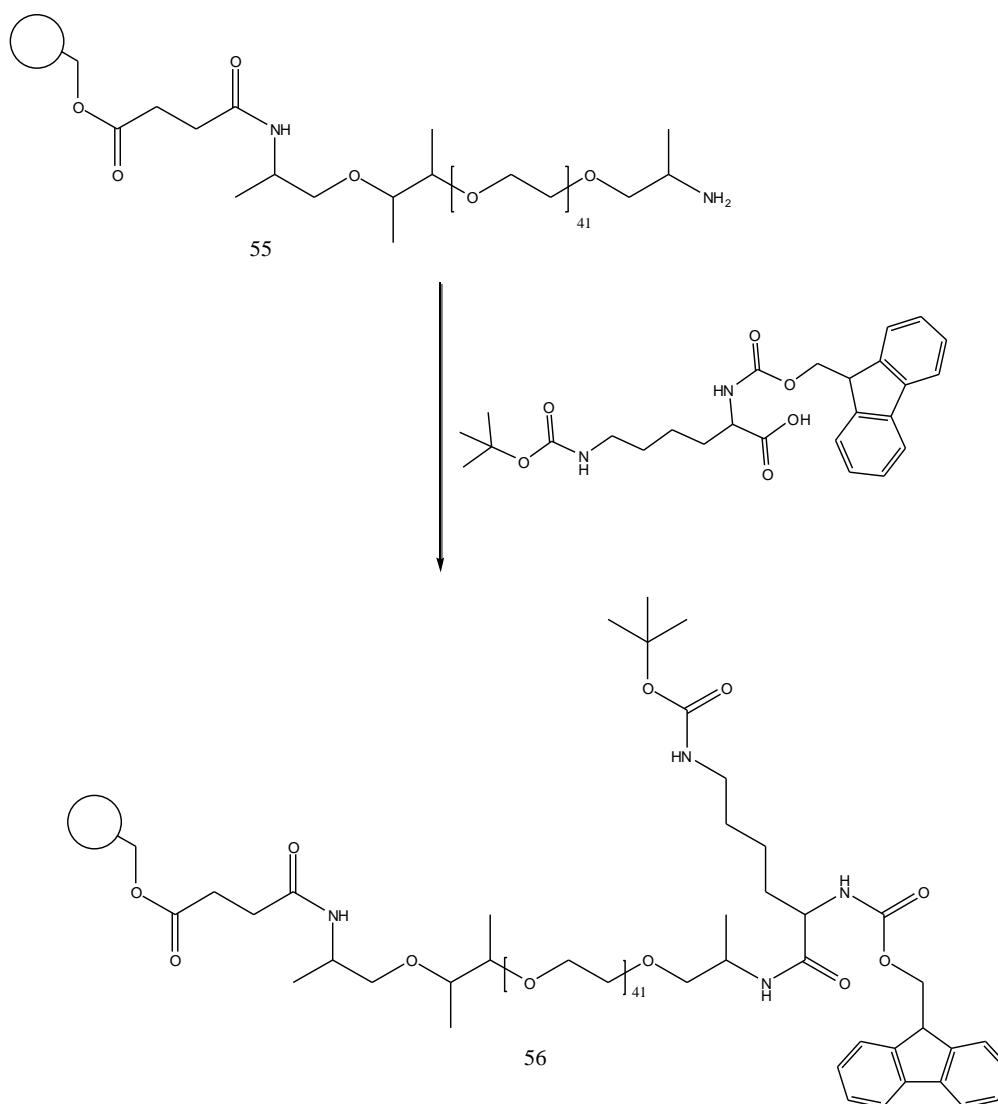
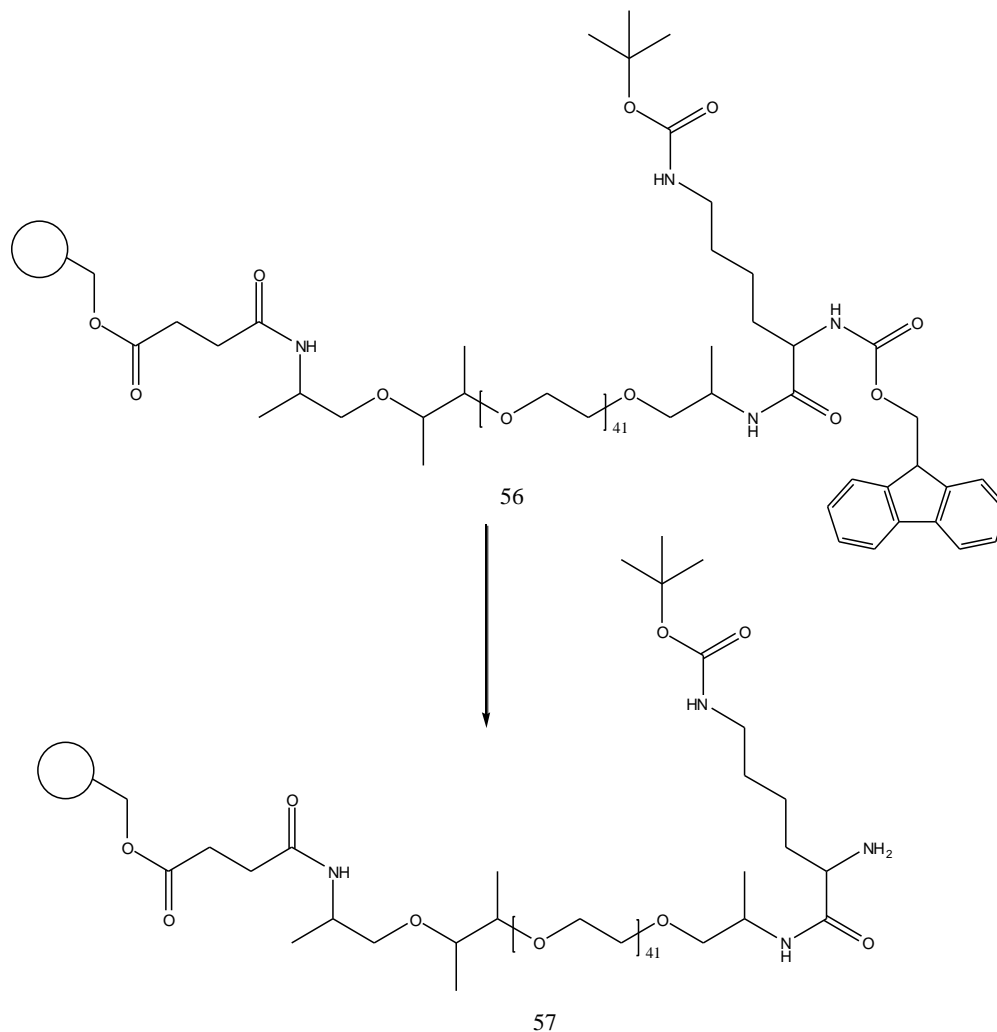


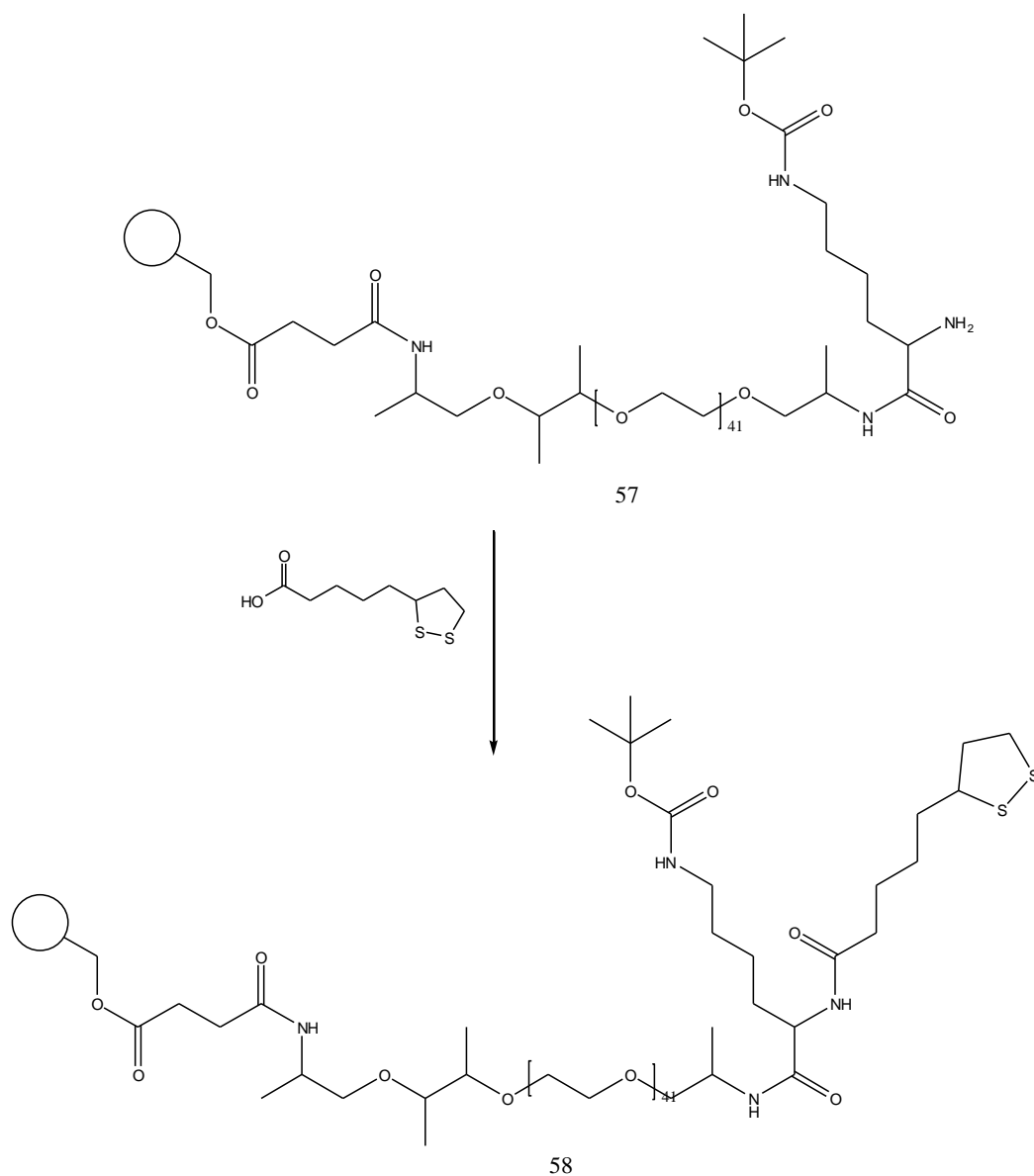
Figure 5.45: Formation of amide bond between resin bound PEG to lysine carboxylic acid.

Once more the resin was collected by filtration. The nihydrin tested was carried out on product [56] on the basis that the resin would not change colour. This was the case and the next stage could proceed. This was the deprotection of the Fmoc group; the deprotection of Fmoc groups on resin is an area well documented, due to the field of peptide synthesis. When synthesising peptides it is necessary to carry out orthogonal protecting group strategy, therefore Fmoc groups are routinely displaced to allow for conjugation of the next amino acid, yet retain the product on the resin. It was surmised that this methodology should be followed to deprotect the Fmoc group yet ensure the product remained on the resin which is shown in scheme 5.46.



Scheme 5.46: Deprotection of Fmoc group

The standard *on resin* Fmoc removal procedure was followed: the resin was washed with DMF; then suspended in a 20% piperidine solution in DMF. The solution was agitated for 30 minutes at room temperature; following which the resin was collected by filtration and washed once more with DMF before drying over vacuum. Once more the ninhydrin test was used which gave a positive result. With the primary amine now free, thioctic was dissolved in DCM to which the modified resin was added with DIC and the reaction was agitated at room temperature for 18 hours under light sensitive conditions (see scheme 5.47).



Scheme 5.47: Amide coupling

The penultimate stage was the deprotection of the BOC group. The typical conditions for the removal of such groups are a 1:1 TFA:DCM solution. However, under these conditions this would cleave the product from the resin. This is undesirable; ideally the final product would be obtained from the cleavage of the resin. A paper published by Lejeune *et al.* had shown that BOC groups could be deprotected while retaining the product attached to the resin.<sup>214</sup> These conditions involved the use of 1,4 Lutidine and TMSOTf. The resin was suspended in DCM to which 1,4-lutidine and TMSOTf and the reaction was stirred at room temperature for 45 minutes; during the course of the reaction the resin changed to an orange colour, scheme 5.48.

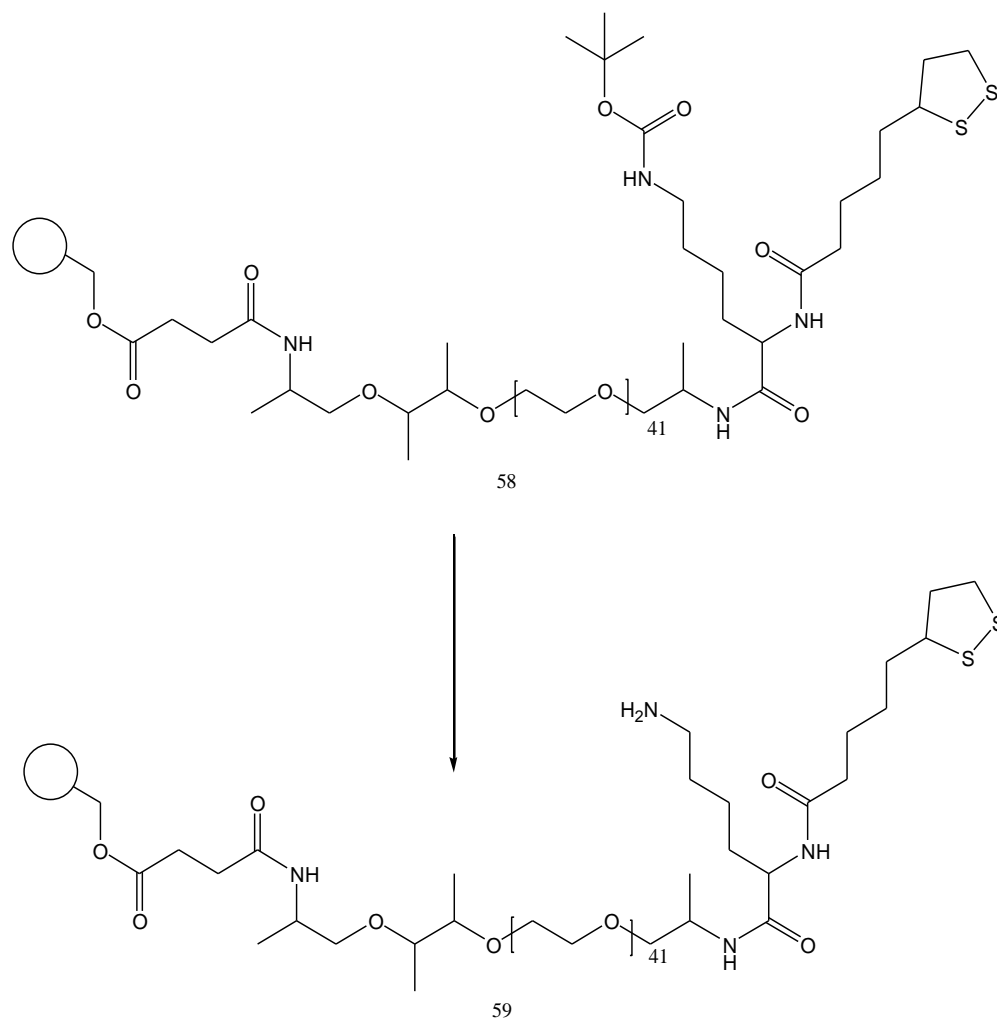


Figure 5.48: On resin deprotection of FMOC group of linker molecule.

The next stage would have been the reaction between the resin and a dye. However due to the small quantities of the dyes and the excess ratios that were required for resin based synthesis, it was decided to cleave the product from the resin at this stage. This was to confirm if this methodology would prove successful in the synthesis of the PEG<sub>41</sub> linker, in order not to waste the dye.

The cleavage was carried out using a 1:1 TFA:DCM solution as shown in scheme 5.49. The resin was suspended in this solution and the reaction mixture was agitated for 3 hours at room temperature. The resin was filtered and discarded, allowing the filtrate to be analysed by MALDI. Upon analysis, the desired molecular weight was not present; the reaction had failed. It was decided that this line of investigation would end as the synthesis of linkers can be a lengthy and complicated process. It

was therefore decided to investigate the prospect of incorporating the feature of the linker directly onto the dye.

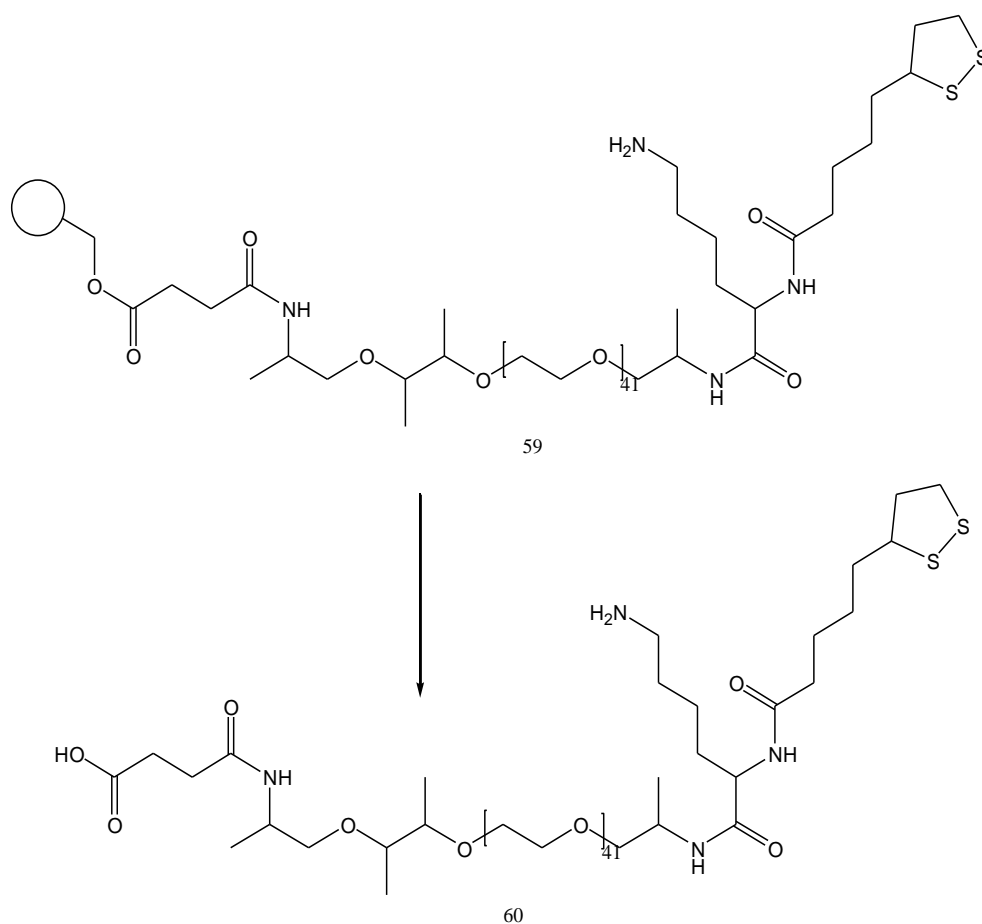


Figure 5.49: Cleavage of linker molecule using TFA:DCM solution

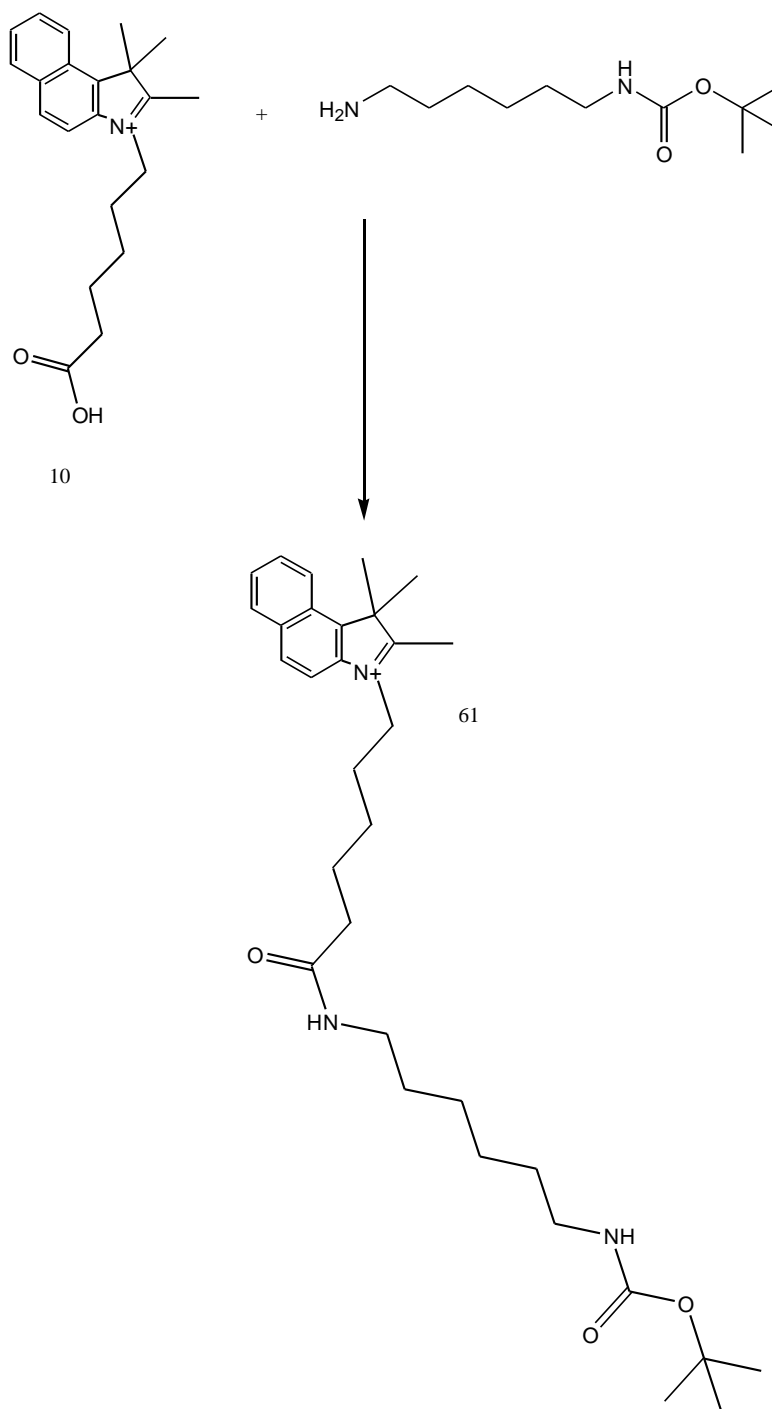
## 5.8 LINKER FREE INVESTIGATIONS

It was hypothesised that if asymmetrical dyes could be synthesised successfully, thioctic acid and PEG<sub>3</sub> could be incorporated directly into the dye. This would allow conjugation of the protein directly via the carboxylic acid on the PEG.

### 5.8.1 LINKER FREE SQUARAIN DYES

Discussed in section 5.5, the asymmetrical synthesis of squaraine dyes is difficult to achieve. However, derivatives of a TMB nature - as documented in literature - have been made with more success. Therefore for the successful synthesis of a linker free dye these derivatives were used.

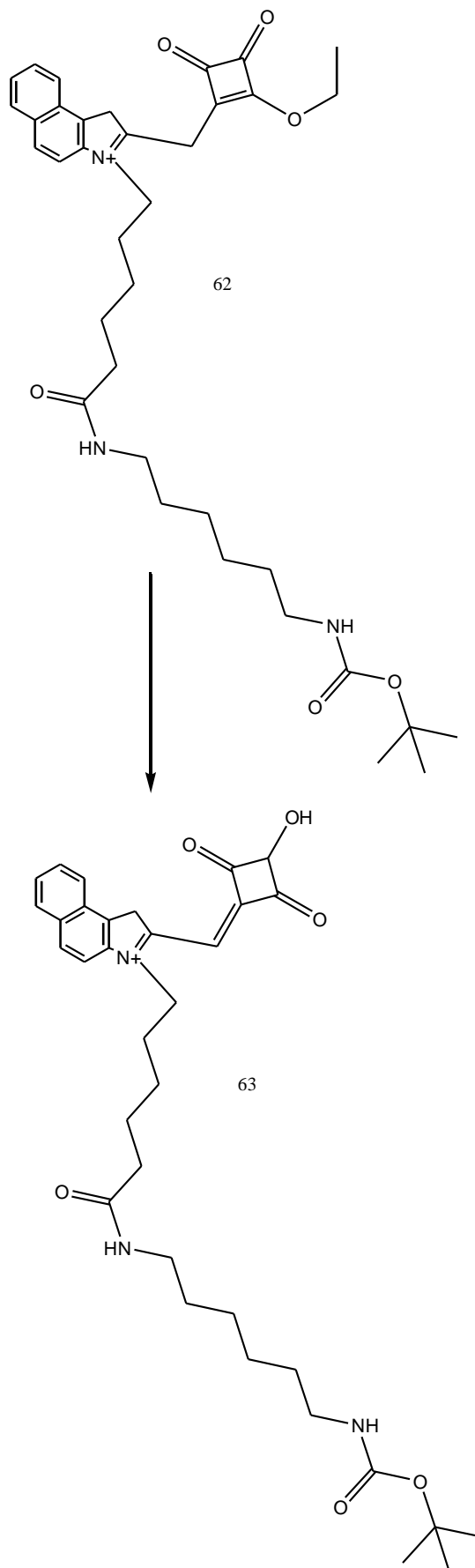
In order to attach thioctic acid to the dye directly, the TMB compound had to contain a primary amine. This was achieved through the coupling of TMB-COOH [10] and BOC protected 1,6 diaminohexane. Compound [10] was dissolved in DCM to which BOC 1,6 diaminohexane and the coupling agent EDC was added and stirred at room temperature for 18 hours as scheme 5.50 explains.



Scheme 5.50: Amide coupling

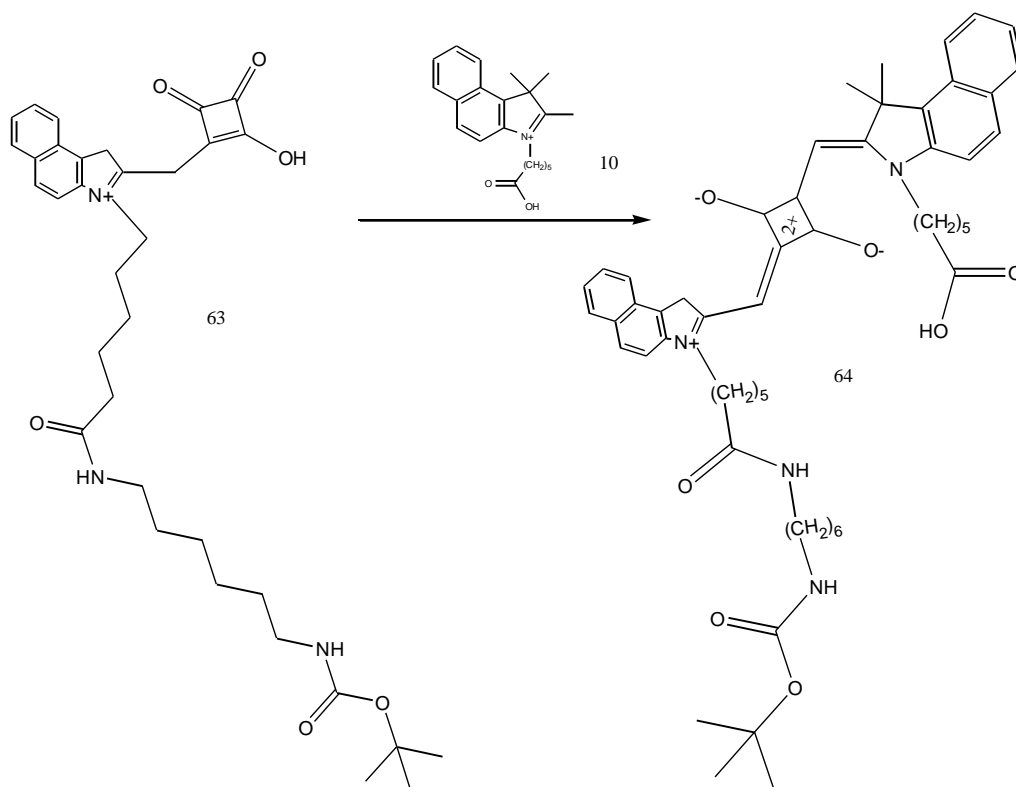


Once again this reaction was used without purifying the crude mixture as it was deemed that the purification by column chromatography would be time consuming and difficult. It was expected that in the next stage, a precipitate would form on the completion of the reaction and therefore eliminate any impurities. Therefore the next stage was to deprotect the remaining ethyl group; this was carried out using a solution of 40% NaOH solution which was added to a solution of compound [62] in ethanol. The reaction mixture was then refluxed for 30 minutes. On this occasion no precipitate was formed but oil was obtained. However, the  $^1\text{H}$  NMR when analysed revealed that the desired product was present (see scheme 5.52).



Scheme 5.52: Deprotection of half squaraine

The Dean-Stark apparatus was used to encourage the formation of the dye as shown in scheme 5.53. Compound [63] and [10] were dissolved in a mixture of butanol and toluene. The reaction was refluxed for 18 hours.



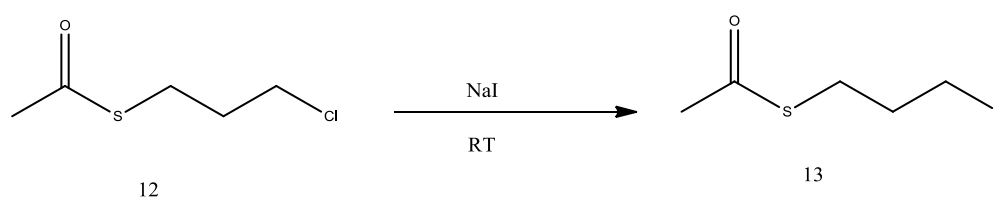
Scheme 5.53: Synthesis of squaraine dye using a step-by-step method.

The reaction failed and the desired product was not obtained. This could have been due to the unpurified compounds from the previous stages. However, due to time constraints this work was not repeated.

## 5.8.2 LINKER FREE CYANINE DYES

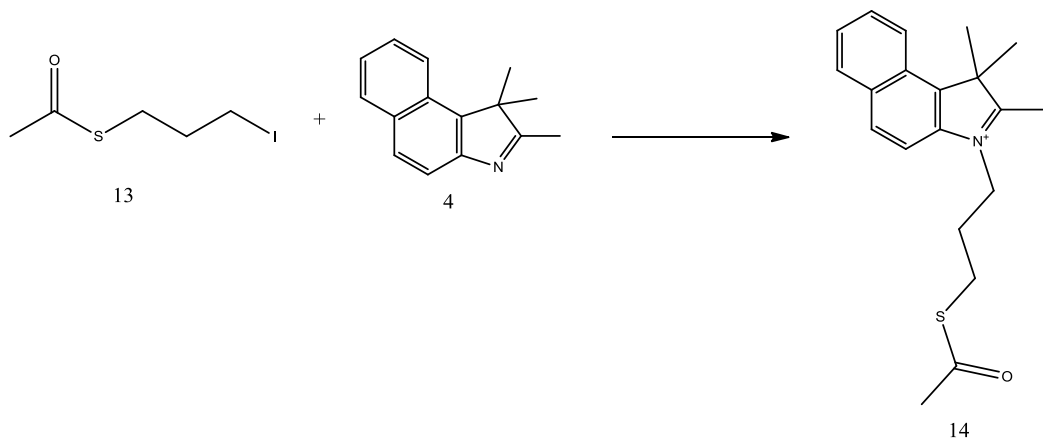
Owing to the strong sulphur-gold/silver interaction, a thiol group was used for attachment to the nanoparticle surface. Thiol acetate was used with the intention of deprotecting the acetate; revealing the free thiol for attachment to the nanoparticle surface. In order to form the direct attachment of the dye to the nanoparticle surface, the TMB molecule was once again used to introduce the thiol containing group.

Chloropropylthiolacetate was used however to promote the formation of the thiolated nitrogen. The chloride group was replaced with an iodide group as this is the better leaving group promoting the formation of the TMB-SAC. To convert the halide, chloropropylthiolacetate was dissolved in acetone, to which the sodium iodide was added. The reaction was allowed to stir at room temperature for 3 hours followed by removal of excess solvent (see scheme 5.54). The product was used without any further purification.



Scheme 5.54: Halide Exchange of Chloropropylthiolacetate

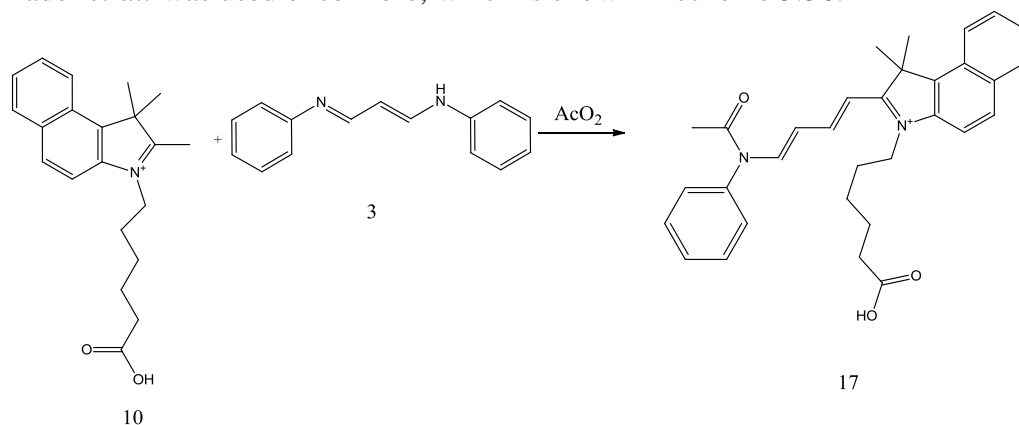
Compound [13] was successfully synthesised and dissolved in acetonitrile with TMB and refluxed for 48 hours - as detailed in scheme 5.55 - After which the excess acetonitrile was removed until slurry remained. This was suspended in 10× the volume of diethyl ether for an hour which produced a precipitate.



Scheme 5.55: Formation of TMB-SAC

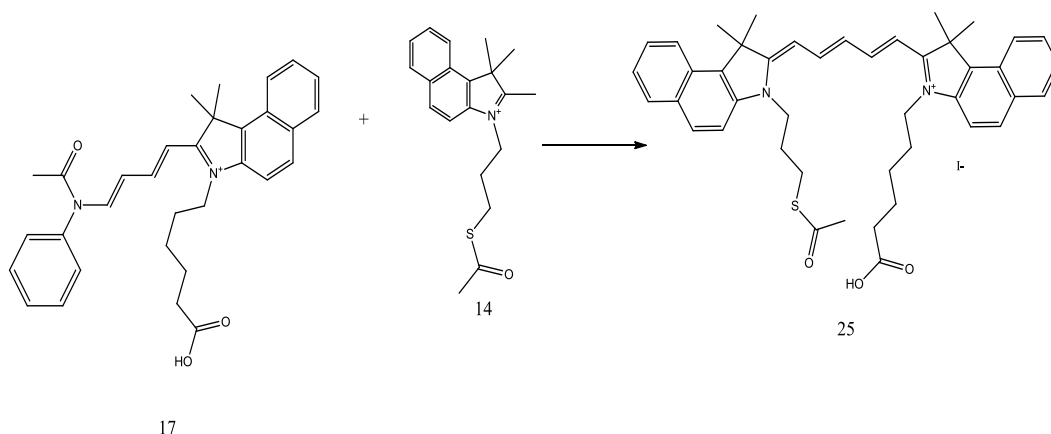
When filtered, the precipitate that had formed was not the expected fine solid but a sticky solid. Further analysis showed that the precipitate was not as pure as anticipated. However, the product was carried onto the next stage of the process. Once the TMB-SAC had been successful synthesised, the next stage of the formation

of the linker free dye was to incorporate the TMB-COOH [10]. This compound was attached to amidine [3], forming the hemicyanine compound. The procedure outlined by Mader *et al.* was used once more, which is shown in scheme 5.56.



Scheme 5.56: Formation of half squaraine, using TMB-COOH

Compound [17] was synthesised in a yield of 2 %. The final stage was to synthesis the dye. Compound [17] and the TMB-SAC [14] were dissolved in pyridine and heated at 50°C for 30 minutes, as shown in scheme 5.57.



Scheme 5.57: Formation of dye C

The free carboxylic acid of the dye was attached to the amino group of the PEG<sub>3</sub> molecule. This was achieved by dissolving compound [25] in DCM to which compound [45] and EDC were added and stirred at room temperature for 18 hours. The crude product was purified by flash column chromatography; producing the desired product in a 32% yield.

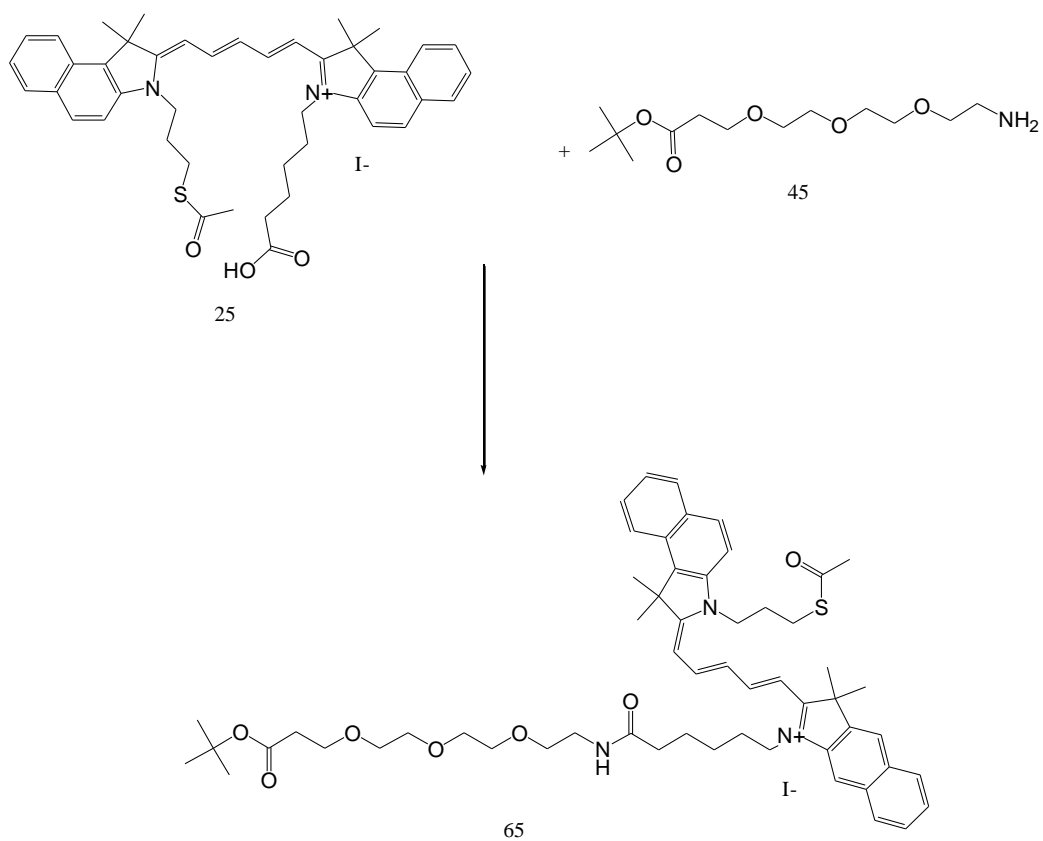
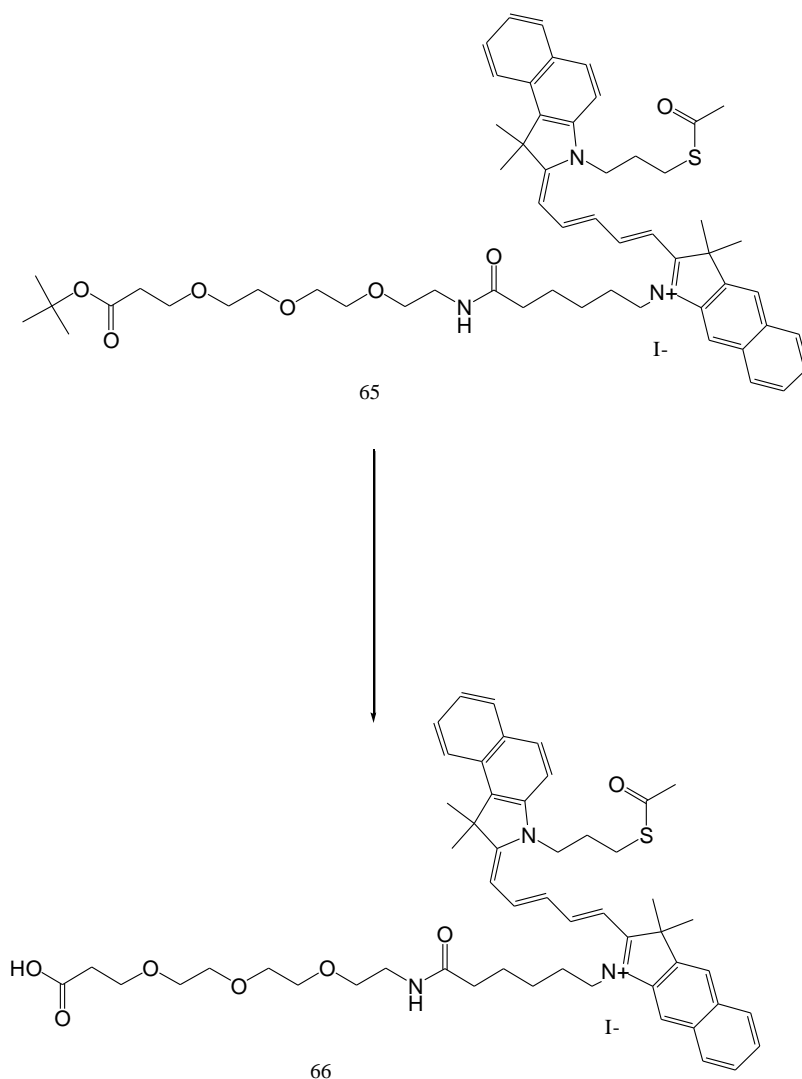


Figure 5.58: Formation of amide bond between PEG<sub>3</sub> and acid group of cyanine 5.5 dye B

The final stage of the scheme was to deprotect the *t*-butyl group of the PEG<sub>3</sub> group to enable conjugation of biomolecules. This was carried out dissolving compound [65] in a 1:1 TFA:DCM solution. This reaction was left to stir at room temperature for 3 hours followed by neutralisation of excess TFA with Et<sub>3</sub>N and the subsequent removal of excess solvent by rotary evaporator (see scheme 5.59).



Scheme 5.59: Deprotection of t-butyl group

Unfortunately the reaction failed. It would appear that the compound had decomposed under the conditions of deprotection. As there was only 10 mg of the product, additional product would have to be synthesised.

It was hypothesised that the reaction had failed due to the impurity of the TMB-SAC product; therefore a slightly different avenue was explored.

To promote the formation of amide bonds it was decided that there would be a benefit to synthesise an amine active heterocycle which could be incorporated into a dye. In addition to this nitrogen groups have been shown to have affinity for silver surfaces. Once again the source of modification was the indole nitrogen. TMB was dissolved in acetonitrile and bromopropylamine was added and the reaction mixture was refluxed over 96 hours. The slurry was suspended in 10x the volume of diethyl

ether producing a precipitate which was collected by filtration. This produced compound [16] in a yield of 60% as scheme 5.60 shows.

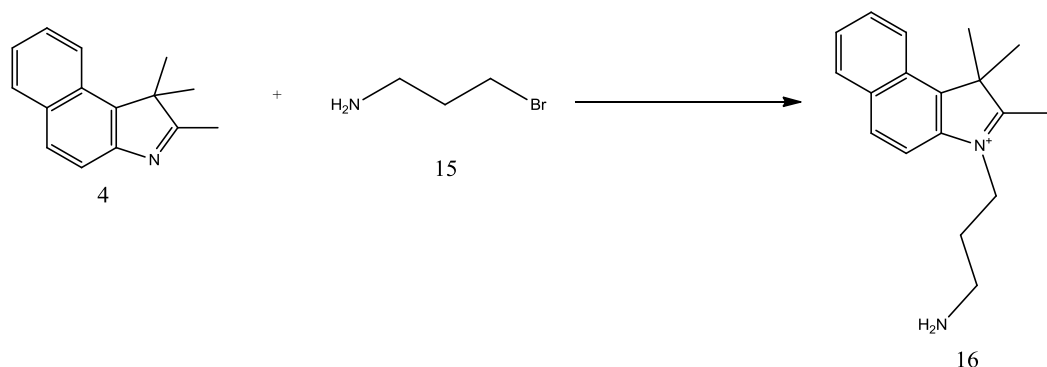
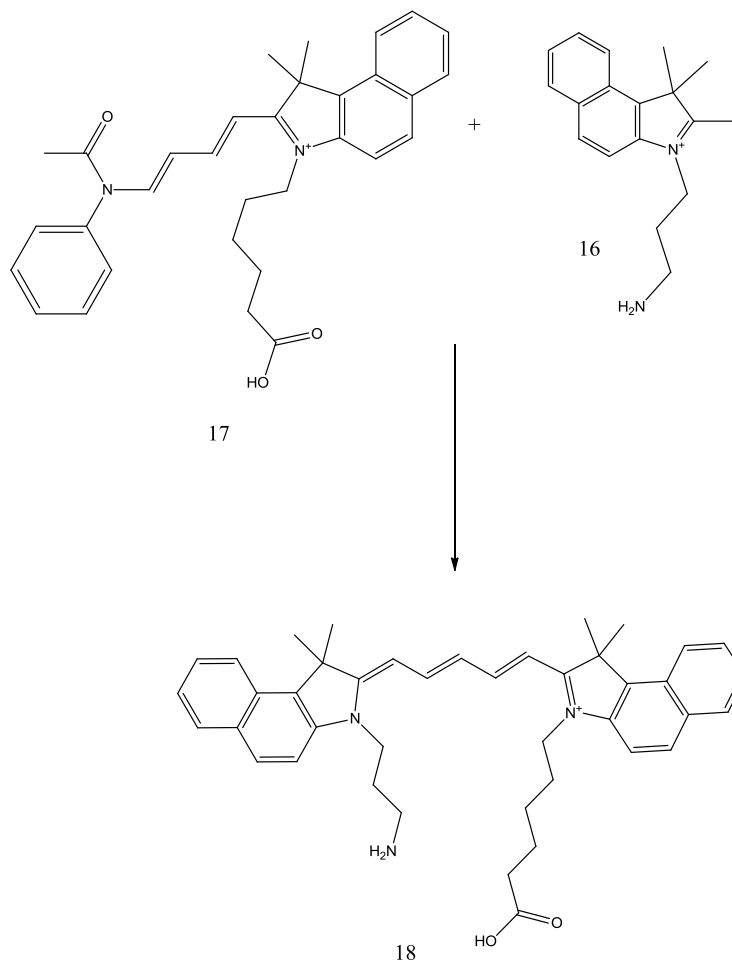


Figure 5.60: Alkylation of TMB with propylamine.

Compound [16] was used further in the reaction with a hemicyanine with a carboxylic acid derivative. The hemicyanine had been formed as before with acetic anhydride and TMB-COOH (scheme 5.12) producing compound [17].

TMB-COOH was dissolved in pyridine with TMB-NH<sub>2</sub> [16] and stirred at 50 °C for 30 minutes (scheme 5.61) and a dull blue solution was obtained. TLC analysis once again showed there to be many by-products. The desired product was attempted to be purified by column chromatography, the column was difficult and the crude material had to be abandoned on the column. This could have been because of the free amine (this functional group is distinctly polar) as the maximum MeOH that can be used in column chromatography is 20% as above this level the MeOH begins to dissolve the silica.



Scheme 5.61: Formation of dye D

The spot that was collected and thought to be the desired product did not move in 20% MeOH: 80% DCM and consequently this product was not collected from the column for further analysis.

## 5.9 USE OF LINKER ONE AS A PROTEIN DETECTOR

Low yields and difficult purifications coupled with time constraints have meant that only one linker molecule had been successfully synthesised. However, this linker had potential to be used in the detection of protein interactions. The linker was examined to assess its feasibility in the detection of the proteins. The first stage was to ascertain their viability as SERS reporters; this was carried out by taking SERS measurements of the dyes as shown in figure 5.12

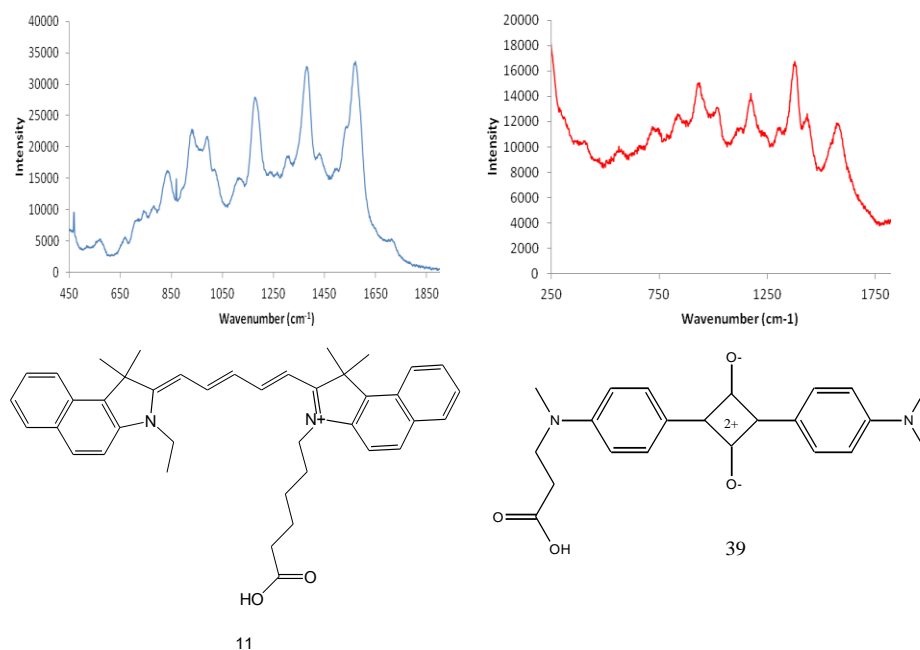


Figure 5.12: The blue line is the SERS obtained from a micromolar solution of the squaraine dye. Compound [39] and the red line indicates SERS from the cyanine dye. Compound [11] were both obtained at 633nm, using a 10 second extended acquisition time.

For the linker, compound [51] shown in figure 5.13, that was successfully synthesised, it was necessary to demonstrate the linker had at least comparable - if not superior - SERS activity when compared to the dye alone (in that as the anchor onto the nanoparticle surface, the linker was necessary). To carry out this experiment, klarite™ was used. This is a nanostructured gold surface, consisting of a lattice of inverted square pyramidal pits. The surface plasmon bands are tuneable due to the concave geometry of the pits, which promotes the formation of hotspots. The dye and linker were bulk coated on to separate klarite™ chips at a micromolar concentration and incubated for 1 hour at room temperature under dark conditions. Following this each piece of klarite™ was washed with ethanol to remove any unbound components. This class of dye also exhibits fluorescence, with an emission at 700 nm. When tested with the linker the fluorescence remained the same. This fluorescence was used to obtain an idea of surface coverage on each chip of klarite™ through examination using a fluorescence microscope; the substrates were examined using a 50x objective with a Texas Red filter.

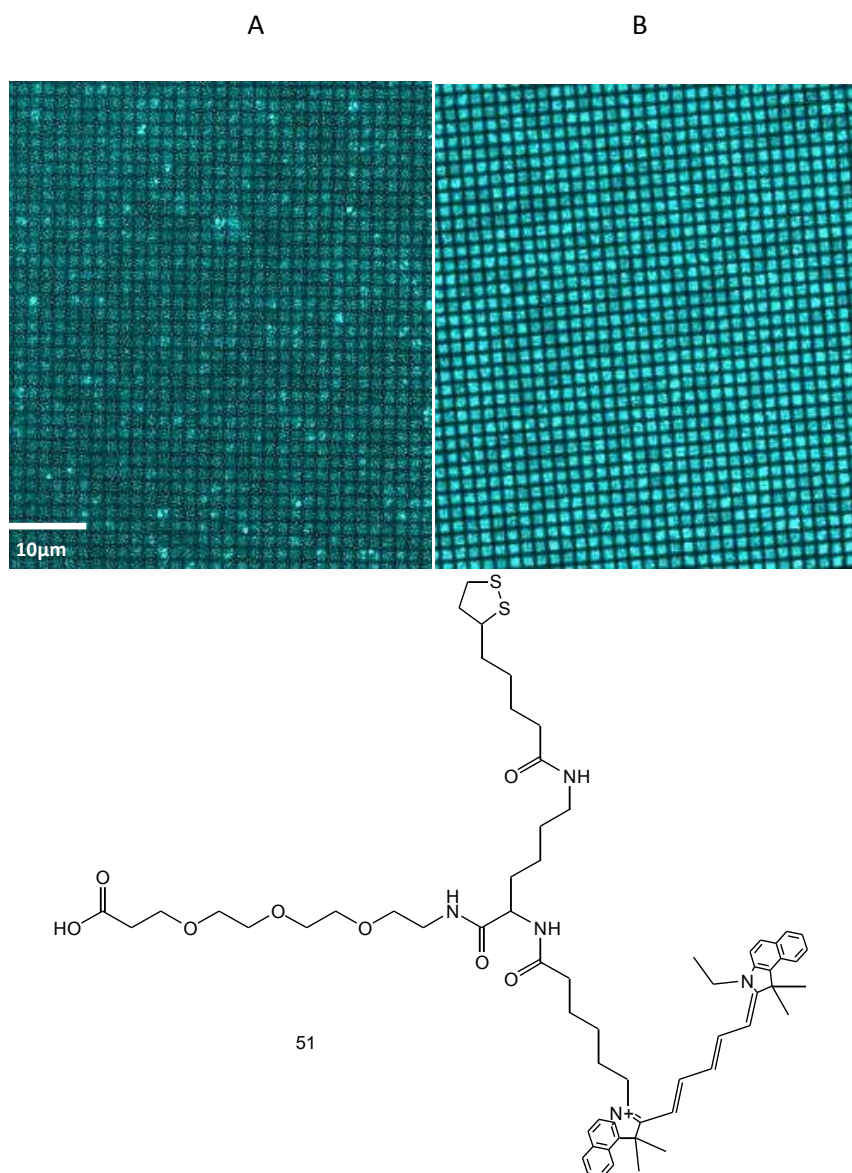


Figure 5.13: Klarite™ chips coated with dye, A, and linker, B. This image was obtained using fluorescence microscopy using a Texas Red filter (Ex. 596, Em. 620) and a 50× objective. Gain and exposure times remained constant for all images taken; using Leica QWin software. Images were processed using Image J software.

The figure shows the fluorescence of each Klarite™ chip: with image A showing the surface functionalised with dye alone; compared with image B in which the surface is coated with the linker. Although fluorescence is observed from image A, this is likely due to non-specific adsorption - probably due to incubation time. In contrast image B shows well formed and uniform coverage of the linker molecule. This was to be expected as it has been well documented that thiol containing compounds form

SAMs on gold surfaces. Therefore this experiment demonstrated that the use of the linker provided a more uniform coverage of the gold surface and thus providing a better signal and a specific orientation for protein reactions. It was therefore necessary to confirm that the good fluorescence observed was mirrored when analysed by SERS. For This purpose, each section of Klarite™ was analysed using a WiTec 633 nm laser.

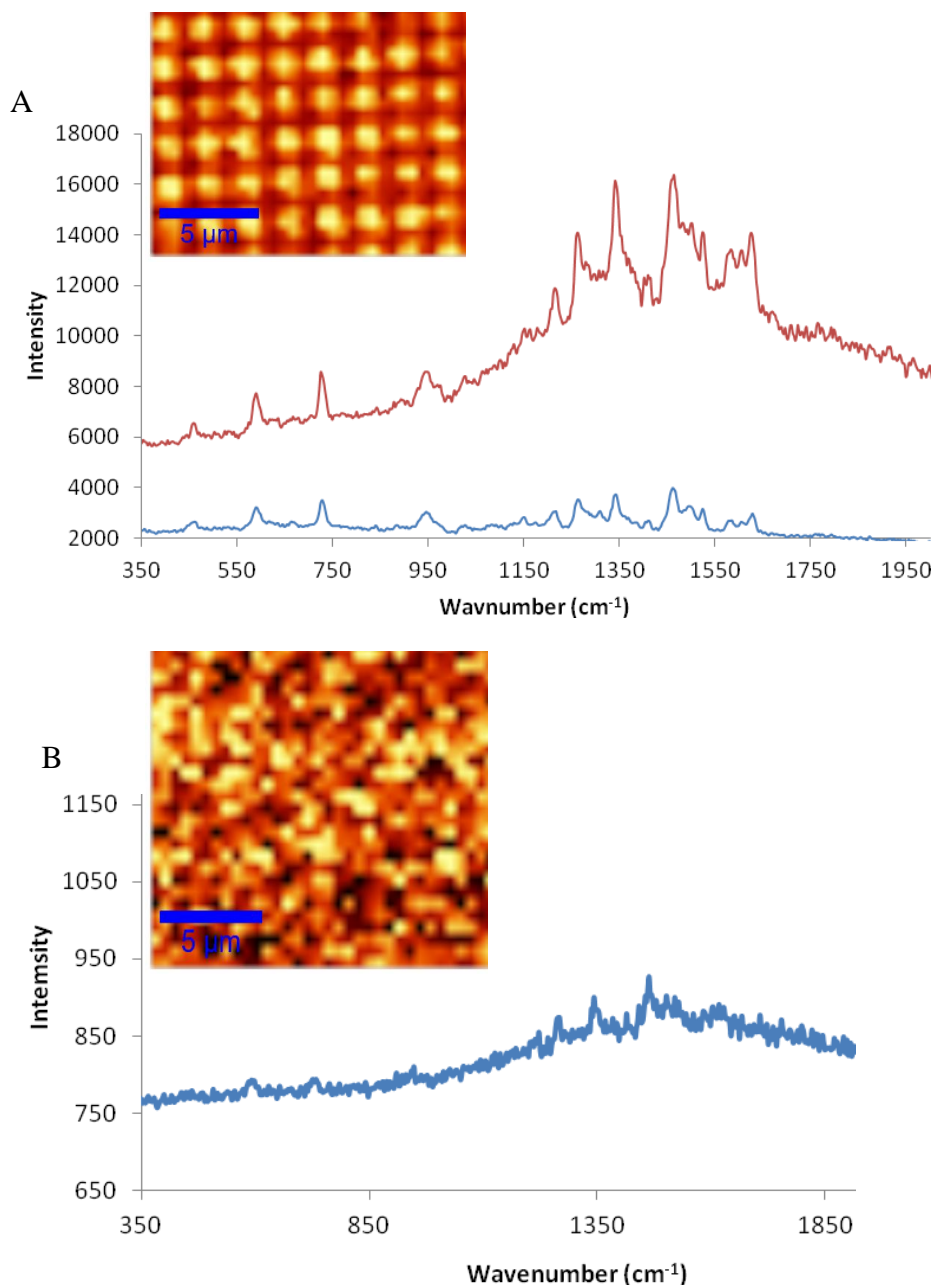


Figure 5.14: False colour images (depicting the SERS response between 1308-1345 cm<sup>-1</sup> at 633 nm) and representative SERS spectra of the Klarite™ chips. A represents the chip coated with 1 mM linker and B the chip coated with 1 mM dye.

Figure 5.14 shows a marked difference in SERS response. Good SERS signals were obtained from the Klarite™ chip when coated with linker when compared with dye alone - a result which was consistent with the fluorescent images obtained.

The good result obtained with the use of this linker meant that further experiments could be carried out and a specific protein interaction could be investigated.

## 5.9.2 ASSAY APPROACH

Assays are commonly used as an analytical approach to investigate protein-protein interactions. ELISAs are often used to investigate these interactions. This type of assay allows for the detection of specific protein-protein interactions. Research has led to a shift towards the development of protein micro/nano-arrays. The reasons for this include the potential to multiplex and far less sample and reagent consumption.<sup>215</sup> Dip-pen nanolithography (DPN) has been shown to efficiently create immunoassays on a small scale.<sup>216</sup> This instrument uses a cantilever which is coated with either an ink or biomolecule. The tip of the cantilever is then brought into contact with the surface and through the formation of a meniscus the ink - or biomolecule - is deposited onto the surface. NLP 2000™ is based on the DPN technique. however it is more specific to the creation of arrays; the process can only form dots and lines. It is a high throughput process that allows fast patterning.

The tip is first coated with a capture antibody by submerging it in a solution contained within a microfluidic inkwell. Once coated, the capture antibody is deposited onto nitrocellulose by placing the tip in contact with the surface by using the NLP 2000™. The tip-substrate contact is controlled through a series of plane calculations where the tip is lowered down and contact can be visualised through a white light microscope.

Monoclonal mouse IgG capture antibody was chosen as the biomolecule to print on the epoxysilane coverslip, to which protein A/G was conjugated. Linker molecule 1 was incubated with the printed coverslip to allow for the protein interaction to occur. Protein A/G was conjugated on to 13 nm gold nanoparticles coated with linker molecule 1 and compound [51] as detailed in section 7. 3.

For each separated area on the slide, 12 arrays were printed with the dimensions of 3 x 3 features and a pitch (distance between spots) of 20 µm. This meant that each pen

on the probe simultaneously contributed 3 x 3 spots within the overall area with the order of patterning for each pen working from left to right (i.e. two spots side-by-side) followed by the pens moving in an upwards direction to print the next row. Only 9 spots per pen were printed since the ink volume and the consistency of the spot size depleted greatly beyond this point. The dwell time used for the array printing was 0.01 seconds for each feature per array. Following the printing of the antibody, the conjugated protein-linker solution was incubated with the slide for 15 minutes, followed by several washing steps. A control - whereby protein was not conjugated to the linker - was also incubated with the printed arrays and analysed.

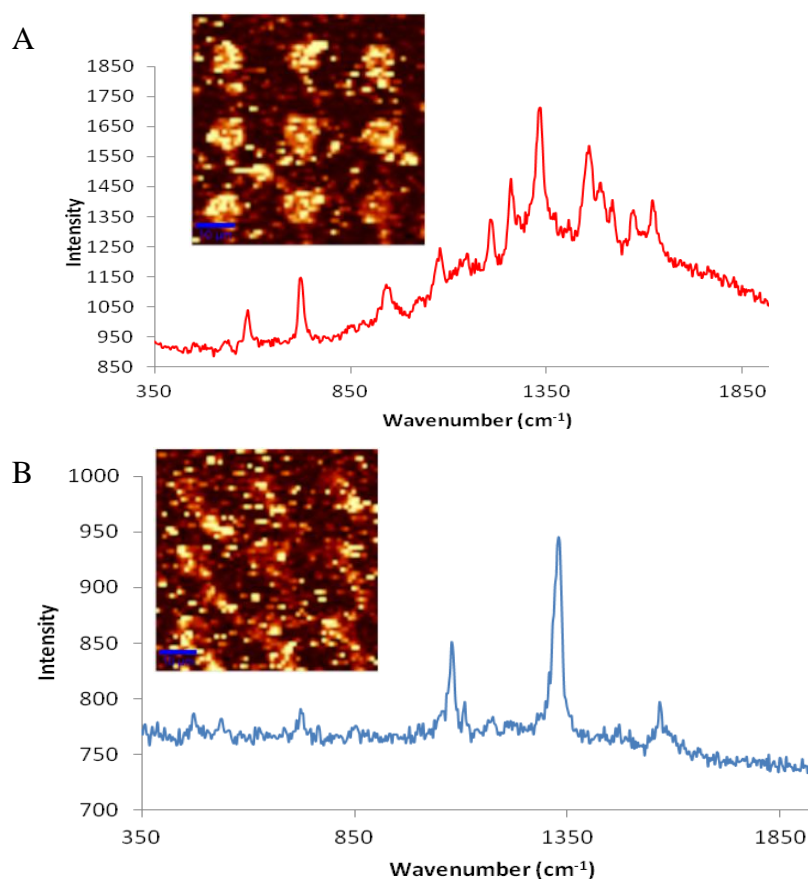


Figure 5.15: SERS spectra of A. Representative of micro-array between antibody and gold nanoparticles anchored protein A/G along with a false colour image of a section of the micro array depicting SERS intensity between 1308 – 1342 cm<sup>-1</sup>. Maps were generated using a 0.1 second integration time and 633 nm wavelength. SERS spectra of B was a control of the array. Gold nanoparticles conjugated with the linker yet no protein was attached. The false colour map was generated using a 0.1 second integration time and shows the SERS intensity between 1308-1342 cm<sup>-1</sup> once more.

It can be seen from figure 5.15 that the samples that contained the control gave minimal signal; most likely due to non-specific binding (B). The false colour image shows that there is no specific binding between the gold nanoparticles conjugated with the linker without protein A/G; whereas the false colour image generated using the protein conjugated linker gold nanoparticles shows uniformity. It indicates the specific interaction between the antibody and protein. The spots depict the area where the antibody has been printed. The spectra obtained under assay conditions match well with the spectra obtained in colloidal solutions.

## CHAPTER 6: CONCLUSIONS

The research presented within this document has striven to demonstrate the different methods for the generation of protein nanoparticle conjugates, their use in the detection of proteins and their associated interactions using Raman based techniques. Fluorescent proteins have been implemented extensively within the cellular biology field as a bio-marker. Through this type of research the cellular biology community has been 'brought into the light' concerning the role of proteins within cellular life. However, the use of fluorescence as an imaging technique has several disadvantages: such as the photo-instability of the fluorophore; and inability to multiplex efficiently. As such there has been great interest to incorporate Raman based technologies as a comparative technique to fluorescence, with the long term goal to implement such technologies - as widely as fluorescence - in the area of detection and diagnostics.

EGFP-NP conjugates using silver nanoparticles have been successfully synthesised through the use of electrostatics by manipulation of pH and the isoelectric point of the fluorescent protein. Nitric acid was used to modify the pH of silver citrate colloid and incubated with EGFP which, over a specified time period, produced a net positively charged protein. The attraction between the negatively charged silver citrate colloid and the positive protein allowed for detection of the intrinsic chromophore of the FP. It has been observed that this manipulation was critical to achieve the intense SERS signal, when compared to the interaction of the FP with unmodified colloid and basic modified colloid which produced poor results.

A series of optimisation experiments, including acquisition time, volume of protein and incubation time ensured that a competitive LOD was obtained for this system.

Once an initial LOD was obtained, a number of different methods were investigated to find an even more competitive LOD. The use of citrate buffer was to create a net positively charged protein and was incubated with unmodified silver citrate colloid. However, this system proved to be less stable and the LOD obtained was not as sensitive as the initial LOD obtained using the electrostatic method.

In a reversal of method, positively charged silver nanoparticles were synthesised using a polyelectrolyte - PDDA. This system was even more unstable, so much so that a LOD could not be obtained.

Once a stable and competitive system was determined, interest in the variants of EGFP occurred. The electrostatic method was used to investigate the detection of RFP using SERS. However, this method failed to produce a successful signal and as such a different method was required. It was hypothesised a formal bond was required between the silver nanoparticles and RFP. Thiocetic acid is a small disulfide organic acid which has a great affinity to silver and gold nanoparticles. Consequently thiocetic acid capped nanoparticles were synthesised successfully using published protocols. RFP was conjugated via amide chemistry and successfully detected. At the time of the writing, this led to the first reported solution based SERS detection of RFP and EGFP.

Due to this development, the potential for multiplexing of FP using SERS was investigated, leading to the observation that there was the possibility to multiplex these biological markers, through identification of unique vibrational peaks present in their SERS spectra.

Following the successful detection of FPs using SERS, a long term goal would be to visualise FPs fused with another protein of interest within a cellular environment. However, before this goal could be realised, investigation into the ability to visualise nanoparticles in cells using SERS was carried out.

Cell penetrating peptides have been documented in literature as possessing the function of crossing the cellular membrane (a notoriously difficult task) and reaching a specific location within that cell. In addition, it has been demonstrated such peptides can carry cargo into the cell which otherwise would have not made it into the cell in the first instance.

One of the initial peptides discovered to possess this feature was TAT. TAT has been used in conjugation with nanoparticles previously. It was determined to synthesise SERS active TAT nanoparticle conjugates capable of detection within cells. Initially gold nanoparticles were chosen due to enhanced stability. Two different linkers were synthesised differing in PEG length. Fluorescein labelled TAT was conjugated to each linker on gold nanoparticles. SERS results were discouraging, after initial investigation into the coupling reaction between linker and peptide showed that this was not the limiting factor. In an attempt to gain signal from this type of conjugates larger gold nanoparticles were used. This did not produce a signal. It was

hypothesised a shorter linker was required which balanced stability, yet allowed creation of hotspots through controlled aggregation of the conjugates. Thiocetic acid which was used in the detection of RFP using SERS was once more employed in the conjugation of TAT. In addition to this, gold nanoparticles were switched to silver nanoparticles to provide resonance with the fluorescein dye.

Thiocetic acid has shown to provide enhanced stability of conjugates when using nanoparticles: this has in part been attributed to the disulfide bond contained within the structure. Thiocetic acid capped nanoparticles were successfully synthesised and fluorescein labelled TAT peptide was conjugated using amide chemistry. The success of this system led to detection of these conjugates in HeLa cells using SERS at 532 nm.

Finally a more traditional approach was investigated. SERS has traditionally used dyes as a reporter. This dye will typically be conjugated to a selected biomolecule and through the presence of the dye signal it is assumed the biomolecule is present. One of the main advantages of Raman based technology is the possibility to multiplex. In order to multiplex efficiently and in large numbers - especially in the area of protein-protein interactions - several different dyes are required; as such, synthesising a family of novel dyes is of interest.

Several different methods were investigated for the synthesis of cyanine and squaraine dyes; with varying degrees of success. It was found that solid phase chemistry provided slightly higher yields when compared to solution phase chemistry. Two unsymmetrical dyes were successfully synthesised (one of each type of dye) however low yields made subsequent reactions difficult. In addition, solubility problems of squaraine dyes made reactions difficult. It was concluded that in future, these dyes should be synthesised with polar side chains to increase solubility in organic solvents.

Selective methods were employed for the synthesis of linker molecules. This was necessary due to the orthogonal protecting group strategy and resin considerations used in this synthetic route.

A linker was successfully synthesised and analysed using a protein micro-array to determine the viability of this compound in the use of protein-protein interactions. It was found that the protein remained active upon conjugation to the said linker

molecule and conjugation to gold nanoparticles, proving that SERS can be implemented within the biological field. This is the first known use of this linker as a protein detecting compound using SERS.

To conclude; the work carried out during the course of this research as shown the variety of different methods which can be used when detecting proteins and their interactions using SERS. Although a small set has been taken with this research it demonstrates the possibility and benefits of using SERS in this field of science.

## CHAPTER 7: FUTURE WORK

The research presented within this thesis has explored the possibility of implementing SERS within the field of proteomics. It is only the opening chapter to what is sure to become an expanding field within the nano-biology community. In order to continue this line of research many different avenues could be investigated.

The potential to utilise FPs with SERS under multiplexing conditions has been demonstrated: it was shown there were peaks in each spectrum that could be - in theory - assigned to each specific protein if they were contained within one solution. This would have to be confirmed experimentally. Initially the proteins would be mixed on a 1:1 basis and following this a series of experiments to determine the sensitivity of each protein when mixed together.

This research has shown the sensitivity of SERS. The chromophores of FPs differ a very slight way; typically there will be a change in conjugation or addition of an atom/bond depending on which amino acid has been substituted. It was found RFP provided a SERS spectrum which differed significantly from that obtained with EGFP even though there was only the addition of a double bond in place.

For future research, the investigation of the SERS potential of the complete FP palette would provide a comprehensive list of FPs which could be used in conjunction with each other when analysing protein interaction using SERS. Additionally, this research showed the electrostatic method did not yield results with RFP - it was unclear as to why this was the case. Through analysis of the range of FPs, similarities could be identified which could provide an explanation e.g. due to RFP existing as a tetramer.

One of the reasons FPs were chosen was due to their popularity within cellular biology to be used as a biomarker. This function allowed proteins of interest to be studied by fluorescence as FPs can be inserted into vectors for other proteins and therefore when the protein of interest is expressed it is fluorescent. It would be ideal to study a FP fusion using SERS - opening up the possibility of using SERS in a cellular situation.

Chapter four investigated the possibility of being able to detect a labelled nanoparticle conjugate within HeLa cells using SERS. One of the worries of using this technique within cells is the interference from cellular components. This was initial research to determine if it would be possible to use SERS as an intracellular reporting technique. It was found fluorescein labelled TAT nanoparticle conjugates could be detected using SERS when contained within cells. However in order to validate these results, several additional experiments would be required. Only white light images were taken of the cells to correspond and align with the SERS maps taken, which confirmed the presence of the nanoparticle conjugates within the cells. However, TEM images would be essential to validate this result, it has been shown previously TEM has a resolution capable of capturing nanoparticles entering the cell and its organelles.

The next stages would be to identify the loading of the nanoparticle with the TAT peptide, this could be achieved using a method developed by McKenzie *et al.*, which used Trypsin to digest a peptide on a nanoparticle surface and determine the loading content using fluorescence.<sup>217</sup> In addition, thioctic acid was conjugated to the peptide without the addition of a stabilising group (such as PEG). It would be interesting to determine the stability of these nanoparticle conjugates.

Finally, the results were obtained at 532 nm, which was in resonance with the fluorescein label, however, at this wavelength there can be plasma and cellular fluorescence which can interfere with results and mask any possible SERS. Ideally one would want to investigate the use of these conjugates off resonance at a longer wavelength such as 633 nm.

Chapter five detailed the synthesis of novel dye molecules to be conjugated to linker molecules capable of binding proteins and nanoparticles. There were several problems in the initial synthesis of dyes. Purification posed a significant issue. Due to the polar nature of the synthesised dyes, using column chromatography with silica yielded small amounts of dye, ensuring that subsequent reactions were difficult to progress. Additionally, separation between the desired product and by-products was poor. Investigation into using reverse phase HPLC for an alternative purification route in the hope a larger yield and better separation could be achieved.

Solubility was also an issue, particularly with the squaraine dyes. Synthesised due to their unique property whereby the anilino version of these dyes exhibit a peak in their Raman spectra in the region of  $1700\text{ cm}^{-1}$  (where no other commercial dye displays any vibrational information), making these types of dyes attractive for use in multiplexing. It was found the solubility of these dyes was very poor. In future research it would be desirable to enhance the solubility through the incorporation of side groups such as  $-\text{SO}_3$ .

In a corresponding research chapter within this thesis, it was found the use of thioctic acid capped nanoparticles provided a great deal of stability without the inclusion of a PEG compound: it would be interesting to investigate the removal of the PEG compound within the linker synthesis to shorten this process and hopefully improve overall yields of the final complete linker.

Initial application work using the linker produced successful results which indicated the linker could be used in conjunction with proteins without deactivating the action of the protein. Future work would include investigation of this interaction in solution using colloidal solutions not on a surface.

# CHAPTER 8: EXPERIMENTAL

## 8.1 GENERAL

All solvents were of laboratory grade, unless stated otherwise. All anhydrous solvents were supplied in Sureseal<sup>TM</sup> bottles from Sigma Aldrich. All reagents were supplied by a commercial source, Aldrich. DNA was supplied by ATDBio, synthesised on a 1  $\mu$ mol scale and purified by HPLC. Fluorescein labelled Tat peptide was supplied by CSS Albachem, off resin and of > 95% purity by HPLC analysis.

Thin layer chromatography was carried out on aluminium sheets, silica gel 60 0.2 mm layer (Merck). TLC visualisation was carried out by UV absorption at 254 nm and at time treatment with ninhydrin/ethanol (0.2 % w/v) or  $\text{KMnO}_4$  (1.5% w/v). Purification was performed by flash column chromatography and carried out with silica gel 60 (Merck).

$^1\text{H}$  and  $^{13}\text{C}$  NMR were recorded on a Brüker DPX 400 spectrometer and J values are quoted in Hz.

Elemental analyses were performed by the University of Strathclyde as a service with a Perkin-Elmer 240 elemental analyser.

Size exclusion HPLC purification was carried out using a C18 Jupiter Phenomex column on a Dionex HPLC system fitted with an UVD170U detector and as P680 pump, with method details specified in the text.

UV-Vis spectroscopy was carried out on a Cary 300 Bio Uv-VIS spectrophotometer fitted with a 6 x 6 cell changer and peltier temperature controller. Fluorescence measurements were recorded on a Varian Cary Eclipse. SEM was carried out by Dr. Iain Larmour at the Department of Physics, University of Strathclyde on a FEI Sirion 200 ultra high resolution shottky field emission scanning electron microscope. Particle size and zeta potential data were recorded on a Malvern High Performance Particle Sizer and a Malvern Zetasizer 2000 respectively.

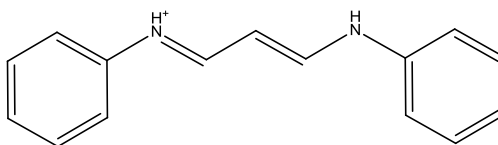
Klarite<sup>TM</sup> chips were obtained from Renishaw Diagnostics.

Bovine serine albumin (BSA), phosphate buffered saline (PBS) and Tween 20 was all purchased from Sigma Aldrich (Dorset, UK). Monoclonal mouse IgG capture antibody and Protein A/G in PBS were obtained pierce.

Nexterion(R) Slide E (epoxy coated) slides and the Nexterion® 16 well incubation chamber were purchased from Schott (Jena, Germany). Array printing by DPN was performed on a NLP 2000™ nanolithography platform (NanoInk Inc., Skokie, IL) using Inkwell arrays (M-6MW) and 12-probe 1D probe arrays (type M-ED).

## 8.2 CHEMICAL SYNTHESIS

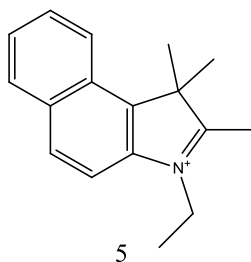
### 8.2.1 Synthesis of (E)-N-((E)-3-(phenyl amino)allylidene)benzenaminium



3

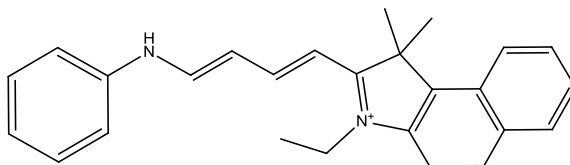
Aniline (3.7 mL, 40 mmol, 1.3 eq) dissolved in distilled water (70 mL) and HCl (5 mL) was added dropwise to a solution of Malondialdehyde bis(dimethylacetal) (5.25 mL, 30 mmol, 1 eq) dissolved in a mixture of distilled water (85.5 mL) and HCl (4.25 mL) with stirring at 50 °C. This produced a precipitate that was obtained by filtration producing 3.2 g of the desired product **3** as an orange solid in a 48 % yield. [Requires C80.68 H 6.77 N 12.55 % Found: C 80.48 H 6.69 N 12.50 % Found 223.1228 M+H; Required 223.1230];  $\delta_{\text{H}}$  (400 MHz;DMSO) 6.35-6.41 (1H,t,Ph(NH), 12Hz), 7.26-7.29 (2H, t, Ph(NH)CHCHCHNH-Ph, 12Hz), 7.39 (4H, d, Ph(NH)CHCHCHNHPh, 8Hz), 7.48-7.52 (4H, m, Ph(NH)CHCHCHNHPh), 8.76-8.83 (2H, m, Ph(NH)CHCHCHNHPh);  $\delta_{\text{C}}$  (100MHz, DMSO) 98.59, 117.24-117.52, 125.61, 129.80-129.90, 139.62-138.66, 158.25

### 8.2.2: Synthesis of 3-ethyl-1,1,2-trimethyl-1H-benzo [e]indol-3-ium



Trimethyl benzo[e] indole (4g, 19.1 mmol, 1 eq) was dissolved in MeCN (100 mL) to which iodoethane (1.836 mL, 22.9 mmol, 1.2 eq) was added. The reaction mixture was heated at 80 °C for 72 Hrs. The excess MeCN was removed until slurry remained, the slurry was suspended into diethyl ether which produced a precipitate. After an hour the precipitate was retrieved by filtration producing 3g of the desired product **5** in a 66% yield as a green solid. [Found 238.15911.58, required 238.1590 M<sup>+</sup>];  $\delta_{\text{H}}$ (500 MHz, CDCl<sub>3</sub>) 1.57 (3H, s, C(CH<sub>3</sub>)), 1.67-1.70 (3H, t, N(CH<sub>2</sub>CH<sub>3</sub>), 8Hz), 1.90 (6H, s, C(CH<sub>3</sub>)<sub>2</sub>), 4.89-4.92 (2H, q, N(CH<sub>2</sub>CH<sub>3</sub>), 8Hz) 7.68-7.80 (3H, m, Ar-H), 8.07-8.15 (3H, m, Ar-H).  $\delta_{\text{C}}$  (500 MHz, CDCl<sub>3</sub>) 13.68, 16.73, 22.66, 45.81, 55.92, 112.40, 122.84, 127.69, 128.71, 130.13, 131.59, 133.77, 137.92, 194.97.

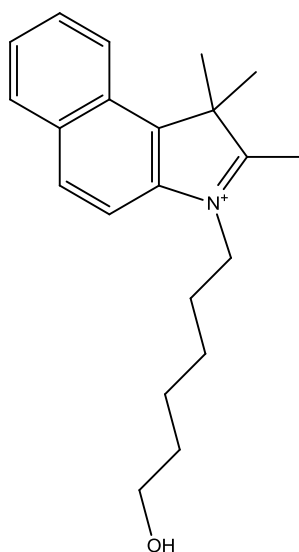
### 8.2.3 Synthesis of 3-ethyl-11-dimethyl-2-((1E,3E)-4-(phenylamino)buta-1,3-dien-1-yl)-1H-benzo[e]indol-3-ium



6

Compound 3 (1g, 4.48 mmol, 1eq) was dissolved in glacial acetic acid (10 mL) to which compound 5 (1.06g, 4.48 mmol, 1eq) was added and the reaction mixture was refluxed for 4 Hrs. The solution was cooled to room temperature and excess solvent was removed under pressure. The compound was used without further purification. [Found 367.25 M; expected 367.22 M ]  $\delta_{\text{H}}$  (400 MHz, DMSO) 1.33-1.37 (3H, t, J 8,  $\text{NCH}_2\text{CH}_3$ ), 1.94 (6H, s,  $\text{CH}_3 \times 2$ ), 4.32-4.36 (2H, q, J 6,  $\text{NCH}_2\text{CH}_3$ ), 6.32-6.38 (1H, t, J 12, CH), 6.50 (1H, s, CH), 7.21-7.24 (1H, t, J 6, CH), 7.37-7.80 (7H, m, Ar-H), 8.07-8.13 (2H, m, Ar-H), 8.29-8.31 (1H, d, J 8, Ar-H), 8.44-8.51 (1H, t, J 14, Ar-H)  $\delta_{\text{C}}$  23.4, 25.3, 125.8, 125.8, 126.9, 128.9, 136.4, 145.8.

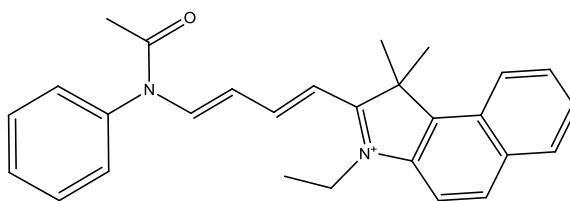
#### 8.2.4: Synthesis of 3-(6-hydroxyhexyl)-1,1,2-trimethyl-1H-benzo [e]indol-3-ium



7

Trimethyl benzo[e] indole (4g, 19.1 mmol, 1 eq) was dissolved in MeCN (100 mL) to which iodoethane (1.836 mL, 22.9 mmol, 1.2 eq) was added. The reaction mixture was heated at 80 °C for 72 Hrs. The excess MeCN was removed until slurry remained, the slurry was suspended into diethyl ether which produced a precipitate. After an hour the precipitate was retrieved by filtration producing 3g of the desired product **7** in a 66% yield as a blue solid. [Found 334.1954 M+Na; expected 334.2097 M+Na]  $\delta_{\text{H}}$  (400 MHz CDCl<sub>3</sub>) 1.53-1.61 (6H, m, CH<sub>2</sub> x 3), 1.92 (6H, s, CH<sub>3</sub> x 2), 2.02-2.09 (2H, m, CH<sub>2</sub>), 3.24 (3H, s, CH<sub>3</sub>), 3.63-3.66 (2H, M, CH<sub>2</sub>), 4.81-4.85 (2H, t, J 8, CH<sub>2</sub>), 7.65-7.77 (2H, m, Ar-H), 7.96-8.14 (4H, m, Ar-H)  $\delta_{\text{C}}$  (100 MHz CDCl<sub>3</sub>) 25.3, 27.3, 33.2, 54.2, 125.6, 127.8, 133.2, 135.4.

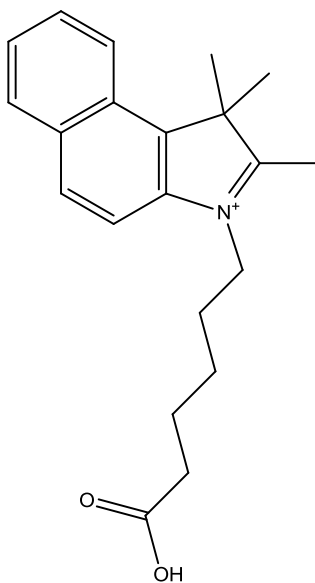
### 8.2.5 Synthesis of 3-ethyl-11-dimethyl-2-((1*E*,3*E*)-4-(*N*-phenylacetamido)buta-1,3-dien-1-yl)-1*H*-benzo[*e*]indol-3-ium



9

Compound 3 (500 mg, 2.1 mmol, 1eq) was dissolved in acetic anhydride (30 mL) to which compound 5 (468 mg, 2.1 mmol, 1eq) was added and the reaction mixture was refluxed for 4 Hrs. The solution was cooled to room temperature and excess solvent was removed under pressure. The compound was purified by flash column chromatography producing 1g of the desired product as a red solid in a 25% yield.  $\delta_{\text{H}}$  (400 MHz,  $\text{CDCl}_3$ ) 1.23-1.27 (3H,t, J 8  $\text{NCH}_2\text{CH}_3$ ), 2.09 (6H, s,  $\text{CH}_3 \times 2$ ), 2.30 (3H,s, $\text{COCH}_3$ ), 4.24-4.29 (2H, q, J 6  $\text{NCH}_2\text{CH}_3$ ), 6.35 (1H,s,CH), 7.15-7.20 (3H,m,Ar-*H*), 7.45-7.54 (5H,m,Ar-*H*), 8.17-8.25 (4H, m,Ar-*H*)  $\delta_{\text{C}}$  (100 MHz  $\text{CDCl}_3$ ) 23.4, 25.3, 125.8, 125.8, 126.9, 128.9, 136.4, 145.8.

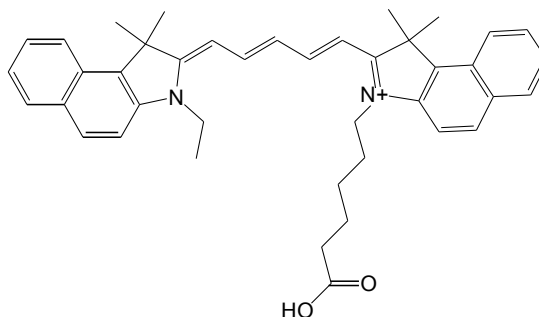
## 8.2.6 Synthesis of 3-(5-carboxypentyl)-1,1,2-trimethyl-1H-benzo [e]indol-3-ium



10

Trimethyl benzo[e] indole (3g, 14.3 mmol, 1 eq) was dissolved in MeCN (100 mL) to which 6-Bromohexanoic acid (2.19g, 14.3 mmol, and 1 eq) was added. The reaction mixture was heated at 80 °C for 72 Hrs. The excess MeCN was removed until a slurry remained, the slurry was suspended into diethyl ether which produced a precipitate. After an hour the precipitate was retrieved by filtration producing 4.5g of the desired product **10** in a 97% yield as a blue solid. [Found 324.1959 M<sup>+</sup> Expected 324.1958 M<sup>+</sup>]  $\delta_{\text{H}}$  (500 MHz, DMSO) 1.42-1.58 (4H, m, CH<sub>2</sub> x 2), 1.75 (6H,s, CH<sub>3</sub> X 2), 1.87-1.93 (2H,m, CH<sub>2</sub>), 2.20-2.27 (2H,t, J 6, CH<sub>2</sub>), 2.94 (3H,s, CH<sub>3</sub>), 4.56-4.59 (2H,t, J 6, CH<sub>2</sub>) 7.70-7.74 (2H, m, Ar-H), 8.13-8.22 (4H, m, Ar-H);  $\delta_{\text{C}}$  (500 MHz, DMSO) 14.23, 22.08, 24.53, 25.88, 27.63, 33.84, 48.12, 55.97, 113.79, 123.89, 127.71, 127.76, 128.88, 130.20, 131.16, 133.52, 137.46, 138.96, 174.78, 196.85. [Required C 77.74 H 8.08 N 4.32 O 9.86; Found C 77.54 H 7.98 N 4.20 O 9.68]

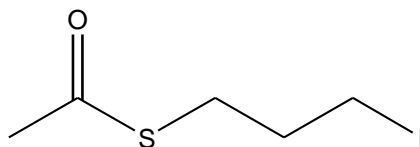
**8.2.7 Synthesis of 3-(5-carboxypentyl)2-((1E,3E,5Z)-5-(3-ethyl-1,1-dimethyl-1H-benzo[e]indol-2(3H)-ylidene)penta-1.3-dien-1-yl)-1,1-dimethyl-1H-benzo[e]indol-3-ium**



11

Compound 9 (2g, 5.6 mmol, 1eq) and compound 10 (1.8g, 5.6 mmol, 1eq) were dissolved in pyridine (10 mL) and stirred at room temperature for 12 Hrs. Removal of excess pyridine under vacuo followed by purification by column chromatography provided 300 mg of the desired product as a green solid in a 13.5% yield.[Found 597.8715  $M^+$ , expected 597.3476  $M^+$ ];  $\delta_H$  (400 MHz,  $CDCl_3$ ) 1.19-1.22 (3H,t,  $NCH_2CH_3$ ), 1.68-1.74 (6H,m, $CH_2 \times 3$ ), 2.07 (12H,s,(  $C(CH_3)_2$ )<sub>2</sub>), 2.35-2.39 (2H,t,  $CH_2$ ), 2.41-2.45 (2H,t,  $CH_2$ ), 4.15-4.21 (2H, q,  $NCH_2CH_3$ ), 6.31-6.40 (2H, m,  $CH \times 2$ ), 6.87-6.93 (1H,t, $CH$ ), 7.34-7.92 (6H, m, Ar-H), 7.90-8.39 (6H, m, Ar-H);  $\delta_C$  (400 MHz,  $CDCl_3$ ) 14.22, 24.34, 24.58, 26.21, 26.37, 27.23, 27.45, 27.72, 27.84, 33.95, 44.33, 51.29, 60.40, 103.26, 110.45, 122.38, 125.04, 126.43, 127.75, 128.21, 129.96, 130.56, 131.78, 134.12, 134.19, 139.27, 152.63, 152.73, 173.59, 174.20, 174.27.

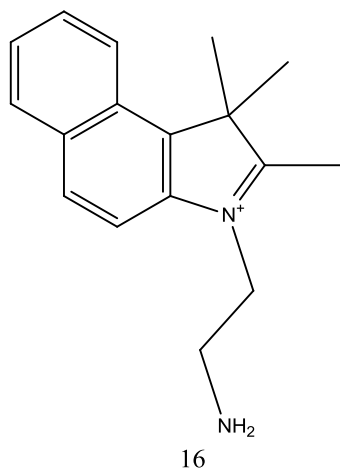
### 8.2.8 Synthesis of S-3(-iodopropyl) ethanethioate



13

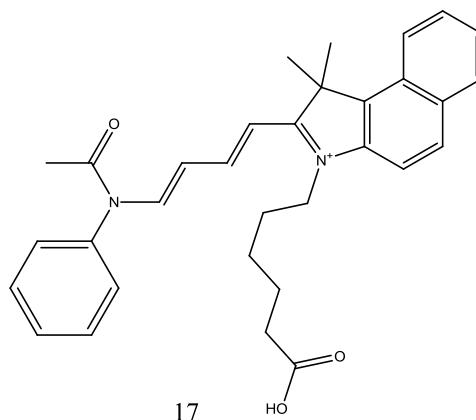
Chloropropylthiolacetate (0.525 mL, 4 mmol, 1.2 eq) and sodium iodide (0.5g, 3.3 mmol, 1eq) were dissolved in acetone and the reaction was stirred for 3 Hrs at room temperature. The excess solvent was removed under vacuo, producing 1g of the desired product as an oil in a quantitative yield. [Found 245.1236  $M^+$ , expected 245.0948  $M^+$ ];  $\delta_H$  (400 MHz, DMSO) 2.30 (3H,s,  $CH_3$ ), 2.65 (2H, t,  $CH_2$ , J 8), 3.10 (2H, t,  $CH_2$ , J 8)<sub>2</sub>, 3.50 (2H,t,  $CH_2$ , J 6);  $\delta_C$  (100 MHz, DMSO) 29.5, 34.5, 180.

### 8.2.9 Synthesis of 3-(3-aminopropyl)-1,1,2-trimethyl-1H-benzo [e]indol-3-ium



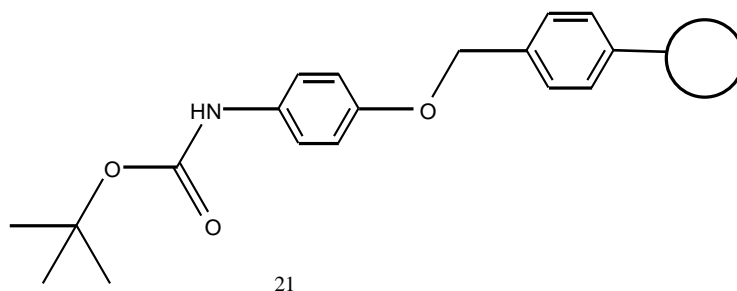
Trimethyl benzo[e] indole (2g, 9.56 mmol, 1eq) was dissolved in MeCN (50 mL) to which 3-bromopropylamine (1.952g, 9.56 mmol, 1 eq) was added. The reaction mixture was heated at 80 °C for 72 Hrs. The excess MeCN was removed until a slurry remained, the slurry was suspended into diethyl ether which produced a precipitate. After an hour the precipitate was retrieved by filtration producing 2.5g of the desired product **16** in a 97% yield as a purple solid. [Found 253.1699 M<sup>+</sup>, expected 253.1699 M<sup>+</sup>];  $\delta_{\text{H}}$  (400 MHz, D<sub>2</sub>O) 1.80 (6H, s, CH<sub>3</sub> x 2), 3.81-3.84 (2H, t, J 6, CH<sub>2</sub>), 4.90-4.94 (2H, t, J 8, CH<sub>2</sub>), 7.70-7.89 (3H, m, Ar-H), 8.14-8.30 (3H, m, Ar-H);  $\delta_{\text{C}}$  (100 MHz D<sub>2</sub>O) 21.7, 26.7, 28.9, 124.3, 125.6, 128.9.

### 8.2.10 Synthesis of 3-(5-carboxypentyl)-1,1-dimethyl-2-((1*E*,3*E*)-4-(*N*-phenylacetamido)buta-1,3-dien-1-yl)-1*H*-benzo[*e*]indol-3-ium



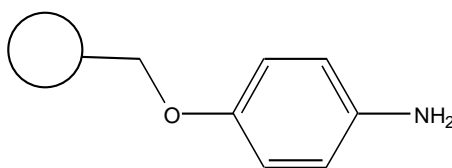
Compound 3 (1g, 4.4 mmol, 1eq) was dissolved in acetic anhydride (30 mL) to which compound 10 (1.4 g, 4.4 mmol, 1eq) was added and the reaction mixture was refluxed for 4 Hrs. The solution was cooled to room temperature and excess solvent was removed under pressure. The compound was purified by flash column chromatography producing 100 mg of the desired product as a red solid in a 4% yield. [Found 453.2529 M-CO<sub>2</sub>H, expected 453.2537 M-CO<sub>2</sub>H]  $\delta_{\text{H}}$  (400 MHz, CDCl<sub>3</sub>) 0.87-0.94 (4H, m, CH<sub>2</sub> x 2), 1.41-1.78 (4H, m, CH<sub>2</sub> x 2), 1.98 (6H, s, CH<sub>3</sub> x 2), 2.30-2.38 (2H, m, CH<sub>2</sub>), 3.49 (3H, s, CH<sub>3</sub>), 4.00-4.04 (2H, t, J 8, CH<sub>2</sub>), 4.18-4.26 (1H, m, CH), 6.19-6.22 (1H, d, J 12, CH), 7.10-8.53 (11H, m, Ar-H);  $\delta_{\text{C}}$  (100 MHz) 23.4, 25.3, 27.9, 29.3, 125.8, 125.8, 126.9, 128.9, 136.4, 145.8.

### 8.2.11 Attachment to Merrifield Resin



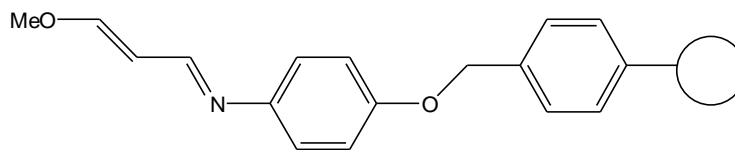
Compound 20 (752 mg, 3.5 mmol, 3 eq) and potassium carbonate (492 mg, 3.5 mmol, 3eq) and 2% DVB cross-linked chloromethyl polystyrene (Merrifield resin, 1g, 1.2 mmol, 1 eq) were suspended in DMF (7.5 mL) the reaction mixture was heated at 50 °C for 32 Hrs. The resin was isolated by filtration and was washed with DMF and DCM three times respectively producing a beige resin.

### 8.2.12 Deprotection of aniline on resin



Resin 21 (500 mg, 0.46 mmol) was shaken at room temperature in a solution of 20% TFA in DCM (4 mL) for 2 Hrs. The resin was filtered and washed with DCM; the filtered resin was then shaken with a 10% solution of Et<sub>3</sub>N in DCM (4 mL) for 15 minutes followed by filtration and washing with DCM to produce the beige resin.

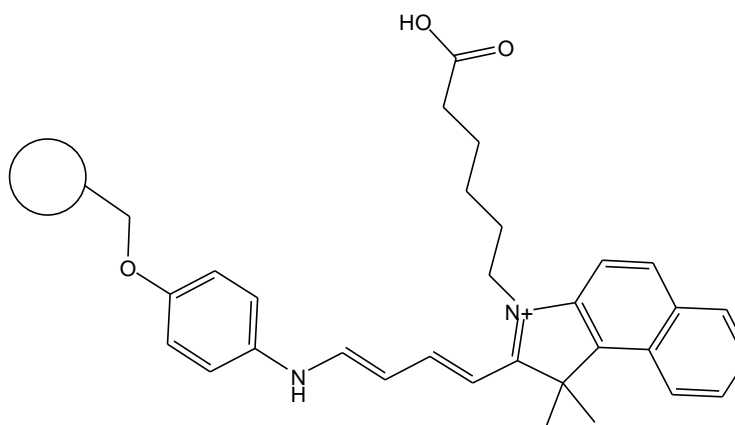
### 8.2.13 Attachment of Malonaldehyde bis(dimethylacetal) to Merrifield resin



23

Malondialdehyde bis(dimethylacetal) (0.6 mL, 4.6 mmol, 1eq) and boron trifluoride diethyletherate (0.06 mL, 0.38 mmol, 0.08eq) in DCM (6 mL) to this solution resin 22 was added and the solution was stirred at room temperature for 6Hrs. Anhydrous DIPEA (0.1 mL, ) was then added and the suspension was stirred for a further 5 minutes. Resin 23 was isolated by filtration and washed with DCM producing the desired product as a beige resin.

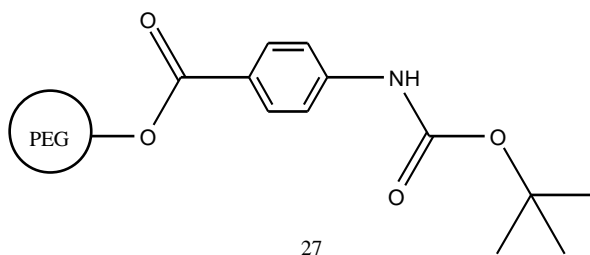
### 8.2.14 Synthesis of hemicyanine on Merrifield resin



24

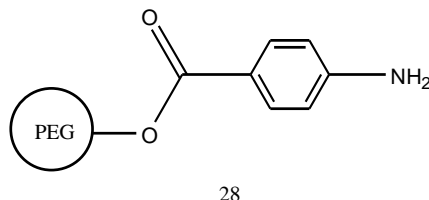
Compound 10 (675 mg, 2 mmol, 6eq) was dissolved in DMF (4 mL) to which the modified resin 23 (300 mg, 0.3 mmol, 1eq) was added and the reaction mixture was heated at 80 °C for 4 Hrs. The resin was isolated by filtration washed with DMF and DCM respectively three times producing a brown resin.

### 8.2.15 Attachment of PEG



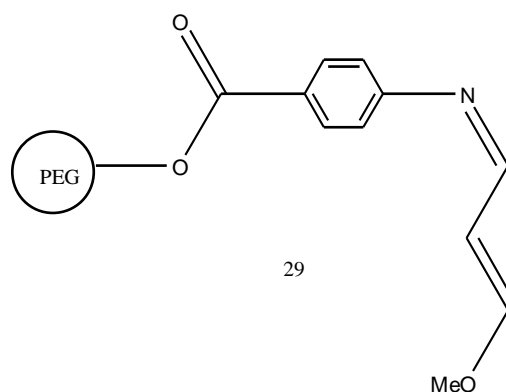
Poly(ethylene glycol), MW2000 (2.5 g, 1.25 mmol, 1eq) and compound 26 (1.2g, 4.2 mmol, 4eq) were dissolved in anhydrous DCM (50 mL) to which DCC (1.07 g, 5.2 mmol, 4 eq) and DMAP (80 mg, 0.65 mmol, 0.52 eq) were added and the solution was stirred at room temperature for 1 Hr. The reaction solution was filter to remove by-products and the filtrate was concentrated under reduced pressure. Diethyl ether was added to the crude produce producing a white precipitate which was collected by filtration producing 1.5g of the desired product as a white solid in a 25% yield.  $\delta_{\text{H}}$  (400 MHz, CDCl<sub>3</sub>) 1.52 (9H, s, CH<sub>3</sub> x 3), 3.60-3.66 (58H, m, PEG), 7.24-7.45 (2H, t, J 8, Ar-H), 7.95-8.03 (2H, m, Ar-H);  $\delta_{\text{C}}$

### 8.2.16 Deprotection of amine on PEG



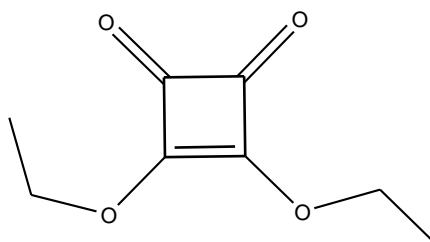
Compound 27 (2.5g, 1.03 mmol) was suspended in 40% TFA in DCM solution (10 mL) and refluxed for 5 Hrs. To this solution diethyl ether was added with vigorous stirring which produced a yellow precipitate. Isolated by filtration the precipitate was dissolved in 20% solution of Et<sub>3</sub>N in DCM (10 mL) which was stirred at room temperature for 15 minutes, once more diethyl ether was added this produced a white precipitate which was isolated by filtration. The excess solvent was removed in vacuo producing 0.5g of the desired product as yellow oil in 10% yield.  $\delta_{\text{H}}$  (400 MHz, CDCl<sub>3</sub>) 3.60-3.66 (62H, m, PEG), 7.06-7.08 (2H, d, J 8, Ar-H), 7.99-8.01 (2H, m, Ar-H);  $\delta_{\text{C}}$

### 8.2.17 Synthesis of Malonaldehyde bis(dimethylacetal) on PEG



Compound 28 (2g, 0.9 mmol, 1eq) and 1,1,3,3- tetramethoxypropane (3.7 mL, 22.2 mmol, 24 eq) were dissolved in glacial acetic acid (9 mL) and heated at 55 °C for 6 Hrs. Diethyl ether was added which cause precipitate of the desired product. Isolated by filtration 5g of the desired product as a yellow solid in a yield.

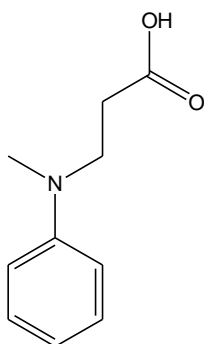
### 8.2.18 Synthesis of 3,4-diethoxycyclobut-3-ene-1,2-dione



31

Squaric acid (3g, 26 mmol, 1eq) was dissolved in ethanol (30 mL) and refluxed for 3 Hrs. Excess solvent was removed in vacuo until only ~5 mL remained. A further 30 mL of ethanol was added and the solution was refluxed for a further 30 minutes, the excess solvent was removed until 5 mL remained once more. Once again 30 mL of ethanol was added and the reaction mixture was refluxed for a final 30 minutes. The excess solvent was removed completely producing 4g of the desired product as a milky suspension in a 90% yield. [Found 171.0648 M+H, expected 171.0657 M+H];  $\delta_{\text{H}}$  (400 MHz, DMSO) 1.32-1.38 (6H, m, CH<sub>3</sub> x 2), 4.58-4.67 (4H, m, CH<sub>2</sub> x 2);  $\delta_{\text{C}}$  (100 MHz, DMSO) 15.20, 56.00, 70.13, 189.85.

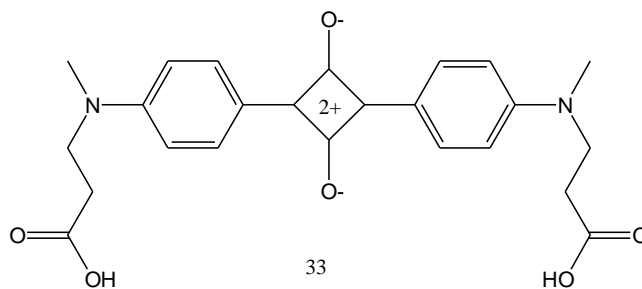
### 8.2.19 Synthesis of 3-(methyl(phenyl)amino)propanoic acid



32

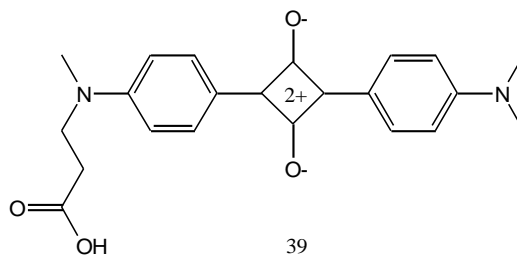
N-methylaniline (1 mL, 9.2 mmol, 1eq) and acrylic acid (0.632 mL, 9.2 mmol, 1eq) were dissolved in toluene (25 mL) and refluxed for 48 Hrs. Excess toluene was removed in vacuo and the crude product was purified using flash column chromatography producing 926 mg of the desired product as a brown oil in a 51% yield. [Found 178.13 M-H, expected 178.08 M-H ];  $\delta_{\text{H}}$  (400 MHz,  $\text{CDCl}_3$ ) 2.59-2.72 (2H, m,  $\text{CH}_2$ ), 2.97 (3H, s,  $\text{CH}_3$ ), 3.68-3.71 (2H, m,  $\text{CH}_2$ ), 6.81 (3H, m, Ar-H), 7.27-7.31 (2H, m, Ar-H);  $\delta_{\text{C}}$  (100 MHz  $\text{CDCl}_3$ ) 41.3, 50.6, 115.7, 115.7, 122.8, 129.7.

### 8.2.20 Synthesis of 2,4-bis(4-((2-carboxyethyl)(methyl)amino)phenyl)cyclobutane-1,3-bis(olate)



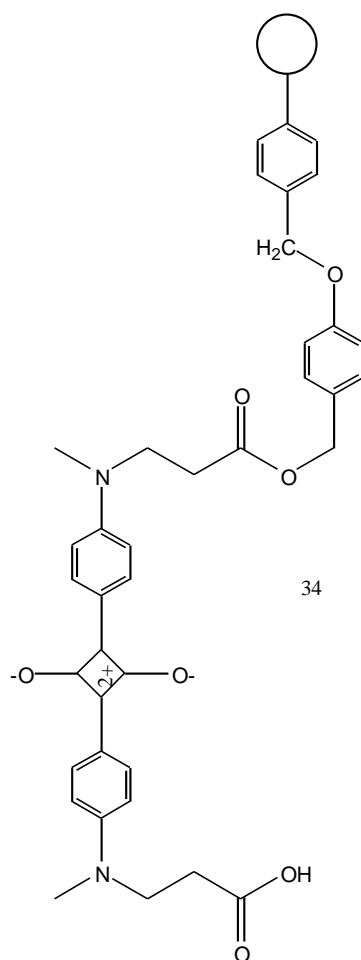
Compound 32 (351 mg, 1.76 mmol, 2eq) and squaric acid (100 mg, 0.88 mmol, 1eq) were dissolved in IPA (15 mL) to which TEOF (1 mL) was added and refluxed for 18 Hrs. The excess solvent was removed and the crude product was suspended in DCM which produced a precipitate. Isolated by filtration producing 152 mg of the desired product as a green solid in a 4% yield. [Found 437.27 M+H, expected 437.17 M+H];  $\delta_{\text{H}}$  (400 MHz,  $\text{CDCl}_3$ ) 2.46 (4H, t,  $\text{CH}_2 \times 2$ ), 2.85 (6H, s,  $\text{CH}_3 \times 2$ ), 3.62 (4H, t,  $\text{CH}_2 \times 2$ ), 6.51-6.95 (8H, m, Ar-H).  $\delta_{\text{C}}$  (100 MHz  $\text{CDCl}_3$ ) 35.4, 42.1, 54.5, 113.9, 128.9, 129.2, 142.5.

**8.2.21 Synthesis of 3-((4-[3-(4-Dimethylamino-phenyl)-2-hydroxy-4-oxo-cyclobut-1-enyl]-phenyl)-methyl-amino)-propanoic acid.**



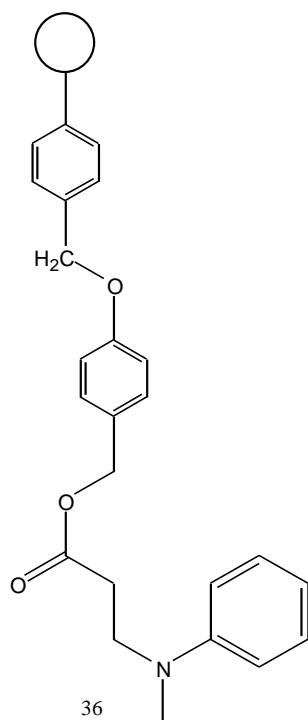
Compound 32 (500 mg, 2.79 mmol, 1eq), dimethylaniline (0.46 mL, 2.79 mmol, 1eq) and squaric acid (318 mg, 2.79 mmol, 1eq) were dissolved in IPA (15 mL) to which TEOF (1 mL) was added and refluxed for 18 Hrs. The excess solvent was removed and the crude product was suspended in DCM which produced a precipitate. Isolated by filtration producing 48 mg of the desired product as a green solid in a 4.5% yield. [Found 180.09 M+H, expected 180.09 M+H];  $\delta_{\text{H}}$  (400 MHz,  $\text{CDCl}_3$ ) 2.46 (4H, t,  $\text{CH}_2 \times 2$ ), 2.85 (9H, s,  $\text{CH}_3 \times 3$ ), 3.62 (4H, t,  $\text{CH}_2 \times 2$ ), 6.51-6.95 (8H, m, Ar-H).  $\delta_{\text{C}}$  (100 MHz  $\text{CDCl}_3$ ) 40.8, 42.1, 53.5, 129.2, 142.5, 177.0.

### 8.2.22 Attachment of compound 33 to Wang resin



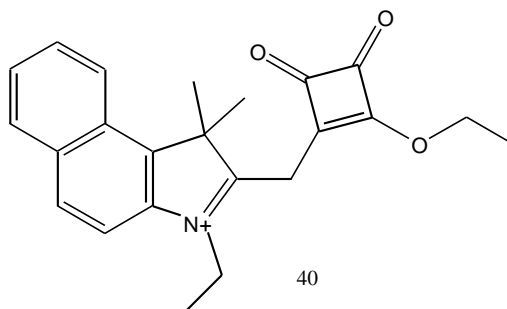
Compound 33 (152 mg, 0.68 mmol, 2.4eq), DPTS (82 mg, x mmol, 1eq) and DIC (0.058 mL, 0.56 mmol, 2 eq) were dissolved in DCM to which Wang resin (280 mg, 0.28 mmol, 1eq) was added the reaction mixture was shaken at room temperature for 18 Hrs. The resin was isolated by filtration producing 250 mg of the dark resin.

### 8.2.23 Synthesis of squaraine on resin.



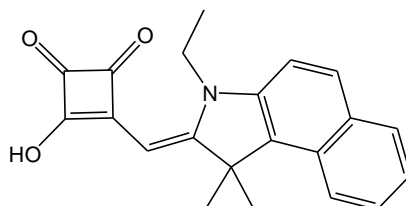
Wang resin (1g, 1 mmol, 1eq) was suspended in a solution of compound 32 (0.895g, 5 mmol, 5eq), DPTS (293 mg, 1 mmol, 1eq), DIC (0.235 mL, 2 mmol, 2eq) and DCM. The solution was shaken at room temperature for 18 Hrs. The resin was isolated by filtration and washed with MeOH and DCM three times respectively.

### 8.2.24 Synthesis of 2-((2-ethoxy-3,4-dioxocyclobut-1-en-1-yl)methyl)-3-ethyl-1,1-dimethyl-1*H*-benzo[*e*]indol-3-ium



Compound 31 (0.5g, 2.9 mmol, 1eq) and compound 5 (1g, 2.9 mmol, 1eq) were dissolved in ethanol (30 mL) and refluxed for 1 Hr. After cooling the crude product was purified by column chromatography producing 250 mg of the desired product as a yellow solid in a 24% yield. [Found 363.3431 M; expected 363.1785 M]  $\delta_{\text{H}}$  (400 MHz,  $\text{CDCl}_3$ ) 1.21 (3H, t, J 8 CH<sub>3</sub>), 1.48-1.52 (3H, t, J 8, CH<sub>3</sub>), 1.76 (6H, s, CH<sub>3</sub> x 2), 4.21 (2H, q, J 9, CH<sub>2</sub>), 4.59-4.64 (2H, q, J 9, CH<sub>2</sub>), 7.71-7.81 (2H, m, Ar-H), 8.13-8.39 (4H, m, Ar-H);  $\delta_{\text{C}}$  (100 MHz  $\text{CDCl}_3$ ) 14.3, 16.1, 45.5, 68.9, 124.5, 125.8, 128.5, 133.5, 176.5, 187.0.

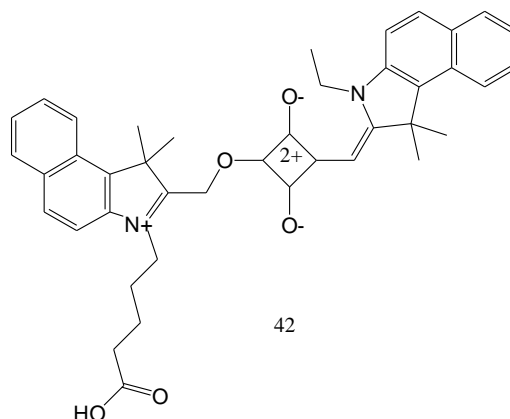
### 8.2.25 Synthesis of (Z)-3-((3-ethyl-1,1-dimethyl-1H-benzo[e]indol-2(3H)-ylidene)methyl)-4-hydroxycyclobut-3-ene-1,2-dione



41

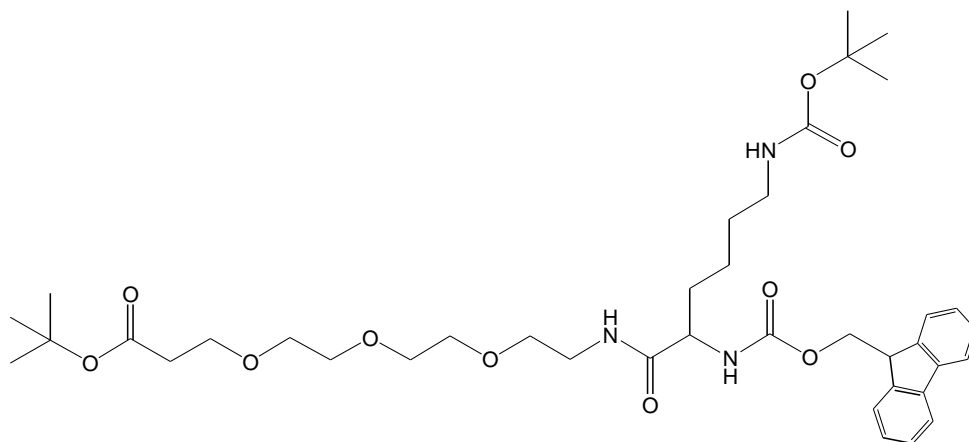
Compound 40 (250mg, 0.73 mmol, 1eq) was dissolved in a mixture of acetic acid (2 mL), water (2 mL) and 2M HCl (0.2 mL) and refluxed for 3 Hrs. Removal of excess solvent and purification by flash column chromatography produced 206mg of the desired product a yellow solid in 84.5% yield. [Found 334.1436 M+H; expected 334.1443 M+H]  $\delta_{\text{H}}$  (400 MHz, DMSO) 1.48-1.52 (3H, t, J 8, CH<sub>3</sub>), 1.76 (6H, s, CH<sub>3</sub> × 2), 4.59-4.64 (2H, q, J 9, CH<sub>2</sub>), 7.71-7.81 (2H, m, Ar-H), 8.13-8.39 (4H, m, Ar-H)  $\delta_{\text{C}}$  (100 MHz DMSO) 14.3, 45.5, 124.5, 125.8, 128.5, 133.5, 176.5, 187.0.

**8.2.26 Synthesis of (Z)-2-((3-(4-carboxybutyl)-1,1-dimethyl-1H-benzo[e]indol-3-ium-2-yl)methoxy)-4-((3-ethyl-1,1-dimethyl-1H-benzo[e]indol-2(3H)-ylidene)methyl)cyclobutane-1,3-bis(olate)**



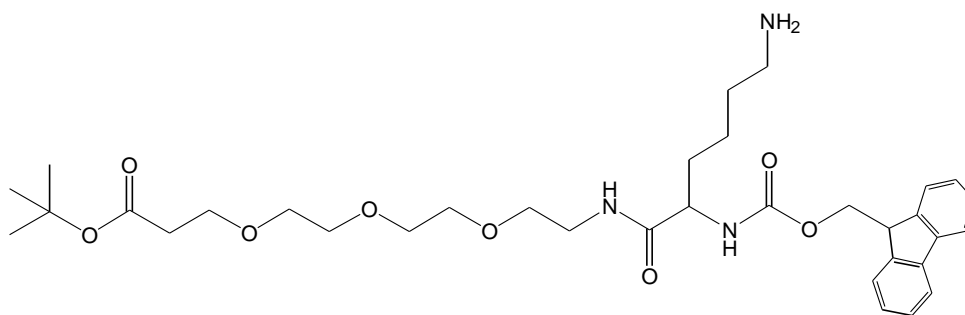
Compound 41 (206 mg, 0.62 mmol, 1eq) and compound 10 (200mg, 0.62 mmol, 1eq) were dissolved in IPA (30 mL) to which TEOF (2 mL) was added and the solution refluxed for 18 Hrs. Purification by flash column chromatography produced 10mg of the desired product as a green solid in a 2.5% yield. [Found 645.3384 M; expected 645.3333 M]  $\delta_H$  (400 MHz, DMSO) 1.09-1.12 (2H, m, CH<sub>3</sub>), 1.54-1.60 (8H, m, CH<sub>2</sub> x4), 1.78-1.80 (2H, m, CH<sub>2</sub>), 1.96 (12H,s, CH<sub>3</sub>x4), 2.20-2.24 (2H, t, J 8, CH<sub>2</sub>), 4.22-4.26 (2H, m, CH<sub>2</sub>), 7.44-7.47 (2H, m, Ar-H), 7.60-7.64 (2H, m, Ar-H), 7.69-7.72 (2H, m, Ar-H), 8.01-8.04 (4H, m, Ar-H), 8.22-8.24 (2H, m, Ar-H)  $\delta_C$  (100 MHz, DMSO) 14.6, 22.9, 27.1, 27.6, 33.7, 50.2, 113.4, 125.8, 126.3, 133.5,178.4.

**8.2.27 Synthesis of tert-butyl 10-(((9H-fluoren-9-yl)methoxy)carbonyl)amino)-2,2-dimethyl-4,11-dioxo-3,15,18,21-tetraoxa-5,12-diazatetracosan-24-oate**



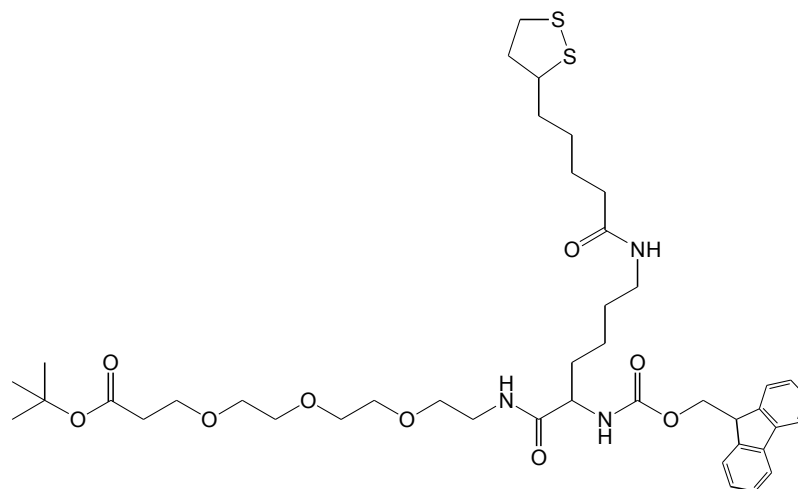
PEG<sub>3</sub> (590mg, 2.1 mmol, 1eq), lysine (1g, 2.1 mmol, 1eq) and EDC (510mg, 2.7 mmol, 1.3 eq) were dissolved in DCM (50 mL). The solution was stirred at room temperature for 18 Hrs. Purification by flash column chromatography produced 450mg of the desired product as a white solid in a 29.5% yield. [Found 728.4116 M+H, expected 728.4112 M+H];  $\delta_{\text{H}}$  (400 MHz, CDCl<sub>3</sub>) 1.25-1.35 (4H, m, CH<sub>2</sub> x2), 1.41 (18H, s, CH<sub>3</sub> x 6), 2.48-2.51 (2H, t, J 6, CH<sub>2</sub>), 3.11 (2H, m, CH<sub>2</sub>), 3.55-3.57 (2H, m, CH<sub>2</sub>), 3.69 (10H, s, CH<sub>2</sub> x 5), 3.70-3.72 (2H, m, CH<sub>2</sub>), 4.11-4.44 (4H, m, CH<sub>2</sub> x 2), 7.31-7.35 (2H, m, CH<sub>2</sub>), 7.39-7.43 (2H, t, J 8, CH<sub>2</sub>), 7.60-7.62 (2H, d, J 8, CH<sub>2</sub>), 7.76-7.78 (2H, d, J 8, CH<sub>2</sub>);  $\delta_{\text{C}}$  (100 MHz, CDCl<sub>3</sub>) 28.4, 28.7, 33.2, 41.3, 57.1, 70.4, 79.5, 82.1, 120.5, 125.2, 126.7, 143.6, 155.9.

### 8.2.28 Synthesis of tert-butyl 5-(4-aminobutyl)-1-(9H-fluoren-9-yl)-3,6-dioxo-2,10,13,16-tetraoxa-4,7-diazanonadecan-19-oate



Compound 46 (200mg, 0.27 mmol, 1eq) was dissolved in a mixture of MeCN (5 mL) and water (100  $\mu$ L) to which BiCl<sub>3</sub> (30 mg, 0.096 mmol, 0.2 eq) and the solution was heated at 55 °C for 1 Hr. A further portion of BiCl<sub>3</sub> (30 mg, 0.096 mmol, 0.2 eq) was added and the reaction mixture was heated for 2Hrs more. A final portion of BiCl<sub>3</sub> (30 mg, 0.096 mmol, 0.2 eq) was added and the reaction mixture was heated for 3 Hrs. Purification by flash column chromatography produced 77mg of the desired product as a white solid in a 45.5% yield. [Found 628.3591 M+H, expected 628.3598 M+H];  $\delta_{\text{H}}$  (400 MHz, CDCl<sub>3</sub>) 1.280-1.30 (2H, m, CH<sub>2</sub>), 1.4 (9H, s, CH<sub>3</sub>  $\times$  3), 1.53-2.06 (8H, m, CH<sub>2</sub>  $\times$  4), 2.52-2.55 (2H, t, J 6, CH<sub>2</sub>), 3.64-3.73 (16H, m, CH<sub>2</sub>  $\times$  8), 7.33-7.41 (4H, m, Ar-H), 7.64-7.78 (4H, m, Ar-H);  $\delta_{\text{C}}$ (100 MHz CDCl<sub>3</sub>) 12.29, 22.51, 24.54, 27.60, 29.00, 33.42, 35.49, 38.61, 44.04, 50.70, 53.25, 66.38, 69.07, 69.83, 120.5, 125.2, 142.6, 143.6.

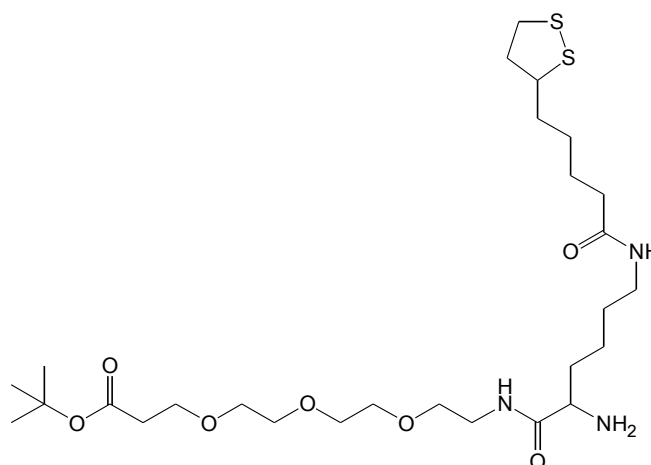
**8.2.29 Synthesis of tert-butyl 5-(4-(5-(1,2-dithiolan-3-yl)pentanamido)butyl)-1-(9H-fluoren-9-yl)-3,6-dioxo-2,10,13,16-tetraoxa-4,7-diazanonadecan-19-oate**



48

Thioctic acid (24mg, 0.11 mmol, 1eq), NHS (13mg, 0.11 mmol, 1eq) and DIC (0.013 mL, 0.11 mmol, 1eq) were dissolved in DCM (5 mL), the solution was stirred at room temperature for 2Hrs. To this solution compound 47 (73mg, 0.11 mmol, 1eq), DIPEA (0.1 mL) and DCM (15 mL) were added the solution was stirred at room temperature for a further 18 Hrs. Purification by flash column chromatography produced 65mg of the desired product in a 72.3% yield. [Found 816.2987 M+H; expected 816.3883 M+H];  $\delta_{\text{H}}$  (400 MHz,  $\text{CDCl}_3$ ) 1.22-1.31 (4H, m,  $\text{CH}_2 \times 2$ ), 1.44 (9H, s,  $\text{CH}_3 \times 3$ ), 1.82-1.96 (4H, m,  $\text{CH}_2 \times 4$ ), 2.13-2.17 (2H, t, J 8,  $\text{CH}_2$ ), 2.47-2.50 (2H, t, J 6,  $\text{CH}_2$ ), 2.61-2.65 (2H, t, J 8,  $\text{CH}_2$ ), 3.085-3.26 (6H, m,  $\text{CH}_2 \times 3$ ), 3.56-3.69 (16H, m,  $\text{CH}_2 \times 8$ ), 7.30-7.34 (2H, t, J 8, Ar-H), 7.39-7.42 (2H, t, J 6, Ar-H), 7.60-7.62 (2H, d, J 8, Ar-H), 7.76-7.78 (2H, d, J 8, Ar-H);  $\delta_{\text{C}}$  (100 MHz  $\text{CDCl}_3$ ) 12.29, 22.51, 24.54, 25.97, 26.80, 27.60, 29.00, 33.42, 35.49, 38.61, 44.04, 50.70, 53.25, 66.38, 69.07, 69.83, 70.05, 120.5, 125.2, 142.6, 143.6.

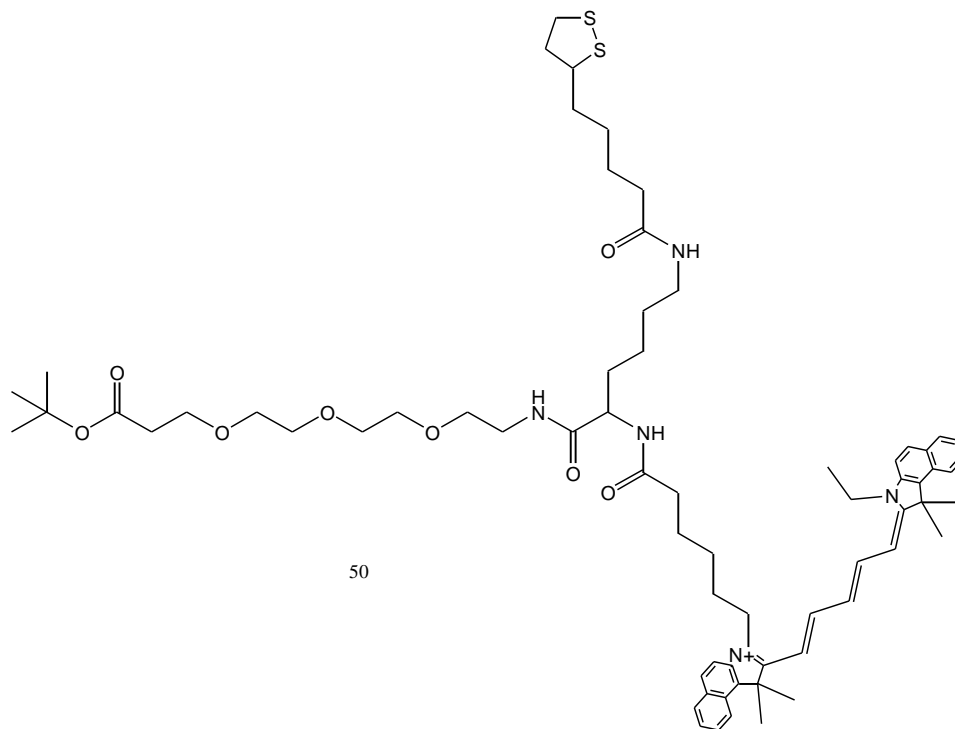
### 8.2.30 Synthesis of tert-butyl 15-amino-25-(1,2-dithiolan-3-yl)-14,21-dioxo-4,7,10-trioxa-13,20-diazapentacosan-1-oate



49

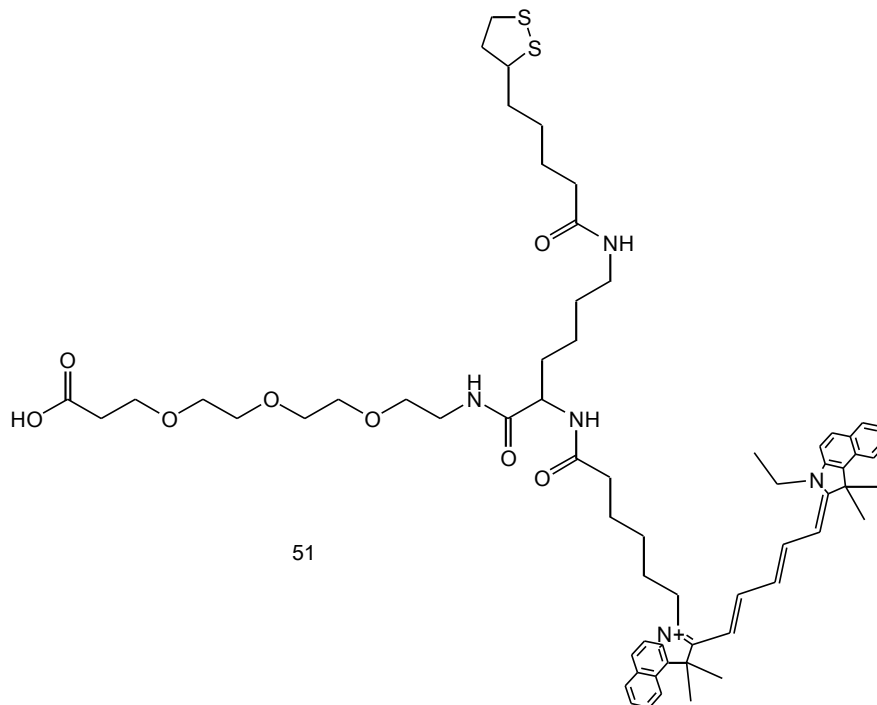
Compound 48 (65mg, 0.079 mmol, 1eq) was dissolved in a 20% piperidine solution in MeCN (20 mL) and stirred at room temperature for 3 Hrs. Removal of excess solvent under vacuo produced the desired product in 100% yield. [Found 593.3681 M+H; expected 593.3168 M+H);  $\delta_{\text{H}}$  (400 MHz,  $\text{CDCl}_3$ ) 1.26 (3H, s,  $\text{CH}_3$ ), 1.41 (9H, s,  $\text{CH}_3 \times 3$ ), 1.48-1.52 (2H, t, J 8,  $\text{CH}_2$ ), 1.57-1.92 (16H, m,  $\text{CH}_2 \times 8$ ) 2.43-2.50 (2H, m,  $\text{CH}_2$ ), 3.09-3.11 (2H, m,  $\text{CH}_2$ ), 3.43-3.73 (14H, m,  $\text{CH}_2 \times 7$ ), 4.26- 4.29 (2H, t, J 6,  $\text{CH}_2$ );  $\delta_{\text{C}}$  (100 MHz,  $\text{CDCl}_3$ ) 12.29, 22.51, 24.54, 25.97, 26.80, 27.60, 29.00, 33.42, 35.49, 38.61, 44.04, 50.70, 53.25, 66.38, 69.07, 69.83, 70.05.

**8.2.31 Synthesis of 3-(18-(4-(5-(1,2-dithiolan-3-yl)pentanamido)butyl)-2,2-dimethyl-4,17,20-trioxo-3,7,10,13-tetraoxa-16,19-diazapentacosan-25-yl)-2-((1E,3E,5Z)-5-(3-ethyl-1,1-dimethyl-1H-benzo[e]indol-2(3H)-ylidene)penta-1,3-dien-1-yl)-1,1-dimethyl-1H-benzo[e]indol-3-ium**



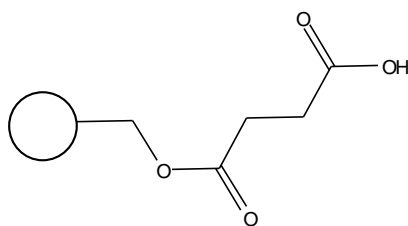
Compound 49 (100 mg, 0.19 mmol, 1eq), compound 11 (113mg, 0.19 mmol, 1eq) and EDC (72mg, 0.38 mmol, 2eq) were dissolved in DCM and stirred at room temperature for 18 Hrs. Purification by column chromatography produced 73 mg of the desired product as a blue solid in a 32% yield. [Found 1172.1564 M+H; expected 1172.6539 M+H];  $\delta_{\text{H}}$  (400 MHz,  $\text{CDCl}_3$ ) 1.26 (3H, s,  $\text{CH}_3$ ), 1.41 (9H, s,  $\text{CH}_3 \times 3$ ), 1.44 (12H, s,  $\text{CH}_3 \times 4$ ), 1.48-1.52 (2H, t, J 8,  $\text{CH}_2$ ), 1.57-1.92 (16H, m,  $\text{CH}_2 \times 8$ ) 2.43-2.50 (2H, m,  $\text{CH}_2$ ), 3.09-3.11 (2H, m,  $\text{CH}_2$ ), 3.43-3.73 (14H, m,  $\text{CH}_2 \times 7$ ), 4.26-4.29 (2H, t, J 6,  $\text{CH}_2$ ), 6.35-6.41 (1H, m, CH), 6.89-6.97 (1H, m, CH), 7.46-7.50 (2H, m, Ar-H), 7.60-7.64 (4H, m, Ar-H), 7.93-7.95 (4H, d, J 8, Ar-H), 8.14-8.26 (4H, m, Ar-H);  $\delta_{\text{C}}$  (100 MHz,  $\text{CDCl}_3$ ) 12.29, 22.51, 24.54, 25.97, 26.80, 27.60, 29.00, 33.42, 35.49, 38.61, 44.04, 50.70, 53.25, 66.38, 69.07, 69.83, 70.05, 80.05, 102.96, 110.06, 121.72, 124.55, 127.25, 129.55, 130.12, 131.32, 138.82, 151.79, 155.99.

**8.2.32 Synthesis of 3-(14-(4-(5-(1,2-dithiolan-3-yl)pentanamido)butyl)-1-carboxy-13,16-dioxo-3,6,9-trioxa-12,15-diazahenicosan-21-yl)-2-((1E,3E,5Z)-5-(3-ethyl-1,1-dimethyl-1H-benzo[e]indol-2(3H)-ylidene)penta-1,3-dien-1-yl)-1,1-dimethyl-1H-benzo[e]indol-3-ium**



Compound 50 (73mg, 0.067mmol, 1eq) was dissolved in a 50% TFA in DCM (6 mL) solution and stirred at room temperature for 3 Hrs. Removal of excess solvent produced 73mg of the desired product as a blue solid in a 100% yield. [Found 1117.584 M+H; expected 1117.5946 M+H],  $\delta_H$  (400 MHz CDCl<sub>3</sub>) 1.26 (3H, s, CH<sub>3</sub>), 1.44 (12H, s, CH<sub>3</sub> x 4), 1.48-1.52 (2H, t, J 8, CH<sub>2</sub>), 1.57-1.92 (16H, m, CH<sub>2</sub> x 8) 2.43-2.50 (2H, m, CH<sub>2</sub>), 3.09-3.11 (2H, m, CH<sub>2</sub>), 3.43-3.73 (14H, m, CH<sub>2</sub> x 7), 4.26- 4.29 (2H, t, J 6, CH<sub>2</sub>), 6.35-6.41 (1H, m, CH), 6.89-6.97 (1H, m, CH), 7.46-7.50 (2H, m, Ar-H), 7.60-7.64 (4H, m, Ar-H), 7.93-7.95 (4H, d, J 8, Ar-H), 8.14-8.26 (4H, m, Ar-H)  $\delta_C$  (100 MHz, CDCl<sub>3</sub>) 12.29, 22.51, 24.54, 25.97, 26.80, 27.60, 33.42, 35.49, 38.61, 44.04, 50.70, 53.25, 66.38, 69.07, 69.83, 70.05, 80.05, 102.96, 110.06, 121.72, 124.55, 127.25, 129.55, 130.12, 131.32, 138.82, 151.79, 155.99.

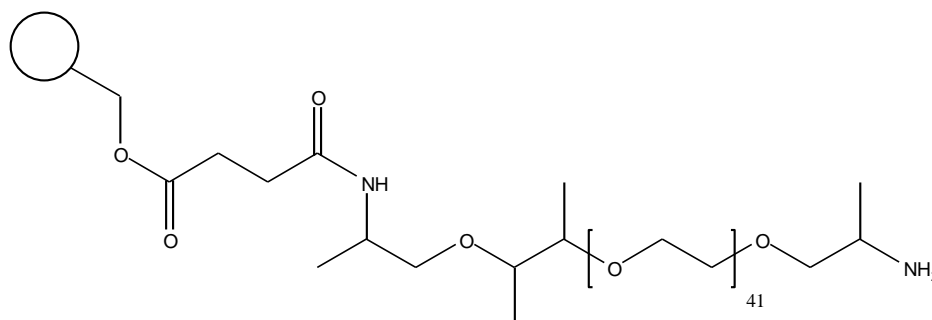
### 8.2.33 Modification of Wang Resin



54

Wang resin (3g, 3 mmol, 1eq), succinic anhydride (1.5g, 15 mmol, 5eq) and DMAP (732mg, 6 mmol, 2eq) were suspended in DCM (50 mL). The solution was refluxed for 6 Hrs, once cooled to room temperature the resin was isolated by filtration, followed by washing with MeOH and DCM three times.

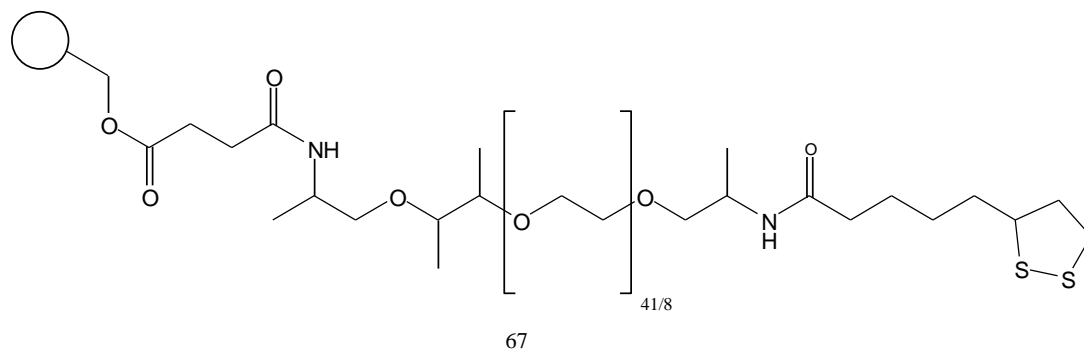
### 8.2.34 Attachment of PEG<sub>41/8</sub> to modified resin



55

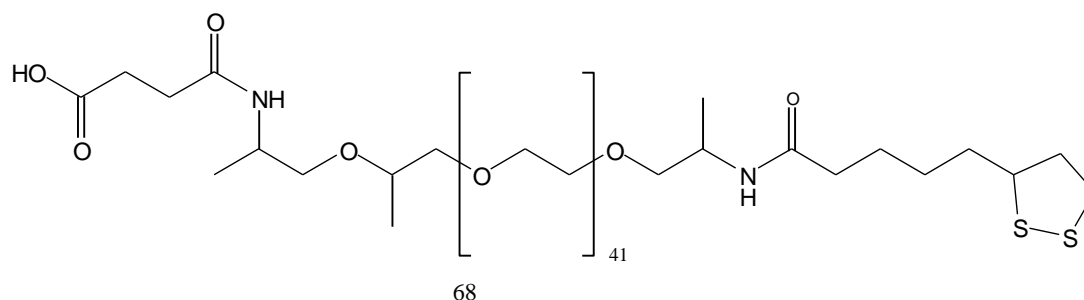
Resin 52 (1g, 1mmol, 1eq), PEG41 (9.5g, 5 mmol, 5eq) and DIC (775  $\mu$ L, 5 mmol, 5eq) were suspended in DCM (50 mL) and shaken for 18Hrs. The resin was isolated by filtration and washed three times with MeOH and DCM respectively.

### 8.2.35 Attachment thioctic acid to modified resin



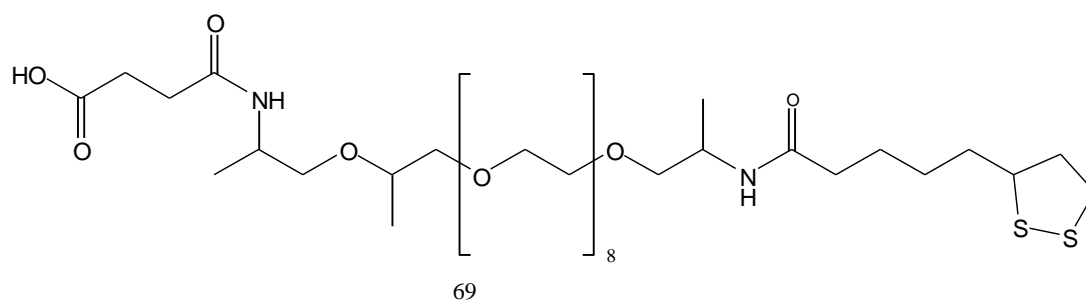
Resin 53 (1g, 1mmol, 1eq), thioctic acid (5g, 5 mmol, 5eq) and DIC (775  $\mu$ L, 5 mmol, 5eq) were suspended in DCM (50 mL) and shaken for 18Hrs. The resin was isolated by filtration and washed three times with MeOH and DCM respectively.

### 8.2.36 Cleavage from of PEG<sub>41</sub> Linker from modified resin.



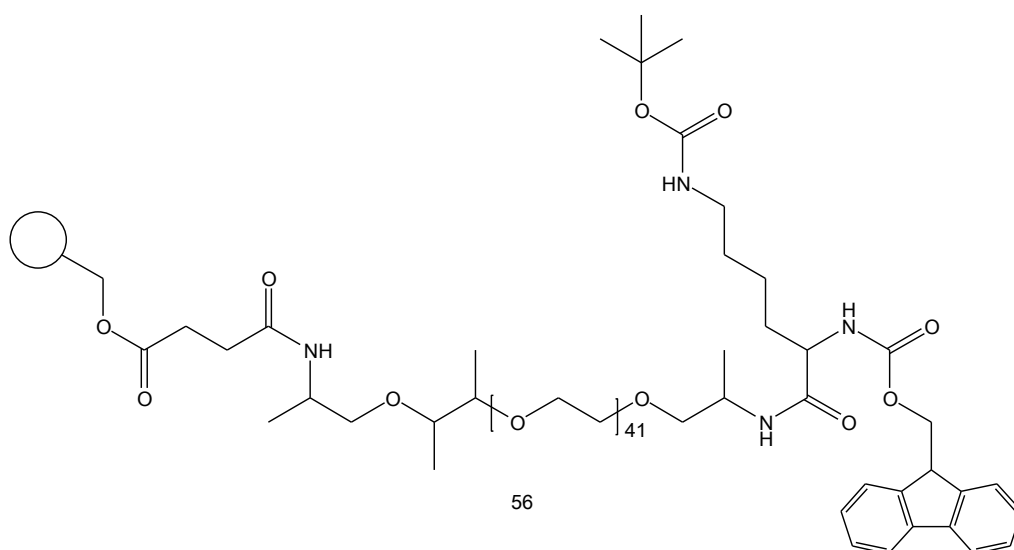
Resin 57 (1g, 1mmol, 1eq) was suspended in a 20% solution of TFA in DCM and agitated for 3 hours at RT. The resin was separated using filtration. The resin was washed three times with MeOH and DCM respectively, before discarding the resin. The filtrate was concentrated using rotary evaporation. The compound was used without further purification. [MALDI-TOF: C<sub>100</sub>H<sub>195</sub>O<sub>47</sub>N<sub>2</sub>S<sub>2</sub> Found: 2056.75; expected 2239],  $\delta$ H (400 MHz CDCl<sub>3</sub>) 1.23 (6H, s, CH<sub>3</sub> x 2), 1.35 (6H, s, CH<sub>3</sub> x 2), 1.40-2.18 (140H, m, , PEG CH<sub>2</sub>), 2.45-2.53 (4H, m, CH<sub>2</sub> x 2)  $\delta$ C (100 MHz, CDCl<sub>3</sub>) 14.9, 18.2, 25.9, 35.2, 38.3, 43.5, 52.5, 70.4, 175.0.

### 8.2.37 Cleavage from of PEG<sub>8</sub> Linker from modified resin.



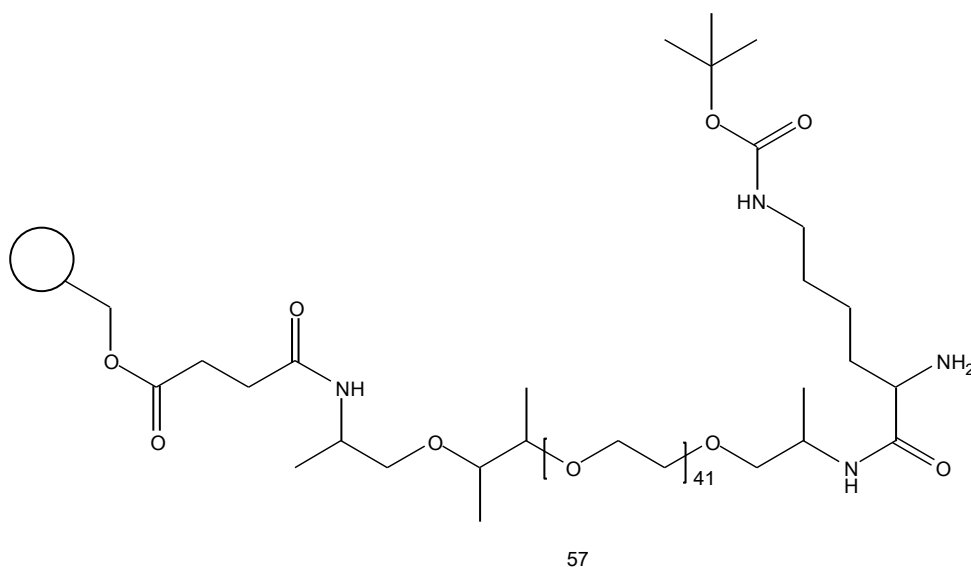
Resin 57 (1g, 1mmol, 1eq) was suspended in a 20% solution of TFA in DCM and agitated for 3 hours at RT. The resin was separated using filtration. The resin was washed three times with MeOH and DCM respectively, before discarding the resin. The filtrate was concentrated using rotary evaporation. The compound was used without further purification. [MALDI-TOF: C<sub>38</sub>H<sub>72</sub>O<sub>14</sub>N<sub>2</sub>S<sub>2</sub> Found: 800.60; expected 844.44],  $\delta$ H (400 MHz CDCl<sub>3</sub>) 1.23 (6H, s, CH<sub>3</sub> x 2), 1.35 (6H, s, CH<sub>3</sub> x 2), 1.40-2.18 (40H, m, PEG CH<sub>2</sub>), 2.45-2.53 (4H, m, CH<sub>2</sub> x 2)  $\delta$ C (100 MHz, CDCl<sub>3</sub>) 15.2, 19.2, 25.9, 36.2, 38.3, 44.5, 55.5, 68.5, 70.4, 177.0

### 8.2.38 Attachment of lysine to resin



Resin 53 (1g, 1mmol, 1eq), lysine (2.34g, 5 mmol, 5eq) and DIC (775  $\mu$ L, 5 mmol, 5eq) were suspended in DCM (50 mL) and shaken for 18Hrs. The resin was isolated by filtration and washed three times with MeOH and DCM respectively.

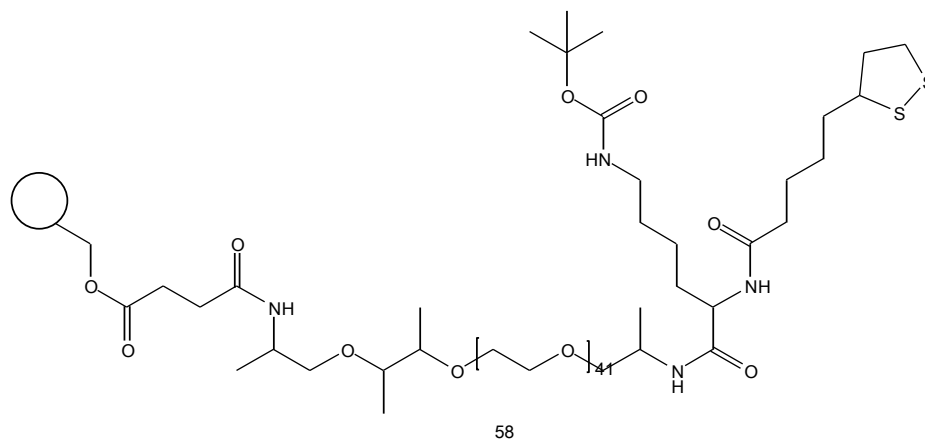
### 8.2.39 Deprotection of Fmoc group



Resin 54 (100mg, 0.1 mmol, 1eq) was washed with DMF (20 mL) and then suspended in a 20% piperidine in DMF (24 mL) solution. The solution was agitated

at room temperature for 2Hrs. The resin was isolated by filtration and washed with DMF the three times with MeOH and DCM respectively.

#### 8.2.40 Attachment of thioctic acid to resin



Resin 54 (100mg, 0.1 mmol, 1eq) and thioctic acid (103mg, 0.5 mmol, 5eq) and DIC (0.052 mL, 0.5 mmol, 5eq) were suspended in DCM (25 mL) and agitated for 18Hrs at room temperature. The resin was isolated by filtration and washed three times with MeOH and DCM respectively.

## 8.3 NANOPARTICLE SYNTHESIS

Prior to colloid synthesis, all glassware was soaked overnight with aqua regia (HNO<sub>3</sub>:HCl 1:3 v/v)

### 8.3.1 Silver Citrate Nanoparticles

500 mL of distilled water was heated to 45°C to which 90 mg of silver nitrate (dissolved in 10 mL of distilled water) was added. The solution was then heated to 98°C where 110 mg of tri-sodium citrate in 10 mL of distilled water was added and the solution was heated at 98°C for 90 minutes with continuous stirring.

### 8.3.2 Gold Citrate Nanoparticles

500 mL of distilled water containing 50 mg of sodium tetrachloroaurate was heated to boiling with continuous stirring to which sodium citrate (1% (w/v) dissolved in 10 mL of distilled water was added). The solution was then maintained at boiling for 15 minutes before cooling to room temperature.

## 8.4 CONJUGATE SYNTHESIS

### 8.4.1 Thioctic acid capped silver nanoparticles

To 10 mL of 1 nM silver citrate colloidal solution, 1 mL of 10 mM NaOH was added to adjust the pH to 9. 10 µL of 0.1 mM thioctic acid solution was added to 1 mL of the pH adjusted colloid and agitated for 16 hours at RT. Centrifuged for 6000 rpm for 20 minutes; the pellet was resuspended in 1 mL of 10 mM carbonate buffer, pH 8. Following a second round of centrifugation the pellet was once more suspended in 1 mL of 10 mM carbonate buffer.

### 8.4.2 EGFP conjugates

To 10 mL of silver citrate colloidal solution, 0.01 % (v/v) nitric acid was added until a pH of 4.5 was reached. 50 µL of EGFP at chosen concentration in 1×PBS was added to 400 µL of pH modified silver colloid and incubated for 50 hours at RT.

### 8.4.3 RFP Conjugates

To 1 mL of 1 nM thioctic acid capped silver nanoparticles, 20 µL EDC, 2 mg/mL, 20 µL sulfo-NHS. 2 mg/mL were added and incubated for 30 minutes at RT. Following which 50 µL of  $3 \times 10^{-7}$  M RFP was added and incubated for 16 hours at RT.

Centrifuged at 5000 rpm for 20 minutes the pellet was resuspended in 650  $\mu$ L of 10 mM carbonate buffer, pH 8.

#### **8.4.4 PDDA-EGFP Conjugates**

To 32 mL of 1 mM NaCl, 8 mL of 1 nM silver citrate colloid was added. To 1 mL of this solution, 100  $\mu$ L of PDDA at a concentration between 1-10 mg/mL was added and incubated for 45 minutes. Followed by centrifugation at 5000 rpm for 20 minutes the supernatant was removed and the pellet was resuspended in 1 mL in 1 mM NaCl. 400  $\mu$ L of the PDDA coated silver citrate colloid was incubated with 50  $\mu$ L of  $3 \times 10^{-7}$  M EGFP and analysed immediately.

#### **8.4.5 PEG<sub>41</sub>/PEG<sub>8</sub>- AuNPs conjugates**

To 17 nM, 13 nm, gold nanoparticles 100  $\mu$ L of PEG<sub>41</sub> linker (8.2.44)/PEG<sub>8</sub> linker at a 1 mM concentration were incubated at RT for 18 hours. Conjugates were centrifuged at 6000 rpm for 20 minutes, the supernatant was removed and the pellet was resuspended in 1 mL of 10 mM carbonate buffer. This cycle was repeated twice more before final resuspension in 1 mL of 10 mM carbonate buffer.

#### **8.4.6 TAT Conjugates**

To 1 mL of 1 nM thioctic acid capped silver nanoparticles, 20  $\mu$ L EDC, 2 mg/mL, 20  $\mu$ L sulfo-NHS. 2 mg/mL were added and incubated for 30 minutes at RT. Following which 20  $\mu$ L of  $1 \times 10^{-6}$  M TAT peptide was added and incubated for 16 hours at RT. Centrifuged for 20 minutes at 6000 rpm, the pellet was resuspended in 1 mL of 10 mM carbonate buffer, pH 8. This cycle was repeated twice more before final suspension in 1 mL of 10 mM carbonate buffer, pH8.

#### **8.4.7 Gold Nanoparticle Linker protein conjugates for NLP micro-assay**

To 1 mL of 5 nM of Au nanoparticles 2  $\mu$ L of 1 mM of compound 51 was incubated for 4 hours at RT. Centrifuged to form a pellet and resuspended in 1 mL of 10 mM carbonate buffer, pH 8 containing 20  $\mu$ L EDC, 2 mg/mL, 20  $\mu$ L sulfo-NHS. 2 mg/mL and 10  $\mu$ L of protein A/G, 2 mg/mL for 16 hours at RT. Following centrifugation at 6000 rpm for 20 min, the supernatant was removed and the pellet resuspended in 1 mL of 10 mM carbonate buffer.

## **8.5 FABRICATION OF IGG CAPTURE ANTIBODY ARRAYS**

12-probe 1D arrays (66  $\mu$ m pitch) were cleaned using an oxygen plasma for 40

seconds (50% power, 72 cm<sup>3</sup>/ min) prior to use. Capture antibody print solution was prepared by reconstituting the lyophilized protein in 5 parts phosphate buffered saline (PBS) and 3 parts protein carrier buffer (supplied by NanoInk Inc, Skokie, IL) with an antibody concentration of 1.2 mg/ml. Ink delivery to the tip array was carried out by placing the array in a 6-channel microfluidic inkwell containing the capture antibody print solution. Excess ink was removed by “bleeding” the ink outside the designated printing area. All NLP experiments were carried out at room temperature (19-21 °C) and a relative humidity of 40-60%. Once desired arrays were fabricated, the epoxysilane coated slides were left to incubate overnight at 4 °C.

The printed slide, after overnight incubation, was washed in wash buffer (WB, 0.05% Tween 20 in PBS) before being blocked with reagent diluent (RD, 1% BSA in PBS) and left to incubate for 1 hour. The slide was placed in a microarray slide incubator at this stage to ensure different treatments could be applied to corresponding arrays. They were washed (x3) with WB before gold nanoparticle linker conjugates (detailed in 8.4.7) were added and incubated for 1 hour. Finally, the slide was washed in WB for 10 minutes followed by de-ionised water and then dried using nitrogen. The processed slides were analysed by Raman microscopy using a 633nm laser and a 100x objective. 60 x 60um raman maps were taken of individual arrays using 0.1s integration time with a 1um resolution. Low laser powers were used to prevent damaging of the arrays. Images were processed using Witech software.

## 8.6 CELLULAR EXPERIMENTS

HeLa cells were routinely grown in Eagles Minimum Essential Medium(EMEM) with 10% heat-inactivated fetal bovine serum and 1% v/v of 200mM L-glutamine and 1% v/v of 10.000IU/ml penicillin-10mg/ml streptomycin at 37°C in a humidified 5% CO<sub>2</sub> atmosphere. After reaching confluence cells were harvested and seeded at 2\*10<sup>5</sup> cells per well in 24-well sterile tissue culture plate to which 13 mm round coverslip had previously been added. HeLa cells were incubated overnight at 37°C, 5% CO<sub>2</sub> to allow the cells to adhere to the coverslip. TAT labelled silver nanoparticles ( 0.2 nM) were added to the cells and incubated for 1 hour. Following

incubation with colloid, the cells were washed four times with phosphate buffered saline to remove any extracellular colloid before fixation with 4% paraformaldehyde. After 15 min the coverslips were washed one time with phosphate buffered saline and one time with distilled water. After fixation the coverslips were air dried for approximately 2 hours before they were mounted on to labelled slides using DPX mountant.

## 8.7 HPLC PROFILE FOR TAT COUPLING

Reverse phase HPLC was carried out on a Dionex UVD170U detector fitted with a P680 pump through a C<sub>18</sub> Phenomenox column. 30 minute gradient 10-90% MeCN, holding at 90% to wash everything off the column. Solvent A: 0.1% TFA in H<sub>2</sub>O Solvent B: 0.1% TFA in MeCN. T=0 90% A:10% B. T=35 minutes A: 10%; B : 90%. T= 40.5; A: 90% B: 10%. 200  $\mu$ L of each sample was injected with water washes (100  $\mu$ L) in-between each sample.

## 8.8 KLARITE™ EXPERIMENTAL

### 8.8.1 Deposition on Klarite™

A Klarite™ surface was immersed in a 1 mM solution (in EtOH) of compound 51 for 60 minutes. A second Klarite™ surface was immersed in a 1 mM solution (in EtOH) of compound 11 for 60 minutes. The surfaces were washed with IPA (5  $\times$  10 mL) then EtOH (5  $\times$  10 mL). The Klarite chips were dried in a dark environment before analysis.

### 8.8.2 SERS analysis of Klarite™ chips and assay

Both the Klarite chips and assay were analysed using a WiTec system at 633 nm and using a laser power of 40  $\mu$ W. 60  $\mu$ m  $\times$  60  $\mu$ m maps were analysed using a 0.1 sec integration time, centred at 1200 cm<sup>-1</sup> and a  $\times$  100 objective

## 8.9 RAMAN ANALYSIS OF EGFP AND RFP

1  $\mu$ L of 3.4 $\times$ 10<sup>-5</sup> M (EGFP) or 3.2 $\times$ 10<sup>-5</sup> M (RFP) were pipetted onto a glass coverslip, which was then dried under dark conditions. Each spot was analysed using WiTec Alpha 300R using 532, 633 and 785 nm. Spectra were obtained using

acquisition times between 90 and 1000 seconds. Each spectrum was centred at  $1800\text{ cm}^{-1}$  and a laser power of approximately  $0.1\text{ mW}$  was used.

## 8.10 UV-VIS SPECTROSCOPY

Carried out on a Cary 300 Bio UV-VIS spectrophotometer, silver citrate samples were diluted by a factor of 100 and gold samples were diluted by a factor of 10. Published extinction coefficients were used for calculation of concentration of colloid samples when using the Beer- Lambert Law.

### 8.11 pH ADJUSTMENT OF SILVER CITRATE COLLOID

10 mL of silver citrate colloid was pH adjusted using an acidic solution which was added dropwise and mixed followed by monitoring of the pH using a Jenway (model 3510) pH meter.

Concentration of acidic solutions:

- Nitric Acid 0.01% v/v
- Sulfuric Acid: 0.01% v/v
- Hydrochloric Acid 0.01% v/v
- Ascorbic Acid 10 mM
- Citric Acid: 10 mM

## 8.12 SERS EXPERIMENTAL

### 8.12.1 SERS of EGFP Conjugate

400  $\mu\text{L}$  of EGFP silver conjugate (either using colloid modification or citrate buffer method) was analysed using a plastic micro-cuvette supplied by VWR. The conjugate solution was analysed using a Renishaw 2000 Raman microprobe with a  $514.5\text{ nm}$  laser source with a 20x objective lens. Each spectrum was observed using a 20 second acquisition and 1 accumulation with the spectrum centred at  $1500\text{ cm}^{-1}$ . Samples were synthesised in triplicate with each sample analysed in triplicate. Prior to each experiment, the instrument was calibrated using  $800\text{ cm}^{-1}$  peak in cyclohexane.

### **8.12.2 SERS of RFP Conjugate**

At 514.5 nm: 400  $\mu\text{L}$  of the RFP was analysed using a plastic microcuvette supplied by VWR. The conjugate solution was analysed using a Renishaw 2000 Raman microprobe with a 20x objective lens. Each spectrum was observed using a 20 second acquisition and 1 accumulation. Each spectrum was observed using a 1 second acquisition and 1 accumulation with the spectrum centred at  $1500\text{ cm}^{-1}$ . Samples were synthesised in triplicate with each sample analysed in triplicate. Prior to each experiment, the instrument was calibrated using  $800\text{ cm}^{-1}$  peak in cyclohexane.

At 633 nm: 250  $\mu\text{L}$  of the RFP conjugate was analysed using a plastic microtitre plate. The conjugate solution was analysed using a Renishaw Raman X-blade with a 633 nm laser source and a 20x objective lens. Each spectrum was observed using a 20 second acquisition and 1 accumulation, focussed on the region between  $100 - 2000\text{ cm}^{-1}$ . As before samples were synthesised in triplicate with each sample analysed in triplicate. Prior to each experiment, the instrument was calibrated using  $520\text{ cm}^{-1}$  peak in silicon.

### **8.12.3 SERS of PDDA-EGFP Conjugates**

400  $\mu\text{L}$  of PDDA-EGFP silver conjugates were analysed using a plastic microcuvette supplied by VWR. The conjugate solution was analysed using a Renishaw 2000 Raman microprobe with a 514.5 nm laser source with a 20x objective lens. Each spectrum was observed using a 20 second acquisition and 1 accumulation with the spectrum centred at  $1500\text{ cm}^{-1}$ . Samples were synthesised in triplicate with each sample analysed in triplicate. Prior to each experiment, the instrument was calibrated using  $800\text{ cm}^{-1}$  peak in cyclohexane.

### **8.12.4 SERS of TAT Conjugate**

400  $\mu\text{L}$  of TAT silver conjugates were analysed using a plastic microcuvette supplied by VWR. The conjugate solution was analysed using a Renishaw 2000 Raman microprobe with a 514.5 nm laser source with a 20x objective lens. Each spectrum was observed using a 1 second acquisition and 1 accumulation with the spectrum centred at  $1450\text{ cm}^{-1}$ . Samples were synthesised in triplicate with each sample analysed in triplicate. Prior to each experiment, the instrument was calibrated using  $800\text{ cm}^{-1}$  peak in cyclohexane.

## 8.13 OPTIMISATION EXPERIMENTAL FOR SERS OF EGFP

All optimisation experiments were carried out using Renishaw 2000 Raman microprobe with a 20x objective lens with a 514.5 nm laser source.

### 8.13.1 Acquisition Investigation

EGFP conjugates at a final protein concentration of  $3.3 \times 10^{-8}$  M were synthesised as previously discussed. Each spectrum was centred at  $1500 \text{ cm}^{-1}$  with each sample synthesised in triplicate with each sample analysed in triplicate.

Samples were observed at 1 second, 10 seconds and 20 seconds. The average of each sample was determined and the intensity of the peak  $1522 \text{ cm}^{-1}$  was used to identify the optimum acquisition time.

### 8.13.2 Incubation time Investigation

EGFP conjugate was analysed using a 20 second acquisition and centred at  $1500 \text{ cm}^{-1}$ , a spectrum was taken every 30 minutes over the course of 54 hours. Once more the peak at  $1522 \text{ cm}^{-1}$  was used to determine the optimum incubation time in order to establish the maximum signal obtained.

## 8.14 GEL ELECTROPHORESIS EXPERIMENTAL

Bare gold nanoparticles, PEG<sub>41</sub>-AuNP conjugates and TAT-PEG<sub>41</sub>-AuNP conjugates (described in section 8.4) were then run on a 1% w/v agarose gel (1g of agarose in 100 mL of TBE buffer.) The gel was poured into a mould, protected from light and allowed to set.

Once set, the gel was placed within an insulated chamber and filled with 1 x TBE buffer until the gel was just covered. To each, volume 2  $\mu\text{L}$  of each conjugate, 20  $\mu\text{L}$  of loading buffer, Bioline 5x DNA loading buffer tri-colour, was added and mixed thoroughly. The gel was run at 160 V for an hour.

Loading buffer was used to visualise the rate of migration. It contained xylene blue, red and orange which will produce blue, pink and yellow bands as the samples move through the gel.

## CHAPTER 9: REFERENCES

1. E. Zubritsky, *Analytical Chemistry*, 2000, **72**, 391 A-391 A.
2. A. Piljic and C. Schultz, *Acs Chemical Biology*, 2008, **3**, 749-755.
3. C. M. Niemeyer, *Chemical & Engineering News*, 2001, **79**, 281-281.
4. A. Mor and M. R. Philips, *Annual Review Immunology*, 2006, **24**, 771-800.
5. A. Mahapatra, *Acs Chemical Biology*, **5**, 343-344.
6. L. Stryer, *Stryer, L. Biochemistry, Third Edition. Xxxiii+1089p. W. H. Freeman and Co.: New York, New York, USA. Illus*, 1988, XXXIII+1089P.
7. D. Baker and A. Sali, *Science*, 2001, **294**, 93-96.
8. F. Sanger and H. Tuppy, *Biochemical Journal*, 1951, **49**, 463-481.
9. F. Sanger and E. O. P. Thompson, *Biochemical Journal*, 1952, **52**, R3-R3.
10. F. H. Crick, *Symposia of the society for Experimental Biology*, 1958, **12**, 138-163.
11. F. H. Crick, *Nature*, 1970, **228**, 613-615.
12. M. G. N Rifai, S Carr, *Nature Biotechnology*, 2006, **24**, 971-983.
13. M. Beeram, A. Patnaik and E. K. Rowinsky, *Journal of Clinical Oncology*, 2005, **23**, 6771-6790.
14. C. C. You, A. Verma and V. M. Rotello, *Soft Matter*, 2006, **2**, 190-204.
15. A. F. Formina, T. J. Deerinck, M. H. Ellisman and M. D. Cahalan, *Experimental Cell Research*, 2003, **291**, 150-166.
16. F. Xie, K. Drozdowicz-Tomsia, T. Shtoyko and E. M. Goldys, *Journal of Nanoparticle Research*, **13**, 613-624.
17. L. Li, Q. Mu, B. Zhang and B. Yan, *Analyst*, **135**, 1519-1530.
18. R. Yuste, *Nature Methods*, 2005, **2**, 902-904.
19. N. C. Shaner, G. H. Patterson and M. W. Davidson, *Journal of Cell Science*, 2007, **120**, 4247-4260.
20. G. S. Baird, D. A. Zacharias and R. Y. Tsien, *Proceedings of the National Academy of Sciences of the United States of America*, 2000, **97**, 11984-11989.
21. J. Zhang, R. E. Campbell, A. Y. Ting and R. Y. Tsien, *Nature Reviews Molecular Cell Biology*, 2002, **3**, 906-918.
22. K. D. Volkova, V. B. Kovalska, A. O. Balanda, R. J. Vermeij, V. Subramaniam, Y. L. Slominskii and S. M. Yarmoluk, *Journal of Biochemical and Biophysical Methods*, 2007, **70**, 727-733.
23. R. E. Carter and A. Sorkin, *The Journal of Biological Chemistry*, 1998, **273**, 35000-35007.
24. Y. L. Yan and G. Marriott, *Current Opinion in Chemical Biology*, 2003, **7**, 635-640.
25. J. W. Lichtman and J. A. Conchello, *Nature Methods*, 2005, **2**, 910-919.
26. K. Faulds, R. P. Barbagallo, J. T. Keer, W. E. Smith and D. Graham, *Analyst*, 2004, **129**, 567-568.
27. G. Valentin, C. Verheggen, T. Pilot, H. Neel, M. Coppey-Moisan and E. Bertrand, *Nature Methods*, 2005, **2**, 801-801.
28. N. C. Shaner, P. A. Steinbach and R. Y. Tsien, *Nature Methods*, 2005, **2**, 905-909.
29. J. Drbohlavova, V. Adam, R. Kizek and J. Hubalek, *International Journal of Molecular Sciences*, 2009, **10**, 656-673.
30. M. A. Walling, J. A. Novak and J. R. E. Shepard, *International Journal of Molecular Sciences*, 2009, **10**, 441-491.
31. M. G. Bawendi, M. L. Steigerwald and L. E. Brus, *Annual Review of Physical Chemistry*, 1990, **41**, 477-496.

32. O. Shimomura, F. H. Johnson and Y. Saiga, *Journal of Cellular and Comparative Physiology*, 1962, **59**, 223-&.
33. O. Shimomura, *Angewandte Chemie-International Edition*, 2009, **48**, 5590-5602.
34. G. D. Malo, M. Wang, D. Wu, A. L. Stelling, P. J. Tonge and R. M. Wachter, *Journal of molecular biology*, 2008, **378**, 871-886.
35. J. Zhang, *Acs Chemical Biology*, 2009, **4**, 85-88.
36. M. Chalfie, *Angewandte Chemie-International Edition*, 2009, **48**, 5603-5611.
37. R. Y. Tsien, *Annual Review of Biochemistry*, 1998, **67**, 509-544.
38. R. Y. Tsien, *Angewandte Chemie-International Edition*, 2009, **48**, 5612-5626.
39. W.-B. Dan, C. Zhang, Z.-B. Guan and S.-Q. Zhang, *Biotechnology Letters*, 2008, **30**, 221-227.
40. G. V. P. Kumar and C. Narayana, *Current Science*, 2007, **93**, 778-781.
41. D. Graham and R. Goodacre, *Chemical Society Reviews*, 2008, **37**, 883-884.
42. R. J. Stokes, A. Macaskill, J. A. Dougan, P. G. Hargreaves, H. M. Stanford, W. E. Smith, K. Faulds and D. Graham, *Chemical Communications*, 2007, 2811-2813.
43. F. G. A Moores, *New Journal of Chemistry*, 2006, **30**, 1121-1132.
44. A. Champion and P. Kambhampati, *Chemical Society Reviews*, 1998, **27**, 241-250.
45. M. C. Daniel and D. Astruc, *Chemical Reviews*, 2004, **104**, 293-346.
46. M. Faraday, *Philosophical Transactions of the Royal Society London*, 1857, **147**, 145.
47. D. Graham, *Angewandte Chemie-International Edition*, **49**, 9325-9327.
48. R. A. Sperling, P. Rivera gil, F. Zhang, M. Zanella and W. J. Parak, *Chemical Society Reviews*, 2008, **37**, 1896-1908.
49. R. Sardar, A. M. Funston, P. Mulvaney and R. W. Murray, *Langmuir*, 2009, **25**, 13840-13851.
50. A. M. Alkilany and C. J. Murphy, *Journal of Nanoparticle Research*, **12**, 2313-2333.
51. G. Frens, *Nature-Physical Science*, 1973, **241**, 20-22.
52. P. C. Lee and D. Meisel, *Journal of Physical Chemistry*, 1982, **86**, 3391-3395.
53. J. A. Creighton, C. G. Blatchford and M. G. Albrecht, *Journal of the Chemical Society-Faraday Transactions II*, 1979, **75**, 790-798.
54. I. Lynch, T. Cedervall, M. Lundqvist, C. Cabaleiro-Lago, S. Linse and K. A. Dawson, *Advances in Colloid and Interface Science*, 2007, **134-35**, 167-174.
55. K. G. Stamplecoskie, J. C. Scaiano, V. S. Tiwari and H. Anis, *Journal of Physical Chemistry C*, **115**, 1403-1409.
56. R. Jones, *Nature Nanotechnology*, 2006, **1**, 85-86.
57. W. Xie, P. Qiu and C. Mao, *Journal of Materials Chemistry*, **21**, 5190-5202.
58. N. L. Rosi and C. A. Mirkin, *Chemical Reviews*, 2005, **105**, 1547-1562.
59. M. Soloviev, *Journal of Nanobiotechnology*, 2007, **5**, 11.
60. W. Zhao, W. Chiuman, J. C. F. Lam, S. A. McManus, W. Chen, Y. Cui, R. Pelton, M. A. Brook and Y. Li, *Journal of the American Chemical Society*, 2008, **130**, 3610-3618.
61. M. E. Aubin-Tam and K. Hamad-Schifferli, *Biomedical Materials*, 2008, **3**.
62. J. F. Hainfeld and J. M. Robinson, *Journal of Histochemistry & Cytochemistry*, 2000, **48**, 459-460.
63. P. Douglas, K. M. McCarney, D. Graham and W. E. Smith, *Analyst*, 2007, **132**, 865-867.
64. A. Sivanesan, H. K. Ly, J. Kozuch, M. Sezer, U. Kuhlmann, A. Fischer and I. M. Weidinger, *Chemical Communications*, **47**, 3553-3555.
65. W. Zhao, M. A. Brook and Y. Li, *ChemBiochem*, 2008, **9**, 2363-2371.
66. J. V. Jokerst, A. Raamanathan, N. Christodoulides, P. N. Floriano, A. A. Pollard, G. W. Simmons, J. Wong, C. Gage, W. B. Furmaga, S. W. Redding and J. T. McDevitt, *Biosensors & Bioelectronics*, 2009, **24**, 3622-3629.

67. M. De, S. Rana, H. Akpınar, O. R. Miranda, R. R. Arvizo, U. H. F. Bunz and V. M. Rotello, *Nature Chemistry*, 2009, **1**, 461-465.
68. A. Onoda, Y. Ueya, T. Sakamoto, T. Uematsu and T. Hayashi, *Chemical Communications*, **46**, 9107-9109.
69. Cannistraro, *Biochemical and Biophysical Research Communications*, 2009, **139**, 1-7.
70. C. Niemeyer, *Chemical Physics and Physical Chemistry*, 2006, **7**, 1112-1118.
71. G. J. Thomas, *Annual Review of Biophysics and Biomolecular Structure*, 1999, **28**, 1-+.
72. R. Tuma, *Journal of Raman Spectroscopy*, 2005, **36**, 307-319.
73. R. F. Aroca, R. A. Alvarez-Puebla, N. Pieczonka, S. Sanchez-Cortez and J. V. Garcia-Ramos, *Advances in Colloid and Interface Science*, 2005, **116**, 45-61.
74. C.V. Raman, *Nature*, 1928, **121**, 501.
75. C. Rodger, W. E. Smith, G. Dent and M. Edmondson, *Journal of the Chemical Society Dalton Transactions*, 1996, 791-799.
76. G. McNay, D. Eustace, W. E. Smith, K. Faulds and D. Graham, *Applied Spectroscopy*, **65**, 825-837.
77. T. Vo-Dinh, D. L. Stokes, G. D. Griffin, M. Volkan, U. J. Kim and M. I. Simon, *Journal of Raman Spectroscopy*, 1999, **30**, 785-793.
78. Fleischm.M, P. J. Hendra and McQuilla.Aj, *Chemical Physics Letters*, 1974, **26**, 163-166.
79. J. A. Creighton, R. J. H. Clark and R. E. Hester, *Spectroscopy of Surfaces* Wiley and sons 1998.
80. D. C. Jeanmarie and R. P. V. Duyne, *Journal of Electroanalytical Chemistry*, 1977, **84**, 1-20.
81. W.-H. Park and Z. H. Kim, *Nano Letters*, **10**, 4040-4048.
82. I. A. Larmour, K. Faulds and D. Graham, *Chemical Science*, **1**, 151-160.
83. K. F. Gibson, D. Correia-Ledo, M. Couture, D. Graham and J.-F. Masson, *Chemical Communications*, **47**, 3404-3406.
84. S. Stewart and P. M. Fredericks, *Spectrochimica Acta Part a-Molecular and Biomolecular Spectroscopy*, 1999, **55**, 1615-1640.
85. M. J. T. Milton. R.J.C Brown, *Journal of Raman Spectroscopy*, 2008, **39**, 1313-1326.
86. B. N. Rospendowski, K. Kelly, C. R. Wolf and W. E. Smith, *Journal of the American Chemical Society*, 1991, **113**, 1217-1225.
87. D. Cunningham, R. E. Littleford, W. E. Smith, P. J. Lundahl, I. Khan, D. W. McComb, D. Graham and N. Laforest, *Faraday Discussions*, 2006, **132**, 135-145.
88. K. Kneipp, Y. Wang, H. Kneipp, L. T. Perelman, I. Itzkan, R. Dasari and M. S. Feld, *Physical Review Letters*, 1997, **78**, 1667-1670.
89. P. C. Andersen and K. L. Rowlen, *Applied Spectroscopy*, 2002, **56**, 124A-135A.
90. L. C. Martin, I. A. Larmour, K. Faulds and D. Graham, *Chemical Communications*, **46**, 5247-5249.
91. I. A. Larmour, K. Faulds and D. Graham, *Journal of Physical Chemistry C*, **114**, 13249-13254.
92. J. Neng, M. H. Harpster, H. Zhang, J. O. Mecham, W. C. Wilson and P. A. Johnson, *Biosensors & Bioelectronics*, **26**, 1009-1015.
93. C. L. Haynes, C. R. Yonzon, X. Y. Zhang and R. P. Van Duyne, *Journal of Raman Spectroscopy*, 2005, **36**, 471-484.
94. K. K. Maiti, A. Samanta, M. Vendrell, K.-S. Soh, M. Olivo and Y.-T. Chang, *Chemical Communications*, **47**, 3514-3516.
95. K. Faulds, W. E. Smith, D. Graham and R. J. Lacey, *Analyst*, 2002, **127**, 282-286.

96. S. A. Hilderbrand, K. A. Kelly, R. Weissleder and C. H. Tung, *Bioconjugate Chemistry*, 2005, **16**, 1275-1281.
97. R. J. Stokes, A. Ingram, J. Gallagher, D. R. Armstrong, W. E. Smith and D. Graham, *Chem. Commun.*, 2008, 567-569.
98. K. Faulds, R. Jarvis, W. E. Smith, D. Graham and R. Goodacre, *Analyst*, 2008, **133**, 1505-1512.
99. N. M. S. Sirimuthu, C. D. Syme and J. M. Cooper, *Analytical Chemistry*, **82**, 7369-7373.
100. J. Llopis, J. M. McCaffery, A. Miyawaki, M. G. Farquhar and R. Y. Tsien, *Proceedings of the National Academy of Sciences of the United States of America*, 1998, **95**, 6803-6808.
101. L. Cognet, C. Tardin, D. Boyer, D. Choquet, P. Tamarat and B. Lounis, *Proceedings of the National Academy of Sciences of the United States of America*, 2003, **100**, 11350-11355.
102. D. Graham and K. Faulds, *Chemical Society Reviews*, 2008, **37**, 1042-1051.
103. D. Graham, R. Stevenson, D. G. Thompson, L. Barrett, C. Dalton and K. Faulds, *Faraday Discussions*, **149**, 291-299.
104. D. Graham, L. Fruk and W. E. Smith, *Analyst*, 2003, **128**, 692-699.
105. A. M. Ingram, K. Stirling, K. Faulds, B. D. Moore and D. Graham, *Organic & Biomolecular Chemistry*, 2006, **4**, 2869-2873.
106. L. Sun, C. Yu and J. Irudayaraj, *Analytical Chemistry*, 2007, **79**, 3981-3988.
107. R. J. Stokes, A. Macaskill, P. J. Lundahl, W. E. Smith, K. Faulds and D. Graham, *Small*, 2007, **3**, 1593-1601.
108. D. G. Thompson, A. Enright, K. Faulds, W. E. Smith and D. Graham, *Analytical Chemistry*, 2008, **80**, 2805-2810.
109. D. Graham, R. Brown and W. E. Smith, *Chemical Communications*, 2001, 1002-1003.
110. S. E. J. Bell and N. M. S. Sirimuthu, *Journal of the American Chemical Society*, 2006, **128**, 15580-15581.
111. K. Faulds, W. E. Smith and D. Graham, *Analyst*, 2005, **130**, 1125-1131.
112. C. A. Mirkin, R. L. Letsinger, R. C. Mucic and J. J. Storhoff, *Nature*, 1996, **382**, 607-609.
113. N. K. Howell, G. Arteaga, S. Nakai and E. C. Y. Li-Chan, *Journal of Agricultural and Food Chemistry*, 1999, **47**, 924-933.
114. F. M. Campbell, A. Ingram, P. Monaghan, J. Cooper, N. Sattar, P. D. Eckersall and D. Graham, *Analyst*, 2008, **133**, 1355-1357.
115. X. X. Han, L. J. Cai, J. Guo, C. X. Wang, W. D. Ruan, W. Y. Han, W. Q. Xu, B. Zhao and Y. Ozaki, *Analytical Chemistry*, 2008, **80**, 3020-3024.
116. H.-Y. Park, J. D. Driskell, K. M. Kwarta, R. J. Lipert, M. D. Porter, C. Schoen, J. D. Neill and J. F. Ridpath, *Surface-Enhanced Raman Scattering: Physics and Applications*, 2006, **103**, 427-446.
117. C. H. Munro, W. E. Smith and P. C. White, *Analyst*, 1995, **120**, 993-1003.
118. A. Enright, L. Fruk, A. Grondin, C. J. McHugh, W. E. Smith and D. Graham, *Analyst*, 2004, **129**, 975-978.
119. G. McAnally, C. McLaughlin, R. Brown, D. C. Robson, K. Faulds, D. R. Tackley, W. E. Smith and D. Graham, *Analyst*, 2002, **127**, 838-841.
120. X. X. Han, G. G. Huang, B. Zhao and Y. Ozaki, *Analytical Chemistry*, 2009, **81**, 3329-3333.
121. M. Kahraman, I. Sur and M. Culha, *Analytical Chemistry*, **82**, 7596-7602.
122. I. Pavel, E. McCarney, A. Elkhaled, A. Morrill, K. Plaxco and M. Moskovits, *Journal of Physical Chemistry C*, 2008, **112**, 4880-4883.

123. D. Graham, C. McLaughlin, G. McAnally, J. C. Jones, P. C. White and W. E. Smith, *Chemical Communications*, 1998, 1187-1188.
124. I. I. S. Lim, F. Goroleski, D. Mott, N. Kariuki, W. Ip, J. Luo and C. J. Zhong, *Journal of Physical Chemistry B*, 2006, **110**, 6673-6682.
125. X. Wang, H. Wen, T. J. He, J. Zuo, C. Y. Xu and F. C. Liu, *Spectrochimica Acta. Part A*, 1997, **53**, 2495-2504.
126. A. Ingram, L. Byers, K. Faulds, B. D. Moore and D. Graham, *Journal of the American Chemical Society*, 2008, **130**, 11846-11847.
127. F. McKenzie, A. Ingram, R. Stokes and D. Graham, *Analyst*, 2009, **134**, 549-556.
128. S. Sun, D. Thompson, U. Schmidt, D. Graham and G. J. Leggett, *Chemical Communications*, **46**, 5292-5294.
129. S. Thobhani, S. Attree, R. Boyd, N. Kumarswami, J. Noble, M. Szymanski and R. A. Porter, *Journal of Immunological Methods*, **356**, 60-69.
130. J. G. Morin and J. W. Hastings, *Journal of Cellular Physiology*, 1971, **77**, 313-&.
131. T. D. Craggs, *Chemical Society Reviews*, 2009, **38**, 2865-2875.
132. S. Kojima, T. Hirano, H. Niwa, M. Ohashi, S. Inouye and F. L. Tsuji, *Tetrahedron Letters*, 1997, **38**, 2875-2878.
133. R. Y. Tsien, *Annual Review of Biochemistry*, 1998, **67**, 509-544.
134. B. P. Cormack, G. Bertram, M. Egerton, N. A. R. Gow, S. Falkow and A. J. P. Brown, *Microbiology-Uk*, 1997, **143**, 303-311.
135. A. A. Heikal, S. T. Hess, G. S. Baird, R. Y. Tsien and W. W. Webb, *Proceedings of the National Academy of Sciences of the United States of America*, 2000, **97**, 11996-12001.
136. , US 6054321.
137. M. De, P. S. Ghosh and V. M. Rotello, *Advanced Materials*, 2008, **20**, 4225-4241.
138. M. De, C.-C. You, S. Srivastava and V. M. Rotello, *Journal of the American Chemical Society*, 2007, **129**, 10747-10753.
139. M. De, O. R. Miranda, S. Rana and V. M. Rotello, *Chemical Communications*, 2009, 2157-2159.
140. S. Habuchi, M. Cotlet, R. Gronheid, G. Dirix, J. Michiels, J. Vanderleyden, F. C. De Schryver and J. Hofkens, *Journal of the American Chemical Society*, 2003, **125**, 8446-8447.
141. V. Tozzini, A. R. Bizzarri, V. Pellegrini, R. Nifosi, P. Giannozzi, A. Iuliano, S. Cannistraro and F. Beltram, *Chemical Physics*, 2003, **287**, 33-42.
142. A. F. Bell, X. He, R. M. Wachter and P. J. Tonge, *Biochemistry*, 2000, **39**, 4423-4431.
143. R. Bandichhor, A. D. Petrescu, A. Vespa, A. B. Kier, F. Schroeder and K. Burgess, *Bioconjugate Chem.*, 2006, **17**, 1219-1225.
144. K. J. Zanotti, G. L. Silva, Y. Creeger, K. L. Robertson, A. S. Waggoner, P. B. Berget and B. A. Armitage, *Organic & Biomolecular Chemistry*, **9**, 1012-1020.
145. C. D. McGuinness, A. M. Macmillan, J. Karolin, W. E. Smith, D. Graham, J. C. Pickup and D. J. S. Birch, *Analyst*, 2007, **132**, 633-634.
146. H. Gunnar, E. Ann-Kristin, J. Gunnar and L. Per, *Electrophoresis*, 1995, **16**, 1377-1380.
147. R. A. O'Neill, A. Bhamidipati, X. Bi, D. Deb-Basu, L. Cahill, J. Ferrante, E. Gentalen, M. Glazer, J. Gossett, K. Hacker, C. Kirby, J. Knittle, R. Loder, C. Mastroieni, M. MacLaren, T. Mills, U. Nguyen, N. Parker, A. Rice, D. Roach, D. Suich, D. Voehringer, K. Voss, J. Yang, T. Yang and P. B. Vander Horn, *Proceedings of the National Academy of Sciences of the United States of America*, 2006, **103**, 16153-16158.
148. N. R. Yaffe, A. Ingram, D. Graham and E. W. Blanch, *Journal of Raman Spectroscopy*, **41**, 618-623.

149. M. Kahraman, A. I. Zamaleeva, R. F. Fakhruddin and M. Culha, *Analytical and Bioanalytical Chemistry*, 2009, **395**, 2559-2567.
150. D. M. Dotzauer, J. Dai, L. Sun and M. L. Bruening, *Nano Letters*, 2006, **6**, 2268-2272.
151. Y. Luo, *Indian Journal of Chemistry Section a-Inorganic Bio-Inorganic Physical Theoretical & Analytical Chemistry*, 2007, **46**, 1266-1269.
152. L. A. Gross, G. S. Baird, R. C. Hoffman, K. K. Baldrige and R. Y. Tsien, *Proceedings of the National Academy of Sciences of the United States of America*, 2000, **97**, 11990-11995.
153. D. Yarbrough, R. M. Wachter, K. Kallio, M. V. Matz and S. J. Remington, *Proceedings of the National Academy of Sciences of the United States of America*, 2001, **98**, 462-467.
154. J. A. Dougan, C. Karlsson, W. E. Smith and D. Graham, *Nucleic Acids Research*, 2007, **35**, 3668-3675.
155. B. A. Lodish, H. Matsudaira, P. Kaiser, C. Krieger, M. Scott, M. Zipursky, S.L. Darnell, *J. Mol. Cell. Biol.*, 2003.
156. M. Lindgren, M. Hallbrink, A. Prochiantz and U. Langel, *Trends in Pharmacological Sciences*, 2000, **21**, 99-103.
157. M. Silhol, M. Tyagi, M. Giacca, B. Lebleu and E. Vives, *European Journal of Biochemistry*, 2002, **269**, 494-501.
158. S. L. Fatemeh Madani, Ulo Langel, Shiroh Futaki, Astrid Grasland, *Journal of Biophysics*, 2011, **4**.
159. P. Jarver and U. Langel, *Drug Discovery Today*, 2004, **9**, 395-402.
160. A. F. S. F Said Hassane, R. Abes, M. J. Gait, B, Lebleu *Cellular and Molecular Life Sciences*, 2010, **67**, 715-726.
161. K. K. Mattias Hallbrink, Anna Elmquist, Pontus Lundberg, Maria Lindgren, Yang Jiang, Margus Pooga, Ursel Soomets, Ulo Langel, *International Journal of peptide research and therapeutics* 2005, **11**, 249-269.
162. V. Steven and D. Graham *Organic & Biomolecular Chemistry*, 2008, **6**, 3781-3787.
163. S. Nie, *Journal of the American Chemical Society*, 2007, **129**, 14759-14766.
164. A. Astriab-Fisher, D. Sergueev, M. Fisher, B. R. Shaw and R. L. Juliano, *Pharmaceutical Research*, 2002, **19**, 744-754.
165. P. C. Patel, D. A. Giljohann, D. S. Seferos and C. A. Mirkin, *Proceedings of the National Academy of Sciences of the United States of America*, 2008, **105**, 17222-17226.
166. N. Nitin, L. LaConte, W. J. Rhee and G. Bao, *Annals of Biomedical Engineering*, 2009, **37**, 2018-2027.
167. J. M. de la Fuente and C. C. Berry, *Bioconjugate Chemistry*, 2005, **16**, 1176-1180.
168. J. S. Molly Gregas, Benoit Lauly, Tuan Vo-Dinh *Applied Spectroscopy*, 2010, **64**, 858-866.
169. B. D. Chithrani, A. A. Ghazani and W. C. W. Chan, *Nano Letters*, 2006, **6**, 662-668.
170. H. K. Patra, S. Banerjee, U. Chaudhuri, P. Lahiri and A. K. Dasgupta, *Nanomedicine-Nanotechnology Biology and Medicine*, 2007, **3**, 111-119.
171. C. J. Murphy, A. M. Gole, J. W. Stone, P. N. Sisco, A. M. Alkilany, E. C. Goldsmith and S. C. Baxter, *Accounts of Chemical Research*, 2008, **41**, 1721-1730.
172. B. D. Chithrani and W. C. W. Chan, *Nano Letters*, 2007, **7**, 1542-1550.
173. V. Mailaender and K. Landfester, *Biomacromolecules*, 2009, **10**, 2379-2400.
174. E. Podstawka, Y. Ozaki and L. M. Proniewicz, *Applied Spectroscopy*, 2004, **58**, 1147-1156.
175. E. Byun, J. Kim, S. M. Kang, H. Lee, D. Bang and H. Lee, *Bioconjugate Chemistry*, **22**, 4-8.

176. T. Arakawa and S. N. Timasheff, *Biochemistry*, 1985, **24**, 6756-6762.
177. M. Popa, T. Pradell, D. Crespo and J. M. Calderon-Moreno, *Colloids and Surfaces a-Physicochemical and Engineering Aspects*, 2007, **303**, 184-190.
178. C.-J. Liu, C.-H. Wang, S.-T. Chen, H.-H. Chen, W.-H. Leng, C.-C. Chien, C.-L. Wang, I. M. Kempson, Y. Hwu, T.-C. Lai, M. Hsiao, C.-S. Yang, Y.-J. Chen and G. Margaritondo, *Physics in Medicine and Biology*, **55**, 931-945.
179. A. M. Kulkarni, A. P. Chatterjee, K. S. Schweizer and C. F. Zukoski, *Journal of Chemical Physics*, 2000, **113**, 9863-9873.
180. J. M. Harris and R. B. Chess, *Nature Reviews Drug Discovery*, 2003, **2**, 214-221.
181. S. D. Brown, P. Nativo, J.-A. Smith, D. Stirling, P. R. Edwards, B. Venugopal, D. J. Flint, J. A. Plumb, D. Graham and N. J. Wheate, *Journal of the American Chemical Society*, **132**, 4678-4684.
182. X. Qian, X.-H. Peng, D. O. Ansari, Q. Yin-Goen, G. Z. Chen, D. M. Shin, L. Yang, A. N. Young, M. D. Wang and S. Nie, *Nature Biotechnology*, 2008, **26**, 83-90.
183. M. Hanauer, S. Pierrat, I. Zins, A. Lotz and C. Sonnichsen, *Nano Letters*, 2007, **7**, 2881-2885.
184. S. M. A. J H Choi, R Ragan *Nanotechnology*, 2009, **20**, 1-6.
185. L. L. Wang, A. Roitberg, C. Meuse and A. K. Gaigalas, *Spectrochimica Acta Part a-Molecular and Biomolecular Spectroscopy*, 2001, **57**, 1781-1791.
186. Z. Zhu, *Dyes and Pigments*, 1995, **27**, 77-111.
187. M. E. Cooper, S. Gregory, E. Adie and S. Kalinka, *Journal of Fluorescence*, 2002, **12**, 425-429.
188. I. W. James, *Tetrahedron*, 1999, **55**, 4855-4946.
189. S. R. Mujumdar, R. B. Mujumdar, C. M. Grant and A. S. Waggoner, *Bioconjugate Chem.*, 1996, **7**, 356-362.
190. T. Hirata, H. Kogiso, K. Morimoto, S. Miyamoto, H. Taue, S. Sano, N. Muguruma, S. Ito and Y. Nagao, *Bioorganic & Medicinal Chemistry*, 1998, **6**, 2179-2184.
191. M. V. Kvach, A. V. Ustinov, I. A. Stepanova, A. D. Malakhov, M. V. Skorobogatyi, V. V. Shmanai and V. A. Korshun, *European Journal of Organic Chemistry*, 2008, 2107-2117.
192. R. J. Stokes, F. McKenzie, E. McFarlane, A. Ricketts, L. Tetley, K. Faulds, J. Alexander and D. Graham, *Analyst*, 2009, **134**, 170-175.
193. N. H. Alison McLintock, Alastair Wark *Chemical Communications*, 2011, **47**, 3757-3759.
194. M. E. Jung and W. J. Kim, *Bioorganic and Medicinal Chemistry*, 2006, **14**, 92-97.
195. O. Mader, K. Reiner, H. J. Egelhaaf, R. Fischer and R. Brock, *Bioconjugate Chem.*, 2004, **15**, 70-78.
196. S. J. Mason, J. L. Hake, J. Naire, W. J. Cummins and S. Balasubramanian, *Journal of the American Chemical Society*, 2004, **70**, 2939.
197. S. J. Mason, J. L. Hake, J. Nairne, W. J. Cummins and S. Balasubramanian, *Journal of Organic Chemistry*, 2005, **70**, 2939-2949.
198. R. B. Merrifield, *Journal of the American Chemical Society*, 1963, **85**, 2149-2154.
199. L.-L. Jiang, B.-L. Li, F.-T. Lv, L.-F. Dou and L.-C. Wang, *Tetrahedron*, 2009, **65**, 5257-5264.
200. A. Triebs and K. Jacobs, *Angewandte Chemie International Chemistry*, 1965, **77**, 680.
201. K.-Y. Law and F. C. Bailey, *Dyes and Pigments*, 1992, **20**, 25-40.
202. K. Y. Law and F. C. Bailey, *Canadian Journal of Chemistry-Revue Canadienne De Chimie*, 1993, **71**, 494-505.
203. A. Ajayaghosh, P. Chithra and R. Varghese, *Angewandte Chemie-International Edition*, 2007, **46**, 230-233.

204. H. B. Zhou, J. Zhang, S. M. Lu, R. G. Xie, Z. Y. Zhou, M. C. K. Choi, A. S. C. Chan and T. K. Yang, *Tetrahedron*, 2001, **57**, 9325-9333.
205. D. Keil and H. Hartmann, *Dyes Pigm.*, 2001, **49**, 161-179.
206. H. Nakazumi, T. Ohta, H. Etoh, T. Uno, C. L. Colyer, Y. Hyodo and S. Yagi, *Synthetic Metals*, 2005, **153**, 33-36.
207. A. L. Tatarets, I. A. Fedyunyayeva, T. S. Dyubko, Y. A. Povrozin, A. O. Doroshenko, E. A. Temetschnig and L. D. Patsenker, *Analytica Chimica Acta*, 2006, **570**, 214-223.
208. K. D. Volkova, V. B. Kovalska, A. L. Tatarets, L. D. Patsenker, D. V. Kryvorotenko and S. M. Yarmoluk, *Dyes and Pigments*, 2007, **72**, 285-292.
209. E. Terpetschnig, H. Szmecinski and J. R. Lakowicz, *Analytica Chimica Acta*, 1993, **282**, 633-641.
210. S. Yagi, Y. Hyodo, S. Matsumoto, N. Takahashi, H. Kono and H. Nakazumi, *Journal of the Chemical Society-Perkin Transactions 1*, 2000, 599-603.
211. J. V. Ros-Lis, R. Martinez-Manez, F. Sancenon, J. Soto, M. Spieles and K. Rurack, *Chemistry-a European Journal*, 2008, **14**, 10101-10114.
212. S. S. Wang, *J. Am. Chem. Soc.*, 1973, **95**, 1328.
213. R. S. Navath, K. B. Pabbisetty and L. Q. Hu, *Tetrahedron Letters*, 2006, **47**, 389-393.
214. V. Lejeune, J. Martinez and F. Cavelier, *Tetrahedron Letters*, 2003, **44**, 4757-4759.
215. A. H.-S. E Irvine, K Faulds, D Graham *Analyst*, 2011, **136**, 2925-2930.
216. R. J. Stokes, J. A. Dougan, E. Irvine, J. Ohayon, S. Rozhok, T. Levesque, B. Dudzik, M. Nelson and D. Graham, in *Microfluidics, Biomems, and Medical Microsystems Vii*, Editon edn., 2009, vol. 7207.
217. F. McKenzie, V. Steven, A. Ingram and D. Graham, *Chemical Communications*, 2009, 2872-2874.
218. V. Steven, PhD Thesis: Novel Approaches to Oligonucleotide Conjugation to a Cell penetrating (Tat) Peptide, 2009.
219. T. Li, L. Guo and Z. Wang, *Analytical Sciences*, 2009, **24**, 907-910